STATE OF THE CLIMATE IN 2022

REGIONAL CLIMATES

P. Bissolli, C. Ganter, A. Mekonnen, A. Sánchez-Lugo, and Z. Zhu, Eds.

Special Online Supplement to the *Bulletin of the American Meteorological Society* Vol. 104, No. 9, September, 2023

https://doi.org/10.1175/2023BAMSStateoftheClimate_Chapter7.1

Corresponding authors:
North America: Ahira Sánchez-Lugo / Ahira.Sanchez-Lugo@noaa.gov.
Central America and the Caribbean: Ahira Sánchez-Lugo / Ahira.Sanchez-Lugo@noaa.gov
South America: Ahira Sánchez-Lugo / Ahira.Sanchez-Lugo@noaa.gov
Africa: Ademe Mekonnen / amekonne@ncat.edu
Europe: Peter Bissolli / Peter.Bissolli@dwd.de
Asia: Zhiwei Zhu / zwz@nuist.edu.cn
Oceania: Catherine Ganter / Catherine.Ganter@bom.gov.au

STATE OF THE CLIMATE IN 2022
Regional Climates

Editors

Ellen Bartow-Gillies
Jessica Blunden
Tim Boyer

Chapter Editors

Peter Bissolli
Kyle R. Clem
Howard J. Diamond
Matthew L. Druckenmiller
Robert J. H. Dunn
Catherine Ganter
Nadine Gobron
Gregory C. Johnson
Rick Lumpkin
Ademe Mekonnen
John B. Miller
Twila A. Moon
Marilyn N. Raphael
Ahira Sánchez-Lugo
Carl J. Schreck III
Richard L. Thoman
Kate M. Willett
Zhiwei Zhu

Technical Editor

Lukas Noguchi

BAMS Special Editor for Climate

Michael A. Alexander

American Meteorological Society

Cover Credit:
Photo by Jiangxi Meteorological Bureau

Poyang Lake, China's largest freshwater lake in the Yangtze River basin, is dry on 2 September 2022 after the strongest recorded heatwave and drought on record in the region.

How to cite this document:
Regional Climates is one chapter from the *State of the Climate in 2022* annual report and is available from https://doi.org/10.1175/2023BAMSStateoftheClimate_Chapter7.1. Compiled by NOAA's National Centers for Environmental Information, *State of the Climate in 2022* is based on contributions from scientists from around the world. It provides a detailed update on global climate indicators, notable weather events, and other data collected by environmental monitoring stations and instruments located on land, water, ice, and in space. The full report is available from https://doi.org/10.1175/2023BAMSStateoftheClimate.1.

Citing the complete report:
Blunden, J., T. Boyer, and E. Bartow-Gillies, Eds., 2023: "State of the Climate in 2022". Bull. Amer. Meteor. Soc., 104 (9), Si–S501 https://doi.org/10.1175/2023BAMSStateoftheClimate.1.

Citing this chapter:
Bissolli, P., C. Ganter, A. Mekonnen, A. Sánchez-Lugo, and Z. Zhu, Eds., 2023: Regional Climates [in "State of the Climate in 2022"]. Bull. Amer. Meteor. Soc., 104 (9), S366–S473, https://doi.org/10.1175/2023BAMSStateoftheClimate_Chapter7.1.

Citing a section (example):
Aldeco, L. S., J. S. Stella, A. J. Reyes Kohler, N. Misevicius, and G. Jadra, 2023: Southern South America [in "State of the Climate in 2022"]. Bull. Amer. Meteor. Soc., 104 (9), S393–S396, https://doi.org/10.1175/2023BAMSStateoftheClimate_Chapter7.1.

Editor and Author Affiliations (alphabetical by name)

Abida, A., Agence Nationale de l'Aviation Civile et de la Météorologie, Moroni, Union of the Comoros

Agyakwah, W., NOAA/NWS National Centers for Environmental Prediction Climate Prediction Center, College Park, Maryland

Aldeco, Laura S., Servicio Meteorológico Nacional, Buenos Aires, Argentina

Alfaro, Eric J., Center for Geophysical Research and School of Physics, University of Costa Rica, San José, Costa Rica

Alves, Lincoln. M., Centro Nacional de Monitoramento e Alertas de Desastres Naturais CEMADEN, São Paulo, Brazil

Amador, Jorge A., Center for Geophysical Research and School of Physics, University of Costa Rica, San José, Costa Rica

Andrade, B., Seychelles Meteorological Authority, Mahe, Seychelles

Avalos, Grinia, Servicio Nacional de Meteorología e Hidrología del Perú, Lima, Perú

Bader, Stephan, Federal Office of Meteorology and Climatology MeteoSwiss, Switzerland

Baez, Julian, Universidad Católica Nuestra Señora de la Asunción, Asunción, Paraguay

Bardin, M. Yu, Yu. A. Izrael Institute of Global Climate and Ecology, Institute of Geography, Russian Academy of Sciences, Moscow, Russia

Bekele, E., NOAA/NWS National Centers for Environmental Prediction Climate Prediction Center, College Park, Maryland

Bellido, Guillem Martín, Govern d'Andorra, Andorra la Vella, Andorra

Berne, Christine, Meteo France, Toulouse, France

Bhuiyan, MD A. E., NOAA/NWS Climate Prediction Center, Silver Spring, Maryland

Bissolli, Peter, Deutscher Wetterdienst, WMO RA VI Regional Climate Centre Network, Offenbach, Germany

Bochníček, Oliver, Slovak Hydrometeorological Institute, Bratislava, Slovakia

Bukunt, Brandon, NOAA/NWS Weather Forecast Office, Tiyan, Guam

Calderón, Blanca, Center for Geophysical Research, University of Costa Rica, San José, Costa Rica

Campbell, Jayaka, Department of Physics, The University of the West Indies, Kingston, Jamaica

Chandler, Elise, Bureau of Meteorology, Melbourne, Australia

Chen, Hua, Nanjing University of Information Science and Technology, Nanjing, China

Cheng, Vincent Y. S., Environment and Climate Change Canada, Toronto, Ontario, Canada

Clarke, Leonardo, Department of Physics, The University of the West Indies, Kingston, Jamaica

Correa, Kris, Servicio Nacional de Meteorología e Hidrología del Perú, Lima, Perú

Costa, Felipe, Centro Internacional para la Investigación del Fenómeno de El Niño (CIIFEN), Guayaquil, Ecuador

Crhova, Lenka, Czech Hydrometeorological Institute, Prague, Czech Republic

Cunha, Ana P., Centro Nacional de Monitoramento e Alertas de Desastres Naturais CEMADEN, São Paulo, Brazil

De Bock, Veerle, Royal Meteorological Institute of Belgium (KMI), Brussels, Belgium

Demircan, Mesut, Turkish State Meteorological Service, Igdir, Türkiye

Deus, Ricardo, Portuguese Sea and Atmosphere Institute, Lisbon, Portugal

Dhurmea, K. R., Mauritius Meteorological Service, Vacoas, Mauritius

Dirkse, S., Namibia Meteorological Service, Windhoek, Namibia

Drumond, Paula, Portuguese Sea and Atmosphere Institute, Lisbon, Portugal

Dulamsuren, Dashkhuu, Institute of Meteorology, Hydrology and Environment, National Agency for Meteorology, Ulaanbaatar, Mongolia

Ekici, Mithat, Turkish State Meteorological Service, Ankara, Türkiye

ElKharrim, M., Direction de la Météorologie Nationale Maroc, Rabat, Morocco

Espinoza, Jhan-Carlo, Université Grenoble Alpes, Institut des Géosciences de l'Environnement, IRD, CNRS, Grenoble INP, Grenoble, France

Fenimore, Chris, NOAA/NESDIS National Centers for Environmental Information, Asheville, North Carolina

Fogarty, Chris, Environment and Climate Change Canada, Dartmouth, Nova Scotia, Canada

Fuhrman, Steven, NOAA/NWS NOAA/NWS National Centers for Environmental Prediction Climate Prediction Center, College Park, Maryland

Ganter, Catherine, Bureau of Meteorology, Melbourne, Australia

Gleason, Karin, NOAA/NESDIS National Centers for Environmental Information, Asheville, North Carolina

Guard, Charles "Chip" P., Tropical Weather Sciences, Sinajana, Guam

Hagos, S., Pacific Northwest National Lab, Department of Energy, Richland, Washington

Heim, Richard R. Jr., NOAA/NESDIS National Centers for Environmental Information, Asheville, North Carolina

Hellström, Sverker, Swedish Meteorological and Hydrological Institute, Norrköping, Sweden

Hicks, J., NOAA/NWS National Centers for Environmental Prediction Climate Prediction Center, College Park, Maryland

Hidalgo, Hugo G., Center for Geophysical Research and School of Physics, University of Costa Rica, San José, Costa Rica

Huang, Hongjie, Nanjing University of Information Science and Technology, Nanjing, China

Jadra, Gerardo, Instituto Uruguayo de Meteorología, Montevideo, Uruguay

Jumaux, G., Meteo France, Direction Interregionale Pour L'Ocean Indien, Reunion

Kabidi, K., Direction de la Météorologie Nationale Maroc, Rabat, Morocco

Kazemi, Amin Fazl, Iran National Climate and Drought Crisis Management, National Meteorology Organization, Tehran, Iran

Kendon, Mike, Met Office National Climate Information Centre, Exeter, United Kingdom

Kerr, Kenneth, Trinidad and Tobago Meteorological Service, Piarco, Trinidad

Khan, Valentina, Hydrometcenter of Russia, WMO North EurAsia Climate Center, Moscow, Russia

Khiem, Mai Van, Vietnam National Center for Hydro-Meteorological Forecasting, Vietnam Meteorological and Hydrological Administration, Hanoi, Vietnam

Kim, Mi Ju, Climate Change Monitoring Division, Korea Meteorological Administration, Seoul, South Korea

Korshunova, Natalia N., All-Russian Research Institute of Hydrometeorological Information, World Data Center, Obninsk, Russia

Kruger, A. C., Climate Service, South African Weather Service, Pretoria, South Africa

Lakatos, Mónika, Climatology Unit, Hungarian Meteorological Service, Budapest, Hungary

Lam, Hoang Phuc, Vietnam National Center for Hydro-Meteorological Forecasting, Vietnam Meteorological and Hydrological Administration, Hanoi, Vietnam

Lavado-Casimiro, Waldo, Servicio Nacional de Meteorología e Hidrología del Perú, Lima, Perú

Lee, Tsz-Cheung, Hong Kong Observatory, Hong Kong, China

Leung, Kinson H. Y., Environment and Climate Change Canada, Toronto, Ontario, Canada

Likso, Tanja, Croatian Meteorological and Hydrological Service, Zagreb, Croatia

Lu, Rui, Nanjing University of Information Science and Technology, Nanjing, China

Mamen, Jostein, Climate Division, Norwegian Meteorological Institute, Oslo, Norway

Marcinonienė, Izolda, Lithuanian Hydrometeorological Service, Vilnius, Lithuania

Marengo, Jose A., Centro Nacional de Monitoramento e Alertas de Desastres Naturais CEMADEN, São Paulo, Brazil

Marjan, Mohammadi, Iran National Climate and Drought Crisis Management, National Meteorology Organization, Tehran, Iran

Martínez, Ana E., National Meteorological Service of Mexico, Mexico City, Mexico
McBride, C., Climate Service, South African Weather Service, Pretoria, South Africa
Mekonnen, A., North Carolina A&T University, Greensboro, North Carolina
Meyers, Tristan, National Institute of Water and Atmospheric Research, Ltd. (NIWA), Auckland, New Zealand
Misevicius, Noelia, Instituto Uruguayo de Meteorología, Montevideo, Uruguay
Moise, Aurel, Centre for Climate Research Singapore, Meteorological Service Singapore, Singapore
Molina-Carpio, Jorge, Universidad Mayor de San Andrés, La Paz, Bolivia
Mora, Natali, Center for Geophysical Research, University of Costa Rica, San José, Costa Rica
Morán, Johnny, Centro Internacional para la Investigación del Fenómeno de El Niño (CIIFEN), Guayaquil, Ecuador
Morehen, Claire, Environment and Climate Change Canada, Vancouver, British Columbia, Canada
Mostafa, A. E., Department of Seasonal Forecast and Climate Research, Cairo Numerical Weather Prediction, Egyptian Meteorological Authority, Cairo, Egypt
Nieto, Juan J., Centro Internacional para la Investigación del Fenómeno de El Niño (CIIFEN), Guayaquil, Ecuador
Oikawa, Yoshinori, Tokyo Climate Center, Japan Meteorological Agency, Tokyo, Japan
Okunaka, Yuka, Tokyo Climate Center, Japan Meteorological Agency, Tokyo, Japan
Pascual Ramírez, Reynaldo, National Meteorological Service of Mexico, Mexico City, Mexico
Perčec Tadić, Melita, Croatian Meteorological and Hydrological Service, Zagreb, Croatia
Pires, Vanda, Portuguese Sea and Atmosphere Institute, Lisbon, Portugal
Quisbert, Kenny, Servicio Nacional de Meteorología e Hidrología de Bolivia, La Paz, Bolivia
Quispe, Willy R., Servicio Nacional de Meteorología e Hidrología de Bolivia, La Paz, Bolivia
Rajeevan, M., Ministry of Earth Sciences, New Delhi, India
Ramos, Andrea M., Instituto Nacional de Meteorología, Brasilia, Brazil
Recalde, Cristina, NOAA/NWS National Centers for Environmental Prediction, Climate Prediction Center, College Park, Maryland
Reyes Kohler, Alejandra J., Dirección de Meteorológica de Chile, Santiago de Chile, Chile
Robjhon, M., NOAA/NWS National Centers for Environmental Prediction Climate Prediction Center, College Park, Maryland
Rodriguez Guisado, Esteban, Agencia Estatal de Meteorología, Madrid, Spain
Ronchail, Josyane, Laboratoire LOCEAN-IPSL, Paris, France
Rösner, Benjamin, Laboratory for Climatology and Remote Sensing, Faculty of Geography, University of Marburg, Marburg, Germany
Rösner, Henrieke, Humboldt University, Berlin, Germany
Rubek, Frans, Danish Meteorological Institute, Copenhagen, Denmark
Salinas, Roberto, Dirección de Meteorología e Hidrología / Dirección Nacional de Aeronáutica Civil, Asunción, Paraguay
Sánchez-Lugo, Ahira, NOAA/NESDIS National Centers for Environmental Information, Asheville, North Carolina
Sayouri, A., Direction de la Météorologie Nationale Maroc, Rabat, Morocco
Schimanke, Semjon, Swedish Meteorological and Hydrological Institute, Norrköping, Sweden
Segele, Z. T., NOAA/NWS National Centers for Environmental Prediction Climate Prediction Center, College Park, Maryland
Sensoy, Serhat, Turkish State Meteorological Service, Ankara, Türkiye
Setiawan, Amsari Mudzakir, Division for Climate Variability Analysis, BMKG, Jakarta, Indonesia
Shukla, R., NOAA/NWS National Centers for Environmental Prediction Climate Prediction Center, College Park, Maryland
Sima, F., Division of Meteorology, Department of Water Resources, Banjul, The Gambia
Smith, Adam, NOAA/NESDIS National Centers for Environmental Information, Asheville, North Carolina
Spence-Hemmings, Jacqueline, Meteorological Service, Jamaica, Kingston, Jamaica
Spillane, Sandra, Climate Services Division, Met Éireann, The Irish Meteorological Service, Dublin, Ireland
Spillane, Sandra, Met Éireann, Dublin, Ireland
Sreejith, O. P., India Meteorological Department, Pune, India
Srivastava, A. K., India Meteorological Department, Pune, India
Stella, Jose L., Servicio Meteorológico Nacional, Buenos Aires, Argentina
Stephenson, Tannecia S., Department of Physics, The University of the West Indies, Kingston, Jamaica
Takahashi, Kiyotoshi, Tokyo Climate Center, Japan Meteorological Agency, Tokyo, Japan
Takemura, Kazuto, Tokyo Climate Center, Japan Meteorological Agency, Tokyo, Japan
Taylor, Michael A., Department of Physics, The University of the West Indies, Kingston, Jamaica
Thiaw, W. M., NOAA/NWS National Centers for Environmental Prediction Climate Prediction Center, College Park, Maryland
Tobin, Skie, Bureau of Meteorology, Melbourne, Australia
Trescilo, Lidia, State Hydrometeorological Service, Chisinau, Republic of Moldova
Trotman, Adrian, Caribbean Institute for Meteorology and Hydrology, Bridgetown, Barbados
van der Schrier, Gerard, Royal Netherlands Meteorological Institute (KNMI), De Bilt, The Netherlands
Van Meerbeeck, Cedric J., Caribbean Institute for Meteorology and Hydrology, Bridgetown, Barbados
Vazife, Ahad, Iran National Climate and Drought Crisis Management, National Meteorology Organization, Tehran, Iran
Willems, An, Royal Meteorological Institute of Belgium (KMI), Brussels, Belgium
Zhang, Peiqun, Beijing Climate Center, Beijing, China
Zhu, Zhiwei, Nanjing University of Information Science and Technology, Nanjing, China

Editorial and Production Team

Allen, Jessicca, Graphics Support, Cooperative Institute for Satellite Earth System Studies, North Carolina State University, Asheville, North Carolina

Camper, Amy V., Graphics Support, Innovative Consulting and Management Services, LLC, NOAA/NESDIS National Centers for Environmental Information, Asheville, North Carolina

Haley, Bridgette O., Graphics Support, NOAA/NESDIS National Centers for Environmental Information, Asheville, North Carolina

Hammer, Gregory, Content Team Lead, Communications and Outreach, NOAA/NESDIS National Centers for Environmental Information, Asheville, North Carolina

Love-Brotak, S. Elizabeth, Lead Graphics Production, NOAA/NESDIS National Centers for Environmental Information, Asheville, North Carolina

Ohlmann, Laura, Technical Editor, Innovative Consulting and Management Services, LLC, NOAA/NESDIS National Centers for Environmental Information, Asheville, North Carolina

Noguchi, Lukas, Technical Editor, Innovative Consulting and Management Services, LLC, NOAA/NESDIS National Centers for Environmental Information, Asheville, North Carolina

Riddle, Deborah B., Graphics Support, NOAA/NESDIS National Centers for Environmental Information, Asheville, North Carolina

Veasey, Sara W., Visual Communications Team Lead, Communications and Outreach, NOAA/NESDIS National Centers for Environmental Information, Asheville, North Carolina

7. Table of Contents

7. Table of Contents

Please refer to Chapter 8 (Relevant Datasets and Sources) for a list of all climate variables and datasets used in this chapter for analyses, along with their websites for more information and access to the data.

7. REGIONAL CLIMATES

P. Bissolli, C. Ganter, A. Mekonnen, A. Sánchez-Lugo, and Z. Zhu, Eds.

a. Overview

This chapter provides summaries of the 2022 temperature and precipitation conditions across seven broad regions: North America, Central America and the Caribbean, South America, Africa, Europe and the Middle East, Asia, and Oceania. In most cases, summaries of notable weather events are also included. Local scientists provided the annual summary for their respective regions and, unless otherwise noted, the source of the data used is typically the agency affiliated with the authors. The base period used for these analyses is 1991–2020, unless otherwise stated. Please note that on occasion different nations, even within the same section, may use unique periods to define their normal. Section introductions typically define the prevailing practices for that section, and exceptions will be noted within the text. In a similar way, many contributing authors use languages other than English as their primary professional language. To minimize additional loss of fidelity through re-interpretation after translation, editors have been conservative and careful to preserve the voice of the author. In some cases, this may result in abrupt transitions in style from section to section.

b. North America

—A. Sánchez-Lugo, Ed.

Below-average annual temperatures were observed across central Canada, the northern contiguous United States, and parts of northern and western Mexico during 2022, while the rest of the region experienced near- to above-average annual temperatures. Averaged as a whole, North America's annual temperature was 1.00°C above the 1991–2020 base period and the 16th-warmest year in the 113-year continental record (extends back to 1910).

Precipitation varied across the region, with significant annual deficits across parts of western and central contiguous United States and northeastern and central Mexico. Several significant events occurred during the year, including Hurricanes Fiona and Ian, among others.

Anomalies in this section are all based on the 1991–2020 base period, unless otherwise noted.

1. CANADA

—K. H. Y. Leung, V. Y. S. Cheng, C. Fogarty, and C. Morehen

In Canada, the national 2022 average temperatures for summer and autumn ranked among the six warmest such periods in the nation's 75-year record (1948–2022). The national winter and spring temperatures were below the 1991–2020 average and ranked seasonally as the 27th lowest and 30th highest, respectively. Overall, Canada had its 16th-warmest year on record. The temperature records presented in this section are based on adjusted and homogenized Canadian climate data.

(i) Temperature

The annual 2022 average temperature for Canada was 0.1°C above the 1991–2020 average and ranked as the 16th-warmest year on record (Fig. 7.1). Over the past 75 years (1948–2022), the national annual average temperature exhibited a warming of 1.9°C and 3 of the 10 warmest years have occurred since 2012. Spatially, annual anomalies of more than +1.0°C were recorded in easternmost Canada, and anomalies of more than +0.5°C were recorded mainly in northeastern and small regions of western Canada. In 2022, 4 of the 13 provinces and territories (Nova Scotia, Prince Edward Island, New Brunswick, and Newfoundland and Labrador) experienced annual average temperatures that were among their 10 highest in the 75-year record. Annual anomalies of more than −0.5°C were observed in areas from central Saskatchewan to northern Ontario, along with small areas in southern British Columbia. Temperatures of more than 1.5°C below average were recorded in the regions between the provincial border of southern Manitoba and northern Ontario (Fig. 7.2).

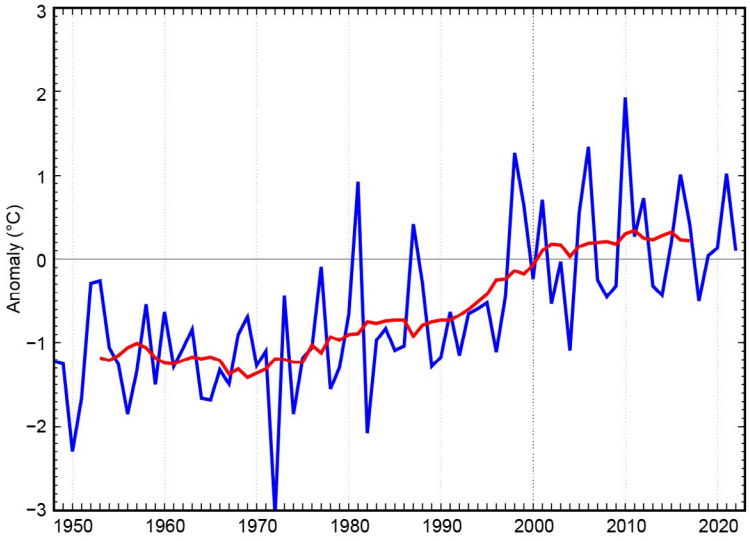

Fig. 7.1. Annual average temperature anomalies (°C; 1991–2020 base period) in Canada for the period 1948–2022. Red line is the 11-year running mean. (Source: Environment and Climate Change Canada.)

Seasonally, the national average temperature for winter (December 2021–February 2022) was 1.6°C below average, making it the 27th-coolest winter on record. Winter anomalies of −4.5°C were recorded over the southeastern portion of Northwest Territories as well as northern Saskatchewan. Most of Canada experienced winter temperatures at least 0.5°C below average. However, above-average temperatures were recorded in most of Labrador, Prince Edward Island, Nova Scotia, and northeastern Nunavut. The national average temperature for winter has increased by 3.4°C over the past 75 years.

During spring (March–May), temperature departures of at least −0.5°C were observed mainly in British Columbia and from central Yukon southeastward to northern Ontario. Above-average temperatures were recorded in northern Nunavut, northern and southern Quebec, southern Ontario, and most of the Atlantic provinces. The rest of the country experienced near-average temperatures. Although the national average temperature for spring 2022 was 0.2°C below the 1991–2020 average, it was still the 30th-warmest spring on record. The most anomalously warm spring was observed in the northernmost region of Nunavut, with temperature departures of more than +2.0°C. The national average spring temperature has increased by 1.6°C over the past 75 years.

The national average temperature for summer (June–August) was 0.8°C above average—the third-warmest summer on record. Most of the Atlantic Provinces, northern Quebec, and the rest of northern, western, and central Canada experienced summer temperatures that were 0.5°C above average or greater. Summer anomalies of more than +1.5°C were recorded in the central region of Nunavut, eastern British Columbia, western Alberta, and

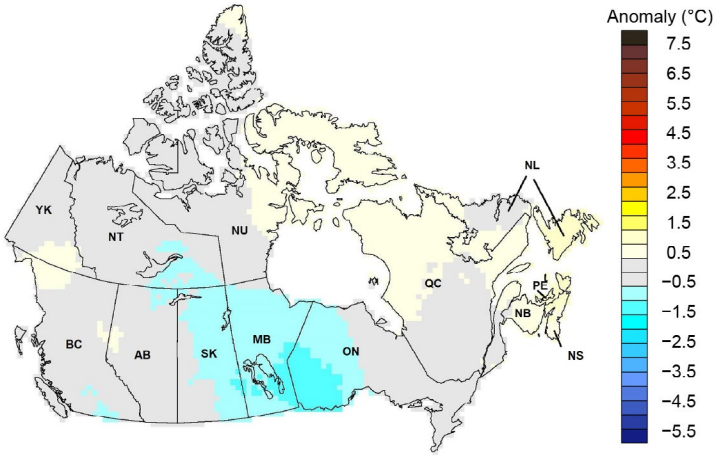

Fig. 7.2. Annual average temperature anomalies (°C; 1991–2020 base period) in Canada for 2022. (Source: Environment and Climate Change Canada.)

Labrador. Nine of the 13 provinces and territories had temperatures among their 10 highest on record for summer. The national average summer temperature has increased by 1.6°C over the past 75 years.

The national average temperature for autumn (September–November) was 1.0°C above average and the sixth highest on record. Most of Canada experienced temperatures at least 0.5°C above average, with the Northwest Territories, New Brunswick and some areas in Yukon, northern British Columbia, Alberta, Saskatchewan, Manitoba, Ontario, Quebec, and Nova Scotia experiencing temperatures 1.5°C to 3.0°C above average. Only a small region in northern and eastern Nunavut experienced below-average temperatures. Prince Edward Island had its highest autumn temperature on record, Nova Scotia had its second highest, and New Brunswick and Northwest Territories had their third highest. The national average autumn temperature has increased by 1.8°C over the past 75 years.

(ii) Precipitation

Over the past decade, precipitation monitoring technology has evolved and Environment and Climate Change Canada (ECCC) and its partners have implemented a transition from manual observations to the use of automatic precipitation gauges. Extensive data integration is required to link the current precipitation observations to the long-term historical manual observations. The updating and reporting of historical adjusted precipitation trends and variations will be on temporary hiatus pending an extensive data reconciliation, and will be resumed thereafter. ECCC remains committed to providing credible climate data to inform adaptation decision-making while also ensuring that necessary data reconciliation occurs as monitoring technology evolves.

(iii) Notable events and impacts

On 21 May, a line of widespread and fast-moving thunderstorms traversed 1000 km from southwestern Ontario to Quebec City. These storms featured torrential rains, hail, and a cluster of straight-line downburst winds (i.e., a derecho). Four tornadoes were also associated with this event, with two Enhanced Fujita (EF)-1s occurring in the London area (with maximum winds between 160 km h^{-1} and 175 km h^{-1}) along with two EF-2s near Toronto and Oshawa (with maximum winds between 180 km h^{-1} and 195 km h^{-1}). Most of the weather stations along the derecho's path recorded wind gusts near or above 100 km h^{-1}. The derecho lasted approximately 11 hours and caused 11 fatalities and widespread damage in a swath over 100 km wide. Winds devastated farm properties in rural areas, while more than a million customers across Ontario and Quebec were left without power. The event caused more than $1 billion Canadian dollars ($750 million U.S. dollars) in damage—the sixth-costliest natural disaster in Canadian history in terms of insured losses. The last time Canada experienced a derecho of this ferocity was in July 1999, when a long line of storms swept into Ontario from Minnesota.

Hurricane Fiona, another devastating storm, made landfall in eastern Nova Scotia on 24 September as a Category 2-strength post-tropical cyclone with a minimum extrapolated sea-level pressure of 931 hPa. Fiona was the most intense and destructive tropical or post-tropical cyclone ever recorded for Canada's Atlantic coast. Fiona's maximum sustained winds at the time of landfall in Nova Scotia were around 165 km h^{-1}. It was the strongest storm in Canadian history (as gauged by barometric pressure), with a pressure of 932.7 hPa measured on Hart Island, Nova Scotia, which was used to determine the extrapolated central pressure of 931 hPa at the moment of landfall. A record-high water height (before waves) of 2.73 meters was also recorded in Channel-Port aux Basques, Newfoundland. Numerous homes were damaged or destroyed in Newfoundland, with almost 200 people displaced and more than 500,000 left without power. Fiona became the costliest weather event in Atlantic Canada's history with insured losses estimated to be at least $800 million Canadian dollars ($600 million U.S. dollars). Please refer to section 4g2 and Sidebar 4.1 for more information about Hurricane Fiona.

2. UNITED STATES

—K. Gleason, C. Fenimore, R. R. Heim Jr., and A. Smith

The annual average temperature for the contiguous United States (CONUS) in 2022 was 11.9°C, which was 0.1°C above the 1991–2020 average and equal with 1953 as the 18th-warmest year in the 128-year record (Fig. 7.3a). Below-average temperatures were concentrated across the Upper Midwest while above-average temperatures were scattered across parts of California, Texas, Florida, and New England (Fig. 7.4a). Based on a linear regression of data from 1895 to 2022, the annual CONUS temperature is increasing at an average rate of 0.09°C decade^{-1} (0.27°C decade $^{-1}$ since 1970). Average precipitation for the nation totaled 722 mm, which is 91% of the 1991–2020 average (Fig. 7.3). However, the annual precipitation total has been increasing at an average rate of 5 mm decade^{-1} since 1895 (2 mm decade^{-1} since 1970). The average annual temperature across Alaska in 2022 was 0.4°C above average and was 16th highest on record. The annual temperature for Alaska over its 98-year record is increasing at an average rate of 0.17°C decade^{-1} since 1925 (0.44°C decade^{-1} since 1970).

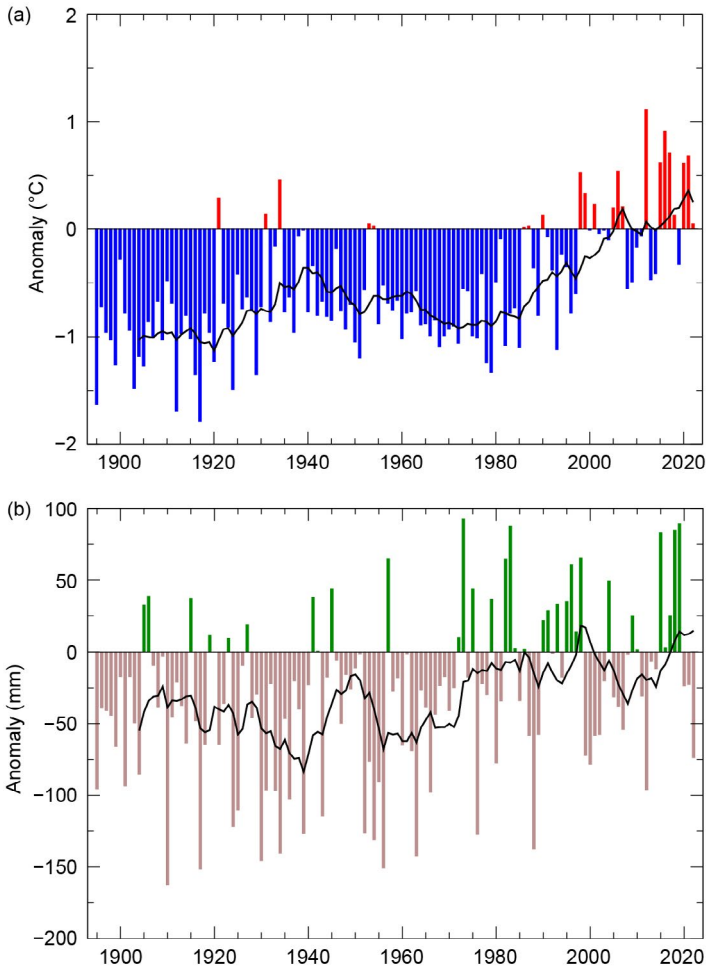

Fig. 7.3. Annual (a) mean temperature anomalies (°C) and (b) precipitation anomalies (mm; 1991–2020 base period) for the contiguous United States during 1895–2022. The black line is the lagged 10-year running mean. (Source: NOAA/NCEI.)

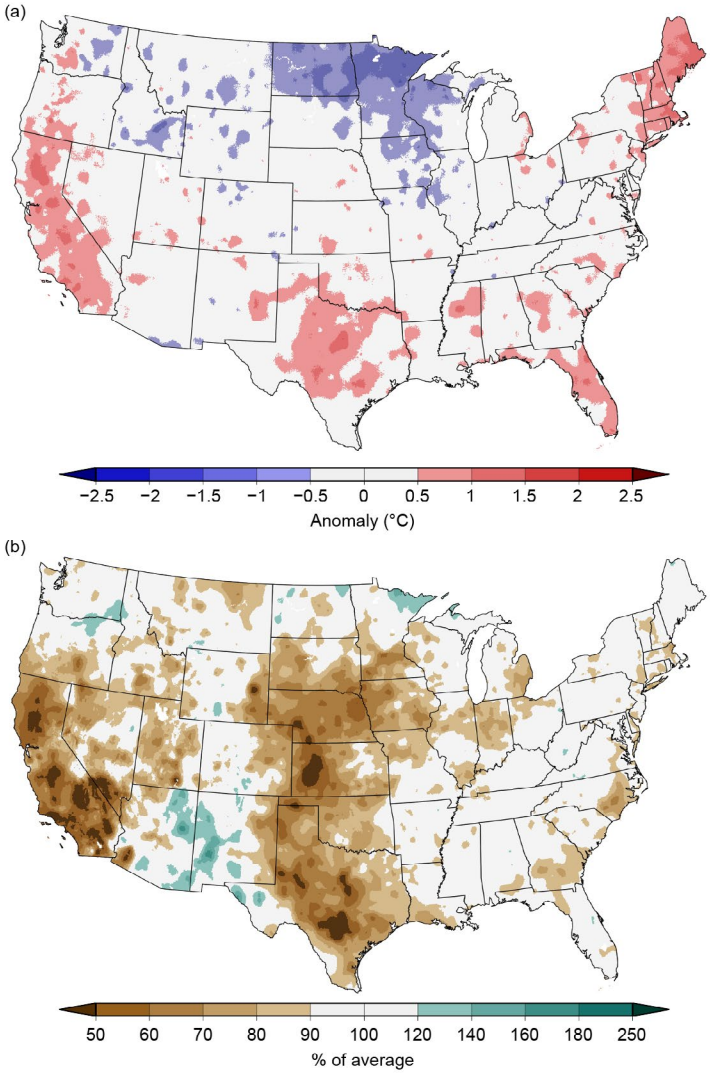

Fig. 7.4. Annual (a) average temperature anomalies (°C) and (b) total precipitation (% of average) in the contiguous United States for 2022 (1991–2020 base period). (Source: NOAA/NCEI.)

(i) Temperature

The winter (December–February) 2021/22 CONUS temperature was 0.4°C above average, with most of the anomalous warmth in the Southeast. The CONUS spring (March–May) temperature was near average, with above-average temperatures spanning from California to the Mississippi River and from the Gulf Coast to New England and below-average temperatures extending from Washington State to the Great Lakes. The summer (June–August) CONUS temperature was 0.9°C above average, the third highest on record. Above-average temperatures dominated the western half of the CONUS as well as the southern Plains and parts of the Northeast. Massachusetts, Rhode Island, and Texas each had their second-warmest summer while California observed its third warmest. The autumn (September–November) CONUS temperature was 0.1°C above average, with the highest anomalies occurring across portions of the West, Great Lakes, and Northeast. Maine had its fifth-warmest autumn on record.

(ii) Precipitation

The climate of the CONUS in 2022 was driven by ridges of high pressure along both the East and West coasts, which exacerbated the multi-year drought by suppressing precipitation across much of the West. Nebraska had its fourth-driest year on record while California ranked ninth driest (Fig. 7.4b).

Winter precipitation across the CONUS was 83% of average and ranked in the driest third of the historical record. Precipitation was above average across portions of the Upper Midwest and from the middle of the Mississippi River Valley to the eastern Great Lakes. Dry conditions prevailed across much of the Plains and Gulf Coast as well as parts of the West and East coasts. Precipitation totals for Louisiana, Nebraska, and Kansas were third, fourth, and fifth lowest on record, respectively. Spring precipitation was 97% of average, but was above average from the Northwest to the Great Lakes as well as in portions of the central Plains, Southeast, and the Northeast. North Dakota had its third-wettest spring on record. Below-average precipitation occurred from California to the western Plains and Texas. Summer precipitation was 95% of average, with above-average wetness occurring across parts of the Northwest, Southwest, Gulf Coast, and Ohio Valley. West Virginia experienced its seventh-wettest summer on record while monsoon rains across Arizona and New Mexico resulted in a ranking of eighth wettest for each state. It was drier than average across much of the Plains and in parts of the Northeast where Nebraska and New Jersey each had their fourth-driest summer on record. The autumn CONUS precipitation total was 81% of average, ranking in the driest third of the record. Precipitation was above average across portions of the Northeast and Florida while drier-than-average conditions were present across parts of the Northwest and from the Plains to the Ohio Valley. Nebraska had its seventh-driest autumn on record.

Drought coverage across the CONUS remained significant for the third consecutive year, with a minimum spatial extent of 44% occurring on 6 September and a maximum coverage of 63% on 25 October—the largest CONUS footprint since the drought of 2012. The rapid intensification and expansion of drought at times during 2022 resulted from the low precipitation occurring with record and near-record high temperatures that, in combination with sunny skies, low humidity, and windy conditions, led to a "flash drought" which rapidly reduced soil moisture, especially in parts of the Plains to the lower and middle parts of the Mississippi Valley during the summer and early autumn. Drought impacted much of the western half of the United States for a majority of the year with some improvement resulting from the summer monsoon across the Southwest. Nonetheless, the multi-year western U.S. drought resulted in water stress/shortages across many locations as some major reservoirs dropped to their lowest levels on record.

(iii) Notable events and impacts

There were 18 weather and climate events across the United States during 2022 with losses each exceeding $1 billion (U.S. dollars): six severe storms, three tropical cyclones, three hail events, two tornado events and one each for drought, flood, winter storm, and wildfire events (Fig. 7.5). Total disaster costs for these events in 2022 exceeded $175 billion (U.S. dollars; adjusted to the Consumer Price Index)—the third-highest cost on record. The costliest event of the year was Hurricane Ian ($114 billion U.S. dollars) which ranks as the third-costliest hurricane on record (1980–2022; see section 4g2 and Sidebar 4.1 for more details about Hurricane Ian). Over the last seven years (2016–2022), 122 separate billion-dollar disasters have killed at least 5000 people and incurred costs greater than $1 trillion (U.S. dollars) in damage.

The tornado count for 2022 was slightly below average with 1143 tornadoes reported across the CONUS. March had triple its average number of verified tornadoes (234) and the most tornadoes for any March in the 1950–2022 record. One of the most significant severe weather days occurred on 5 April when approximately 68 tornadoes were reported from Mississippi to South Carolina, including an EF-4 tornado that struck the town of Pembroke, Georgia, causing damage, injuries, and one fatality.

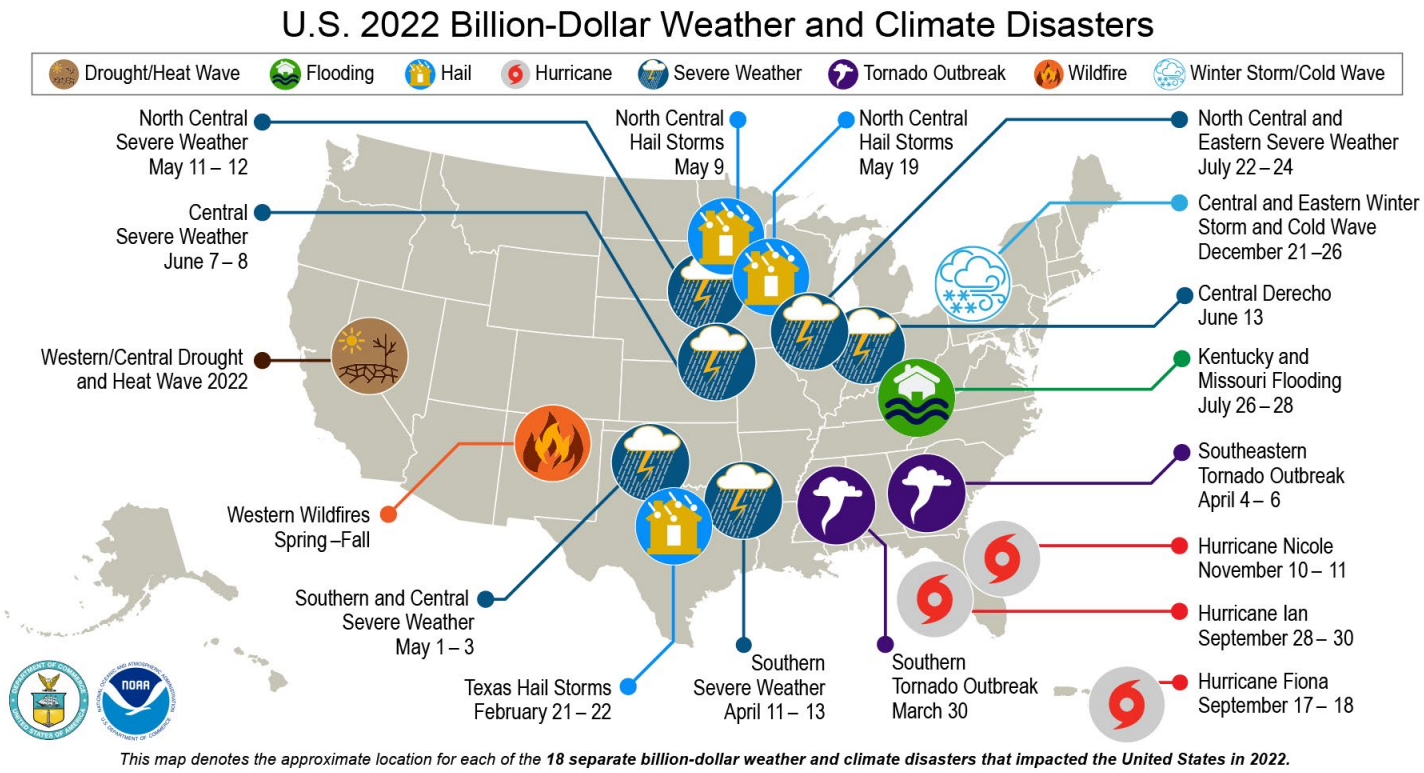

Fig. 7.5. Map depicting date, approximate location, and type of the 18 weather and climate disasters in the United States in 2022 whose losses each exceeded $1 billion (U.S. dollars). (Source: NOAA/NCEI.)

3. MEXICO

—R. Pascual Ramírez and A. E. Martínez

Mexico's mean annual temperature for 2022 was the eighth highest since national records began in 1950 (Fig. 7.6a). The national precipitation total for 2022 was 743.6 mm, which is slightly below the 1991–2020 average and ranked in the middle of the 73-year record (Fig. 7.6b). Precipitation was below average across the northeast, central region, and the northern coast of the Gulf of Mexico. Conversely, the northwest, southern Baja California Peninsula, and the Yucatan Peninsula had above-average annual rainfall through the year (Fig. 7.7b).

(i) Temperature

The 2022 national average annual temperature was 22.0°C, which was 0.6°C above the 1991–2020 average (Fig 7.6a), marking the eighth-warmest year in the 73-year record. Although 2022 did not rank among Mexico's five warmest years, the nation continued its warming trend, and 2022 marked the 13th consecutive year with an above-average national temperature. The year was characterized by above-average temperatures across much of the nation, although parts of the northwest and areas along the Gulf of Mexico coast experienced near- to below-average annual temperatures (Fig. 7.7a). February, March, October, and November each had monthly temperatures slightly below average, while the remaining months had above-average temperatures, with the month of May setting a record high.

During January–March, below-average temperatures were observed in the northwest and along the states in the Gulf of Mexico. The rest of the country had slightly above-average temperatures. From April through June, temperatures were near average from the central to southern regions of the country as the rainy season began;

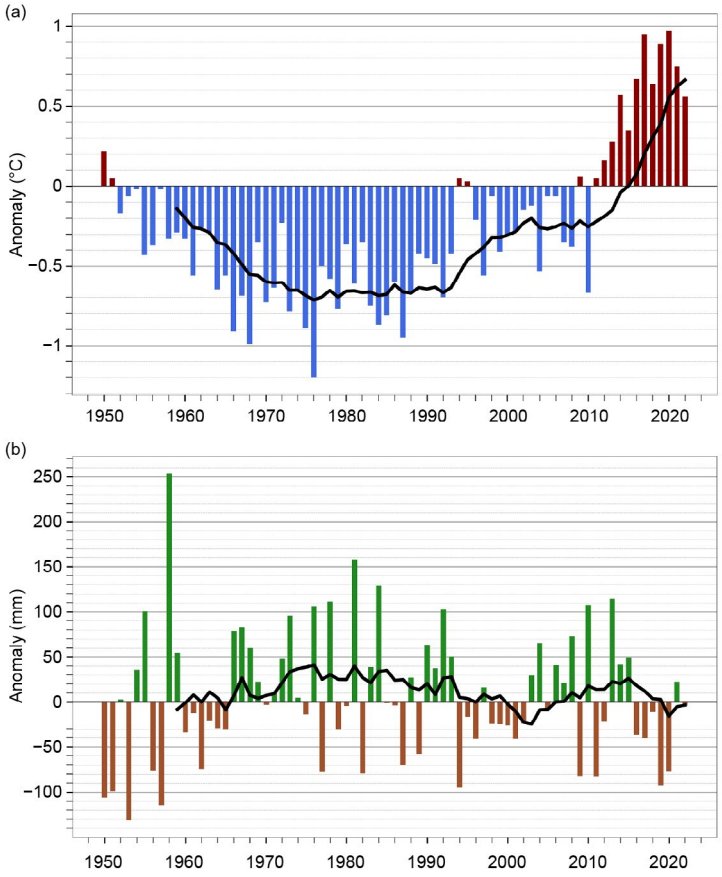

Fig. 7.6. Annual anomalies of (a) temperature (°C) and (b) precipitation (mm) for Mexico for the period 1950–2022 (1991–2020 base period). Black solid lines represent a 10-year running mean. (Source: National Meteorological Service of Mexico.)

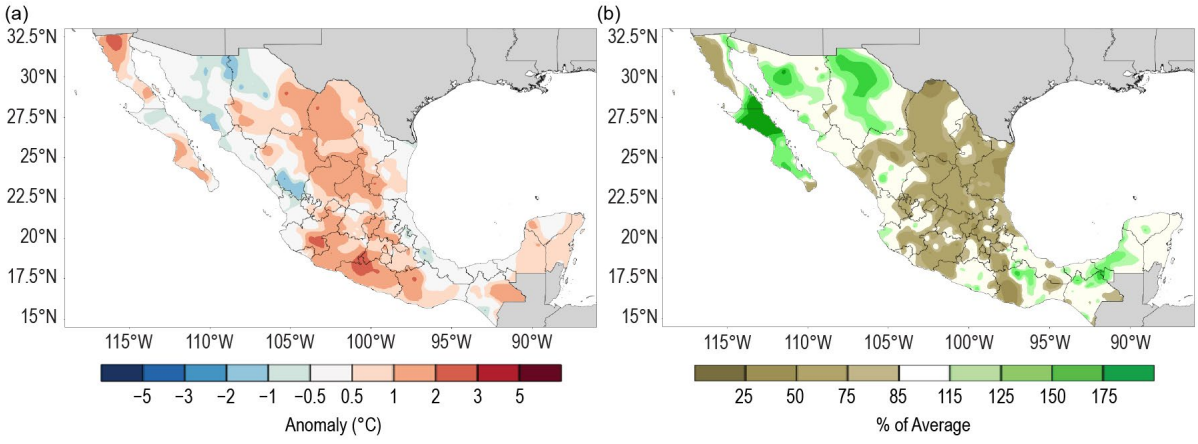

Fig 7.7. Annual anomalies of (a) mean temperature (°C) and (b) precipitation (% of average) over Mexico in 2022 (1991–2020 base period). (Source: National Meteorological Service of Mexico.)

above-average temperatures were present across northern Mexico. When the rains reached the northwest region and the Sierra Madre Occidental, temperatures in the region dropped to below average between July and September. During October–December, above-average temperatures were present across central and southern Mexico, while slightly below- to near-normal temperatures prevailed in the northwest and along the states of the Gulf of Mexico.

(ii) Precipitation

The national precipitation total for 2022 was 743.4 mm (99.4% of average). Climatologically, September tends to be the nation's rainiest month. However, similar to 2021, August 2022 contributed more than any other month to the annual precipitation total. Meanwhile, March was the driest month for the year and contributed the least to the annual total among all months, coinciding with the driest month climatologically.

During January–March, below-average rainfall was observed across most of the country, especially along the Sierra Madre Occidental and in Baja California, exacerbating drought conditions in the region. The Yucatan Peninsula and the Isthmus of Tehuantepec in southern Mexico received above-average rainfall in January.

The onset of the rainy season from central to southern Mexico occurred in late May and early June. Tropical Storm Alex in the Gulf of Mexico and Hurricane Agatha in the Pacific were the main precursors of rainfall in early June. Monsoon rain began in the northwest at the end of June and continued through September. During the summer (June–August), rains associated with tropical cyclones were less than typical in the foothills of the Gulf of Mexico and the northeast. On the Pacific side, Hurricane Kay and Tropical Storm Lester brought considerable amounts of precipitation on the Pacific coast and in Baja California Sur. See sections 4g2 and 4g3 for more details about these hurricanes.

The last quarter of the year marks the transition between the end of the rainy season and the beginning of the dry season in Mexico. During this transition period, it is common to see a combination of tropical and winter systems. From September through December, three tropical cyclones (Orlene and Roslyn from the Pacific and Lisa from the Gulf of Mexico) and several cold fronts were the main sources of rainfall in Mexico. Mexico's drought footprint was at its lowest for the year (7.48%) by 31 October, according to the North American Drought Monitor. The dry season began in late November, and the dry conditions led to an increase in drought, with close to 19% of the nation experiencing moderate to exceptional drought by the end of the year.

(iii) Notable events and impacts

Northeastern Mexico was severely affected by the lack of precipitation during most of the year. Rainfall deficits combined with high temperatures during March and April resulted in a wildfire in the state of Nuevo León that lasted more than 20 days. The fire spread rapidly due to strong winds, burning at least 5000 hectares. According to Mexico's Drought Monitor, during the first half of the year, severe to exceptional drought prevailed in most of the northern portion of the country. During this time, there were 6305 forest fires and over 400,000 hectares burned. At the end of the year, a total of 6755 forest fires were recorded that burned 739,626 hectares (National Forestry Commission), the second-largest area burned by fires, behind only 2011 (956,404 hectares), according to fire data that began in 1998.

Only three tropical cyclones (Tropical Storms Alex and Karl and Hurricane Lisa) from the Atlantic basin (see section 4g2 for details) affected Mexico's eastern coast during 2022. On the Pacific side, Hurricanes Agatha, Blas, Kay, Orlene, and Roslyn, as well as Tropical Storm Lester, made landfall or tracked near the country and brought significant rainfall to the western region (see section 4g3 for details). Precipitation from these Pacific systems caused floods and landslides, mainly around the Isthmus of Tehuantepec in the Pacific coast, as well as the Baja California Peninsula.

c. Central America and the Caribbean

—A. Sánchez-Lugo, Ed.

1. CENTRAL AMERICA

—H. G. Hidalgo, J. A. Amador, E. J. Alfaro, B. Calderón, and N. Mora

For this region, nine stations from five countries were analyzed (see Fig. 7.8 for data and station list). The station distribution is representative of the relevant seasonal and intraseasonal regimes of precipitation (Amador 1998; Magaña et al. 1999; Amador et al. 2016a,b), wind (Amador 2008), and temperature (Hidalgo et al. 2019) on the Caribbean and Pacific slopes of Central America (CA). Precipitation and temperature records for the stations analyzed and regional winds were provided either by CA National Weather Services (CA-NWS), NOAA, or the University of Costa Rica. Anomalies are reported using a 1991–2020 base period and were calculated from CA-NWS data. The methodologies used for all variables can be found in Amador et al. (2011).

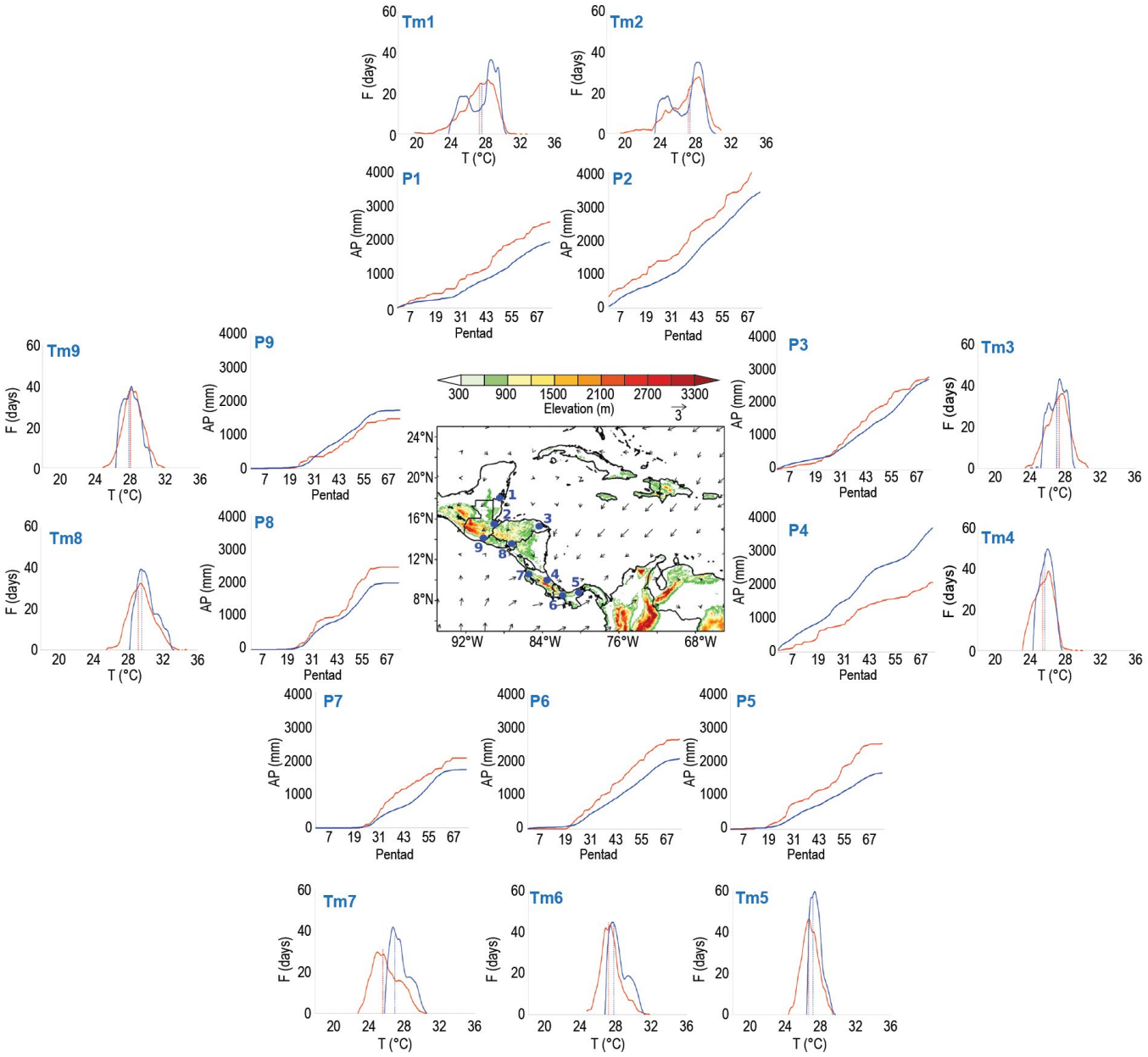

Fig. 7.8. Mean surface temperature (Tm; °C) frequency (F; days) and accumulated pentad precipitation (P; mm) time series are presented for nine stations (blue dots) in Central America: (1) Philip Goldson International Airport, Belize; (2) Puerto Barrios, Guatemala; (3) Puerto Lempira, Honduras; (4) Puerto Limón, Costa Rica; (5) Tocumen International Airport, Panamá; (6) David, Panamá; (7) Liberia, Costa Rica; (8) Choluteca, Honduras; (9) Puerto San José, Guatemala. The blue solid line represents the 1991–2020 average values and the red solid line shows 2022 values. Vertical dashed lines show the mean temperature for 2022 (red) and the 1991–2020 period (blue). Vectors indicate July wind anomalies at 925 hPa (1991–2020 base period). Shading depicts regional elevation (m). (Sources: NOAA/NCEI and CA-NWS.)

(i) Temperature

The mean temperature (Tm, °C) pentad frequency distributions in 2022 as well as the climatology for all stations analyzed are shown in Fig. 7.8. Most stations across Central America had near-average annual temperatures. Only the stations of David, Panamá (Tm6), and Liberia, Costa Rica (Tm7) had significant (in the tails of the 95% confidence distributions using a t-test) below-average annual temperature anomalies of –0.8°C and –1.3°C, respectively. The two northernmost stations in the Caribbean coast, Philip Goldson International Airport, Belize (Tm1), and Puerto Barrios, Guatemala (Tm2), had a bimodal temperature distribution over the course of the seasonal cycle during 1991–2020. This was also reported in the last two yearly climate reports. However, contrary to what was found for the 2021 data, the two-peak distribution in mean temperature is not clearly visible in both stations in 2022, a feature observed in the temperature records of this location in the period 2017–21 (Amador et al. 2018). In terms of seasonal changes, only Liberia, Costa Rica (Tm7) had significant (in the tails of the 95% confidence distributions) below-average temperatures in all seasons.

(ii) Precipitation

The accumulated pentad precipitation (P, mm) time series for the nine stations in Central America is presented in Fig. 7.8. Most stations had near-average annual rainfall totals, with the exceptions of Puerto Barrios, Guatemala (P2), which had an above-average total accumulation of 751 mm (119% of normal) and Puerto Limon, Costa Rica (P4), which had an exceptionally dry year with a deficit of 1618 mm (56% of normal). Most of the stations in the Pacific coast had above-average annual accumulations, consistent with the cold phase of the El Niño–Southern Oscillation (La Niña) teleconnection response in the area. The prevailing wind patterns (Fig. 7.8) increased flow from the Pacific Ocean to the coast in the southernmost regions and resulted in larger accumulations in those stations (David, Panamá [P6]; Liberia, Costa Rica [P7]; and Choluteca, Honduras [P8]). However, farther north near the El Salvador and Guatemala border, the anomalies were much weaker, and the annual precipitation totals were below average (San Jose, Guatemala [P9]). Another contributor to the anomalously wet Pacific coast in the southern countries is that 2022 was the third consecutive year with an anomalously active hurricane season in both basins. At seasonal scales, extreme precipitation (in the tail of the distribution of the annual values from 1991 to 2020) occurred during winter in Puerto Barrios, Guatemala (P2), and in spring and autumn in Tocumen, Panamá (P5).

(iii) Notable events and impacts

Tropical cyclone activity in the Caribbean in 2022 consisted of five named storms in the basin: Tropical Storm Bonnie (1–2 July) and Hurricanes Fiona (17–19 September), Ian (23–27 September), Julia (7–9 October), and Lisa (31 October–3 November). Three of the five storms affected the Central American isthmus. Bonnie made landfall and crossed Central America near the Costa Rican-Nicaraguan border. Strong winds and heavy rains from Bonnie affected the region, and two fatalities in El Salvador were associated with the storm. Bonnie exited into the eastern Pacific basin, moving westward, away from the Central American coast by 4 July.

Julia was a Category 1 hurricane that made landfall on the Caribbean coast of Nicaragua on 9 October. Direct and indirect effects were observed across Central America, as Julia became the deadliest cyclone of the season with over 30 fatalities in the region. Julia also managed to survive its passage through the isthmus and continued its path into the eastern Pacific basin. The system moved to the west and then to the west-northwest, parallel to and near the coasts of Nicaragua and El Salvador. On 10 October, the center of the storm crossed the coast of El Salvador and later affected Guatemala. (see Sidebar 7.1 for additional details)

Hurricane Lisa made landfall as a Category 1 hurricane on the coast of Belize on 2 November. There were no systems from the eastern tropical Pacific that impacted Central America.

Other rain-producing systems caused landslides and flooding that killed 110 people: 2 in Panamá, 10 in Costa Rica, 7 in Nicaragua, 27 in El Salvador, 12 in Honduras, and 52 in Guatemala. Lightning strikes caused 13 fatalities in the region during the season (three in Costa Rica, three in Nicaragua, one in El Salvador, four in Honduras, and two in Guatemala).

Please refer to sections 4g2 and 4g3 for more information on these tropical cyclones.

2. CARIBBEAN

—T. S. Stephenson, M. A. Taylor, A. Trotman, C. J. Van Meerbeeck, J. Spence-Hemmings, L. Clarke, J. Campbell, and K. Kerr

(i) Temperature

The Caribbean had relatively small positive temperature anomalies in 2022 compared to the previous four years (2018–21, as analyzed from European Centre for Medium-Range Weather Forecasts Reanalysis version 5 [ERA5] reanalysis data). The annual temperature anomaly for the region was 0.42°C above average, marking the eighth-warmest year since records began in 1950 (Fig 7.9a). Annual temperatures have increased at a rate of 0.11°C decade^{-1} since 1950 (0.17°C decade^{-1} since 1970). Much of the region had above-average annual temperatures for 2022 (Fig. 7.10a). Freeport, Bahamas, had its warmest year on record since 1973, with an annual average maximum temperature of 29.7°C (1.0°C above average) and Canefield, Dominica, equaled its highest annual average maximum temperature at 31.8°C (0.7°C above average) since 1985. The Sancti Spiritus Airport and the National Airport at Camagüey in Cuba each recorded their third-warmest year in the 52-year record with annual average maximum temperatures of 31.5°C (0.9°C above average) and 31.3°C (0.7°C above average), respectively. Conversely, Grantley Adams, Barbados, had its ninth-lowest annual average maximum temperature since 1979 at 29.7°C, which was 0.5°C below average.

Seasonally, December–February and March–May temperatures were above average for most of the region. The temperature anomaly averaged regionally for March–May was +0.46°C and the eighth-warmest such period on record. June–August temperatures were near average across much of the Caribbean, but parts of Barbados, northern Belize, Curaçao, Jamaica, and Trinidad had below-average temperatures. There were fewer heatwaves (defined by the Caribbean Climate Outlook Forum as periods of at least two consecutive days with daily maximum temperatures exceeding the 90th percentile) in 2022 than in recent years (May–October). St. Kitts recorded its highest daytime maximum temperature of 33°C on 5 July and again on 8 July. The September–November temperature anomaly for the region was 0.50°C above the 1991–2020 average and the seventh warmest on record since 1950.

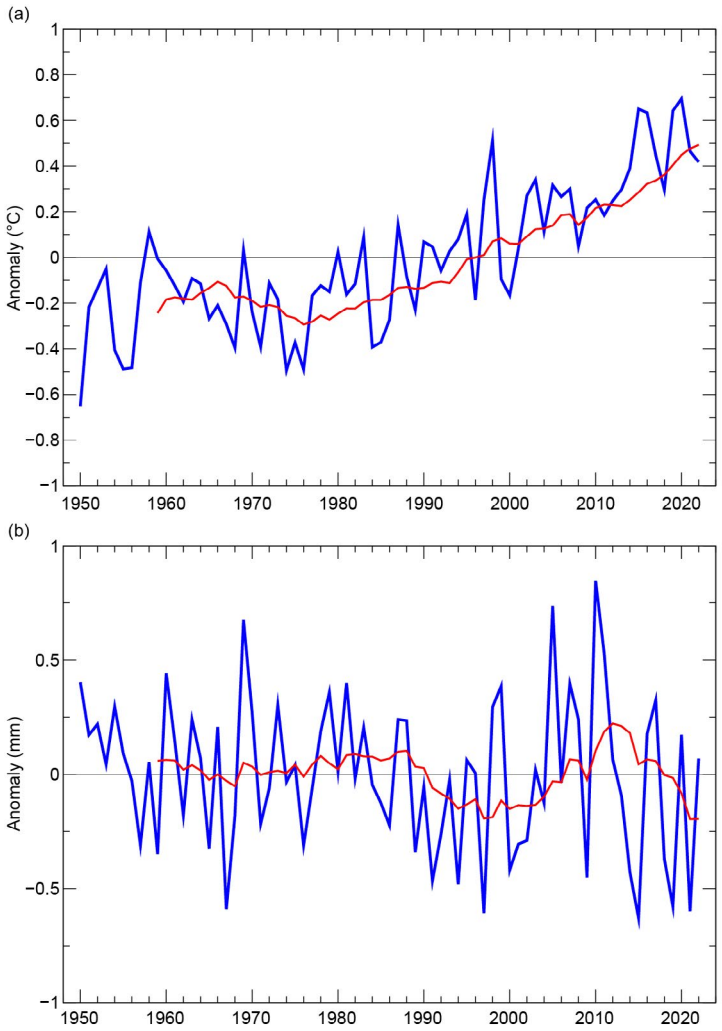

Fig. 7.9. Annual average (a) 2-m temperature anomalies (°C) and (b) rainfall anomalies (mm day^{-1}) for the Caribbean (9°N–27°N, 58°W–90°W) for 1950–2022 relative to the 1991–2020 average. The red line is the 10-yr running mean. (Sources: ERA5 from the KNMI Climate Explorer.)

(ii) Precipitation

Most of the Caribbean islands had near-average rainfall during 2022 (Fig. 10b). The average rainfall anomaly for the region was −0.22 mm day^{-1} (Fig 7.9b). Moderately-to-exceptionally wet conditions were observed across the northern Bahamas (in the far north Caribbean) and Trinidad (eastern Caribbean). Three locations in Trinidad reported their highest rainfall totals: Caroni (3422.9 mm, 158% of average; since 1985), Hillsborough (3264.9 mm, 147% of average; since 1971), and Hollis (4281.5 mm, 144% of average; since 1971). Two other locations in Trinidad had their second-highest amounts since 1971: Navet (3141.9 mm, 143% of average) and Piarco (2378.9 mm, 132% of average). Rancho Coloso, Aguada, Puerto Rico, had its second-highest annual rainfall total (2403.1 mm, 132% of average) since 1971. It was also dry in places. With records dating from 1979, E.T. Joshua, St. Vincent, recorded its lowest annual rainfall total (1511.1 mm, 70% of average). Since 1971, El Valle, Hato Mayor, Dominican Republic, experienced its second-driest year (717.9 mm, 50% of average), Rivière, Martinique, had its fourth-driest year (1797.6 mm,70% of average), and La Trinité, Martinique, recorded its fifth-driest year (1522.3 mm, 72% of average).

December–February was characterized by a lingering seasonal dryness throughout most of the eastern Caribbean, with many islands experiencing moderate-to-severely dry conditions. During spring (March–May), the region transitioned to near- to above-average rainfall, with the exception of the Cayman Islands and the Leeward Islands where below-average conditions prevailed. Summer (June–August) rainfall anomalies were mixed over the region with most islands recording above-average precipitation, consistent with the ongoing La Niña event in the eastern tropical Pacific Ocean. The La Niña signature continued into September–November, with Cuba and southwest Haiti receiving below-average rainfall while other locations (generally in the south and east) had above-average precipitation.

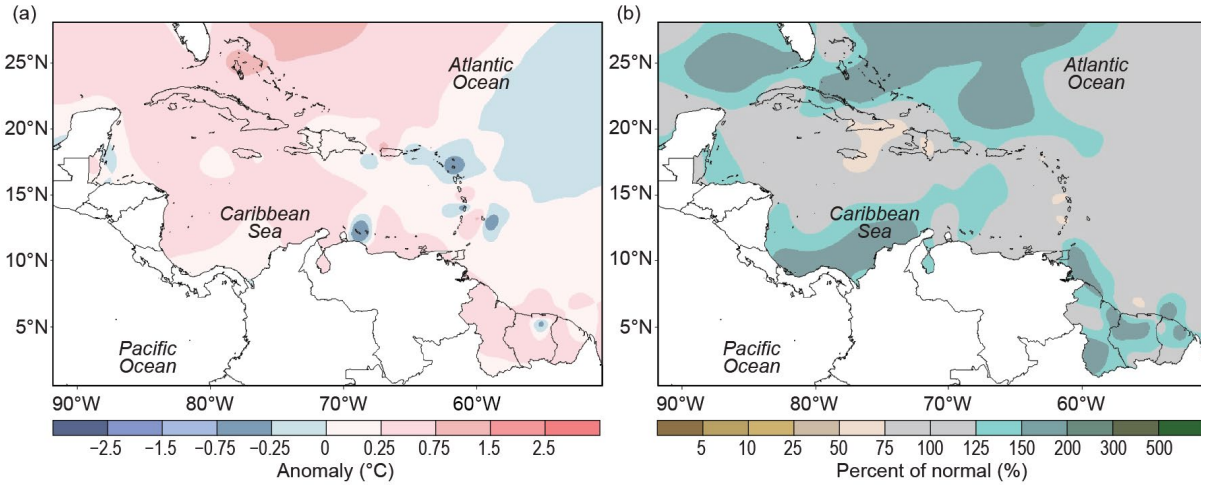

Fig. 7.10. Annual (a) mean temperature anomalies (°C) and (b) total precipitation anomalies (% of normal) relative to 1991–2020. (Source: Caribbean Climate Outlook Forum [CariCOF] and the Caribbean Institute for Meteorology and Hydrology.)

(iii) Notable events and impacts

Hurricane Fiona crossed the eastern Caribbean as a tropical storm on 16–20 September, causing minor damage for most locations. However, Fiona left considerable damage to infrastructure in Guadeloupe and caused one fatality. Hurricane Fiona made landfall in Puerto Rico on 18 September and resulted in widespread flooding and loss of power across the entire island, impacting over one million people. The storm intensified and severely impacted the Dominican Republic on 19 September and the Turks and Caicos Islands on 20 September. Fiona was associated with two fatalities each in Puerto Rico and the Dominican Republic.

Hurricane Ian impacted Jamaica as a tropical storm on 26 September and resulted in landslides, mudslides, fallen trees, and floods, and left some communities inaccessible. Damage to the road network was estimated to be $2.3 million (U.S. dollars). Ian impacted the Cayman Islands

as a Category 1 hurricane on 26 September. Debris generated from flooding made some areas inaccessible. Hurricane Ian made direct landfall in Pinar del Rio, western Cuba, with maximum sustained winds of 185 km h^{-1}. The storm reportedly caused three deaths and, in Pinar del Rio province, damaged 63,000 homes.

Nicole made landfall on Grand Bahama Island on 9 November as a Category 1 hurricane. Coastal flooding from storm surge was reported around the Abaco Islands. Flooding in coastal areas near Nassau, New Providence, reportedly caused two road closures.

Please refer to section 4g2 for more details on these storms and to Sidebar 4.1 for more information about Hurricanes Fiona and Ian.

Sidebar 7.1: **Notable events across Central America**

—S. FUHRMAN, C. RECALDE, AND W. M. THIAW

Heavy rains plagued Central America for large portions of the year. In February, Honduras's national disaster agency Permanent Contingency Commission of Honduras (COPECO) reported high river levels, flooding, damaged houses, and infrastructure over the Atlántida, Yoro, the Bay Islands, and Cortés Departments of Honduras. Notably, the León River overflowed its banks in Atlántida department, where around 500 homes were affected and at least 300 families were evacuated.

During the end of May, dangerous rains were widespread across Guatemala where the National Coordination for Disaster Reduction agency (CONRED) reported that over 38,900 people were affected in the municipalities of Villa Nueva, Aguacatán, Nebaj, Chiquimulilla, Solola, Estanzuela, Gualán, and Zacapa.

Continued heavy rains, 150%–200% of normal September totals (Fig. SB7.1), caused deadly and destructive impacts in several countries. In El Salvador, the General Directorate of Civil Protection reported that homes were damaged and one person died after rivers overflowed in La Paz and San Salvador departments. The agency also reported five fatalities from a landslide in the La Libertad department. In Costa Rica, the National Emergency Commission (CNE) said personnel responded to floods in 191 locations. According to the Red Cross, about 80 homes were damaged and 50 people evacuated in San Jose province after the Cañas River overflowed.

Landslides and floods affected Panama during November. According to the National Civil Protection System (SINAPROC), more than 300 families in three south-central provinces were affected by flooding on 10 November. SINAPROC also reported two fatalities in a landslide in Cativá, Colón Province, on 21 November.

Conversely, two periods of insufficient rain during the first and second rainy seasons impacted Central America, which resulted in abnormal dryness and degraded vegetation health. In Guatemala and western Honduras, rainfall was less than 50% of normal during April, according to Climate Prediction Center morphing technique (CMORPH) analysis, which led to a period of abnormal dryness in May. While May rainfall improved in central Guatemala and Honduras, continued suppression (less than 50% of normal rainfall) during May and June kept abnormal dryness in place over northern Guatemala until the third week of June. A second period of insufficient rains led to a short period of abnormal dryness in northern Guatemala, eastern Honduras, and Nicaragua during the third dekad (10-day period) of September and the first dekad of October. Rainfall deficits in these regions exceeded 100 mm and September's rainfall was 25%–80% of average, according to CMORPH (Fig. SB7.1).

Two tropical cyclones made landfall in Central America during the 2022 Atlantic hurricane season: Tropical Storm

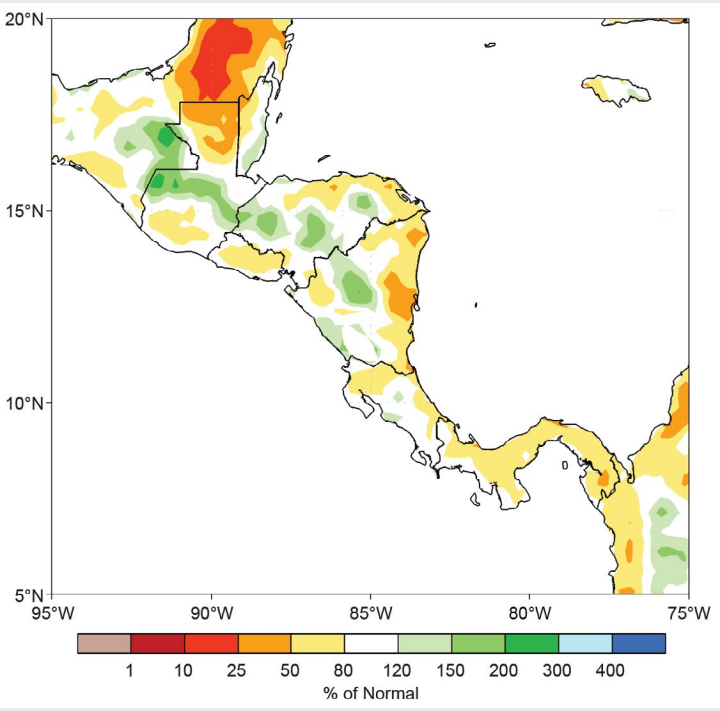

Fig. SB7.1. Satellite-estimated rainfall (% of normal) during Sep 2022. Anomalies are computed with respect to the 1998–2020 base period. (Source: NOAA Climate Prediction Center's CMORPH.)

Bonnie and Hurricane Julia (Fig. SB7.2). Tropical Storm Bonnie made landfall on 2 July near the Caribbean coast in southern Costa Rica with sustained winds of 85 km hr^{-1} and traversed southern Nicaragua, moving northwest across the country to the Pacific Ocean coast near El Salvador. In Nicaragua, heavy rains flooded 21 municipalities, resulting in four casualties, over 400 houses damaged, and more than 3000 people displaced, according to the country's National System for the Prevention, Mitigation and Attention of Disasters.

Although no deaths were reported in Costa Rica, heavy rainfall caused floods and landslides, and about 1600 people were evacuated to storm shelters; damage to highway bridges and agriculture was also reported. Heavy rain in El Salvador caused floods and damaged infrastructure, which led to three casualties and the evacuation of about 243 people to shelters, according to Civil Protection.

Julia made landfall in Nicaragua on 9 October as a Category 1 hurricane, weakening into a tropical storm before affecting several Central America countries. Hurricane Julia's impacts in Nicaragua affected approximately 7500 people, flooded 3000 houses, displaced 2000 roofs from winds, overflowed 78 rivers, and collapsed walls; however, no casualties were reported. Meanwhile, the storm's passage in Guatemala affected about 66,350 people, led to 15 casualties, and damaged roads and bridges. Impacts to El Salvador included floods, landslides, over 10 casualties, and the overflow of at least 78 rivers. Damage in Panama was less severe; there, the storm caused landslides, the collapse of some infrastructures, and the evacuation of people in the province of Chiriquí.

Forest fire activity was high in Central America, especially in Guatemala, Honduras, and Costa Rica. In Guatemala, the National Coordination for Disaster Reduction organization reported that during the fire season, there were 950 incidents, which affected 21,877 hectares, and local news reported that there were at least 10 fatalities. The report also added that much of the wildfire activity was due to human activities such as agriculture or pasture burning. Meanwhile, the Honduran Forest Conservation Institute reported more than 98,000 hectares were affected by 1202 forest fires. One of the most intense wildfire incidents occurred during March in the Biological Reserve Lomas de Barbudal in the province of Guanacaste, Costa Rica, where 1715 hectares burned, affecting diverse flora and fauna.

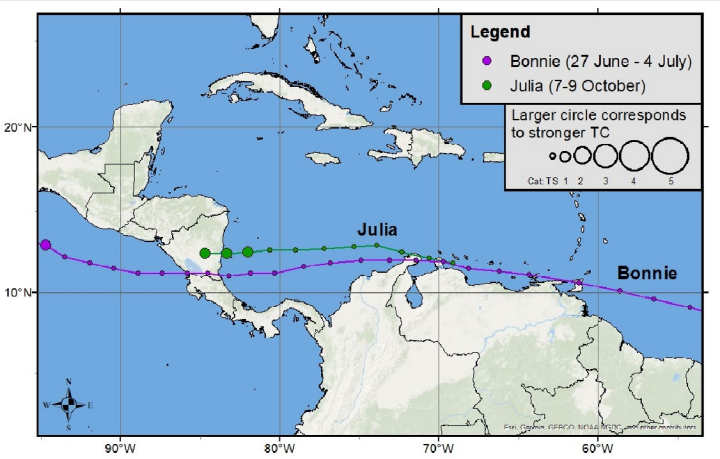

Fig. SB7.2. Plot of the tracks of the two tropical cyclones (Bonnie and Julia) that made landfall in Central America during the 2022 hurricane season. Size of the circle indicates the relative strength of the storm. (Source: National Hurricane Center best track archive.)

d. South America

—A. Sanchez-Lugo, Ed.

Much of South America had near- to above-average annual temperatures in 2022, with several locations across the north experiencing below-average annual temperatures. As a whole, South America had an annual temperature that was 0.11°C above average, tying with 2018 as the 11th highest since continental records began in 1910. Nine of South America's 10 warmest years have occurred since 2010.

Precipitation varied greatly across the continent, with much of the north and northwest receiving above-average annual rainfall, while much of the western and southern regions had below-average annual rainfall.

Anomalies in this section are all based on the 1991–2020 base period, unless otherwise noted.

1. NORTHERN SOUTH AMERICA

—J.J. Nieto, F. Costa, and J. Morán

The northern South America region includes Colombia, Ecuador, French Guiana, Guyana, Suriname, and Venezuela.

(i) Temperature

Mean annual temperature anomalies for most of the region were near to below average (Fig. 7.11). The most notable cool temperature anomaly was along the Caribbean coast of Colombia. Parts of southern Colombia, on the other hand, had near- to above-average mean annual temperatures. In northern Ecuador, temperature anomalies were between 0.5°C and 1.0°C below average.

While temperatures were near to below average for much of the region (where data were available) during March–May, June–July, and September–October, there were some locations, specifically in the southern half of Colombia, that had above-average temperatures during March–May and June–July. An analysis was not available for December–February for the region due to lack of data at the time of this writing.

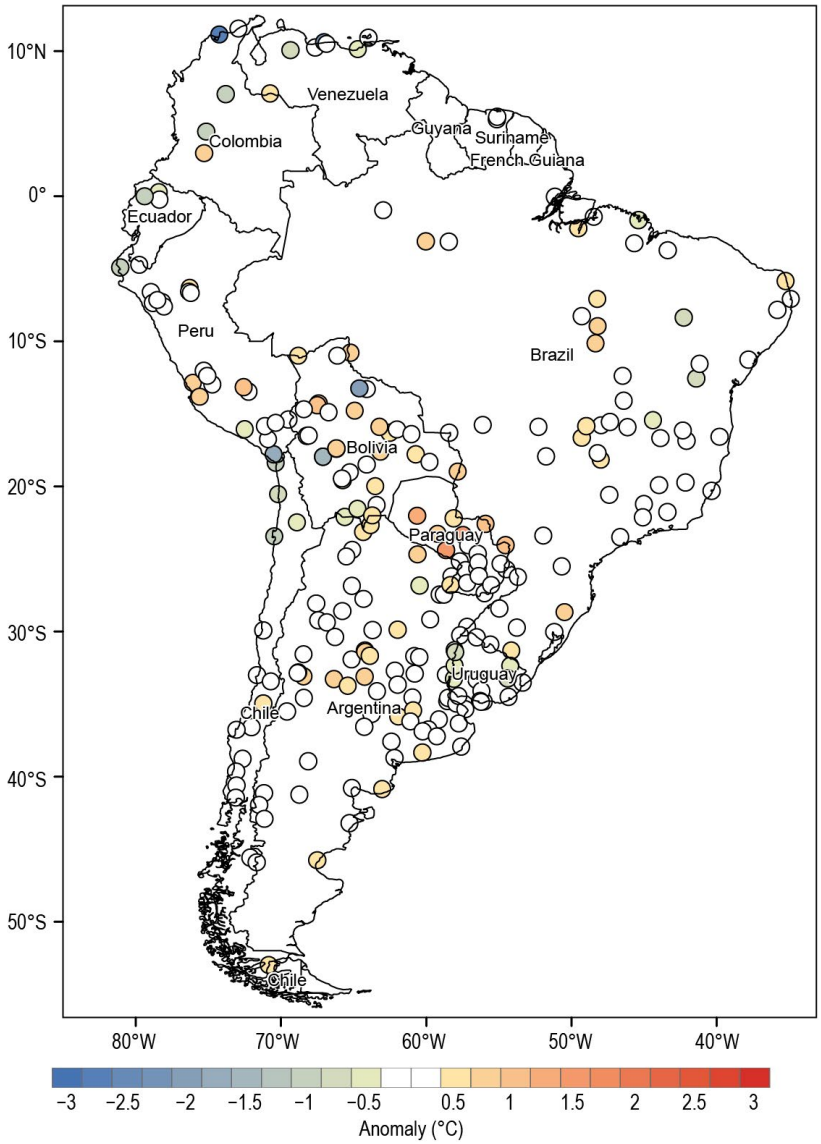

Fig. 7.11. 2022 mean annual temperature anomalies (°C; 1991–2020 base period). (Source: data from NMHSs of Argentina, Bolivia, Brazil, Chile, Colombia, Ecuador, Paraguay, Peru, Suriname, Uruguay, and Venezuela. Processed by CIIFEN.)

(ii) Precipitation

Precipitation across northern South America was generally above average during 2022 (Fig. 7.12). This could be associated with the warm sea-surface temperatures (SSTs) across the Caribbean region throughout much of the year, as well as the La Niña that was present across the central and eastern tropical Pacific Ocean during 2022.

Suriname had on average 30% above-normal precipitation for the year, with most of the rain falling during winter (December–February 2021/22) and autumn (September–November). Precipitation varied throughout the year for Venezuela. Most locations along the northern coast of Venezuela had near- to below-average precipitation during spring and summer (June–August); however, above-average conditions predominated during autumn, with some locations receiving twice their normal precipitation. The annual precipitation totals across most locations in Venezuela were near average. Much of the Caribbean and the Andean region of Colombia had above-average precipitation throughout the year, with annual totals 20%–30% above average. The highest seasonal precipitation totals fell during June–August, with some stations recording precipitation anomalies as high as +150%. In Ecuador, most locations also had near- to above-average annual precipitation, while the coastal region had anomalies close to 20% below average.

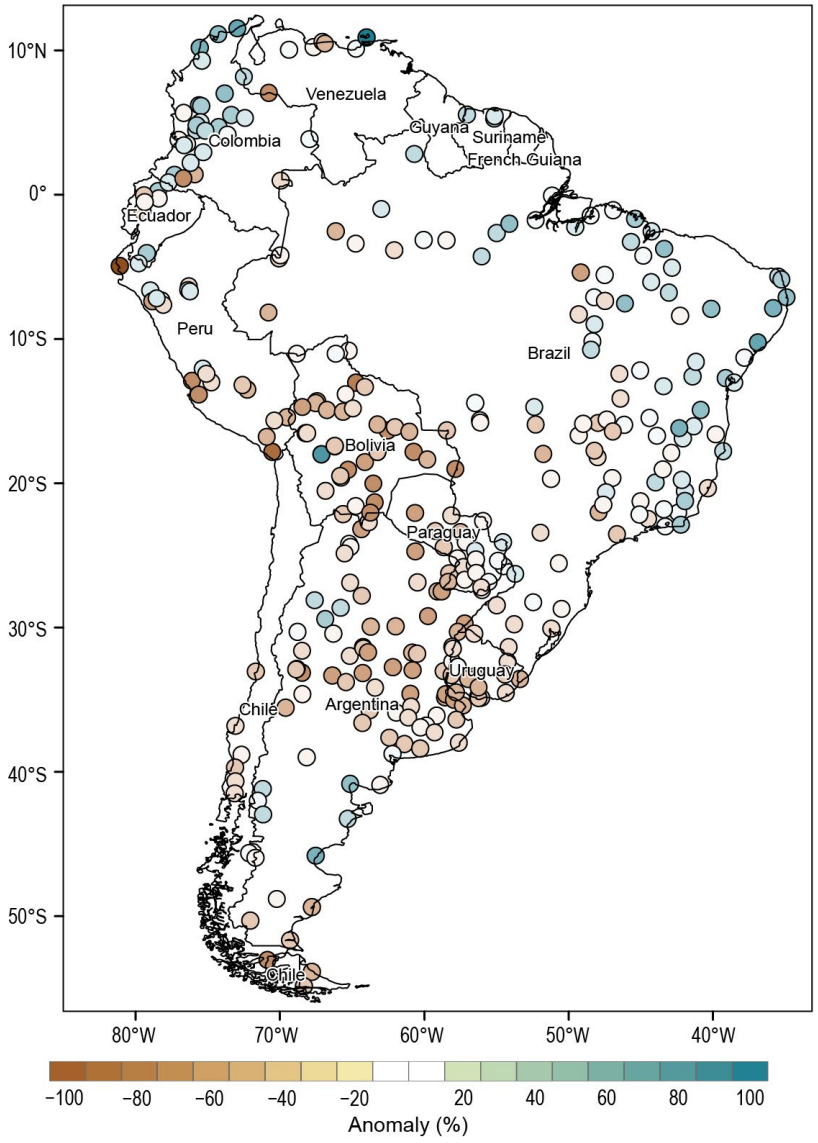

Fig. 7.12. Annual precipitation anomalies (%; 1991–2020 base period) for 2022. (Source: data from NMHSs of Argentina, Bolivia, Brazil, Chile, Colombia, Ecuador, Paraguay, Peru, Suriname, Uruguay, and Venezuela. Processed by CIIFEN.)

(iii) Notable events and impacts

An intense rainfall event occurred on 8 October in the city of Las Tejerías, Aragua, Venezuela, when 108 mm fell in six hours, equivalent to the average monthly rainfall for this region. The main cause of this event was the passage of Hurricane Julia in the Caribbean. The heavy rain fell over an area that was already saturated after receiving 180% of its normal precipitation in September. As a result of the October storm, a torrential flow of mud and debris inundated the city, resulting in 56 fatalities, forcing 10,000 residents to relocate, and damaging or destroying almost 800 homes. Economic losses were estimated at $500 million (U.S. dollars). Hurricane Julia also affected parts of Colombia. La Guajira received 120 mm of rain in 12 hours. The storm affected over 48,000 people and 174 homes were destroyed. On the islands of San Andrés and Providencia, more than 490 people were affected, roads were damaged, and more than 120 homes were damaged or destroyed.

Rainfall totals were atypical during 2022 in Barranquilla, a city in northern Colombia, with some places receiving as much as twice their normal precipitation. This event could be associated with La Niña since it increases the probability of tropical wave occurrences in the Caribbean. Notably, on 4 November, rainfall totals exceeding 70 mm in a 40-minute period were reported in the city.

In the city of Babahoyo, Province of Los Ríos, Ecuador, 140 mm of rain fell in the early hours of 12 March, prompting floods that inundated roads, damaged homes, affected over 100 families, and caused the San Pablo River to rise by 6.5 meters. The heavy rain was associated with increased convection due to sea-surface warming on the Ecuadorian coast.

2. CENTRAL SOUTH AMERICA

—J. A. Marengo, J. C. Espinoza, L. M. Alves, J. Ronchail, A. P. Cunha, A. M. Ramos, J. Molina-Carpio, K. Correa, G. Avalos, W. Lavado-Casimiro, J. Baez, R. Salinas, W. R. Quispe, and K. Quisbert

The central South America region includes Brazil, Peru, Paraguay, and Bolivia.

(i) Temperature

The 2022 mean temperature for central South America was 0.23°C above the 1991–2020 average (Fig. 7.13). Much of the region had near- to above-average mean annual temperatures (Fig. 7.11). Seasonally, during December–February, much of the northern half of Brazil and some areas in northwestern Peru and southwestern Bolivia had near- to below-average temperatures. Meanwhile, the rest of region had near- to above-average conditions. During boreal autumn (March–May), most of the region experienced near- to above-average temperatures, with southern Peru and southwestern Bolivia observing below-average temperatures. Above-average temperatures also encompassed much of the region during boreal winter (June–August), with some locations experiencing mean temperature anomalies that were +2°C or higher. Parts of southern Peru continued to experience near- to below-average conditions during their winter. Below-average temperatures were observed in southern Brazil, Bolivia, and Paraguay during September–November, while the rest of the region experienced near- to above-average temperatures.

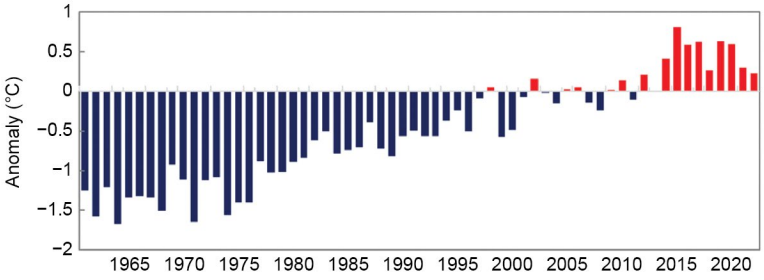

Fig. 7.13. Time series of mean annual regional air-temperature anomalies (°C; 1991–2020 base period) for the period 1961–2022 for central South America (Brazil, Bolivia, Paraguay, and Peru). (Source: NOAA /NCEP GHCN CAMS data.)

(ii) Precipitation

Above-average annual precipitation was observed across parts of northern and eastern Brazil, while the rest of central South America had below-average annual precipitation (Fig. 7.12). Abundant rainfall in the central and northern Amazon and drought in the southern Amazon and Parana-La Plata basin (LPB) were associated with La Niña in 2022.

Below-average rainfall was dominant during the austral summer in southern Peru, eastern Bolivia, southeastern Brazil, and parts of Paraguay, suggesting an early ending to the South American Monsoon. Above-average rainfall was observed across much of eastern Brazil and southwestern Bolivia during the austral summer. During boreal autumn, below-average rainfall extended across southern Peru, Bolivia, and southern parts of Brazil. Southern Paraguay and the northern region and southern tip of Brazil had above-average autumn rainfall. Much of southern Peru, the western half of Bolivia, and parts of southern Brazil reported little to no rain during the boreal winter. Meanwhile, northern Peru, eastern Bolivia, and northeastern and southeastern Brazil had above-average rainfall during winter. Boreal spring was characterized by below-average conditions across much of the region, with central Paraguay and northeastern Brazil experiencing above-average rainfall.

(iii) Notable events and impacts

Several significant weather extremes occurred across central South America in 2022, as shown in Fig. 7.14. Some of these events are discussed in more detail below.

The La Plata Basin had drought-induced damage to agriculture and reduced crop production, including soybeans and maize, which affected global crop markets. The 2022 drought conditions across the Basin were the worst since 1944 (Fig. 7.15). Several locations across Bolivia had record-dry conditions since the 1950s throughout the year when rainfall totals were between 4% and 45% of normal. The dry conditions affected over 160 Bolivian municipalities, including more than 3100 communities, 171,000 families, and 247,000 hectares (SENAMHI-Bolivia). In the southern Andes of Peru, drought conditions were the worst they had been since 1965, with rainfall ranging from none to 40% of normal. The rainfall deficits in the region were associated with the persistence of the continuous La Niña event in the tropical Pacific Ocean.

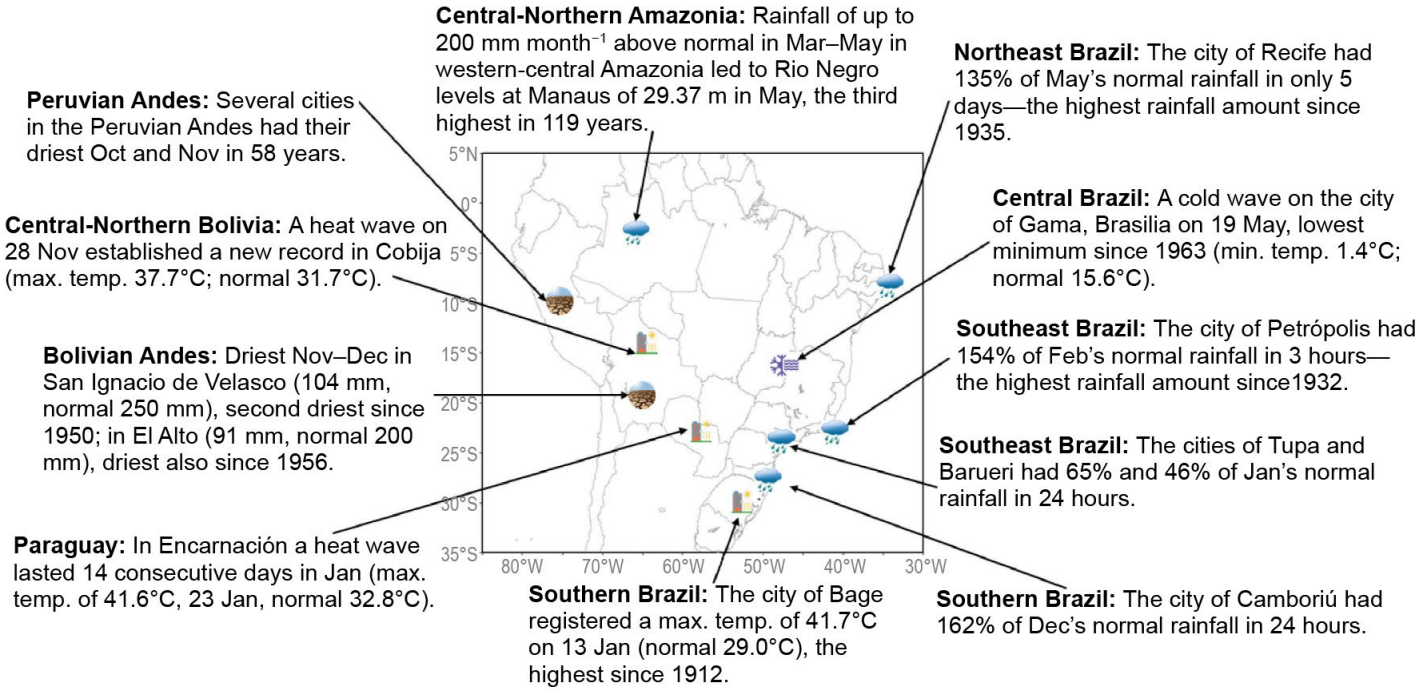

Fig. 7.14. Extreme and notable events across central South America in 2022. (Sources: Peru: SENAMHI; Bolivia: SENAMHI, Paraguay: DMH; Brazil: INMET, CEMADEN, CLIMATEMPO, INPE; International: UN OCHA, Flood list, UNDRR.)

An intensely invigorated mesoscale convective system on 15 February brought heavy rain to parts of Brazil. Of note, Petrópolis (Rio de Janeiro) received 258 mm of rain in just three hours and a total of 530 mm in 24 hours (the monthly February average is 210 mm). This caused the worst disaster in Petrópolis since 1931 with over 230 fatalities (Alcantara et al. 2023). During 2–4 April, Petrópolis and the city of Angra dos Reis (coastal region in the state of Rio de Janeiro) were affected by record rainfall when over 800 mm fell in 48 hours in each location. The torrential rain prompted floods and landslides that caused widespread damage to the area. Paraty was one of the worst-affected areas. A landslide destroyed seven houses, burying at least eight residents.

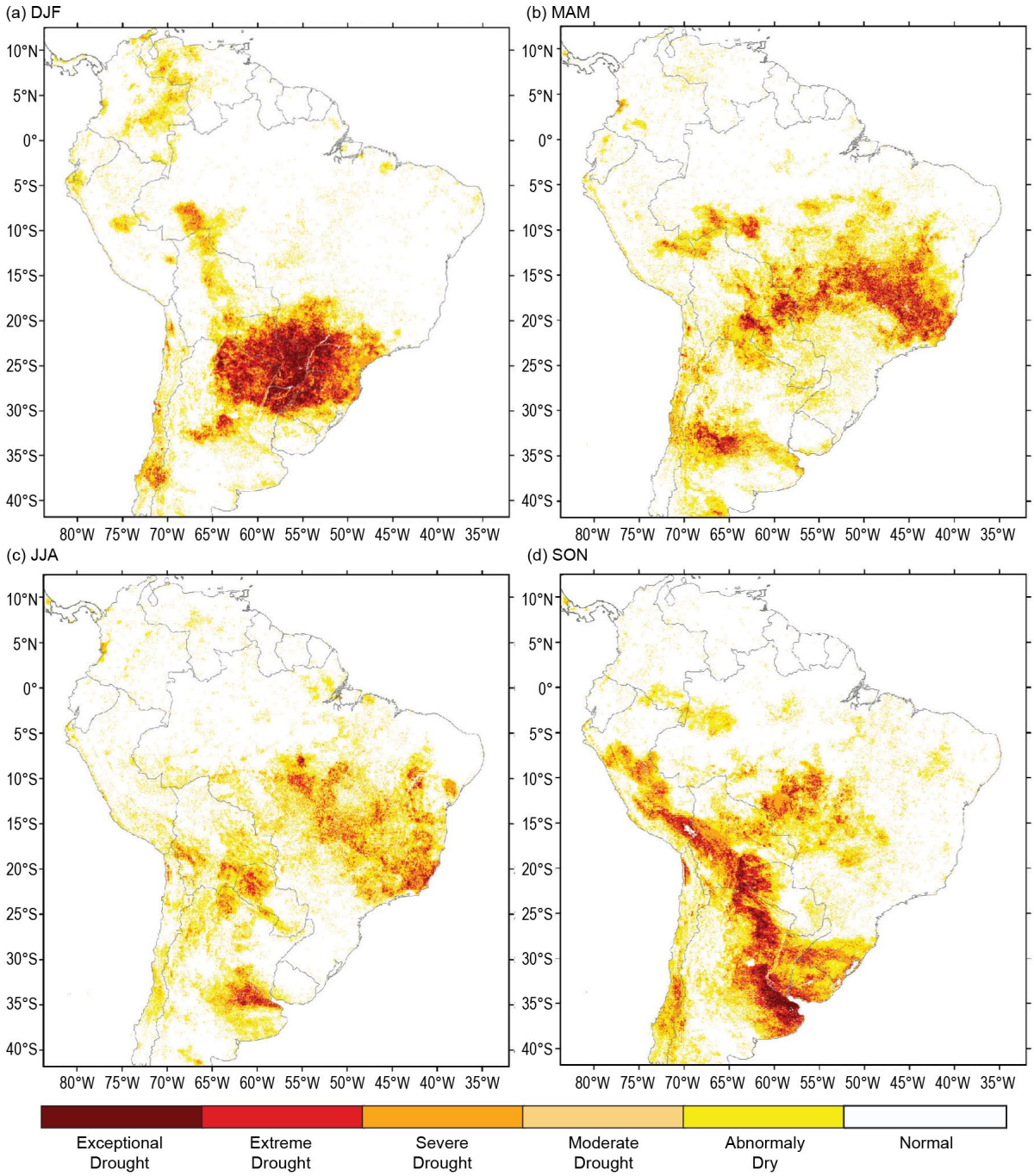

Fig. 7.15. Integrated Drought Index (IDI) maps for central South America during (a) DJF 2021/22, (b) MAM 2022, (c) JJA 2022, and (d) SON 2022. (Source: CEMADEN.)

Heavy rain on 20 February in the Bolivian Tarija department caused a 2 m-high torrent of water, mud, and debris to slide down a narrow ravine, destroying homes, crops, and livestock in various Guarani communities. The precipitation was mainly due to intense convective activity in the region associated with a cold front that crossed the southern Bolivia-northern Argentina region. In Rondônia in western Brazilian Amazonia, heavy rain from early February increased river levels, causing flooding in the municipality of Cacoal and the evacuation of 19,400 families. Damaged roads and bridges left many communities isolated.

The Rio Negro at Manaus reached the severe flood stage of 29 m in early May and 29.37 m by 23 May, the fourth-highest level since 1903. The three highest levels occurred in 2021, 2012, and 2009 (Espinoza et al. 2022). The Civil Defense reported that flooding affected over 306,000 people across the Amazonas state, and 35 municipalities declared a state of emergency.

Exceptional heavy rain fell in northeastern Brazil at the end of May. The city of Recife received 551 mm during 25–30 May, which is 140 mm more than its average total for May. The torrential rains affected 130,000 people and caused over 90 fatalities, and the city declared a state of emergency (Marengo et al. 2023). In Alagoas, 97.6 mm of rain fell in 24 hours in Porto de Pedras Largo on 2 July, resulting in more than 39,000 people evacuating their homes due to flooding.

In southern Brazil, parts of the state of Santa Catarina received over 300 mm of rain in a 72-hour period during 3–5 May. By 6 May, at least three people died, and thousands of people were displaced due to floods and landslides. On 20 December, in Camboriu (in Brazil's state of Santa Catarina), a total of 256 mm of rain fell in 24 hours, which is more than the monthly normal of 158 mm. The heavy rain triggered intense flash floods in the affected region.

On 16 May, Subtropical Storm Yakecan favored the intensification of a cold air surge that reached most of subtropical South America east of the Andes. In Brazil, a cold wave from 16 to 23 May, the country's longest cold event in 2022, affected most of the country, along with western Amazonia and Bolivia. On 18 May, the city of São Paulo recorded its third-lowest May minimum temperature in 32 years when temperatures dropped to 6.6°C, which is 6.5°C below average. In Gama (Brasilia), the minimum temperature was 1.4°C on 19 May (normal is 15.6°C), the lowest there since 1963. In the Bolivian Altiplano, the El Alto station reported its lowest May temperature on record when temperatures dropped to –9.8°C on 23 May, which is 9.2°C below average.

The central coastal region of Peru recorded its lowest minimum temperature in 15 years when temperatures dropped to 12.7°C on 13 August, which is 2.3°C below average. During 18–23 August, a cold spell impacted Santa Catarina (southern Brazil), bringing snow to the region's mountains and below-freezing temperatures (–6.4°C, or 16.4°C below average) on 19 August in Bom Jardim da Serra. This was the second-coldest event in southern Brazil in 15 years.

During 13–26 January, a heatwave event was recorded at 90% of the meteorological stations in Paraguay. The warmest day was 24 January; Concepción recorded a maximum temperature of 43.0°C, which was 8.8°C above average. The longest heatwave, which lasted for 14 consecutive days, was detected in Encarnación.

3. SOUTHERN SOUTH AMERICA

—L. S. Aldeco, J. S. Stella, A. J. Reyes Kohler, N. Misevicius, and G. Jadra

The southern South America region includes Argentina, Chile, and Uruguay.

(i) Temperature

Near- to below-average temperatures were observed across most parts of southern South America (SSA) during 2022. The most notable below-average temperatures were recorded across Uruguay and northern Chile. The national mean temperature anomaly for Argentina was +0.2°C, marking its 20th-warmest year since national records began in 1961; Chile had its 10th-coldest year since 1961 at 0.24°C below normal; Uruguay had its second-coldest year since 1991 at 0.5°C below normal (Figs. 7.16a,b,c).

During austral summer (December–February) 2021/22, above-average mean temperatures were recorded across much of the region, with the exception of the northern half of Chile, which had below-average temperatures. The highest positive anomalies, up to +3°C, were in north-eastern Argentina. Heatwaves affected the region, leading to new multiple historical maximum temperature records. The city of Florida in Uruguay recorded a maximum temperature of 44.0°C on 14 January, the highest value for this location since 1991; Rivadavia, Argentina, recorded 46.5°C on 1 January, which was the highest value for this location since 1961 and the highest value for the region and nation during 2022. Overall, Argentina observed its second-warmest summer since 1961, while Uruguay's department of Artigas had its warmest summer since 1991.

During autumn (March–May), temperatures were below average across much of the region, while above-average temperatures were recorded across parts of northern, central, and southern Argentina and Chile. Cold irruptions on 31 May led to new historical minimum temperatures records in the region. Among the most notable were: –12.6°C in Chapelco, Argentina, the lowest minimum temperature record for May for this location since 1961; –4.3°C in Mercedes, Uruguay, the lowest minimum temperature for May for this location since 1991; and –5.9°C in Chillán, Chile, also a monthly record for this location.

Winter (June–August) was characterized by near- to above-average temperatures across Argentina, while below-average temperatures were present across Uruguay and most of Chile. Cold irruptions affected central Argentina and southern Patagonia, while a warm air mass affected northern Argentina, leading to both new minimum and maximum temperature records for July. Several cities across Uruguay, including Treinta y Tres, Colonia, and Rocha, set new low minimum monthly temperatures records (since the start of the record in 1991) during June and August.

Spring (September–November) temperatures were below average across much of Uruguay, Chile, and northern Argentina. Above-average temperatures were observed south of 33°S. An early heatwave in November affected the southern half of Argentina, with the highest temperatures (>30.0°C) in southern Argentina. Several locations set new daily and monthly maximum temperature records. Of note, temperatures of 31.2°C

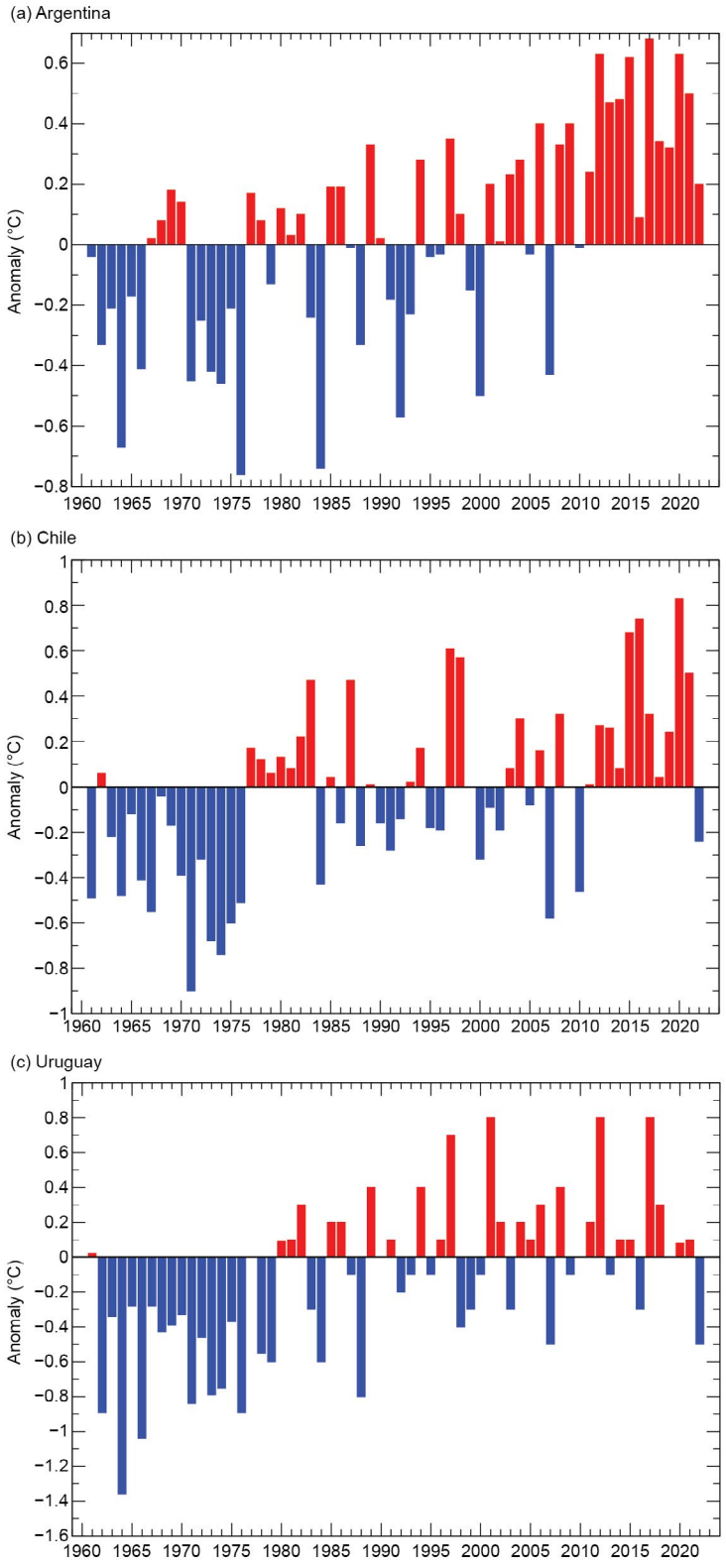

Fig. 7.16. National annual temperature anomalies (°C; 1991–2020 base period) for (a) Argentina, (b) Chile, and (c) Uruguay for the period 1961–2022.

in Esquel on 3 November and 38.6°C in Ezeiza on 5 November were recorded. This was the highest maximum temperature for November since 1961 for each location. Meanwhile, the city of Treinta y Tres in Uruguay recorded its lowest monthly minimum temperature for September (6.8°C) since 1991.

(ii) Precipitation

Similar to previous years, most of SSA had below-average annual rainfall during 2022. The most-affected regions were Uruguay, Chile, northwestern Patagonia, and north-central Argentina (Fig. 7.12). The year 2022 adds to a long period of rainfall deficit in south-central Chile, which has been called "Mega Drought" and also marks the third consecutive year of rainfall deficit in most of the region due to La Niña (Fig. 7.17). Punta Arenas in southern Chile had its second-driest year since 1966. Eastern Patagonia and northwestern Argentina had above-average annual rainfall, as much as 20%–60% above average.

During austral summer 2021/22, drier-than-average conditions were observed across northern Argentina and northern Uruguay, mostly due to the effects of La Niña. In Argentina, rainfall was 60%–87% below average in the northern region and, in Uruguay, the greatest deficits were 40%–50% below average in Rivera and Artigas. However, sub-seasonal variability favored some precipitation events that led to above-average rainfall in southern Uruguay, northern Patagonia of Chile and Argentina, and central and northwestern Argentina. In Argentina, the highest anomalies were recorded in Patagonia, with several stations receiving 100%-above-average precipitation, and in some cases, more than 150% above average. In Uruguay, Cerro Chato recorded 477 mm in January, setting its highest January rainfall total since 1991. In northwestern Argentina, Tartagal recorded 163 mm on 4 February—the highest daily rainfall for February for this location since 1961.

During autumn, drier-than-average conditions were present across most of the region; nevertheless, frontal activity favored above-average rainfall in northeastern Argentina and northern Uruguay, ranging from +72% to +89%. In central and northwestern Argentina, most stations recorded little to no rain. In Uruguay, the stations in Colonia Rivera and Javier de Viana recorded 210 mm on 25 April, which was the highest daily April rainfall since 1991 for both locations.

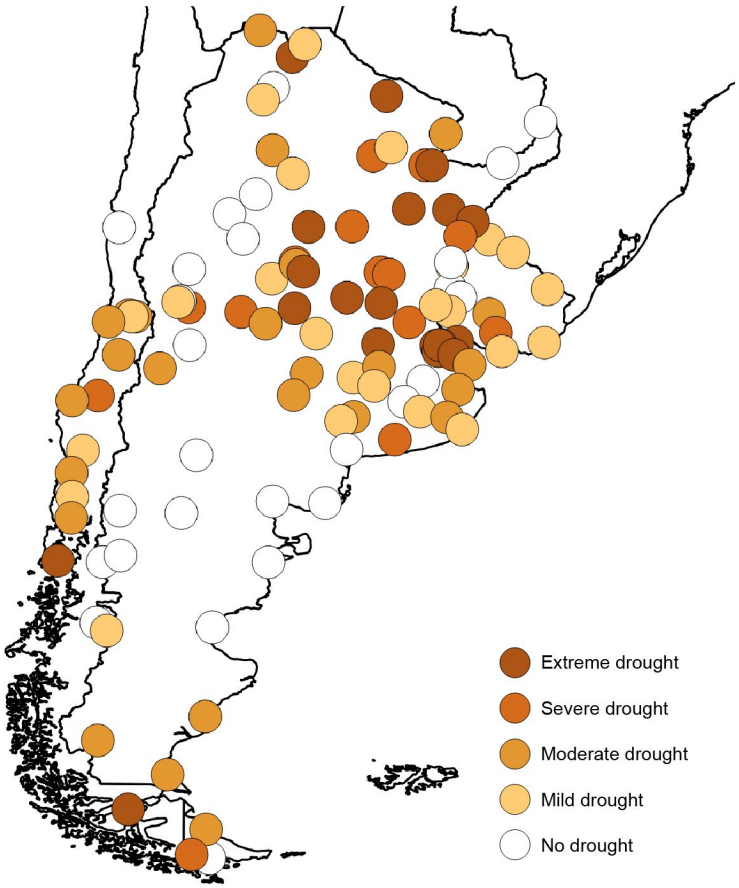

During winter, below-average precipitation was recorded across most of the region, with several stations having their driest June on record (since 1961 in Argentina and 1991 in Uruguay). Northern Patagonia had above-average precipitation of +45% to +88%, mainly due to snow events during the season. Local precipitation events led to new records. Quebracho, Uruguay, received 205 mm on 25 August—its highest daily precipitation total for August since 1991; Freirina Nicolasa in Chile recorded its most intense precipitation event since 1991, with 33.1 mm in six hours on 11 July.

Fig. 7.17. Standardized precipitation index (SPI) for January–December 2022. SPI values can be referenced here: https://droughtmonitor.unl.edu/About/AbouttheData/DroughtClassification.aspx.

During spring, drought intensified with the peak of La Niña. The driest regions were recorded in Uruguay and central and northeastern Argentina, with some areas receiving little to no rainfall. Above-average rainfall was recorded in eastern Patagonia, with the highest daily rainfall for September since 1961 recorded in Comodoro Rivadavia (82.1 mm on 20 September, 228% of normal).

(iii) Notable events and impacts

Figure 7.18 shows numerous notable events that occurred across the region during 2022. Several are discussed in more detail below.

Argentina, parts of Uruguay, and Chile experienced severe drought conditions throughout much of 2022 (Fig. 7.17), which affected the region's hydrology. Extreme drought conditions prevailed across central Argentina and southern Uruguay from May onward, mostly due to the prolonged La Niña event. Between October and December, severe drought conditions spread to northeastern Argentina. Several locations in Argentina observed their driest year on record, ranging between 50% and 60% of normal precipitation: Corrientes (818.8 mm); Paso de los Libres (773.3 mm); Rosario (561.1 mm); Junín (591.7 mm); Ezeiza (507.0 mm); Río Cuarto (457.0 mm); La Plata (567.1 mm). Due to the impacts across most of the region, this drought is considered one of the worst on record.

During January, a blocking event led to persistent heatwaves in central and northern Argentina and Uruguay, with several locations recording maximum temperatures above 40.0°C. In Argentina, the heatwave lasted for most of the month and was considered one of the most intense and prolonged heatwaves. In Uruguay, two heatwaves occurred: 12–16 January and 20–23 January. Summer 2022 was the driest summer for Corrientes, northern Argentina, which received only 83.1 mm (21% of normal) of precipitation. Drought conditions combined with high temperatures enabled the development of fires and bushfires during summer, burning close to 800,000 hectares.

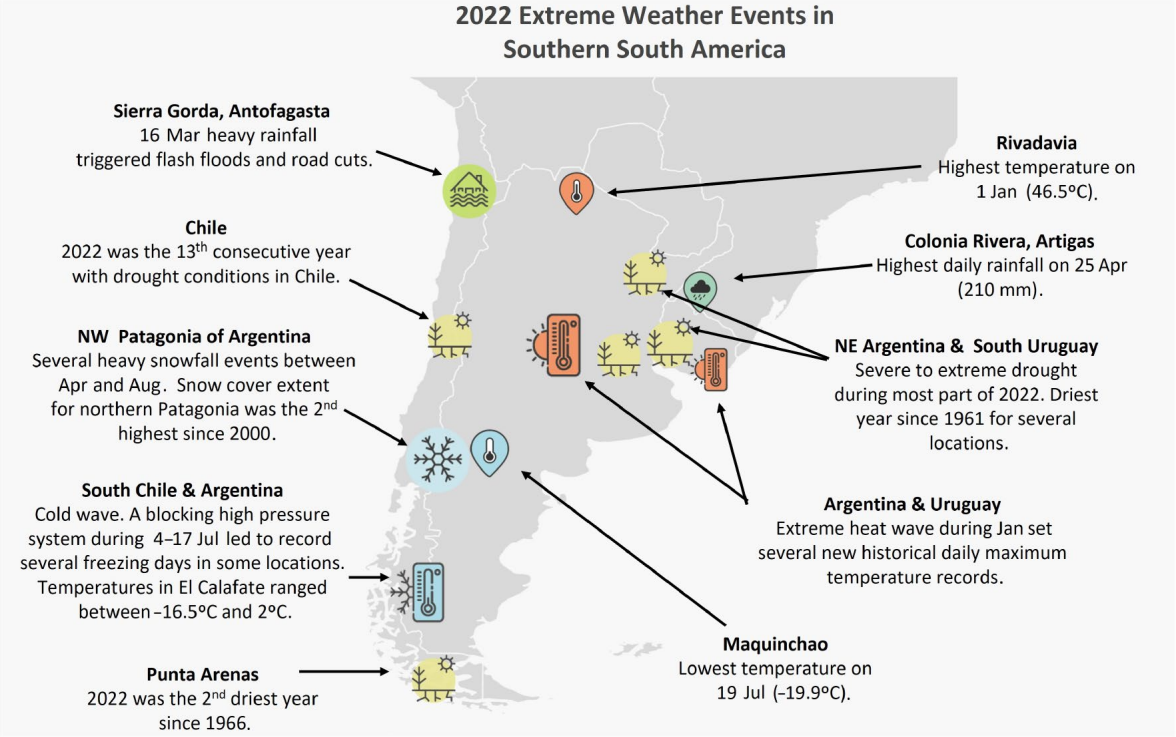

Fig. 7.18. Extreme and notable events in southern South America (Argentina, Chile, and Uruguay) during 2022.

e. Africa

—A. Mekonnen, Ed.

This analysis for Africa is based on observational records from meteorological and hydrological services across the region, rainfall from the Global Precipitation Climatology Project (GPCP), and reanalysis products from the National Centers for Environmental Prediction/National Center for Atmospheric Research (NCEP/NCAR). Notable events in 2022 were compiled based on reports from government agencies, regional and international organizations, and research/Early Warning organizations. The climatological base period is 1991–2020, and the terms "normal" and "average" are interchangeably used to refer to this climatology.

Figure 7.19 presents the 2022 mean temperature anomalies for Africa. Annual temperatures greater than 1°C above normal were observed over most of northwest Africa (Algeria, Mauritania, Morocco, and Tunisia), while Mali, Niger, Chad, and northern Nigeria had annual mean temperatures as much as 2°C below normal. Most of eastern and equatorial Africa experienced above-normal temperatures (Fig. 7.19). Except for some areas across the western half of Angola, most of Africa south of the equator remained within their annual normal temperature ranges.

West Africa north of 10°N received above-average annual rainfall, while rains over the Guinea Highlands and Nigeria were below normal. Rainfall over Ethiopia, Kenya, northern Uganda, and northern Tanzania in eastern Africa were below normal. Rainfall over the adjoining areas of the Democratic Republic of the Congo, Zambia, and Angola were more than 1 mm day^{-1} below normal (Fig. 7.20a).

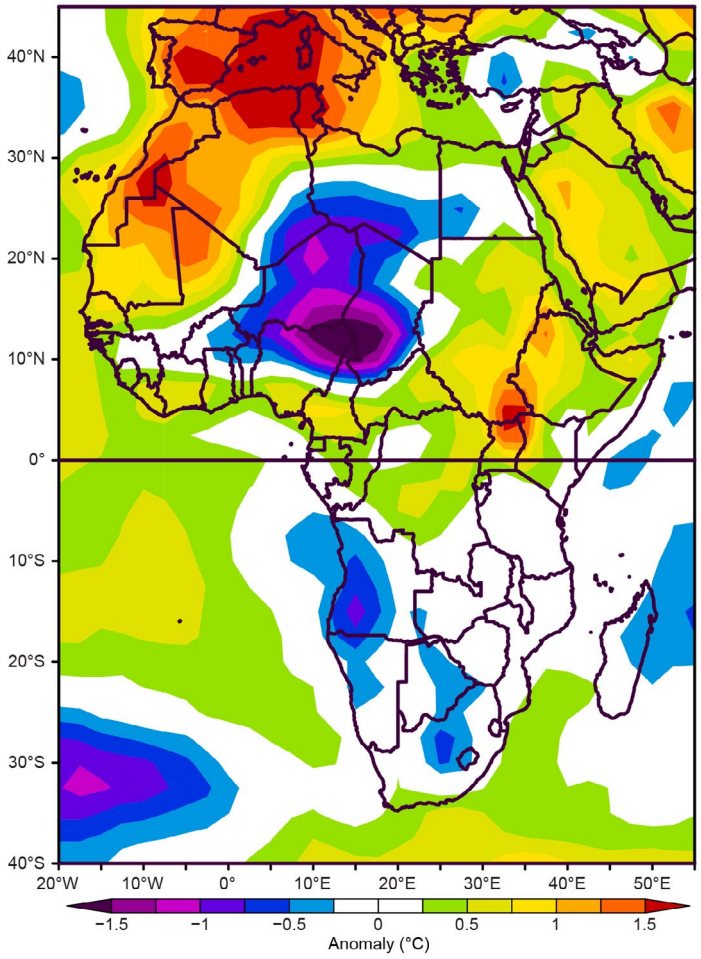

Fig. 7.19. 2022 annual mean temperature anomalies for Africa (°C; base period 1991–2020). (Source: NCEP/NCAR.)

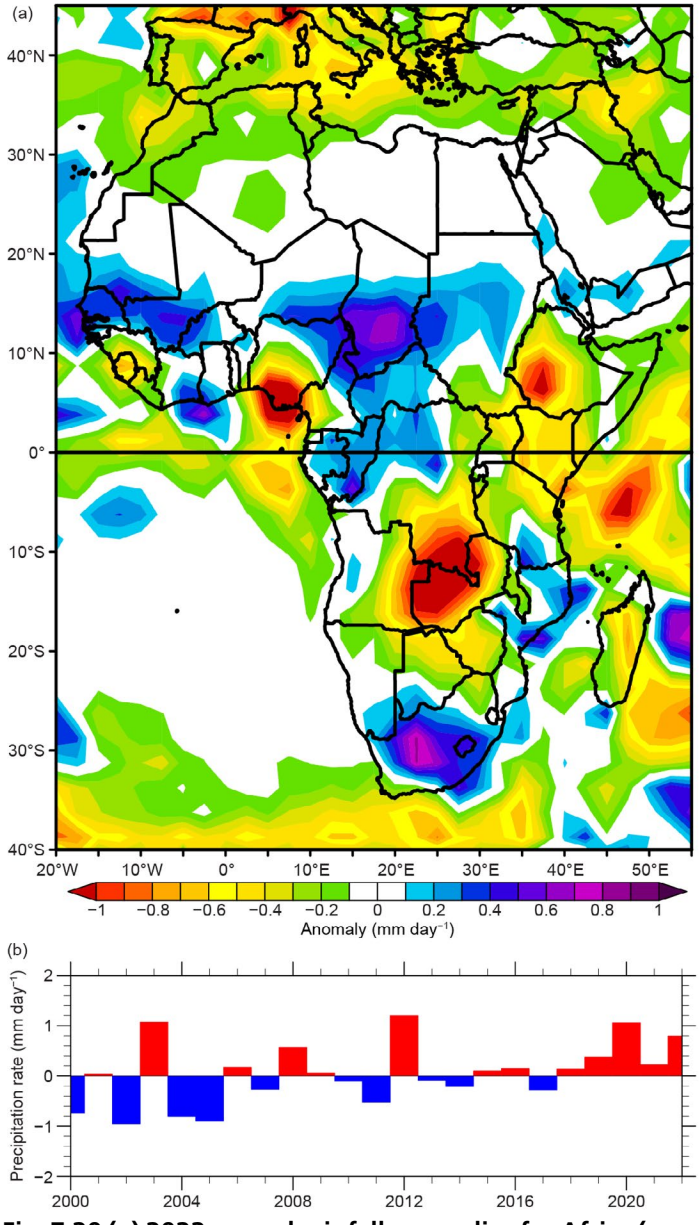

Fig. 7.20 (a) 2022 annual rainfall anomalies for Africa (mm day^{-1}; base period 1991–2020). (Source: NCEP/NCAR.) (b) Rainfall anomalies (mm day^{-1}) for West Africa (10°N–15°N, 15°W–10°E; base period 1991–2020) for the period Jul–Sep from 2000 to 2022. (Source: GPCP v2.3.)

After the devastating droughts in the 1970s through the 1990s, a rainfall "recovery" has been reported in the literature (e.g., Giannini 2015; Biasutti 2019). Although there is no consensus on the recovery, a significant increase in seasonal rainfall has been reported (*c.f.* Nicholson et al. 2018). To provide context, the West African (10°N–15°N, 15°W–10°E) rainfall trend for the July–September period, the peak rainfall season over West Africa north of 5°N, for 2000–22 is presented in Fig. 7.20b. Rainfall has been above normal since 2018, with July–September 2022 being the fourth-wettest such period in this record (~0.8 mm day^{-1} above normal)

Extreme weather events and high climate variabilities were also reported from regions, the details of which are compiled below.

1. NORTH AFRICA

—K. Kabidi, A. Sayouri, M. ElKharrim, and A. E. Mostafa

North Africa comprises Mauritania, Morocco, Algeria, Tunisia, Libya, and Egypt. Much of this region is characterized by arid and semi-arid climate, while northern parts exhibit Mediterranean climates. Precipitation over the region was highly variable, but in general, below-normal precipitation was observed in winter (December 2021–February 2022) and heatwaves were observed during summer (June–August).

(i) Temperature

During winter, most of the region experienced temperatures greater than 0.5°C above normal (Fig. 7.21a). Moroccan records show above-average minimum temperatures over its southern and coastal Atlantic regions. Mean minimum temperatures over Tunisia, Libya, Algeria, and Egypt remained near normal (not shown). Mean temperature anomalies ranging from –1°C over Tunisia to more than –3°C over southeastern Algeria, southern Libya, and most of Egypt were observed in January. A minimum temperature of about –2°C was recorded on 5 February at Saint Catherine in Egypt.

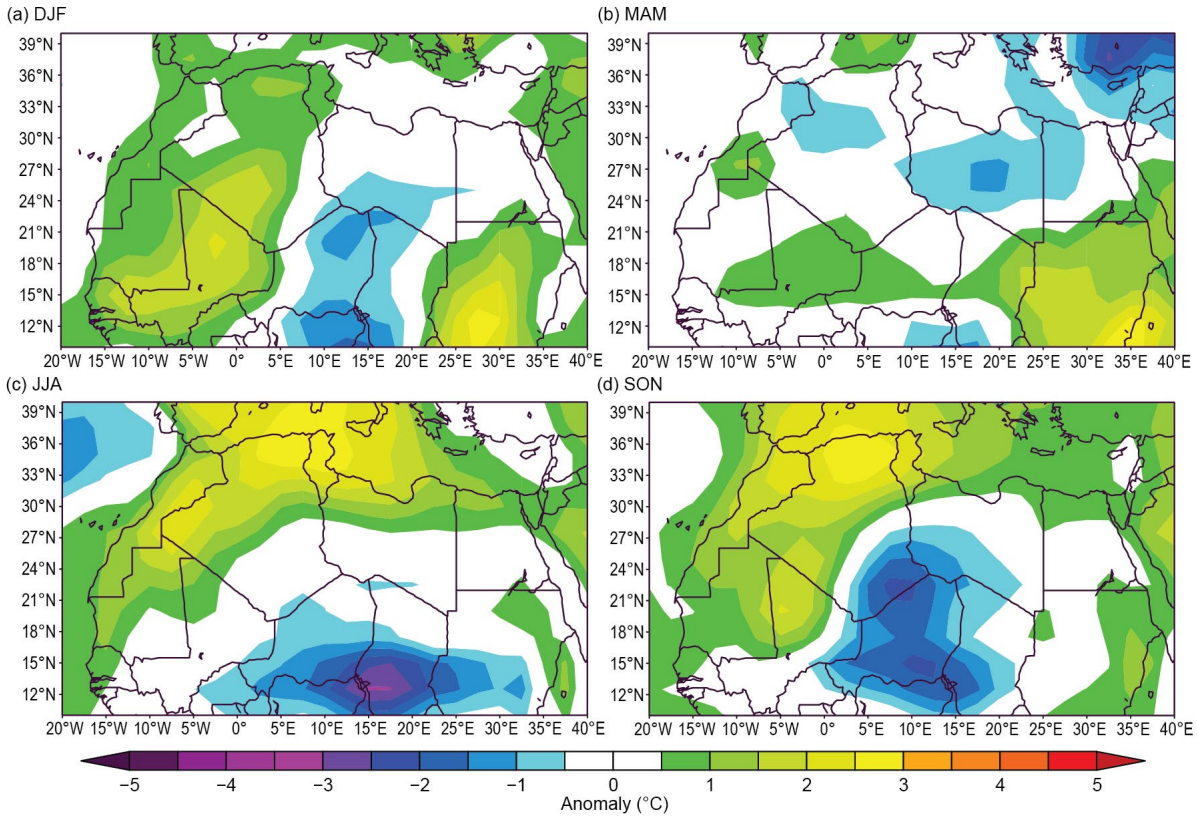

Fig. 7.21. North Africa seasonally averaged temperature anomalies (°C; 1991–2020 base period) for (a) Dec–Feb 2021/22, (b) Mar–May 2022, (c) Jun–Aug 2022, and (d) Sep–Nov 2022. (Source: NOAA /NCEP.)

In general, spring (March–May; Fig. 7.21b) temperatures were near normal across North Africa, with a slight positive anomaly over southern Morocco and slight negative anomaly over Libya (Fig. 7eb). However, a new record of 47.3°C on 20 May broke the previous May maximum temperature of 45.8°C on 23 May 2015 at Sidi Slimane in Morocco. A maximum temperature of 47°C was reported at Aswan, Egypt, on 14 May 2022.

Summer (June–August; Fig. 7.21c) temperatures were more than 2°C above normal over north-northwest Mauritania, Morocco, and adjoining Algeria, Tunisia, and the northern half of Libya and Egypt. A high maximum temperature of 49.1°C was observed during summer at Smara, Morocco. The overall average maximum temperature in June in Tunisia exceeded the normal by 4.2°C, marking the highest average June maximum temperature on record for the country. Record maximum temperatures ranging from 46°C to 47°C were recorded at Monastir, Jerba, and Gafsa in Tunisia during July and August.

Above-average mean temperatures dominated the region during autumn (September–November, Fig. 7.21d), except for extreme southeastern Algeria where below-average mean temperatures were observed. In December, temperatures of 1°C to 5°C above normal dominated central and southern Algeria and extended into the southern half of Tunisia, the northern half of Egypt, and western Libya (not shown). Records show that mean temperatures in December 2022 over Tunisia were about 3.4°C above normal, the highest since 1950.

(ii) Precipitation

Below-normal precipitation dominated much of the region during winter (Fig. 7.22a). The lack of winter precipitation over Morocco and adjacent countries was associated with expansive dominance of Azores high pressure. The precipitation deficit over Morocco in January and February ranged from 62% to 74% of normal. However, above-normal winter precipitation was reported from meteorological stations at Errachidia and Ouarzazate in southeast Morocco. Reports from various observatories show that winter precipitation was generally below normal over Egypt. However, extremely heavy rainfall was reported from stations in January.

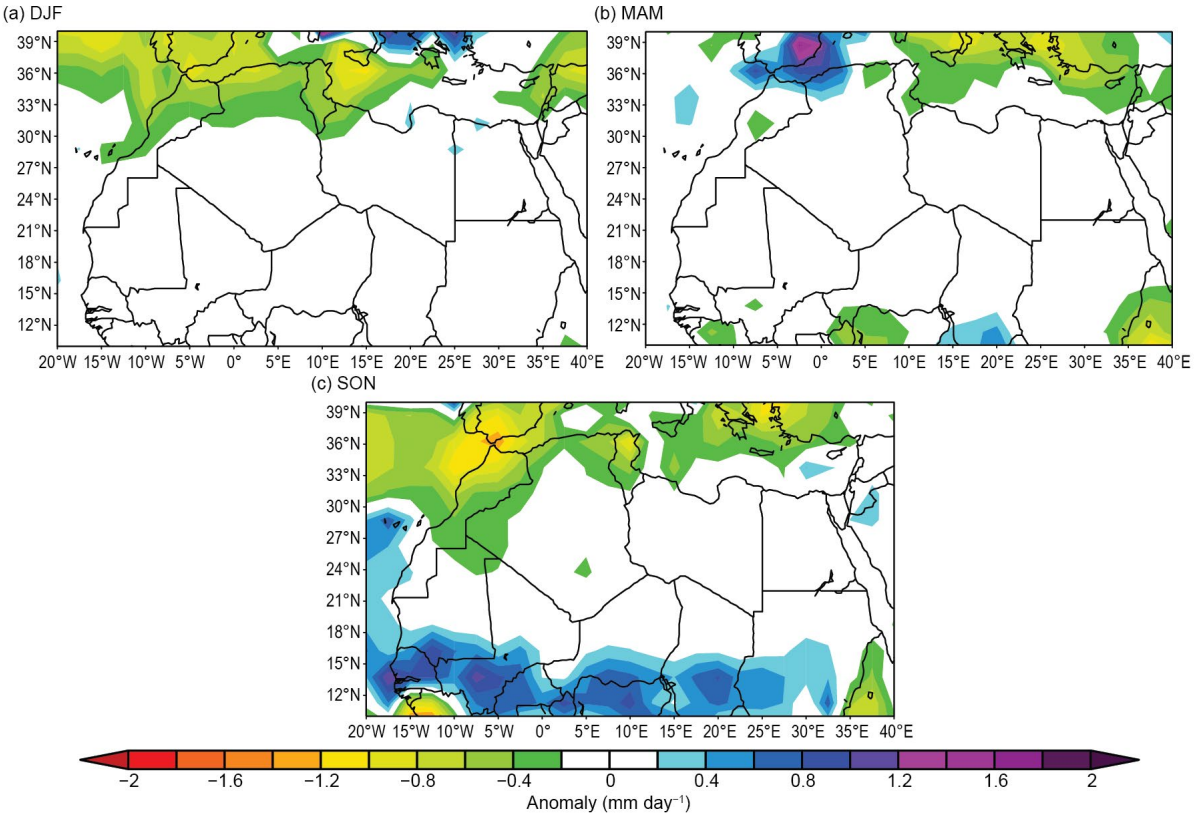

Fig. 7.22. North Africa seasonally averaged rainfall anomalies (mm day^{-1}; 1991–2020 base period) for (a) Dec–Feb 2021/22, (b) Mar–May 2022, and (c) Sep–Nov 2022. (Source: GPCP NOAA/NCEP.)

For example, Alexandria received 60 mm on 8 January and Elkollia-ElBaharia received 75.4 mm on 9 January. Precipitation in January and February was near normal in Algeria.

Spring mean precipitation did not ameliorate winter deficits, although precipitation was near normal (Fig. 7.22b). Above-normal precipitation was reported in March over northern Morocco, but drought conditions prevailed in April and May over most of the country. In Algeria, March and April precipitation was above normal. In Tunisia, record precipitation fell in some areas, including 92 mm at Kairouan on 19 March (previous record 76.6 mm on 15 March 1991) and 79 mm at Tozeur on 19 March (previous record 25.7 mm on 26 March 1993).

Rainfall during June–August is not discussed in this analysis because the season is normally dry over North Africa, north of 20°N–25°N. Autumn precipitation (Fig. 7.22c) was below normal for the region, but some stations in Morocco reported above-average precipitation during the last 10 days of September (Smara ~194% of normal, Dakhla 280%, Agadir ~120%). Rainfall deficits during October and November were associated with the extension of the Azores high into the region. October was the driest on record since 1960 in Tunisia. Wet conditions were observed in northern Tunisia during November (above normal in some stations), while drier-than-normal conditions were reported in central and southern parts of the country (deficits were approximately 30% of normal). December 2022 was the driest December on record for Tunisia since 1950 (e.g., Enfidha 100%, Jerba 97%, Gafsa 37% below normal). On the other hand, in Egypt, Ras Elitine received 84.2 mm on 25 December 2022, marking the highest one-day rainfall in the country in 2022.

(iii) Notable events and impacts

In late January, heavy snowfall (10 cm–20 cm) affected northern regions of Libya (Sidi AlHamri, Shahat, Al-Bayda, Qandula, and Belqes), including some road closures. The snow was associated with a cold air mass centered on the northeastern regions.

During summer 2022, a series of forest fires broke out in Morocco, Algeria, and Tunisia. Heatwaves due to exceptional drought and water stress especially affected Morocco in July and August. Forest fires destroyed about 11,000 hectares of forest and 1156 families had to be relocated in the Moroccan provinces of Larache, Ouezzane, Tetouan, Chefchaouen, Taza, and Al Hoceima. In Tunisia, 219 forest fires were reported between June and September, which destroyed 5900 hectares. Nabeul, Tunis, Bizerte, Siliana, Béja, and Jendouba were the main regions affected. In addition, several forest fires broke out in northern and eastern Algeria during August and September, causing 43 deaths and the destruction of 800 hectares of forest and 1800 hectares of coppice. The areas of Bejaia, Jijel, Setif, Khenchela, El Tarf, Tebessa, Souk Ahras, and Skikda et Tipaza were all affected.

In October, violent floods due to heavy rains hit northeastern regions of Algeria, especially in the region of Bordj Bou Arreridj, killing four people. Flash floods in late November affected Tripoli and western areas of Libya as 128 mm of precipitation fell within a 24-hour period. The main roads were flooded and schools were disrupted.

2. WEST AFRICA

—W. Agyakwah, J. Hicks, W. M. Thiaw, S. Hagos, and F. Sima

West Africa extends from the Guinea coast to about 20°N and from the eastern Atlantic coast to Niger. West Africa consists of two sub-regions: 1) The Sahel (12°N to 17°N; Senegal and The Gambia in the west to Niger in the east) and 2) the Gulf of Guinea region to the south (from about 4°N to 10°N; the Guineas to the west along the east Atlantic coast and Nigeria and Cameroon to the east).

(i) Temperature

The highest mean annual temperatures ranged between 28°C and 30°C, mainly across the western and central Sahel (Senegal, Mauritania, and Mali; Fig. 7.23a). Most countries in the Gulf of Guinea region had lower mean annual temperatures ranging from 22°C to 24°C. Areas in the central Sahel region (northern Nigeria and southern Niger) had mean annual temperatures between 22°C and 26°C, which were 1°C to 2°C below normal (Fig. 7.23b).

Mean annual maximum temperatures were normal to below normal over the Sahel region, with anomalies as much as –3°C in southern Niger. Conversely, above-normal annual maximum temperatures were recorded in the Gulf of Guinea countries, including Liberia, Cote d'Ivoire, Ghana, Togo, Benin, and southern Nigeria. The highest positive anomalies of +1.5°C to +3°C were recorded in southern Nigeria. Mean annual minimum temperatures were 0.5°C to 1.5°C below normal in northeastern Nigeria and southeastern Niger and 0.5°C to 2.5°C above average across western parts of West Africa.

The warmest months in the Sahel were April, May, June, and July, with mean daily temperatures ranging from 34°C to more than 36°C, with the highest temperatures over Mauritania and Mali during June. However, compared with climatology, April had the highest above-average temperature, with anomalies from +0.5°C to +2°C over the western and central Sahel regions.

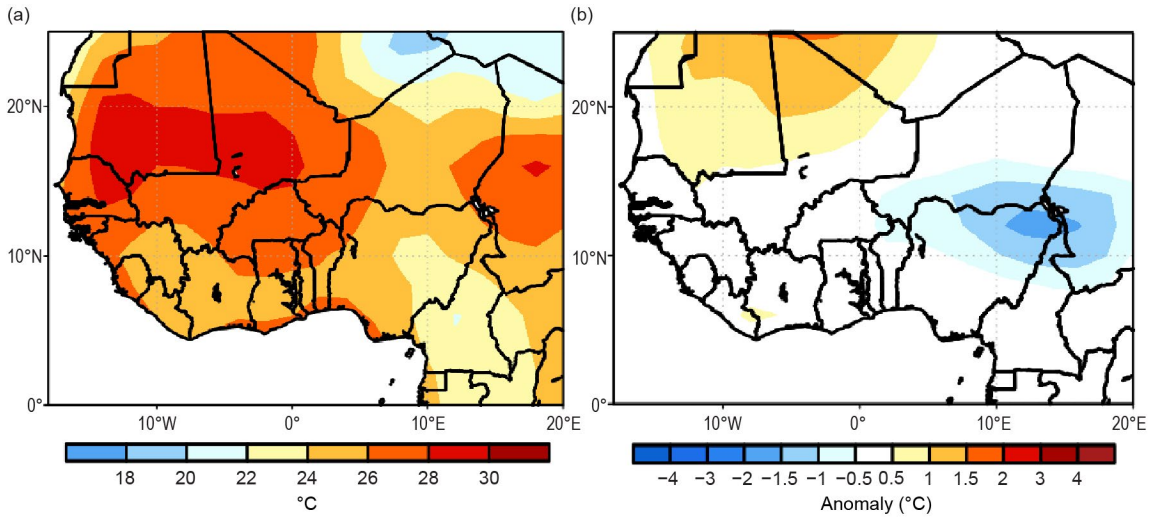

Fig. 7.23. Annual (a) mean temperatures and (b) mean temperature anomalies in 2022 for West Africa (°C; 1991–2020 base period). (Source: NOAA/NCEP.)

(ii) Precipitation

In the Sahel, annual rainfall ranges from 200 mm to 1500 mm, and increases to the south. The highest rainfall amounts, between 1000 mm and 1500 mm, occurred in southern Senegal, The Gambia, and southern Mali (Fig. 7.24a). Average rainfall anomalies of +50 mm to +150 mm were observed over Mauritania, Senegal, The Gambia, southern Mali, Burkina Faso, central and eastern Niger, and northeastern Nigeria. Over Mauritania, Senegal, central Mali, and eastern Niger, recorded rainfall was about 120%–200% of normal rainfall.

Annual rainfall totals over the Gulf of Guinea region ranged from 1000 mm to over 2000 mm, with the highest totals over Sierra Leone. Even with these high totals, Sierra Leone still registered

below-average rainfall (50 mm to 150 mm below normal; Fig. 7.24b). The most significant anomalies of –50 mm to more than –300 mm occurred in Nigeria. The greatest deficits (more than –300 mm) occurred in southeastern Nigeria (10th percentile). Above-average rainfall (+50 mm to +200 mm) was recorded over eastern Cote d'Ivoire and Ghana. The highest departures from the mean (+150 mm to +200 mm) were observed in southwestern Ghana (90th percentile).

Significant rainfall totals were observed in the southern Sahel and the Gulf of Guinea from April to October, with the highest occurring from June to September, resulting in much of the annual cumulative rainfall. In August and September, almost the entire Gulf of Guinea region received more than 200 mm of rain, which was reflected in the July–September (JAS) and August–October (ASO) seasonal rainfall, with surpluses of +50 mm to +150 mm. During JAS and ASO, rainfall totals were above average (+20 mm to +150 mm) over western Guinea, southwestern Sierra Leone, Liberia, Cote d'Ivoire, Ghana, Togo, Benin, and Nigeria. The highest departures from average (+100 mm to +150 mm) were recorded over Cote d'Ivoire and Ghana, which received 120%–200% of their average rainfall (90th percentile). Throughout the seasons, as mentioned above, rainfall deficits (–20 mm to more than –150 mm) were registered over Guinea, Sierra Leone, Liberia, and Nigeria. In addition, over the Gulf of Guinea, the highest rainfall anomalies (more than +150 mm) occurred in southern Ghana during April–June, the peak rain season over the region. Surpluses between +50 mm and +100 mm (120%–200% of normal) were observed during April and June.

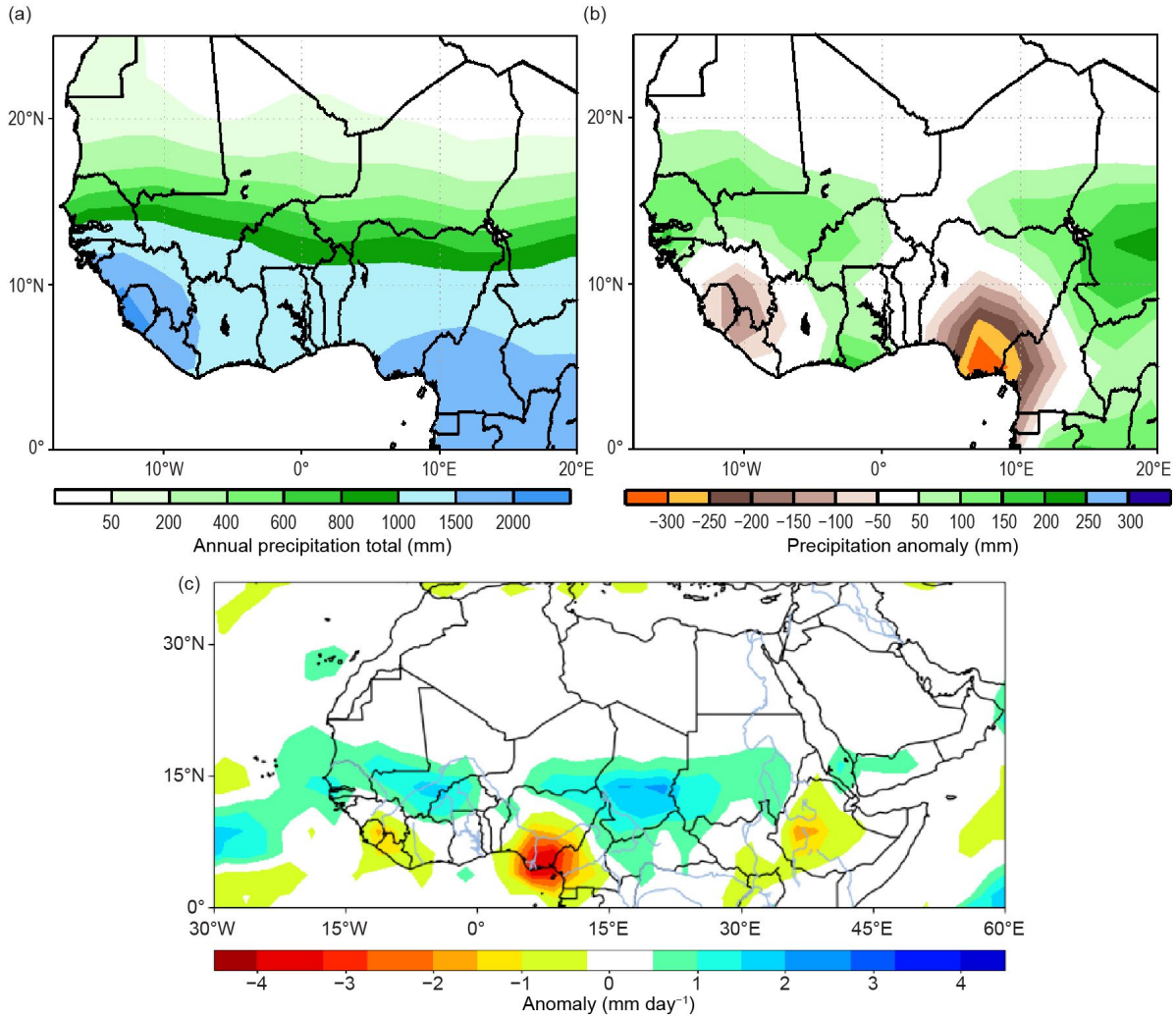

Fig. 7.24. Cumulative (a) annual total precipitation (mm), (b) annual total precipitation anomalies (mm), and (c) Jun–Sep precipitation anomalies (mm day^{-1}) in 2022 for West Africa (1991–2020 base period). (Source: NOAA/NCEP.)

Substantial rainfall occurred in the Sahel region during June–August (JJA), JAS, and ASO, with more than 500 mm recorded over the southern Sahel region, 20 mm–150 mm above normal, with the highest anomalies (+100 mm to +150 mm, 120%–200% of normal) over southern Mauritania, southern Mali, and western Burkina Faso. Among the three seasons (JJA, JAS, and ASO), southern Mali, western Burkina Faso, southeastern Niger, and northeastern Nigeria registered substantial rainfall surpluses ranging from +100 mm to more than +150 mm during JAS. At the northeastern tip of Nigeria, surpluses exceeding +150 mm were recorded. Over the Sahel, rainfall surpluses of about +20 mm to +30 mm occurred in July and August, and surpluses reached their peak of about +50 mm to +100 mm in September over southern Mali, Burkina Faso, northern Nigeria, and southern Nigeria.

Overall, widespread above-normal precipitation throughout the West African Sahel region from the western coast to the eastern border of Chad during June–September was observed (Fig. 7.24c). The seasonal mean precipitation was particularly high over southern Mali and southern Chad, which led to several extreme precipitation events.

(iii) Notable events and impacts

Above-average rainfall and heavy rain events led to widespread flooding across the region during the boreal summer. The Civil Protection Directorate of Niger indicated that eight people lost their lives due to heavy rain and flooding between June and July. Heavy rain on 15 July damaged roads and homes in the Diffa, Zinder, Maradi, and Tahoua regions, causing one additional fatality. In Senegal, short-duration heavy rainfall totaling 127 mm in Dakar was reported on 5 August, leaving city streets inundated. Flood waters ~1 m deep caused widespread traffic disruption. In Mali, the government of the Mopti Region reported rivers overflowing in several places in September. Several places in Mauritania and The Gambia were also affected by floods during June–September. The flash floods that impacted The Gambia were among the worst there in nearly half a century. Torrential rain and thunderstorms caused widespread damage that affected large parts of the country, particularly the densely populated Banjul area. According to the Department of Water Resources of The Gambia, 276 mm of rain fell during 30–31 July at Banjul International Airport. The National Disaster Management Agency of The Gambia reported that four people were killed by lightning in the North Bank region.

In the Gulf of Guinea region, the United Nations reported flood conditions in Cote d'Ivoire (16 July), Sierra Leone (29 August), Benin (throughout September), and Guinea (17 September). The flooding affected thousands of people and houses. Significant livestock losses were recorded, and several hectares of crops and farmlands were also affected. The United Nations Children's Fund (UNICEF) reported that since September 2022, the worst floods in a decade affected 3.2 million people across Nigeria. It is estimated that 60% of the people affected were children, and the highest number of displaced persons occurred in Anambra, Bayelsa, Cross River, and Jigawa States. Heavy rainfall and river overflow damaged public health facilities, water systems, and sanitation facilities, which increased the risk of waterborne diseases, such as cholera, diarrhea, and malaria, and heightened the chances of an epidemic as well as childhood illnesses. The children living in makeshift displacement sites lacked basic facilities and were exposed to additional risks, such as separation from their families and gender-based violence.

3. CENTRAL AFRICA

—W. Agyakwa, J. Hicks, and W. M. Thiaw

Central Africa features a unique climate system marked by a strong annual cycle as it spans a wide area of Africa across both the Northern and Southern Hemispheres. The region extends from the southern tip of the Democratic Republic of Congo (DRC) northward into the central areas of Chad. Longitudinally, the region extends from about 5°E to ~35°E. Given the overlap with areas in West Africa and East Africa, this analysis focuses strictly on the sub-region encompassing Cameroon, Chad, Central Africa Republic (CAR), DRC, Congo, Gabon, Equatorial Guinea, and Sao Tome and Principe.

(i) Temperature

Mean annual temperatures ranged from 21°C to 25°C throughout Central Africa and approached 27°C in central Chad and 19°C in east-central DRC. These temperatures correspond to anomalies that were about 0.75°C above the mean in northeastern DRC and 1°C –1.5°C below the mean in northern Cameroon and central and southern Chad. In central portions of DRC and east-central portions of CAR, annual mean temperatures were above the 85th percentile (Fig. 7.25a). Southwestern portions of Chad experienced their lowest annual mean temperatures. Annual maximum temperatures were mostly between 24°C and 32°C, but up to 37°C in central Chad. This translated to maximum temperatures that were 1°C–2°C above the mean from southern Cameroon to central and southern CAR and 1°C–2.25°C above the mean in southern and eastern DRC (Fig. 7.25b). Conversely, maximum temperatures were about 1°C–3°C below the mean in southern and central Chad, where much of the region experienced its lowest maximum temperatures.

The northern sector of Central Africa experiences its highest mean temperatures from March–June, from around 28°C in northern CAR to more than 32°C in northern Cameroon and central Chad. Central CAR observed mean temperatures in March that were 1°C–2.25°C above normal, placing this region above the 90th percentile for that month. However, mean temperatures north of the Mbang Mountains in Cameroon were more than 2°C below the mean for May, ranking as the coldest or second-coldest May on record. This region—including southern and central Chad—had an additional six consecutive months (June–November) where mean temperatures ranked as the coldest or second coldest on record relative to the climatological mean. Conversely, the southern sector of Central Africa (southern Cameroon to DRC) had nine months where a majority of this region experienced mean temperatures ranking above the 70th percentile, including central DRC, which experienced three months (May, July, and August) with

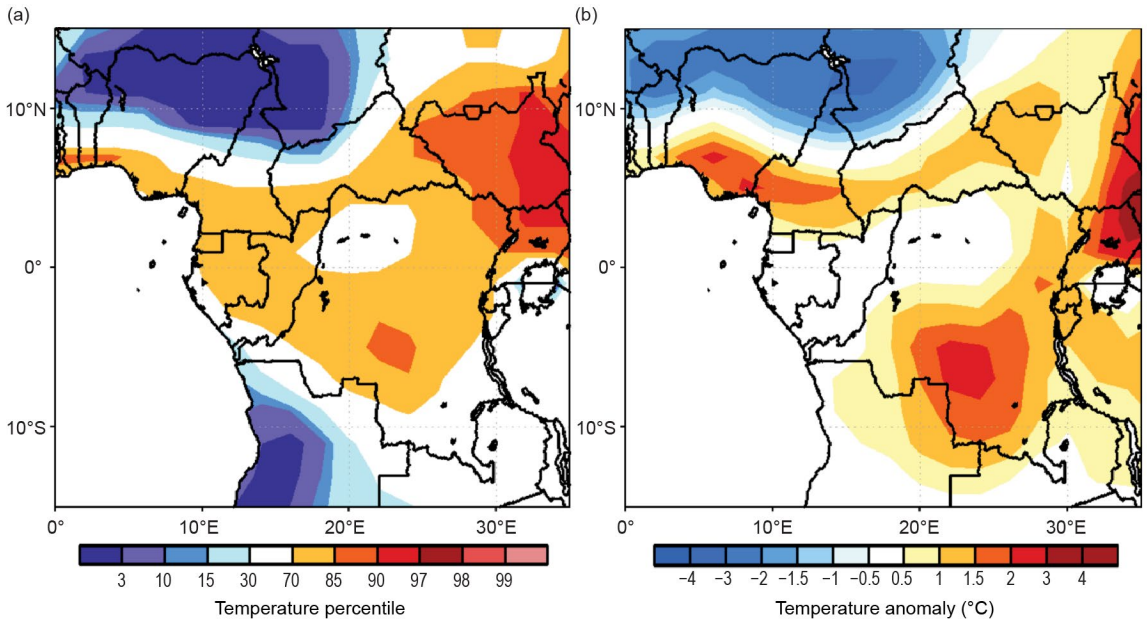

Fig. 7.25. Annual (a) mean temperature percentile rank and (b) maximum temperature anomalies (°C) in 2022 for Central Africa (1991–2020 base period). (Source: NOAA/NCEP.)

mean temperatures above the 90th percentile (up to 3°C above normal). Maximum temperatures ranged from 32°C in central Cameroon/southern CAR to about 43°C in central Chad in March before transitioning to below-normal maximum temperatures by May—more than 5°C below the mean—especially throughout northern Cameroon and central/southern Chad. This cold pattern extended from May until the end of the year, resulting in some regions experiencing their lowest maximum temperatures on record, particularly during May–August. As maximum temperatures plummeted in this region around May, maximum temperatures throughout central and southern DRC soared to 30°C to 31°C. This corresponded to anomalies that were 4°C to nearly 7°C above the mean from July to October, with two months (July and August) ranking above the 90th percentile. Annual minimum temperature anomalies were less pronounced than the maximum temperature anomalies. Northern Cameroon and western Chad observed annual minimum temperatures up to about 1°C below the mean. Southern Cameroon, Equatorial Guinea, Gabon, western Congo, eastern CAR, and northeastern DRC observed annual minimum temperatures up to 1°C above normal.

The monthly evolution of the minimum temperatures was highly variable throughout the year. Most of DRC, Gabon, and Congo observed near- to above-normal minimum temperatures during January–May. From Gabon to central and southern DRC, minimum temperatures ranked above the 90th percentile—particularly in April and May—before observing near- to below-normal minimum temperatures in June that ranked below the 10th percentile in central DRC and most of Congo. June also saw the greatest below-average minimum temperatures for portions of east-central Congo and west-central DRC. In addition, a large swath of below-normal minimum temperatures covered northern Cameroon and southern and western Chad in February, June, and November, with much of the region experiencing its coldest or second-coldest minimum temperatures on record. Southern Cameroon observed minimum temperatures above the 90th percentile, particularly in April, May, July, and October. Eastern CAR also experienced minimum temperatures above the 90th percentile in April.

(ii) Precipitation

Most of the rainfall in Central Africa is tied to the summer season across both sides of the equator. In the northern part of the region, greater rainfall totals typically begin after April and extend until October, giving way to heavier rainfall in the southern part of the region from October to April. Closer to the equator, rainfall is persistent throughout the year and changes in intensity due to the north–south movement of the Intertropical Convergence Zone. On average, rainfall totals are highest in coastal Cameroon, which receives just over 2000 mm of rainfall. This region received below-average rainfall in 2022, with deficits exceeding –250 mm, yielding rainfall totals below the 10th percentile. Annual rainfall deficits extended from coastal Cameroon to coastal Gabon, ranking below the 30th percentile from Equatorial Guinea to coastal Gabon. Farther inland, central Chad to southeastern DRC experienced annual rainfall surpluses. From central to southern Chad, a tight north–south gradient in annual precipitation existed, from around 200 mm in central Chad to over 1000 mm in southern Chad (Fig. 7.26a). Central Chad observed annual rainfall surpluses upwards of +200 mm (Fig. 7.26b), ranking above the 90th percentile. Eastern Gabon to western DRC—an area that typically receives up to 1800 mm of rainfall each year—experienced rainfall surpluses of over +150 mm, yielding a rainfall ranking of greater than the 90th percentile in a small area of central Congo (in the higher elevations near Djambala). Southeastern DRC typically receives around 1300 mm of rainfall each year. This region was drier than normal in 2022, as much as 300 mm below average, placing it below the 10th percentile.

Coastal Cameroon experienced nine months of near- to below-normal rainfall, especially in March, June, and August, which saw deficits of up to –100 mm. Rainfall deficits up to –50 mm in August extended into northern Congo, resulting in monthly rainfall below the 10th percentile from southwestern Cameroon to northern Congo and below the 30th percentile around coastal Cameroon. Farther north, the beginning of the rainy season lasting from April to June resulted in seasonal rainfall surpluses of +20 mm to +60 mm, particularly over CAR and southern Chad.

These surpluses increased, as up to 275 mm of precipitation fell in northern Cameroon, southern Chad, and throughout most of CAR in July and September. This resulted in seasonal (July–September) and monthly (July and September) rainfall above the 90th percentile for much of the region. In southeastern DRC, significant deficits were observed in January (–50 mm to > –100 mm) and February/March (–50 mm to –70 mm), resulting in the driest month (January) and three-month (January–March) period on record.

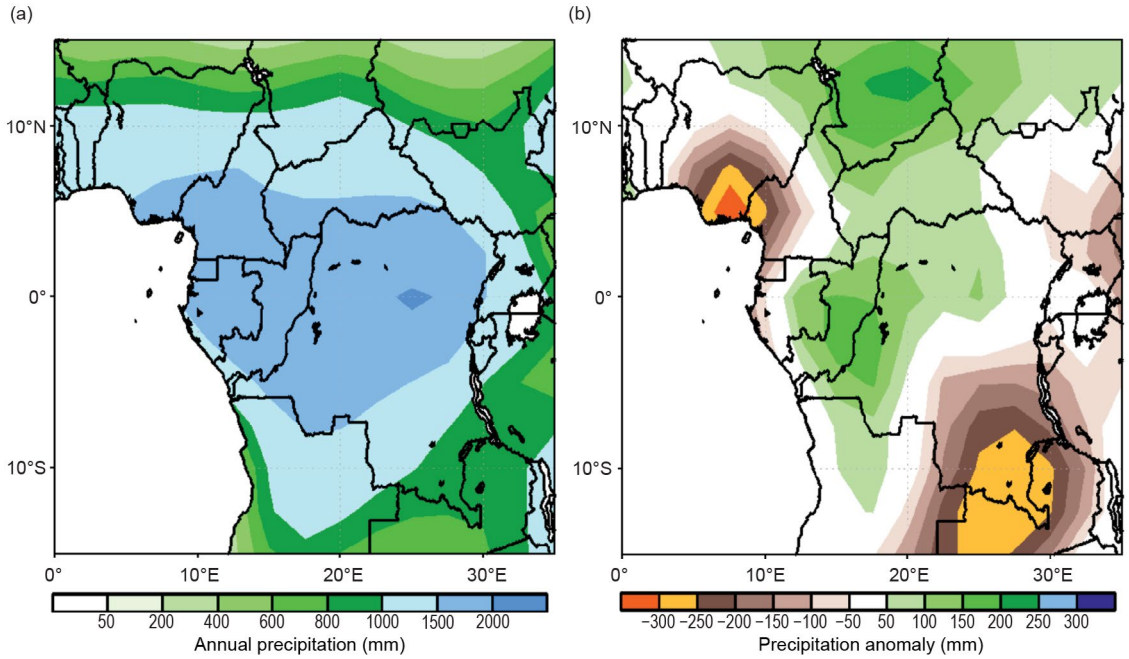

Fig. 7.26. Cumulative annual (a) precipitation totals and (b) precipitation anomalies in 2022 for Central Africa (mm; 1991–2020 base period). (Source: GPCP data, NOAA/NCEP.)

(iii) Notable events and impacts

According to the U.S. Agency for International Development, heavy rainfall from June to October triggered extensive flooding in 19 of Chad's 23 provinces and affected more than a million people. Following months of persistent heavy rainfall, over 190,000 people were displaced in and around the capital city of N'Djamena after up to 160 mm of rain fell in 24 hours beginning on 2 August. According to the United Nations, 22 people were killed and approximately 55,000 houses were damaged or destroyed due to flooding in July and August. The U.S. ambassador declared the need for humanitarian assistance in September, resulting in the distribution of cash funds, shelter, water, sanitation, hygiene, and food. Flooding occurred during the season of heightened malnutrition risks, resulting in more than 2.1 million people across Chad requiring emergency food assistance.

The aforementioned flooding was part of a widespread pattern that also led to heavy rains and flooding in the far north region of Cameroon. Flooding began in mid-August, and by September had affected more than 150,000 people, damaged over 18,000 houses, destroyed over 27,000 hectares of farmland, and killed over 5800 livestock in the departments of Mayo-Danay, Logone-et-Chari, and Mayo-Tsanaga. In addition, a reported 200 mm of rain fell in 48 hours ending on 11 August in the coastal city of Douala in southwest Cameroon. On the same day, heavy rainfall exceeding 100 mm according to the NOAA's Climate Prediction Center satellite rainfall estimates version 2 (RFE2) triggered landslides that killed five people in the northwest town of Widikum.

DRC also experienced a destructive landslide during 12–13 December that killed 169 people and displaced over 5000 households in the capital city of Kinshasa after heavy rainfall exceeding 80 mm, according to the RFE2.

4. EAST AFRICA

—E. Bekele, Z. T. Segele, and W. M. Thiaw

The Greater Horn of Africa (GHA), or East Africa, encompasses 11 countries and extends 12°S–24°N and 21°E–52°E. Its northern sector comprises Sudan, South Sudan, the northern two-thirds of Ethiopia, Eritrea, Djibouti, and the northern two-thirds of Somalia. Southern Somalia, southern and southeastern Ethiopia, Kenya, northern Tanzania, Uganda, Rwanda, and Burundi are in its equatorial sector, while the southern sector encompasses central and southern Tanzania. The region has a complex terrain, with elevation ranging from about 160 m below sea level at Ethiopia's northern exit of the Rift Valley to more than 5000 m above sea level at glaciated Mount Kilimanjaro. This complex topography is further typified by the presence of large lakes and is reflective of multi-faceted climate zones modulated by local and large-scale forcing such as the deep convective and moisture convergence zone, the El Niño–Southern Oscillation, the Indian Ocean dipole, the Madden-Julian Oscillation, and tropical–extratropical interactions. Rainfall is bimodal in the equatorial sub-region, with two distinct rainfall seasons in March–May (MAM) and October–December (OND). Seasonal rainfall is unimodal in the northern and southern sectors, spanning November–April in the south and June–September (JJAS) in the north.

(i) Temperature

Annual mean temperatures exceeded 26°C over most of Sudan, Somalia, Djibouti, Eritrea, eastern Ethiopia, and Kenya (Fig. 7.27a). Although it was anomalously warm over Ethiopia (1.5°C–2°C above normal), annual mean temperatures were less than 20°C across most of central

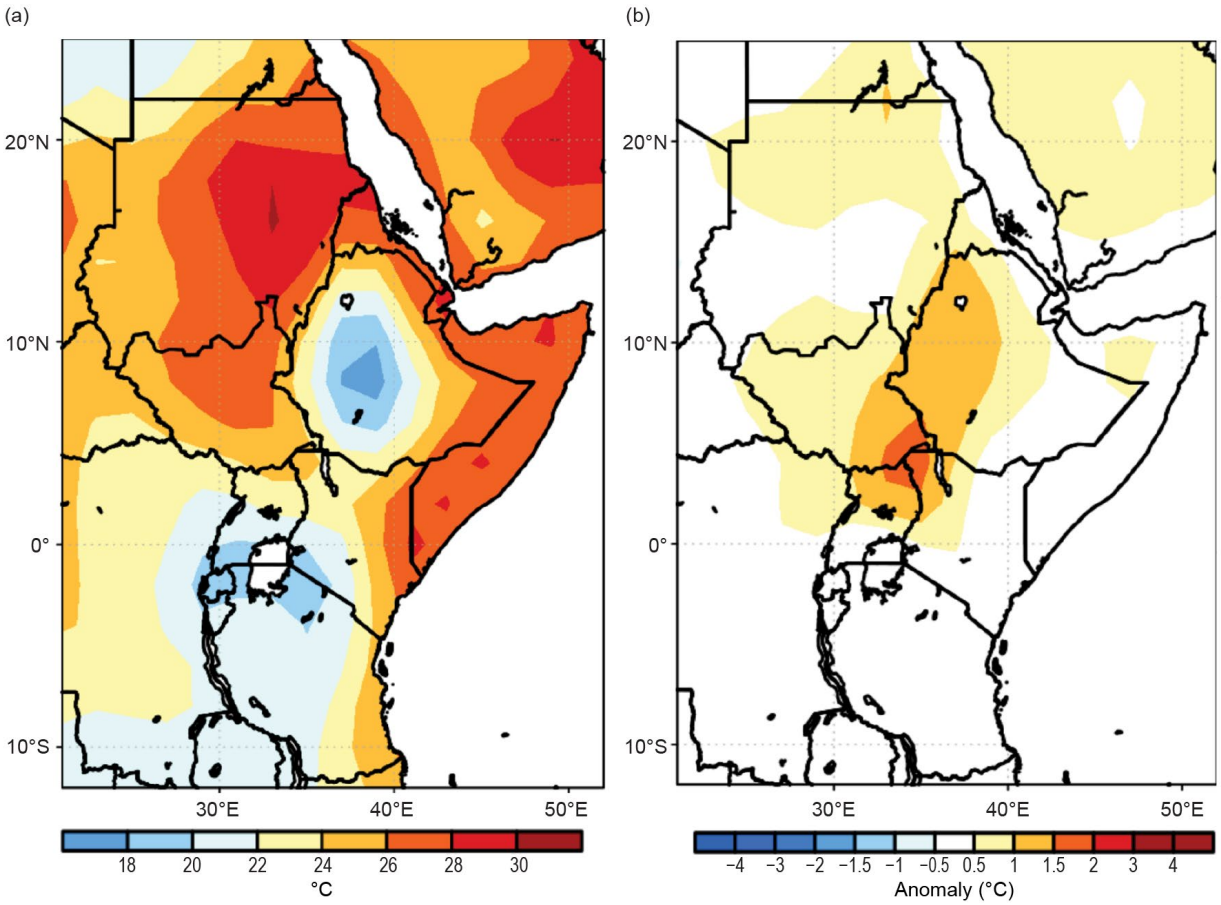

Fig. 7.27. Annual (a) mean temperature and (b) mean temperature anomalies (°C; 1991–2020 base period) in 2022 for East Africa. (Source: NOAA/NCEP.)

Ethiopia and in the Lake Victoria regions of equatorial East Africa (Fig. 7.27b). Anomalous warm mean temperatures were most pronounced during March–May over Ethiopia, South Sudan, Sudan, and northern Uganda due to higher-than-average minimum and maximum temperatures. On the other hand, seasonal mean temperatures were 0.5°C–1.5°C below average over eastern Tanzania, southeastern Ethiopia, and parts of Sudan during June–September.

Annual maximum temperatures exceeded 36°C in central and eastern Sudan but were 24°C–26°C across central Ethiopia and the Great Lake regions of East Africa. However, annual maximum temperatures were 2°C–3°C above normal across the Karamoja cross-border regions of Uganda, South Sudan, Kenya, and Ethiopia. Annual minimum temperatures exceeding 24°C were recorded in the coastal regions of Sudan, Eritrea, Djibouti, Kenya, Somalia, and Tanzania, while central Ethiopia and parts of Tanzania had annual minimum temperatures below 16°C. The greatest negative annual minimum temperature anomalies of >–3°C were observed over Tanzania during June–September.

(ii) Precipitation

Annual rainfall surpassed 1000 mm across western Ethiopia, parts of South Sudan, Uganda, Rwanda, Burundi, and northwestern and southern Tanzania (Fig. 7.28a). Western Kenya, central Ethiopia, eastern South Sudan, northeastern Uganda, and much of Tanzania received rainfall between 600 mm and 1000 mm. Totals were less over northern Sudan, Eritrea, Djibouti, southeastern Ethiopia, northeastern Kenya, and Somalia, with amounts between 50 mm and 600 mm. Overall, rainfall was below normal over much of equatorial East Africa (Fig. 7.28b).

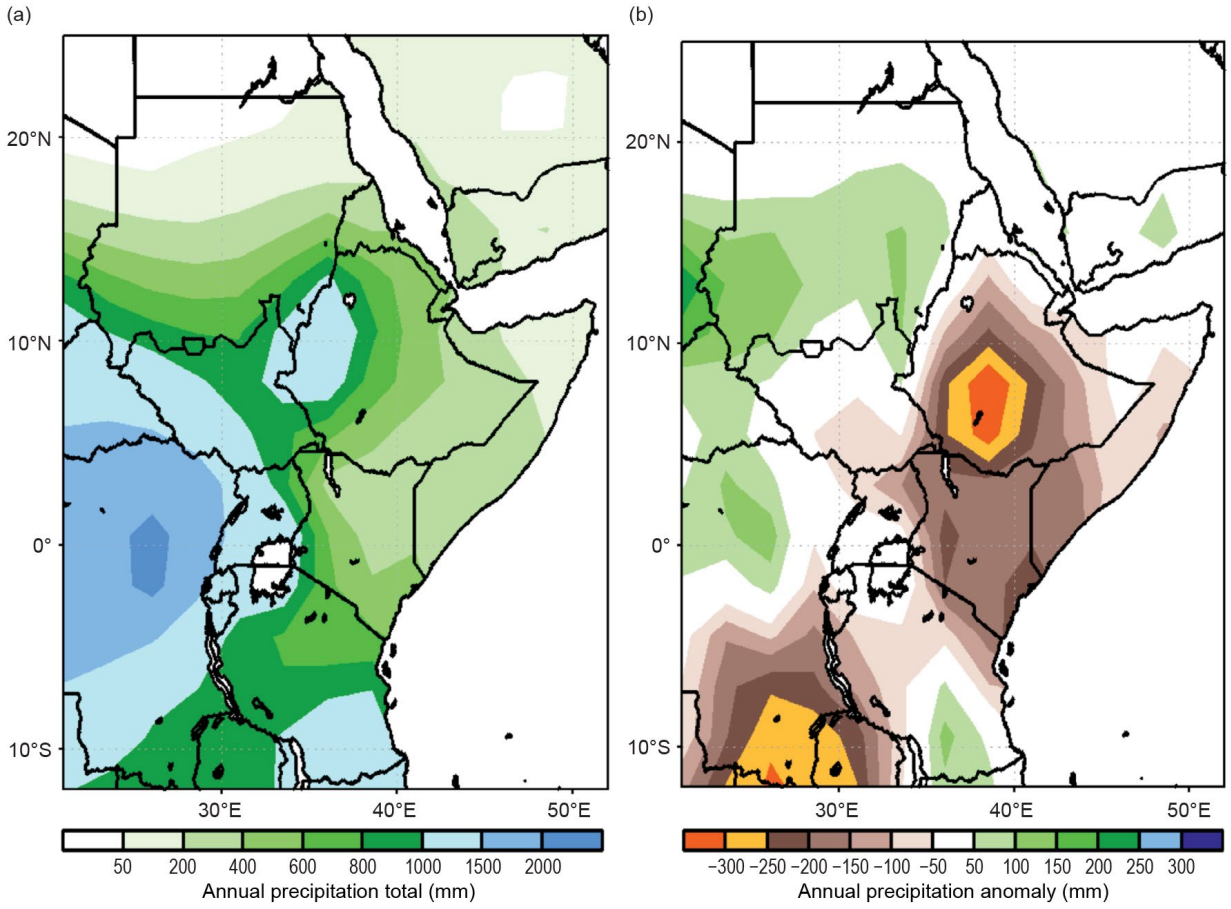

Fig. 7.28. Cumulative annual (a) rainfall totals and (b) rainfall anomalies (mm; 1991–2020 base period) in 2022 for East Africa. (Source: GPCP, NOAA/NCEP.)

Negative rainfall anomalies of –100 mm month^{-1} began in March over Tanzania and extended into Kenya, Somalia, and southern Ethiopia in April and May. Annual rainfall deficits exceeded –250 mm (–150 mm) over parts of southern Ethiopia (Kenya).

Annual rainfall was below the third percentile over southern Ethiopia and below the 10th percentile over much of Kenya and central Ethiopia. The dryness over southern and equatorial regions was pronounced during April, May, and October, and contributed to the excessively deficient MAM and OND rainfall seasons. In particular, during MAM, many locations in the equatorial regions received rainfall below the 10th percentile of their respective records.

(iii) Notable events and impacts

Over 100 mm of rainfall per day on average was observed over local areas in Sudan and upstream areas of northwestern Ethiopia during the June–September season, according to RFE. The annual and JJAS rainfall over central and western Sudan was above the 90th percentile. These persistent heavy rains led to widespread flooding in many places in Sudan.

According to the United Nations and Sudan's Humanitarian Aid Commission, around 226,200 people were affected by flooding and heavy rains across 15 states as of 28 August 2022. The most affected states were Gedaref, Central Darfur, South Darfur, White Nile, Kassala, River Nile, and West Darfur. Nine other states were also affected: West Kordofan, South Kordofan, North Kordofan, East Darfur, Sennar, Al Jazirah, Khartoum, and North Darfur. The rains and floods destroyed at least 13,200 houses and damaged another 34,200 since the beginning of the rainy season in June. Government authorities reported that 89 people died and more than 30 people were injured.

A large part of equatorial Eastern Africa (especially in Kenya, Somalia, and Ethiopia) experienced consecutive failed rainy seasons during OND 2020 through 2022. The annual total rainfall for 2022 was the lowest on record since 1991 in portions of equatorial East Africa. The March–May season was exceptionally dry over Tanzania, Kenya, central Somalia, and southern Ethiopia. Northeastern Tanzania and southern Ethiopia recorded deficient rainfall totals below the third percentiles of their historical records. Similarly, most of Kenya, south-central Somalia, and southern Ethiopia received 50 mm–150 mm below their average seasonal rain during OND 2022.

According to the U.S. Agency for International Development Famine Early Warning Systems Network (FEWS NET), the five-season drought (ongoing for 2.5 years) is the most extensive and persistent drought event in decades, leading to crop failure, millions of livestock deaths, water scarcity, and soaring staple food prices.

5. SOUTHERN AFRICA

—A. C. Kruger, C. McBride, M. Robjhon, W. M. Thiaw, and S. Dirkse

Southern Africa extends from about 5°S to 35°S and comprises Angola, Namibia, Zambia, Botswana, Zimbabwe, Malawi, South Africa, Lesotho, Eswatini, and Mozambique. The region is characterized by two main seasons: the wet and warm season from November of the previous year to April, and the dry and cold season from May to October.

(i) Temperature

Annual mean temperatures below 22°C dominated the central and southern sectors of southern Africa, whereas temperatures up to 26°C were observed in northwestern Angola and Mozambique (Fig. 7.29a). Annual mean temperatures were near normal across most areas, except southwestern Angola and northwestern Namibia, where abnormally low temperatures, with negative anomalies of up to –1.5°C, were observed (Fig. 7.29b). South Africa experienced a warm

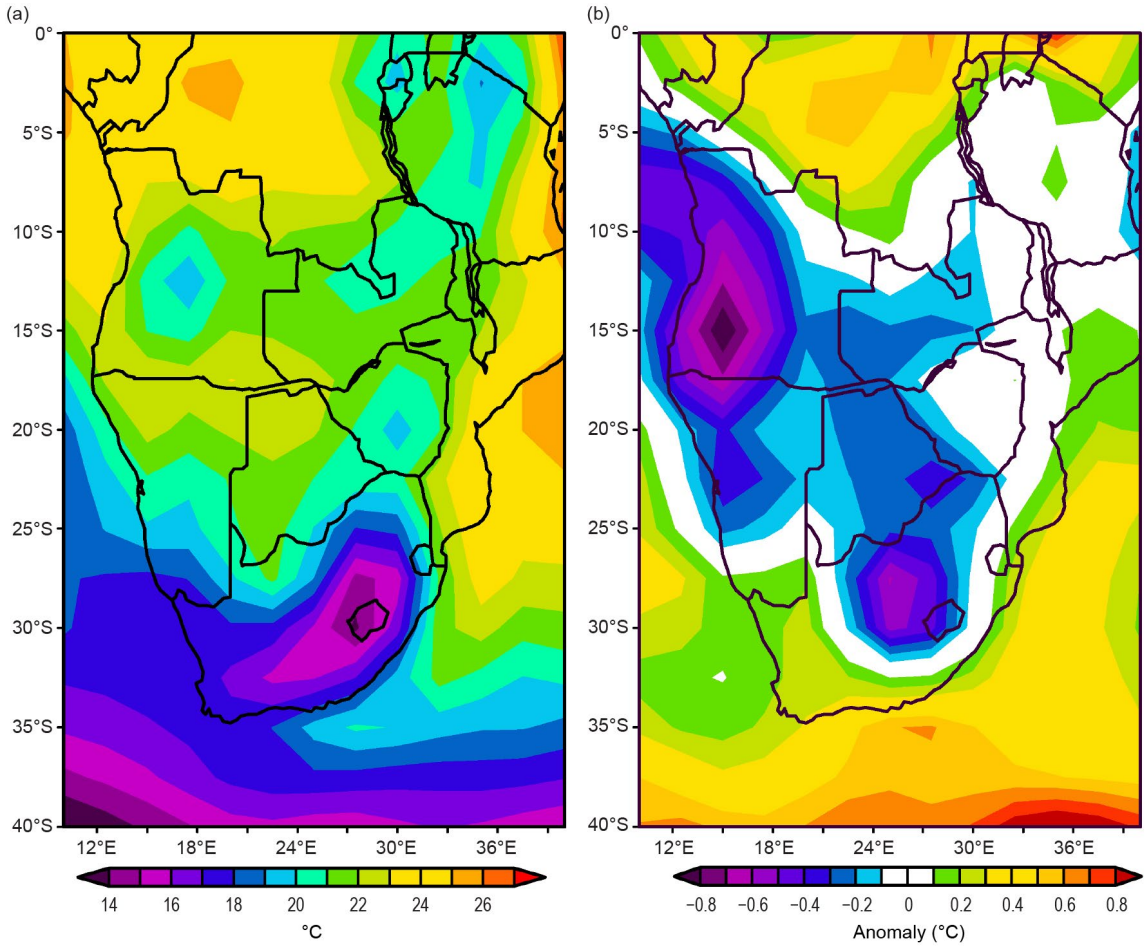

Fig. 7.29. Annual (a) mean temperatures and (b) mean temperature anomalies (°C; 1991–2020 base period) for southern Africa. (Source: NCEP/NCAR.)

year, especially in the western interior and southern and eastern coastal regions. The annual mean temperature anomaly for 2022, based on the data of 26 climate stations, was about 0.4°C above average, the fourth highest on record since 1951 (Fig. 7.30). A warming trend of +0.16°C per decade is indicated for the country, statistically significant at the 5% level.

Seasonally, the warmest period was austral spring (September–November), when abnormally high mean temperatures (anomalies of up to +2°C) were observed over most areas of South Africa, parts of Namibia, and portions of Botswana (not shown). October was the warmest month, with maximum temperatures above 36°C across the central sector, including southern Angola, western Zambia, much of Botswana, western Zimbabwe, and western Mozambique, which corresponded to anomalies as high as +5°C in eastern Angola, northwestern Zambia, western South Africa, southeastern Namibia, and southern Botswana, placing this October among the three warmest Octobers on record.

The coldest season occurred during austral winter (June–August), when minimum temperature dropped below 10°C across the southern two-thirds of southern Africa, with negative anomalies as low as –3.5°C in Angola and northern Namibia (not shown). August was the coldest month of 2022 and the coldest August on record, when minimum temperatures reached as low as 5°C below normal over Angola, western Zambia, and northern Namibia.

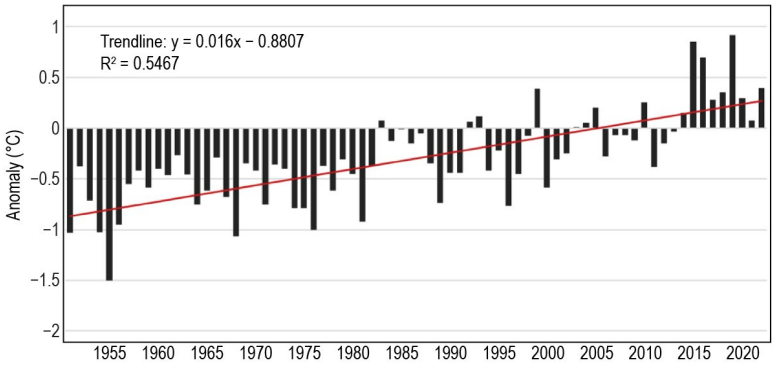

Fig. 7.30. Time series of annual average surface temperature anomalies (°C; 1991–2020 base period) over South Africa based on 26 climate stations for the period 1951–2022. The dark red line shows the linear trend. (Source: South African Weather Service.)

(ii) Precipitation

Annual rainfall exceeded 1000 mm over northern Angola, Malawi, northern Mozambique, eastern Lesotho, and eastern South Africa, varied between 600 mm and 1000 mm across Zambia, and totaled less than 600 mm across the central and western sectors of the region (Fig. 7.31a). Annual rainfall was well above normal in central South Africa and Lesotho, with surpluses of up to 300 mm, placing the year above the 90th percentile in their historical records.

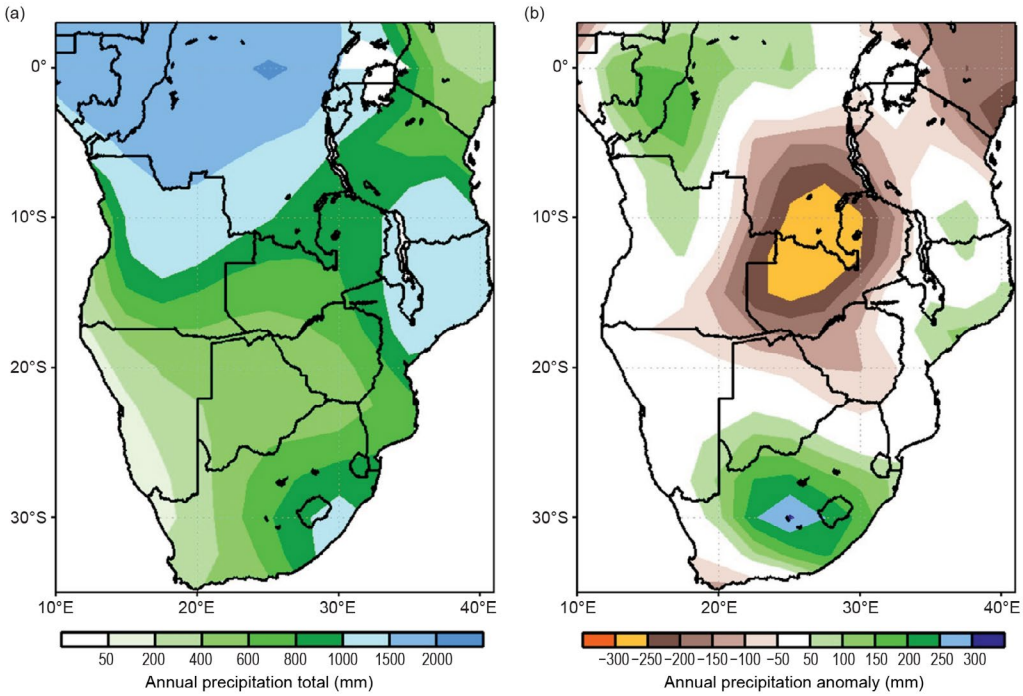

Fig. 7.31. Annual (a) rainfall totals and (b) rainfall anomalies (mm; 1991–2020 base period) in 2022 for southern Africa. (Source: GPCP, NOAA/NCEP.)

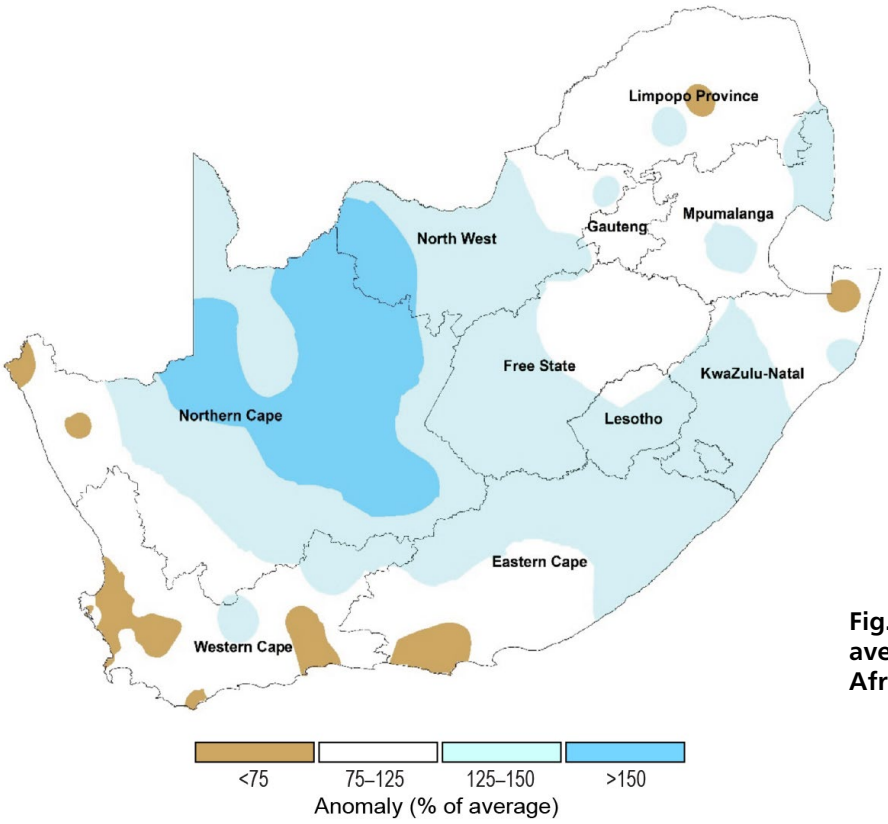

However, annual rainfall amounts were well below normal in Zambia, where deficits reached –300 mm (Fig. 7.31b; 3rd to 10th percentiles). Additionally, extensive areas in central South Africa received well-above-normal rainfall, but there were clear signals of drying in the western parts of the Northern Cape and Western Cape Provinces. Dry conditions persisted in parts of the Eastern Cape Province (Fig. 7.32).

Fig. 7.32. Annual rainfall anomalies (% of 1991–2020 average) in 2022 for South Africa. (Source: South African Weather Service.)

Seasonally, rainfall was above normal in the southern tier of southern Africa during December–February (DJF) 2021/22, March–May, and September–November, with the largest surpluses of over 100 mm recorded across eastern South Africa, Lesotho, Eswatini, and coastal Mozambique during March–May. November was the wettest month, where anomalies of up to +100 mm were observed in central South Africa, Lesotho, eastern Zimbabwe, central Mozambique, and parts of northern Angola (90th to 97th percentile, not shown).

Rainfall was more than 100 mm below normal over the northern sector extending from eastern Angola, Zambia, and Malawi, to northern Mozambique during DJF. February was the driest month, with rainfall deficits surpassing –50 mm across eastern Angola, Zambia, north-eastern Botswana, Zimbabwe, and southern Mozambique (not shown).

(iii) Notable events and impacts

Tropical Storm Ana caused severe flooding and infrastructure damage in Nsanje in the Chikwawa District of Malawi, with local rainfall totaling up to 200 mm during 22–25 January. This resulted in 64 deaths, 206 injuries, and more than 940,000 people affected, according to the Emergency Events Database (EM-DAT), an international disaster database. The government in Malawi declared a state of disaster on 26 January due to the substantial impacts of the storm.

During 11–14 March, Category 3 Cyclone Gombe, with sustained winds of 185 km h^{-1} and a 24-hour rainfall total over 200 mm, triggered flooding in the Nampula, Zambezia, Sofala, Beira, Tete, and Niassa Provinces in Mozambique. The impacts from the storm left 63 people dead, 108 injured, and over 736,000 affected.

Heavy rain with a 24-hour accumulation of over 300 mm during 8–18 April led to flooding and landslides in Umlazi Town in Durban in the KwaZulu-Natal Province of South Africa, leading to 544 deaths, 50 injuries, and affecting more than 140,000 people. The government in South Africa considered this storm event among the worst in history and declared a nation-wide state of disaster. Infrastructure was badly damaged, more than 4000 homes were destroyed, and more than 40,000 people were displaced from their homes. The event was caused by a cut-off low that moved from the interior eastward over the ocean before strengthening. The wet conditions continued in May, with more damaging floods in the eastern KwaZulu-Natal Province.

Although August had some heavy rainfall episodes over parts of the southwestern, southern, and eastern coastal regions, some parts of the Eastern Cape Province remained dry; the Nelson Mandela Bay Metropole in the Eastern Cape was the hardest hit by water shortages due to drought after seven years of below-normal rainfall. However, rainfall brought some relief to some places in September and October. In November, normal to above-normal rainfall occurred mainly over the eastern half of the country, as well as isolated areas of the Northern and Western Cape. Some urban areas experienced severe flooding; more than 300 families at the Nancefield Hostel in Soweto, Gauteng Province, were left destitute as water from heavy floods entered their homes from 11 to 13 November.

A cold front with its associated cut-off low-pressure system along with a reported 24-hour rainfall of more than 100 mm on 21 June brought sub-zero temperatures, snowfall, strong winds, and freezing rain to Helmeringhausen in the southern parts of the western escarpment and central regions in Namibia. This led to road and infrastructure damage and livestock deaths.

A convective hailstorm with strong winds on 5 November destroyed infrastructure in the Nsingizini and Nsubane communities under the Hosea and Somntongo in the Shiselweni region of Eswatini, which affected over 1000 people.

On 14 December, a thunderstorm with strong winds, hail, lightning, and heavy rain totaling 85 mm in less than an hour impacted Windhoek (capital of Namibia), killing two people and causing costly infrastructure damage.

6. WESTERN INDIAN OCEAN ISLAND COUNTRIES

—G. Jumaux, K. R. Dhurmea, A. Abdallah, B. Andrade, M. Robjhon, and W. M. Thiaw

The Western Indian Ocean island countries consist of Madagascar, Seychelles, Comoros, Mayotte (France), Réunion (France), Mauritius, and Rodrigues (Mauritius). There are two distinct main seasons: a warm and wet period spanning from November of the antecedent year to April and a cold and dry season lasting from May to October.

Overall, temperatures in 2022 were near normal, but lower than those of the last decade (Fig. 7.33). Near-normal temperatures were associated with large-scale prevailing environmental conditions of La Niña and a negative Indian Ocean dipole. Annual rainfall was below normal over Comoros and near normal across the rest of the Western Indian Ocean island countries (Fig. 7.33).

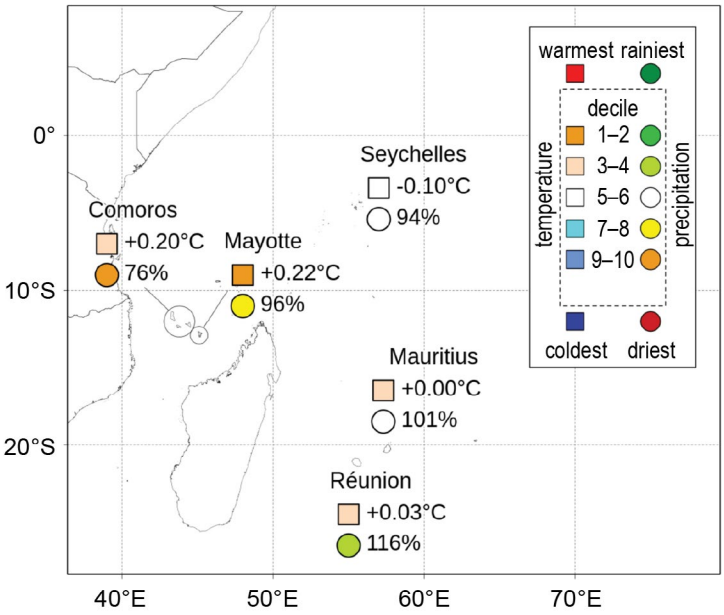

Fig. 7.33. Mean annual temperature anomalies (°C, squares), annual rainfall ratio to normal (%, circles), and their respective deciles for the western Indian Ocean islands countries in 2022 (top right inset box). Base period is 1991-2020. (Sources: Météo France and Meteorological Services of Mauritius, Seychelles, and Comoros.)

(i) Temperature

In Madagascar, annual mean temperatures were 20°C–22°C across the central highlands and up to 26°C along the west coast (Fig. 7.34). Although annual mean temperatures were near normal over the island, their seasonal evolutions showed above-normal mean temperatures of up to +1°C. Maximum temperatures ranked between the 85th and 97th percentile across central Madagascar during December–February 2021/22, and below-normal mean temperatures up to –1°C (below the 10th percentile) and minimum temperatures that ranked between the 3rd and 10th percentile in the northern parts during June–August.

The annual mean temperature over Réunion (based on three stations) was 0.03°C above normal, the 16th highest since records began in 1968 (Fig. 7.33). March, at 0.8°C above normal, was among the three warmest on record. Most months observed near- or slightly below-normal temperatures, especially during austral winter, which was related to a strong negative Indian Ocean dipole and below-normal sea-surface temperatures around the island.

In Mauritius, the annual mean temperature (based on two stations at Vacoas and Plaisance) was near normal. The maximum temperature was 0.18°C below average, and the minimum was 0.18°C above average. May 2022 was the warmest May on record with a mean temperature anomaly of +0.94°C. With a well-established La Niña, below-normal temperatures prevailed during October–December, notably at night.

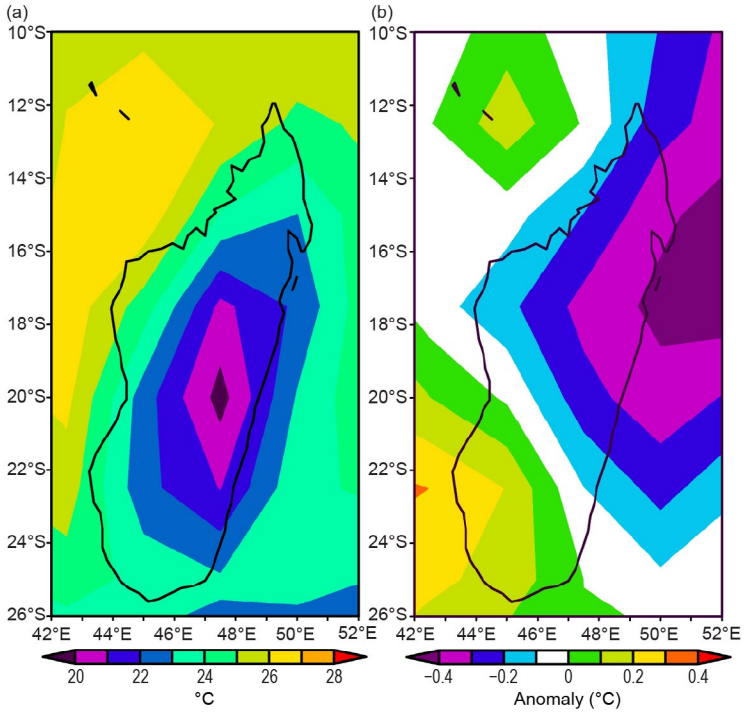

Fig. 7.34. Annual (a) mean temperatures and (b) mean temperature anomalies (°C; 1991–2020 base period) in 2022 for Madagascar. (Source: NOAA/NCEP.)

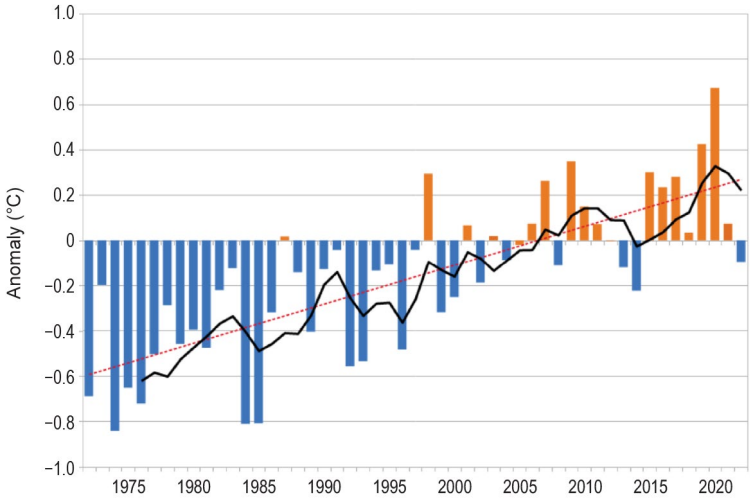

Fig. 7.35. Time series of Seychelles annual mean temperature anomalies (°C; 1991–2020 base period) for the period 1972–2022. The black line is the five-yr running mean and the dotted red line represents the linear trend. (Source: Seychelles Meteorological Authority.)

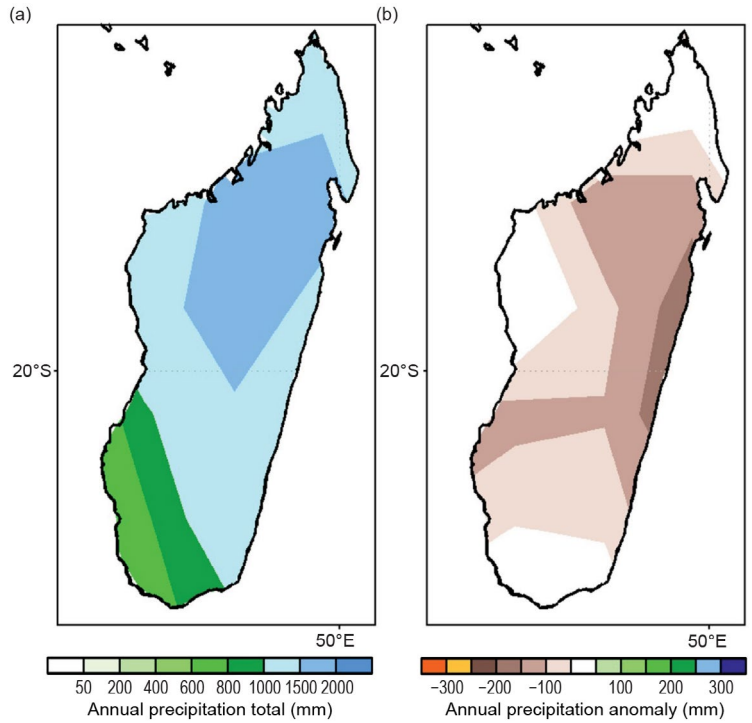

Fig. 7.36. Annual (a) total rainfall and (b) total rainfall anomalies (mm; 1991–2020 base period) in 2022 for Madagascar. (Source: NOAA/NCEP.)

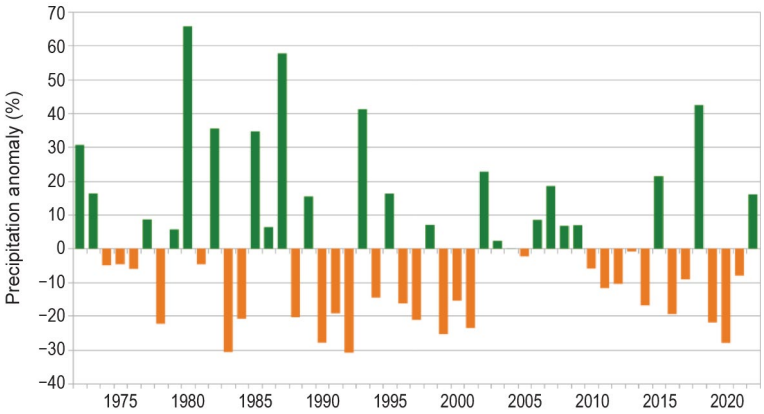

Fig. 7.37. Annual rainfall anomaly time series (%; 1991–2020 base period) in Réunion for the period 1972–2022. (Source: Météo-France.)

In Comoros, the annual mean temperature was the ninth highest since 1981 (0.2°C above normal). December–April was warmer than normal, with the exception of February. During August–October, temperatures were below normal.

In Mayotte (Pamandzi Airport), the annual mean temperature was the 11th highest in the 62-year record, at 27.26°C. The first half of the year was 0.41°C above normal, and the second half was near normal (+0.02°C). The annual maximum and minimum temperatures were above normal by 0.32°C and 0.12°C, respectively.

At Seychelles, the annual mean temperature was 0.1°C below normal (Fig. 7.35). Nearly all months were near normal except March and April, which were above normal, and July and August, which were significantly below normal. July 2022 was the second-coldest July on record (anomaly of –1.1°C).

(ii) Precipitation

Annual rainfall was below normal across most of Madagascar, particularly in the eastern portions of the island, where the annual total was as much as 200 mm below normal (Fig. 7.36b). Seasonally, December–February 2021/22 rainfall was predominantly below normal, with the largest deficits exceeding –150 mm and ranking below the third percentile in the southwest.

The annual rainfall total over Réunion was 116% of normal (Fig. 7.37). The rainy season (December–April) produced 144% of normal precipitation, the fifth-wettest such period on record. Two tropical cyclones (Batsirai and Emnati) influenced the weather in February, the first one generating heavy rains. The dry season (May–November) was the third driest on record (68% of normal), which is often the case during a negative phase of the Indian Ocean dipole (see section 4f for details). October was the driest on record, while April was the wettest.

In Mauritius, normal mean annual rainfall of about 2040 mm was observed (average is 2019 mm). However, there was a marked

seasonal variability (Fig. 7.38). During February–April, above-normal rainfall was observed, with April being the second wettest in the last 20 years. During winter (July–October), rainfall was deficient, and this persisted into November and December.

In Comoros, total annual rainfall was 76% of normal and the fourth-lowest total since 1979. The start of the rainy season was delayed until February. The month of April and the late winter (August–September) were also wetter than normal. Most other months had rainfall deficits.

In Mayotte, total annual rainfall was 96% of normal. April and July were wet but five consecutive months from August to December, during the dry season and the early rainy season, were each drier than normal, leading to a 41% rainfall deficit in this period; this was the sixth-driest such period in the 62-year record.

In Seychelles, the total annual rainfall was 94% of normal, making 2022 the 26th-driest year since the start of the record in 1972. The rainfall was below normal in most months, but January and December were the wettest in 2022. October (18% of normal) was the third driest on record, while December (183% of normal) was the sixth wettest on record.

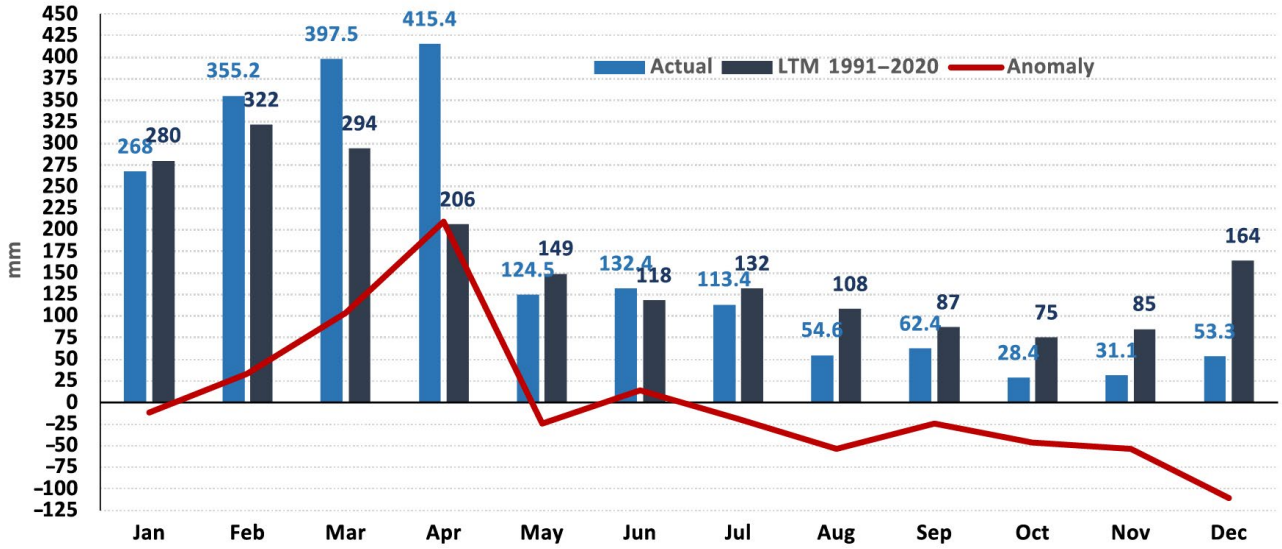

Fig. 7.38. Monthly rainfall totals for 2022 (blue bars), 1991–2020 mean (black bars), and 2022 anomalies (dark red line; 1991–2020 base period). Units are mm. (Source: Meteorological Services of Mauritius.)

(iii) Notable events and impacts

The 2021/22 rainfall season included 12 named tropical storms, including five tropical cyclones, which ranked the season as the fifth most active since 1998/99. Tropical storm Ana brought a total rainfall of 150 mm during 22–25 January, which resulted in floods, landslides, collapsed houses, and damaged infrastructures in the Analamanga Region, including Antananarivo in Madagascar, leading to 55 fatalities and more than 130,000 people affected.

Tropical Cyclone Batsirai, with sustained winds of 165 km h^{-1} and gusts up to 235 km h^{-1}, hit the eastern coast of Madagascar in the evening of 5 February. Its center made landfall just north of the city of Mananjary. Batsirai's impacts were the most violent in this sector of Madagascar for more than 25 years, as the region was exposed to the storm surge and to the strongest winds, with maximum gusts estimated up to 230 km h^{-1}. It brought 48-hour rainfall totals of up to 150 mm during 5–7 February, impacting Mananjary, Nosy Varika, Ikongo District, Manakara Atsimo, Fianarantsoa, and Ambositra in Madagascar and leading to 121 deaths and over 140,000 total people affected.

Prior to landfall on Madagascar, Batsirai affected weather conditions in Mauritius and Réunion from 1 to 5 February. The center of the cyclone passed 170 km north of Mauritius and 190 km north of Réunion. Réunion remained under the influence of the cyclone for a longer period, as Batsirai remained less than 220 km north of the island for 26 hours on 3 February. The storm influence was remarkable in the highlands (Fig. 7.39). Over the five-day period, the highest cumulative rainfall was 2044 mm at the Commerson Crater. Maximum hourly gusts exceeded 100 km h^{-1} at Gillot Airport for 32 consecutive hours, a new record at this station. The following maximum gusts were recorded: 135 km h^{-1} on the coast at the Port and 208 km h^{-1} in the highlands at Piton Maïdo.

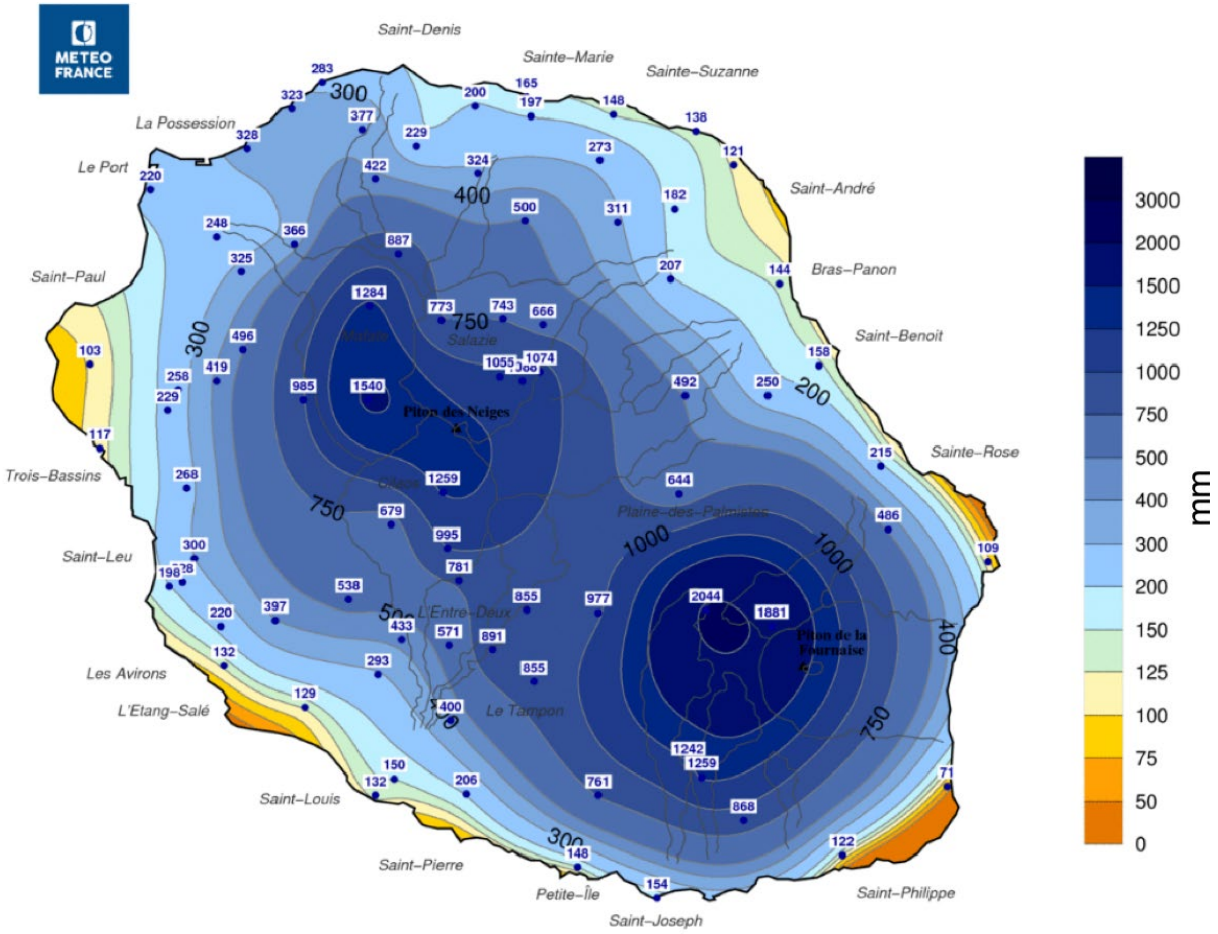

Fig. 7.39. Cumulative five-day rainfall (mm) in Réunion during tropical cyclone Batsirai (1–5 Feb 2022). (Source: Météo-France.)

f. Europe and the Middle East

—P. Bissolli (Ed.), H. Rösner, S. Bader, G. M. Bellido, C. Berne, O. Bochníček, L. Crhova, V. De Bock, M. Demircan, R. Deus, P. Drumond, M. Ekici, S. Hellström, M. Kendon, V. Khan, M. Lakatos, T. Likso, J. Mamen, I. Marcinonienė, M. Perčec Tadić, V. Pires, E. Rodriguez Guisado, B.Rösner, F. Rubek, S. Schimanke, S. Sensoy, S. Spillane, L. Trescilo, G. van der Schrier, and A. Willems

Throughout this section, 1991–2020 is the base period used for both temperature and precipitation, unless otherwise specified. European countries conform to different standards applied by their individual national weather services. All seasons mentioned in this section refer to the Northern Hemisphere. More detailed information can be found in the *Monthly and Annual Bulletin on the Climate* in Regional Association VI (RA VI) – European and the Middle East, provided by the World Meteorological Organization (WMO) RA VI Regional Climate Centre on Climate Monitoring (RCC-CM; http://www.dwd.de/rcc-cm). Anomaly information has been taken from Figs. 7.41–7.44 and aggregations of CLIMAT station data when national reports are not available. The length of national temperature and precipitation records for each country are provided in Supp. Table A7.1.

1. OVERVIEW

Based on the Global Historical Climate Network (GHCN) v4.0.1 dataset (Menne et al. 2018), Europe (36°N–72°N, 23°W–60°E) experienced its second-warmest year in its record with an anomaly of +1.0°C (1991–2020 base period; Fig. 7.40). An evaluation of several other datasets (WMO 2023) has shown that the 2022 annual average temperature for Europe (defined by the area of the WMO RA VI region) was likely between the second and fourth highest on record, with an anomaly between +0.7°C and +0.9°C compared to the 1991–2020 average. All countries reported above-normal annual temperatures (Fig. 7.41). Nationally, it was the warmest year on record for Spain (+1.7°C), Portugal (+1.4°C), Belgium (+1.2°C), France (+1.6°), Luxembourg (+1.1°C), the United Kingdom (+0.9°C), Ireland (+0.7°C), Switzerland (+1.6°C), Hungary (+1.1°C), Germany (+2.3°C), Italy (+1.1°C), Croatia (+1.2°C), Bosnia and Herzegovina (+1.1°C), Monaco (+1.4°C), Montenegro (+1.2°C), and Slovenia (+1.2°C). Many other countries reported an annual temperature among their four highest: Serbia (second warmest, +1.0°C), the Netherlands (third warmest, +1.1°C), Denmark (third warmest, +0.8°C), Finland (third warmest, +0.9°C), Romania (third warmest, +1.0°C), and Bulgaria (fourth warmest, +0.8°C). See Supp. Table A7.1 for a complete list of national temperature anomalies and rankings. Winter 2021/22 was warmer than normal across most of Europe due to a positive phase of the North Atlantic Oscillation (NAO; see further explanation in Lindsey and Dahlman 2009), which persisted throughout the season, with positive temperature anomalies in the Northern Hemisphere midlatitudes ranging from +1.0°C in France and Türkiye to above +3.0°C in southern European Russia and Kazakhstan (Fig. 7.42a). The most intense warmth in Eastern Europe was additionally caused by subtropical air from the south, which flowed to the north at the west flank of the Russian high. The season ended with an exceptionally warm February for all of Europe when the positive NAO phase was strongest, with anomalies above +2.0°C almost everywhere and even above +6.0°C in eastern parts of Europe.

Spring was slightly warmer than normal (anomalies around +1.0°C) in western and northern Europe while it was colder than normal (anomalies around –1.0°C) in much of Eastern Europe (Fig. 7.42b). This reflects an outstanding meridional circulation pattern with anticyclonic conditions in Western Europe and cyclonic conditions in Eastern Europe. France reported its warmest May on record, Italy and Slovenia their second warmest, and Luxembourg and Croatia their third warmest.

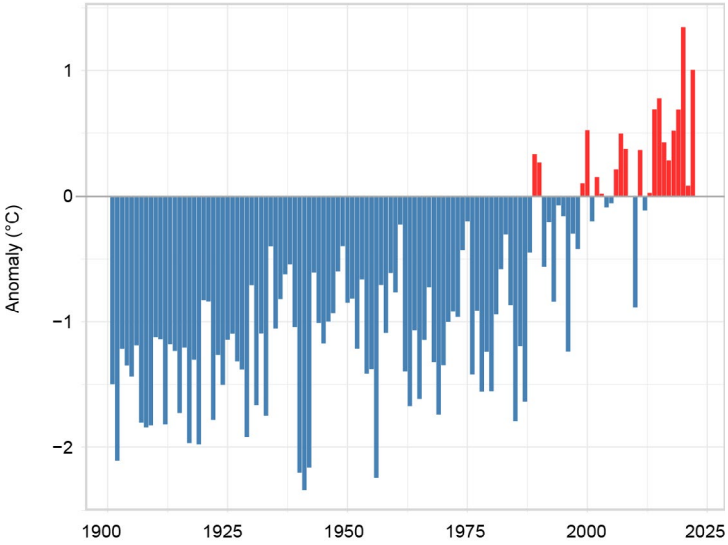

Fig. 7.40. Annual average land–surface temperature anomalies over the period 1900–2022 for Europe (36°N–72°N, 10°W–60°E) relative to the 1991–2020 base period. (Source: GHCN version 4.0.1 [Menne et al. 2018].)

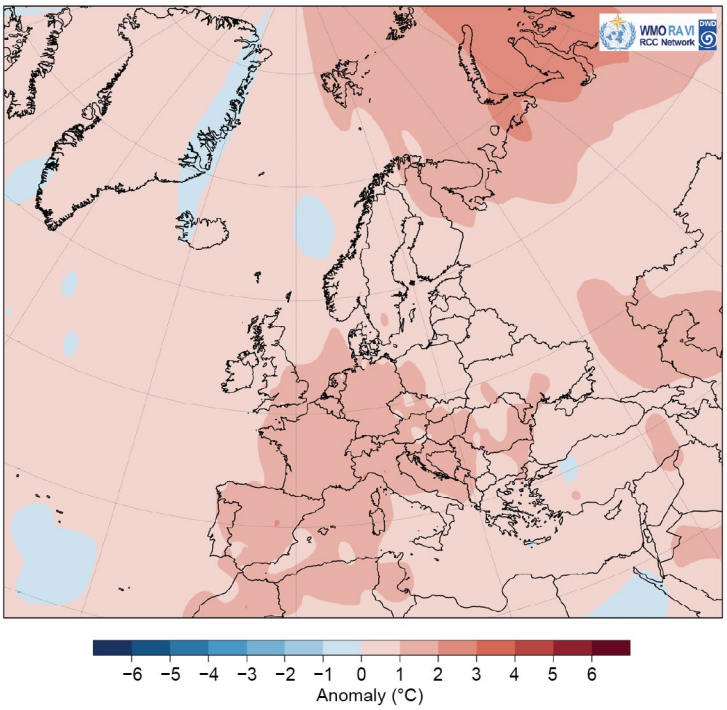

Fig. 7.41. Annual mean temperature anomalies (°C; 1991–2020 base period) for 2022. (Source: interpolated climate station and ship data, Deutscher Wetterdienst [DWD].)

Summer was exceptionally warm across all of Europe with large areas observing anomalies between +2.0°C and +3.0°C (Fig. 7.42c) as warm subtropical air from the southwest spread over much of the region up to the northeast and prevailed under the influence of high pressure. Portugal, Spain, and Hungary reported their warmest summer on record, Switzerland, Romania, Croatia, France, and Italy their second warmest, and Poland, the Russian Federation, the Netherlands, and Serbia their third warmest.

During autumn, anomalies were above +1.0°C across the western half of Europe (Fig. 7.42d), which was continuously influenced by subtropical air from the southwest. Only regions east of Germany and north of the Black Sea reported anomalies around or slightly below normal, since they were occasionally affected by cold air from the northeast. Spain had its warmest autumn on record, Italy and France their second warmest, Switzerland, the United Kingdom, the Netherlands, Luxembourg, Belgium, and Croatia their third warmest, and Denmark and Ireland their fourth warmest. It was the warmest October on record for France, Germany, Austria, Croatia, and Slovenia. December 2022 was colder than normal in northwestern Europe (below −4°C in Iceland) and warmer than normal in the southeast (up to +5°C in eastern Türkiye).

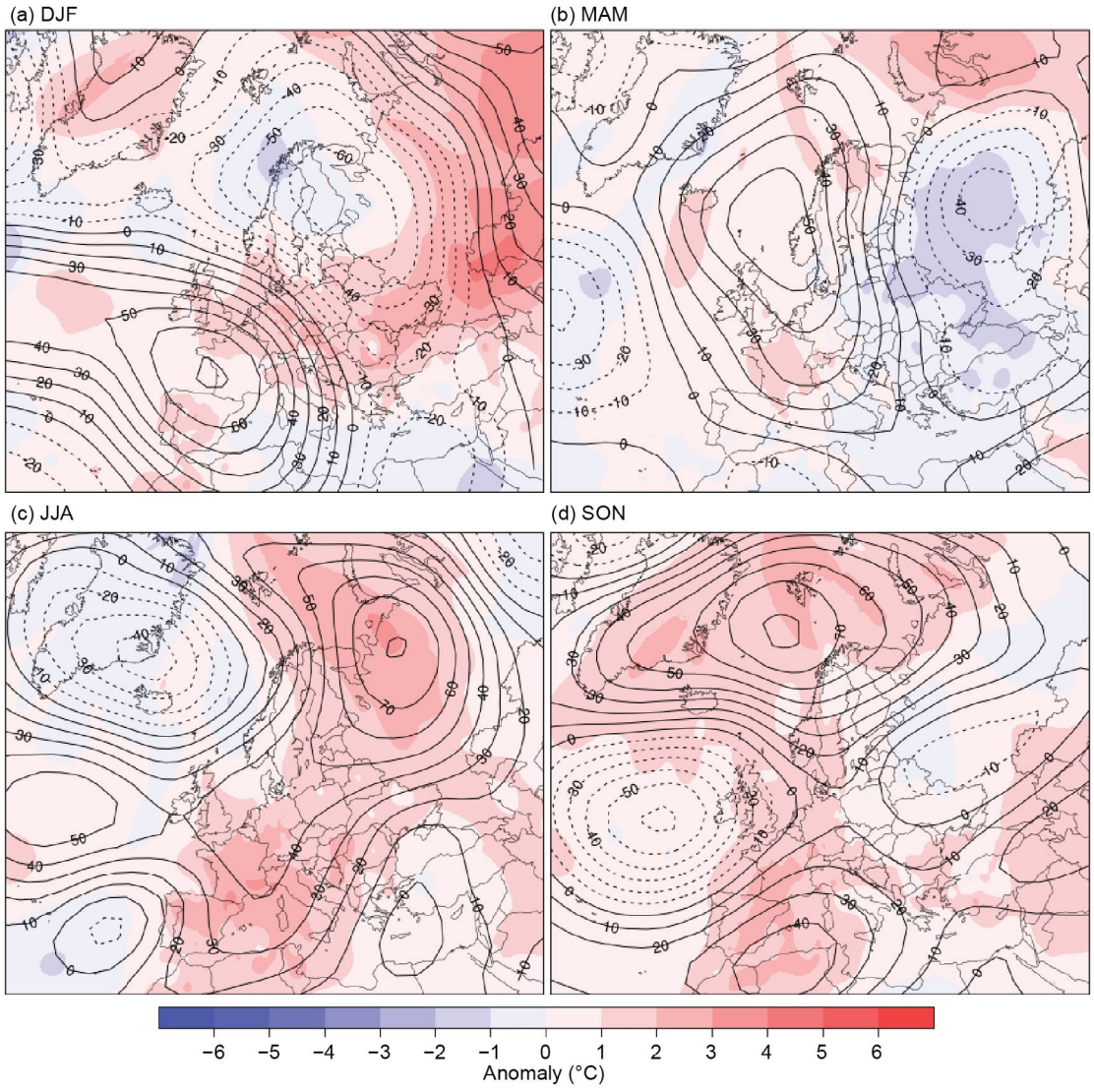

Fig. 7.42. Seasonal anomalies (1991–2020 base period) of 500-hPa geopotential height (contour; m) and surface temperature (shading; °C) using data from the NCEP/NCAR reanalysis and DWD, respectively, for (a) DJF 2021/22, (b) MAM 2022, (c) JJA 2022, and (d) SON 2022.

Annual precipitation was mostly near normal or drier than normal and mainly ranged between below 80% and 125% of normal (Fig. 7.43). Locally, precipitation below 60% of normal was observed in southeastern France, northern Spain, northwestern Italy, Estonia, the Middle East, and on the west coast of the Black Sea.

Winter 2021/22 was drier than normal, particularly on the Iberian Peninsula and in the Middle East with large parts receiving less than 60% of normal precipitation and less than 20% locally, revealing a severe winter drought in regions that normally receive most of their precipitation during the cold season (Fig. 7.44a). The dryness in southwestern Europe was caused by a relatively intense Azores high in combination with dry air advection from northwest Africa, while the Middle East was affected by dry air from the Arabian Peninsula. The winter months were drier than normal for almost all of the Iberian Peninsula and the Middle East (large areas below 40% of normal).

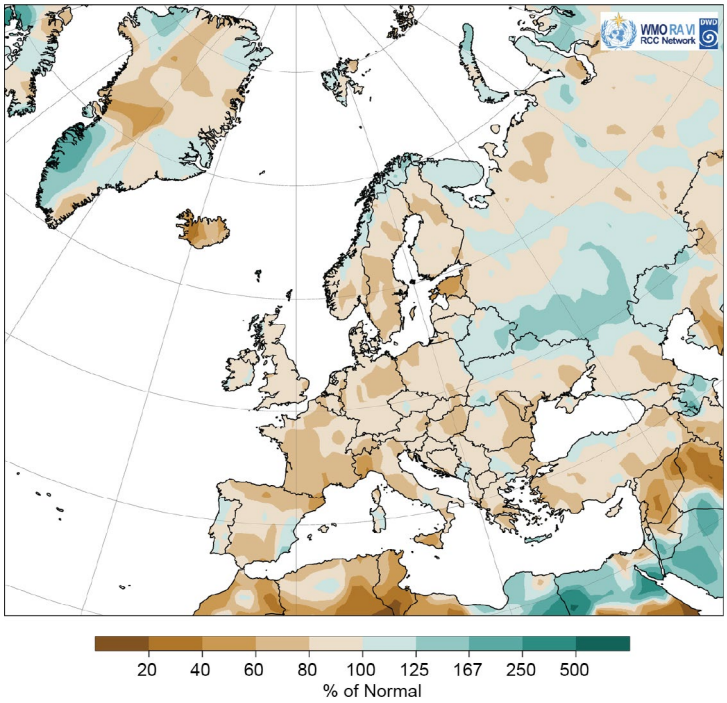

Fig. 7.43. European precipitation totals (% of 1991–2020 average) for 2022. (Source: GPCC, created by DWD.)

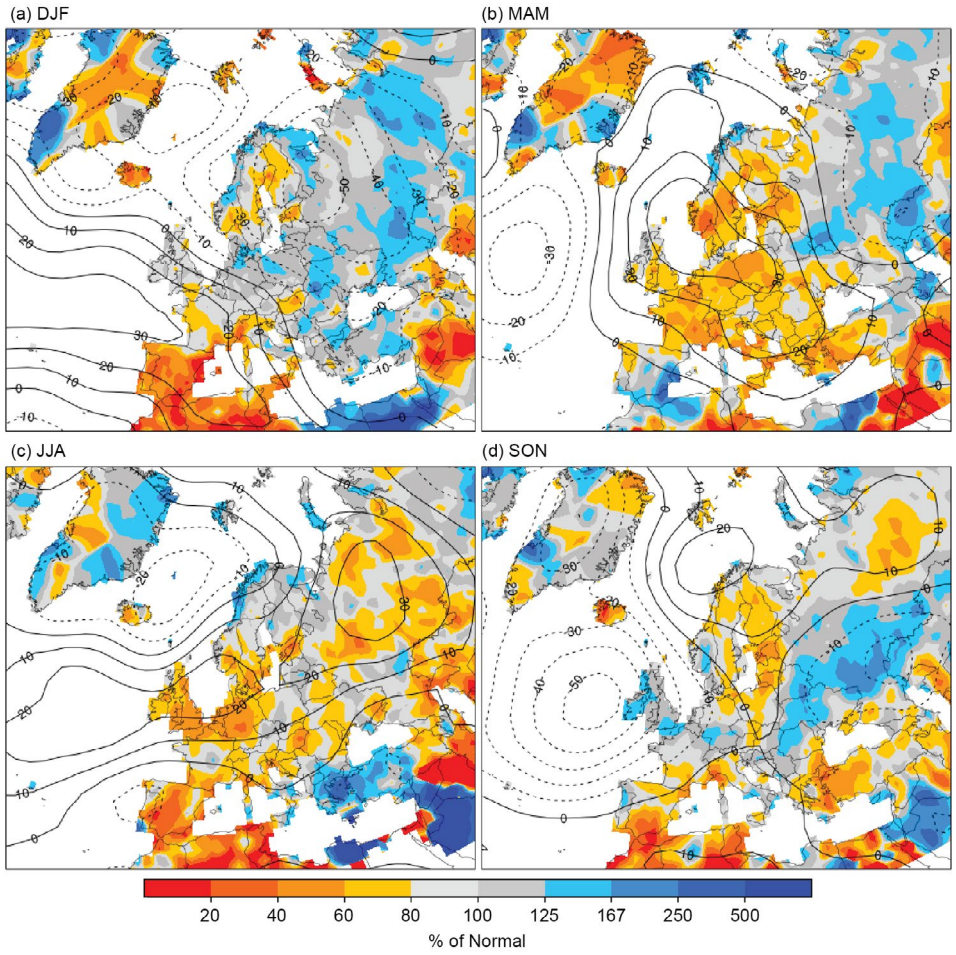

Fig. 7.44. Seasonal anomalies for 2022 (1991–2020 base period) of sea-level pressure (hPa) from NCEP/NCAR reanalysis (contours) for (a) DJF 2021/22, (b) MAM 2022, (c) JJA 2022, and (d) SON 2022. Colored shading represents the percentage of seasonal mean precipitation for 2022 compared with the 1991–2020 mean from GPCC (Schneider et al. 2018).

Spring was drier than normal across most of Europe, with large areas receiving only 60% to 80% of normal precipitation as high-pressure patterns over the continent prevailed (Fig. 7.44b). Above-normal precipitation was observed across most of Belarus, European Russia, and the Caspian Sea as well as most of the Iberian Peninsula, ending its winter drought. Iberia was affected by low-pressure developments over the North Atlantic, which expanded quite far to the south. Cyclonic conditions also occurred over Eastern Europe, expanding southward to the Caspian Sea region. However, not all eastern countries saw cyclonic conditions throughout spring. Poland and Belarus reported their driest March on record, and the Czech Republic had its third driest.

Summer was again a dry season, with most of Europe receiving between 50% and 90% of normal precipitation (Fig. 7.44c). Anticyclonic conditions dominated over much of the continent; however, eastern Mediterranean cyclones contributed to above-normal precipitation across the southern Balkans, Greece, western Türkiye, and large areas of the Middle East.

Autumn was wetter than normal for Eastern Europe with around 130% of normal precipitation where cyclonic conditions prevailed (Fig. 7.44d). Poland, Finland, and the Baltic countries as well as Greece, western Türkiye, and southern Spain received 60% to 80% of their normal precipitation and even lower in some localized areas. High-pressure conditions continued from summer into autumn over Scandinavia and over the western Mediterranean, but no longer dominated over the European midlatitudes. Autumn 2022 was the second wettest autumn in Ireland. During October, it was drier than normal almost everywhere in continental Europe (except for some areas in southern Germany and eastern France) with precipitation locally below 20%. Only Belarus and some areas of central European Russia received above-normal precipitation. Ireland had its wettest October on record (from 1941). November was wetter than normal for the Mediterranean, Balkans, and central parts of Eastern Europe, while Central Europe and the Nordic and Baltic countries received 50% to 80% of normal precipitation in many areas, a result of Scandinavian blocking. In December 2022 (not shown), above-normal precipitation fell over Iberia, southern France, northern Italy, and the northern Balkans up to central parts of eastern European Russia, while the southeast from Kazakhstan to the eastern Mediterranean region was notably dry, often with less than 20% of the normal precipitation.

2. WESTERN EUROPE

This region includes Ireland, the United Kingdom, the Netherlands, Belgium, Luxembourg, and France.

(i) Temperature

The year was the warmest or tied with or close to the warmest year on record for many countries in this region. It was the warmest for France (+1.6°C), Luxembourg (+1.1°C), Belgium (+1.2°C), the United Kingdom (+0.9°C), and Ireland (+0.7°C), and third warmest for the Netherlands (+1.1°C). All seasons were warmer than normal for the region.

During winter 2021/22, anomalies were +0.8°C for France while the other countries of the region reported higher anomalies of +1.1°C in the United Kingdom and Ireland, +1.4°C in Belgium and Luxembourg, and +1.9°C in the Netherlands. In January, anomalies were below +0.8°C in the region, except for the Netherlands (+1.6°C) and Ireland (0.9°C). February saw even higher anomalies, with the highest ranging from +2.3°C in Luxembourg to +2.7°C in the Netherlands.

Spring anomalies were also positive, ranging from +0.3°C in the Netherlands to +1.1°C in France. In March, most of the region except for Ireland (+0.5°C) had anomalies ranging from +1.0°C to +1.5°C. April temperatures were near or slightly below normal. May was exceptionally warm for most of the region. France observed its warmest May on record with an anomaly of +2.4°C. Anomalies in the rest of the region during May ranged from +1.3°C in Ireland (its third warmest) and the United Kingdom to +1.9°C in Luxembourg.

June, July, and August were all warmer than normal. For many countries, summer 2022 was among their five warmest. Anomalies ranged from +0.7°C in Ireland to +2.3°C in France.

Temperatures at the start of summer were near normal for Ireland (+0.3°C) and slightly higher for the United Kingdom. France had its third-warmest June on record (2.3°C above normal) and also its third-warmest July (+2.1°C). In Luxembourg, the July anomaly was close to +2.0°C. August was among the three warmest on record for most countries in the region, with monthly anomalies ranging from +2.3°C in the Netherlands to +3.1°C in Luxembourg. For France, it was the second-warmest August on record (+2.6°C). Only Ireland and the United Kingdom experienced anomalies below +2.0°C.

Autumn was also warmer than normal. Anomalies ranged from +1.1°C in Ireland to +1.6°C in Belgium. For all countries except Ireland, it was either the second- or third-warmest autumn on record. In Ireland, it was the fourth warmest. In September, only France reported an anomaly of +0.7°C while the other countries had temperatures near or slightly below normal. October was very warm across the entire region. France reported its warmest October on record at 3.5°C above normal. In November, temperature anomalies were close to +2.0°C in the region except for Ireland (+1.4°C). It was the third- and fifth-warmest November on record for the United Kingdom and France, respectively. December was colder than normal in the west and warmer than normal in the southeast, with anomalies ranging from –1.4°C in Ireland to +2.0°C in southern France.

(ii) Precipitation

Most of Western Europe received near-normal precipitation over the year. During winter 2021/22, precipitation was mostly near normal; only parts of southern France and the northwest had below-normal precipitation. January was drier than normal in all countries except Luxembourg where precipitation was near normal. France, Ireland, and the United Kingdom received only around 50% of their normal precipitation. February was wetter than normal (120% to 145%) for all countries except France, where most areas only received 40% to 80% of normal precipitation.

Spring was drier than normal across the region. Precipitation ranged from 60% of normal in Luxembourg to 80% in Ireland. All countries saw below-normal precipitation during March. Belgium experienced its driest March on record having received just 5% of its normal precipitation, and the Netherlands had its third driest having received only around 20% of normal. In April, the rest of the region received 70% to 85% of normal precipitation, and parts of England and France were even drier. France reported its driest May in history, receiving only 35% of normal. Luxembourg received around 40% of its normal precipitation.

Summer 2022 was the driest summer since at least 1991 for Belgium and Luxembourg (47% and 34% of normal precipitation, respectively). Ireland, the United Kingdom, and the Netherlands each received around 60% of their normal precipitation. June was wetter than normal (114% to 130%) for all countries except Luxembourg (65% of normal) and the United Kingdom (80%). July was exceptionally dry across the entire region. The Netherlands and France reported only 25% of normal precipitation, making it the second-driest July in history for France and Belgium. Luxembourg had its driest July on record (less than 20% of normal). Ireland and the United Kingdom received around 50% to 60% of normal precipitation in both July and August. All countries also reported below-normal precipitation for August. Some areas in France received well below 50% of normal. Many areas of the Netherlands, Belgium, and Luxembourg received only around 30% of their normal precipitation.

Autumn precipitation was near or slightly wetter than normal across most of the region. All three months of the season were wetter than normal for Ireland and the United Kingdom. During September, most countries received about 120% to 140% of their normal precipitation, while Belgium and northeastern France observed about 150% to 175%. October was drier than normal in the Netherlands, Belgium, and France (45% to 65% of normal). Mesoscale rain events contributed to above-normal precipitation in Luxembourg and some areas in eastern France. November precipitation in the region was near to slightly above normal. December precipitation was also near normal in most areas.

(iii) Notable events and impacts

On 27 June, a tornado hit the city of Zierikzee (Zeeland Province, Netherlands), causing one fatality, 10 injuries, and extensive damage that included torn off roofs and uprooted trees. This was the first tornado in the region since 1992.

On 12 November, North Atlantic low-pressure systems brought mild air to northern and western Europe. This influx of warm air led to new high minimum temperature records in Scotland (14.6°C) and Northern Ireland (14.5°C).

During 16–18 November, heavy rain in Scotland and England caused flooding, damage, and casualties due to flash floods. In Charr, Aberdeenshire, 140 mm of rain was recorded in 48 hours (close to the monthly normal). Aboyne, Aberdeenshire, recorded 71.4 mm in 24 hours. Rail services were suspended and left hundreds of travelers stranded in Newcastle. Several roads were flooded and cars submerged in the region of Angus and Edinburgh. Some residents had to be evacuated. Earlier that week, heavy rain led to flooded roads and submerged cars in West Sussex, England.

During 2–7 June, France was affected by severe thunderstorms that brought hail and heavy rain that led to flooding. Hail diameters measuring up to 7 cm damaged cars, infrastructure, and vineyards. Multiple stations measured 24-hour precipitation totals above 50 mm (some above 70 mm), which are amounts comparable to normal monthly June totals. The station Saint-Yan in Saône-et-Loire, central eastern France, received 108 mm in 48 hours. Thousands of households experienced power outages, and flights at Paris airports were either suspended or delayed.

A 14-day heatwave in France peaked on 18–19 July when 104 stations broke their all-time records (e.g., Brest, 39.3°C; Nantes, 42.0°C; Dieppe, 40.4°C; Calais, 39.9°C). This was the fifth-longest and third-most intense heatwave in France since 1947, after those of July 2019 and August 2003. On the same day, Ireland achieved its highest maximum air temperature since 1887 with 33.0°C. On 19 July, a temperature of 40.0°C was measured in the United Kingdom for the first time on record (Coningsby in Lincolnshire recorded the highest temperature of 40.3°C), and temperature records at several long-running stations were broken by margins of 3°C to 4°C. Additionally, a new high daily minimum record of 25.8°C was set in Kenley (Greater London). In the Netherlands, station De Kooy set a new local all-time high temperature record of 36.1°C on the same day. Overall, monthly temperatures reached 39.5°C in the Netherlands (Beek), 40.0°C in Belgium (Kapelle-op-den-Bos), and 36.3°C in Luxembourg.

3. CENTRAL EUROPE

This region includes Germany, Switzerland, Austria, Poland, the Czech Republic, Slovakia, and Hungary.

(i) Temperature

Overall, 2022 was very warm in the region. Switzerland reported its warmest year on record at 1.6°C above normal, and many other countries observed one of their five warmest years. Except for the Czech Republic, Slovakia, and Poland, which each reported anomalies slightly below +1.0°C, all countries experienced temperatures 1.2°C to 1.6°C above normal.

Winter was warmer than normal, with anomalies ranging from +1.1°C in Switzerland to +2.0°C in Germany and the Czech Republic. February was exceptionally warm. Much of the region reported monthly anomalies between +3.0°C and +3.4°C, while Switzerland and Austria reported slightly lower anomalies of +1.8°C and +2.1°C, respectively.

During spring, only Germany and Switzerland had above-normal temperatures (+1.0°C and +1.4°C, respectively), while the rest of the region reported near- to slightly-below-normal temperatures. April was colder than normal for all countries except Switzerland, which reported near-normal temperatures. May was warmer than normal in Poland, Slovakia, Czechia, Germany, and Hungary (1.0°C to 1.3°C above normal). Austria reported a higher anomaly of +1.8°C and Switzerland reported its second-warmest May on record at 2.6°C above normal.

Summer was exceptional in Central Europe, with many countries experiencing one of their warmest on record. Switzerland and Germany reported their second-warmest summer with anomalies of +2.3°C and +1.7°C, respectively, and Poland had its third warmest (+1.3°C). Slovakia reported +1.8°C, Austria +1.6°C, Poland +1.3°C, and the Czech Republic +1.2°C. June, July, and August were all warm with many countries reporting record or near-record monthly temperatures. Switzerland reported its second-warmest June on record at 2.7°C above normal and Slovakia its third warmest (2.3 °C). Hungary observed its third-warmest June (+2.3°C) and fifth-warmest July on record (+1.6°C) and Switzerland its fourth warmest July (+2.4°C). Germany reported its warmest August on record (+2.3°C), Hungary its second warmest (+2.6°C), Poland and Switzerland their third warmest (+2.1°C and +1.8°C, respectively), Slovakia its fourth warmest (+2.0°C), and Austria and Czechia their fifth warmest (+1.1°C and +1.2°C, respectively).

The year continued with a warmer-than-usual autumn. Switzerland reported its third-warmest autumn on record at 1.7°C above normal. Poland, Slovakia, and Czechia reported anomalies between +0.4°C and +0.7°C, and Germany and Austria reported +1.4°C and +1.3°C, respectively. September was colder than normal for all countries in the region, while October was exceptionally warm. Germany, Austria, and Switzerland each reported their warmest October on record, with anomalies of +3.1°C, +3.4°C, and +3.8°C, respectively. Poland and Czechia reported their fourth warmest October on record (+2.5°C). December was colder than normal in the north, but warm in the south, with anomalies ranging from –1.0°C in northern Poland to +3.0°C in southern Hungary.

(ii) Precipitation

The year was slightly drier than normal across Central Europe, with most areas receiving 80% to 92% of their typical annual totals. Some parts received even less. During winter, precipitation was near normal for Germany, Poland, Austria, and Czechia. Hungary and Slovakia reported only around 70% and 80% of normal, respectively. Switzerland reported 90% of normal precipitation, but only up to 40% of normal on the Alpine Southside. In January, only Poland reported above-normal precipitation, while Hungary, Slovakia, and Switzerland received just 30% to 46% of their normal amounts. February was wetter than normal for Germany and Poland (155% of normal), while Hungary continued to be dry (36%).

Spring was drier than normal, with precipitation 60% to 80% of normal for most of the region. Czechia and Poland each reported their third-driest spring on record (70% and 62% of normal). In March, almost the entire region received less than 35% of normal precipitation. It was the second-driest March for Poland and Austria, third driest for Czechia, fourth driest for Germany, and fifth driest for Switzerland. April precipitation was near normal, but May was dry in Germany, Czechia, and Poland (63% to 71% of normal) and even drier in Switzerland (48%), Hungary (47%), and Slovakia (46%).

Summer was near normal for Czechia but drier than normal elsewhere. Poland and Austria reported 89% of normal, and Slovakia, Switzerland, Germany, and Hungary 78%, 72%, 61%, and 54% of normal, respectively. June was the fourth driest on record for Hungary (59% of normal), and July was drier than normal across the entire region. August was drier than normal for Austria (81% of normal), Switzerland (70%), Hungary (66%), and Germany (64%).

Autumn precipitation was near normal for Germany, Hungary, Switzerland, Czechia, and Slovakia. Austria and Poland reported 88% and 79% of normal precipitation, respectively. The season started with a wetter-than-normal September almost everywhere in the region. Hungary reported its ninth-wettest September on record but also its eighth-driest October. October was drier than normal everywhere in the region except for southwestern Germany and Switzerland, where precipitation was near normal. In November, Slovakia and Poland received only 46% and 48% of normal precipitation, respectively, making it the third-driest November for Poland. December was wetter than normal in eastern Poland, Slovakia, and Hungary, and drier than normal in southwestern Germany, Austria, and parts of Switzerland.

(iii) Notable events and impacts

During 2–4 April, an unusual cold spell accompanied by frost occurred in parts of Europe. Following warmer temperatures in the previous weeks that saw the greening of flora, there was widespread damage to agriculture in Germany, Austria, and France. In Germany, minimum temperatures dropped from –5°C to –10°C, and some stations broke their April minimum temperature records.

On 19–20 May, following the first heatwave of the year over central Europe, two consecutive upper-level troughs led to severe thunderstorms. On 20 May, a strong cell developed over the Eifel Mountain range in western Germany and produced hailstones as large as 5 cm that were accompanied by precipitation rates of 30 mm h^{-1} to 40 mm h^{-1}, which caused local flooding. Wind gusts of up to 113 km h^{-1} were measured. In North Rhine-Westphalia, multiple tornados were spawned by a supercell, one of which struck Paderborn. Trees were uprooted, roofs were damaged, and windows burst. The supercells reached Czechia, causing further damage. At least 3 people were killed during these storms and more than 50 were injured.

Warm air from Spain advanced into Central Europe on 18–19 June, setting new temperature records. In Germany, Cottbus and Dresden-Strehlen stations recorded 39.2°C, which is a new monthly record in time series dating to 1887 (Cottbus) and 1936 (Dresden). Temperatures did not drop below 24°C during the night at some German stations. In Switzerland, Beznau (Aargau Canton) set a new national June record of 36.9°C (previously held by Basel since 1947) on 19 June. That same day, Feldkirch (Austria) set a new regional record for Vorarlberg (northwestern Austria) at 36.5°C. In Slubice (Poland), the temperature of 38.3°C was on par with the previous June record set in 2019. A new June maximum temperature of 39.0°C was recorded in Czechia on 19 June. On 30 June, a new June national maximum temperature record of 39.6°C was set in Berettyóújfalu, Hungary. The temperature did not fall below 24.7°C at the station Budapest Lágymányos, setting a new national high daily minimum temperature record (the previous June record of 24.4°C had been held by Budapest Istvánmező since 1946).

A heatwave in July also led to many new temperature records across Central Europe. In Germany, daily maxima reached over 40°C on 19 July. That same day, 38.1°C was reached in Genève-Cointrin (Switzerland). On 21 July, a new national temperature record of 38.6°C was set in Slovakia.

During yet another heatwave in the region, many new local monthly and all-time records were set during 4–5 August. On 4 August, Bad Kreuznach (Germany) recorded a new maximum temperature of 39.6°C as did the station Weinbiet (553 m a.s.l.) with 38.0°C. The same day, a new record temperature of 38.3°C was measured in Geneva (Switzerland). On 5 August, Stuttgart (Germany) measured a new highest daily minimum temperature of 21.2°C, and Zurich Airport (Switzerland) set a new record with 18.9°C.

4. IBERIAN PENINSULA

This region includes Spain, Portugal (1971–2000), and Andorra.

(i) Temperature

The year was the warmest on record for Andorra, Spain, and Portugal, with anomalies of +2.6°C, +1.7°C and +1.4°C, respectively. All seasons, especially summer and autumn, were warmer than normal for the Iberian Peninsula. In Andorra, May, June, July and October were the warmest on record with anomalies above +4°C. Portugal had its fourth-warmest winter on record with an anomaly of +1.4°C, while Spain was 0.8°C warmer than normal. In February, monthly anomalies reached almost +1.5°C.

Spring temperatures were near normal on the Iberian Peninsula. While the first two months of the season were colder than normal, (anomalies of –0.2°C to –0.6°C), May temperatures were more than 2.0°C above normal in Portugal and Spain, marking the warmest May on record.

Summer was the warmest on record for both Portugal and Spain (anomalies of +1.7°C and +2.2°C, respectively). June, July, and August were all among the four warmest on record for their

respective months for Spain (+1.7°C, +2.3°C, and +1.7°C, respectively). June and August were near normal for Portugal, while July was among the three warmest on record, with an anomaly of +2.0°C.

All three months of autumn were warmer than normal for the Iberian Peninsula. With an anomaly of +2.0°C, it was the warmest autumn on record for Spain and the fifth warmest for Portugal (+1.1°C). October was the warmest month of the season, with temperatures 2.0°C above normal for Portugal (fifth warmest on record) and 2.9°C above normal for Spain (warmest on record). Spain had its fifth-warmest November at 1.8°C above normal. December was record warm for both Spain and Portugal, with temperatures more than 2.0°C above normal over the entire peninsula.

(ii) Precipitation

Total precipitation for the year was around 90% of normal on the Iberian Peninsula. Locally, precipitation was slightly less than 60% of normal in certain places. Winter was dry, seeing only 30% to 60% of normal precipitation. For Portugal, it was the fifth-driest winter on record, with January and February receiving only 20% to 40% of normal precipitation.

Spring was drier than normal in Portugal (80% of normal), while it was near to wetter than normal in Spain, particularly in the southeast (more than 250%). March was wet across the Peninsula (around 180% of normal). During April, most of Portugal received below-normal precipitation while most of Spain was near normal. May was dry, with Portugal reporting only 20% of normal precipitation (fourth-driest May on record). Most of Spain received only 20% to 40% of normal precipitation.

The summer was also drier than normal for both Portugal (47% of normal) and Spain (65%). During June, only the northwestern tip of the Iberian Peninsula received above-normal precipitation. Portugal had 60% of normal precipitation while most of the stations in Spain reported below 20%. In July, most areas on the Iberian Peninsula received less than 20% of normal precipitation or none at all; only a few stations in eastern Spain reported above-normal precipitation. During August, Portugal received only 25% of normal precipitation. Some areas in Spain recorded less than 20% of normal precipitation, while others received 140% to 250% of their normal amounts.

Autumn precipitation was near normal for most areas in Portugal, but less than normal for Spain, particularly in the southeast which saw only 10% to 50% of normal precipitation. September was wet in Portugal (up to 160% of normal precipitation), but in Spain, precipitation was mostly below normal, especially in the south (20% to 40% of normal). October was near normal for Portugal while Spain was again drier than normal. November was drier than normal for the southern Iberian Peninsula with precipitation less than 50% of normal. The northern Peninsula mostly received near to slightly above-normal precipitation. December 2022 was a wet month for much of Iberia, with local reports above 250% of normal precipitation.

(iii) Notable events and impacts

On 20 April, the mountain observatory of Navacerrada in Spain (northwest of Madrid, located at 1894 m a.s.l.) recorded a fresh snow cover of 36 cm, an unusual accumulation of snow for a single day in April.

A notable heatwave (the longest and largest area affected since 2003) occurred during 9–17 June on the Iberian Peninsula. Temperatures surpassed 40°C on several days and broke some June records (Pinhão in Portugal: 42.3°C on 13 June; Andujar in Spain: 44.5°C on 17 June).

More exceptional heat in July on the Peninsula led to multiple temperature records. In Portugal, average daily temperatures were above 25°C beginning on 7 July, and multiple stations reported daily maximum temperatures above 40°C. In Alvega and Mora, the temperature surpassed 40°C for 10 consecutive days. On 14 July, Pinhão recorded a new July record with a maximum temperature of 47°C. In Spain, Madrid reported a new maximum temperature record of 40.7°C and a new high minimum temperature record of 26.2°C. New all-time records with temperatures above

40°C were recorded in Ponferrada, Valladolid, and Ourense (northern Spain). The extreme heat contributed to more than 1000 fatalities in Portugal and Spain. Along with the heat, it was very dry in both countries, and severe and extreme drought developed across large areas. In central Portugal and central western Spain, multiple large wild fires broke out and damaged large areas. Portugal declared a state of emergency during 11–15 July, and efforts to extinguish the fires led to some casualties. In the region of Galicia in Spain, 8000 people had to be evacuated.

On 30 August, hailstones as large as 10 cm caused significant damage to houses, vehicles, and infrastructure in parts of Catalonia (Spain). At least 50 people were injured, and some casualties were reported.

Severe storms during 10–14 November brought heavy rain, hail, and strong winds that caused extensive damage in central and eastern Spain. Flooding was reported in the regions of Valencia, Castile, and León. Valencia airport was closed due to the flooding. Wind caused damage to power infrastructure, leading to power outages for around 7000 homes in Catalonia. Multiple places recorded 48-hour totals of 150 mm to 300 mm of rain during 10–12 November, breaking November precipitation records for the most intense 1-hour total (66.1 mm) and the highest 24-hour total (148.4 mm).

5. THE NORDIC AND BALTIC COUNTRIES

This section includes Iceland, Norway, Denmark, Sweden, Finland, Estonia, Latvia, and Lithuania.

(i) Temperature

Annual temperatures in the Nordic and Baltic countries were normal to above normal, with anomalies from 0.0°C in Iceland to +0.9°C in Finland. Some stations in Sweden reported their second-warmest year (the warmest was 2020). Winter 2021/22 was colder than normal in northern Scandinavia, but warmer than normal in southern Scandinavia and the Baltic countries. Anomalies ranged from –1.0°C in northern Norway to +1.4°C in Lithuania and Denmark. January was mild in the southern parts of the region, up to 3.0°C above normal in Lithuania; February was even more mild (locally +4.0°C). Conversely, Iceland saw a cold February (–2.0°C anomaly) due to a cold air outbreak from Greenland.

Spring was relatively mild in Scandinavia, especially in the north and in Iceland (+1.0°C anomaly), but colder than normal in the Baltic countries, which were influenced by cold troughs over Eastern Europe. The largest negative seasonal anomalies were recorded in Lithuania (–1.0°C). The warmth over Scandinavia reached the Arctic regions in March, resulting in Svalbard being 4.0°C warmer than normal. A cold spell followed in April, resulting in below-normal temperatures in most of the region, with the largest anomalies (–1.5°C) in Lithuania. Similar anomalies occurred in May in the Baltics, having been affected by cold air from northern Russia.

Summer brought near-normal temperatures to western parts of the region, while Finland and the Baltics were 1°C to 2°C above normal. During June and once in August, warm air from the subtropics reached northern Europe. July 2022 had the highest (station-level) daily maximum temperature of all July months in Denmark. August was record warm in parts of Finland; records were broken or equaled at 18 observation stations. Lithuania saw its warmest August on record (anomaly of +2.8°C). Summer was relatively cold in Iceland.

During autumn, Iceland and western Scandinavia (Norway, Denmark, and southern Sweden) were at least 1.0°C warmer than normal, while temperatures were closer to normal farther east. Widespread warmth dominated the whole region during October and to a lesser extent in November. Iceland reported its warmest November on record as warm easterly winds prevailed. The country was almost completely without snow, which is unusual in November. On 12 November, three stations in Sweden reached 16.7°C, the highest temperature ever reported in Sweden so late in the month. December brought a large Arctic cold air outbreak to almost the whole region, with the largest anomalies in western Iceland (–4.0°C). It was the coldest December for the country since 1973 and the coldest December for the capital city of Reykjavík in more than

100 years (equal to December 1916). Some warmth was seen in late December, however. A new daily maximum temperature record (10.7°C) was set on 31 December in Lithuania.

(ii) Precipitation

Precipitation totals for 2022 were below normal across much of the region. Southeastern Sweden was very dry. The lowest annual precipitation amount for the country in 2022 was 281 mm at station Ölands norra udde; this was also the lowest total for that station since 1921. Conversely, Reykjavik, Iceland, reported its eighth-wettest year on record. In Latvia, it was the first year since 2017 that was wetter than normal, although only by 0.2 mm.

Winter 2021/22 precipitation was below 80% of normal across much of southern Norway, Sweden, and Finland, mainly due to dry weather in January, as February was generally wetter. In southern Sweden, Lund recorded 97 mm of precipitation, a new February record for a series dating to 1753. Heavy snow fell over all of Iceland in February.

Spring was also dry in much of the region, with less than 40% of normal precipitation in southern Norway. Only Svalbard and the northern Norwegian coasts had above-normal precipitation. March was particularly wet in Iceland; many weather stations in the south, west, and northwest of the country recorded their highest March precipitation totals on record. Conversely, March was record dry in Denmark, and in southern Sweden 50 stations had no measurable precipitation for the month. Estonia recorded only 4 mm (13% of normal), its lowest March total since 1961. Lithuania was also record dry for the month.

Summer was notably dry in southern Scandinavia. Southern Norway and southern Sweden reported totals that were 60% or less of normal for the season. Helsinki-Vantaa airport (Finland) received its lowest August precipitation total (5.9 mm) on record for its observation station. Other parts of the region were less affected by dryness, as seasonal totals were closer to normal.

Autumn was also dry in much of the region with precipitation less than 80% of normal over large areas, notably in Sweden, Finland, and the Baltics, where some local totals in those places were below 60%. November was particularly dry, with several areas throughout the region receiving 40% or less of their normal precipitation; however, it was very wet in eastern Iceland. Generally dry weather continued in December. It was the driest December in decades for many places in Iceland.

(iii) Notable events and impacts

Strong winds impacted western Lithuania on 30 January with gusts of up to 34.5 m s^{-1} (124 km h^{-1}) along the coast. Klaipėda seaport was closed, and power lines were downed from fallen trees. Flooding was even observed close to the sea at Šventoji resort due to the strong winds.

A heatwave occurred in the last decade of June in Estonia. Temperatures reached 30°C or higher in many places for two to five consecutive days. Five stations set new June high-temperature records.

The highest temperature in the Norwegian Arctic in 2022 (20.1°C) was recorded at Bjørnøya on 29 June, marking only the second time Bjørnøya has surpassed 20°C in that month. The first occurrence was on 22 June 1953, with 23.6°C.

The highest maximum temperature in 2022 in Norway was 33.6°C, recorded on 20 July at Lysebotn (Sandnes, Rogaland). Since 1957, Rogaland has had the highest temperature of the year only once before in 1978, when Sola reached 30.7°C on 31 July. On 21 July, Målilla (Sweden) reported a daily maximum of 37.2°C, marking the highest temperature in the country since 29 June 1947.

On 12 December, snow reached a depth of 55 cm in Kuldīga (western Latvia). This was the thickest snow cover in Latvia since April 2013.

6. CENTRAL MEDITERRANEAN REGION

This section includes Italy, Monaco, Malta, Slovenia, Croatia, Serbia, Montenegro, Bosnia and Herzegovina, Albania, North Macedonia, Greece, and Bulgaria.

(i) Temperature

The year 2022 was the warmest on record for Monaco, Italy, Slovenia, Croatia, and Bosnia and Herzegovina and second warmest for Serbia, behind 2019. Annual mean temperatures in the central Mediterranean region were around 1.0°C above normal.

Winter 2021/22 temperatures were near to above normal. Anomalies ranged from slightly below normal in southernmost Italy, especially Sicily Island, Malta, and southern Greece, to +2.0°C in northern Bulgaria and northern Serbia. January was colder than normal over the Mediterranean (–1.0°C anomaly), while the northern Balkans in particular were affected by a warm westerly flow due to the positive phase of the North Atlantic Oscillation. February anomalies up to around +3.0°C were observed in northern Serbia and northeastern Croatia.

Spring had near- to below-normal temperatures across almost the entire region, except for northwestern Italy (+1.0°C anomaly). March temperatures were below normal, as cold air from Russia advanced to the eastern and central Mediterranean. Greece reported a monthly anomaly of –3.0°C (third-coldest March on record), mainly due to a cold wave during 9–16 March. This wave brought rare snowfall to the northern suburbs of the Attica region and Viotia (East Sterea Periphery) in Greece. In April, the northern Balkans were impacted by cold air from eastern central Europe that advanced southward, resulting in anomalies close to –2.0°C in northern Serbia. The eastern Mediterranean experienced a warming due to subtropical air, which warmed southern Greece (1.0°C above normal). In May, the entire region experienced a flow of warm air from southwestern Europe, leading to temperatures 1°C to 2°C above normal.

Summer was generally warmer than normal, as influxes of warm air from the southwest continued. The highest anomalies (above +3.0°C) were observed in northwestern Italy and eastern Bulgaria. June, July, and August were each warmer than normal across the entire region. Some stations in Slovenia recorded their highest July maximum temperature on record (e.g., Doblice: 39.4°C). The highest temperature of 2022 in Bosnia and Herzegovina (41.5°C) was recorded at Mostar and in Greece (42.0°C) at Ruse, both in July. The highest temperature in Serbia of 2022 (40.6°C) was measured at Smederevska Palanka on 23 July. Greece experienced an early heatwave in June, when temperatures above 38°C were recorded in the central and eastern mainland.

Above-normal temperatures continued in autumn, though with lower anomalies compared to summer (up to +2.0°C in northwestern Italy). September temperatures were mostly near normal, except for the western Mediterranean islands (Sardinia, Sicily, Malta), which were 1°C to 2°C above normal. Anomalies up to +3.0°C were observed in northern Italy in October and in eastern Bulgaria in November. December was mild, with several new local monthly mean records set in Serbia. Greece experienced its warmest December on record.

(ii) Precipitation

It was mainly a dry year for the central Mediterranean region. Italy reported its driest year on record, as the country experienced a critical drought situation in some areas, notably the northwest and the south (Sicily) where both regions received less than 60% of normal precipitation for the year. Other parts of Italy and parts of southern Greece and eastern Bulgaria registered 60% to 80% of normal. Precipitation was closer to normal elsewhere, though it was locally very dry in some areas. Slovenia, for example, experienced a dry spell (defined here as a long period with well-below-normal precipitation) from 28 April to 7 September with agricultural losses estimated at 100 million Euro ($108 million U.S. dollars).

During winter 2021/22, some areas in northwest Italy and Sicily received less than 40% of their normal precipitation, while other parts of the region were occasionally affected by troughs expanding from the northeast. However, due to a frequent expansion of the Azores high into the central Mediterranean region, there were also several drier-than-normal periods throughout the region in January and February.

Spring was generally dry. Seasonal totals were mainly 60% to 80% of normal, although some areas in Italy, including the northwest, again received less than 40%. North Macedonia in the southern Balkans had its driest spring on record. March was dry throughout most of the region.

In April, much of Italy, Greece, and North Macedonia received around 60% of normal precipitation, and much less in localized areas. The rest of the region had normal precipitation. May was drier than normal except in the western Mediterranean (Sardinia and Sicily). Monaco had its second-driest May on record.

Summer precipitation presented a contrasting pattern between north and south. The northern half of Italy and the northwestern half of the Balkans received less than 80% of normal precipitation, while the south had 150% of normal around the Aegean Sea in Greece. This pattern persisted through the season, with a larger dry area in July and a larger wetter-than-normal area in August. Croatia experienced its second-driest summer on record. Drought occurred in northern Serbia from mid-June to mid-August during its critical crop period, as well as in parts of Bulgaria.

Autumn was drier than normal in parts the region. Italy, Greece, and eastern Bulgaria received less than 80% of normal precipitation, with northwestern Italy receiving less than 40%. The remainder of the region had normal to above-normal precipitation. September was rainy in central Italy and much of the Balkans (local totals over 150% to 200% of normal), while October was extremely dry throughout most of the region with less than 20% of normal precipitation in Italy and the Balkans. Bosnia and Herzegovina observed its third-driest October on record. November was generally wetter than normal (local totals over 150%). December was wet in the north, while Greece, North Macedonia, and Bulgaria received less than 80% of normal and Sicily less than 40%.

(iii) Notable events and impacts

Heavy rainfall on 2–3 September in the upper watershed of the Stryama River (around the village of Klisura, Plovdiv District, Bulgaria) led to high wave formation in the mountainous part of the tributaries that swept debris from the slopes, affecting the villages Bogdan, Karavelovo, Stoletovo, Rozino, and Slatina. Most of the infrastructure and many houses were either destroyed or inundated by water and mud. At least 150 people were displaced. An emergency was declared in the municipality of Karlovo. The return period of the high wave formed along the Stryama River is estimated to be around 600 years. The 24-hour rainfall amounts measured on 2 September in Rozino (164 mm) and Klisura (156.5 mm) were the highest on record for this area (return periods are estimated to be about 440 and 600 years, respectively). Damage was estimated to be more than 30 million Euro ($32.5 million U.S. dollars).

Heavy rain fell during 15–17 September in Slovenia. Osilnica station in the Kolpa River region received 423 mm in 56 hours and Šebreljski in the Littoral region received 372 mm in 51 hours, far exceeding their 100-year return levels. Additionally, strong wind affected several counties in Croatia on 15 September, causing damage estimated at more than 6 million Euro ($6.5 million U.S. dollars).

On 14–15 October, a barometric low reached Greece from southern Italy and was intensified by the warm Ionian Sea. The station in Siteia (east Crete) recorded 293 mm of daily precipitation (281.8 mm in 12 hours), which was the third-highest 24-hour rainfall on record for the country. Torrential rain on 15 October triggered flash floods in the Heraklion and Lasithi Regional Units on the island of Crete, causing two fatalities and significant damage to buildings and infrastructure, particularly in coastal areas.

Heavy precipitation in Montenegro and southwestern Serbia during 19–22 November led to high water levels on the Ibar River and its tributaries as well as the Lim River, causing local flooding. On 20 November, an emergency situation was declared in three municipalities in southwestern Serbia.

On 11 December, heavy rain caused the river water levels throughout Croatia to rise. A state of emergency was declared on the Sunja and Una Rivers near Sunja, Dvor, and Hrvatska Kostajnica.

7. EASTERN EUROPE

This section includes the European part of Russia, Belarus, Ukraine, Moldova, Romania, and West Kazakhstan.

(i) Temperature

The year was warmer than normal in Eastern Europe, with anomalies ranging from +0.7°C in Ukraine to +1.0°C in Romania and higher in certain localities. It was the third-warmest year on record for Romania, behind 2019 and 2020.

Winter 2021/22 temperatures were near normal in northern European Russia, but above normal toward the southeast (highest in West Kazakhstan at +4.0°C). This was due to a mild westerly flow from the North Atlantic that advanced far into Eastern Europe while the Russian Blocking High retreated to areas farther east. February was particularly warm, when the westerly flow changed its direction toward the north just over European Russia due to the blocking. The result was a warming, which was most intense just along the 50°E meridian (eastern European Russia to West Kazakhstan) where monthly anomalies exceeded +6.0°C.

A relatively cold spring followed. Belarus, northern and eastern Ukraine, and central European Russia had anomalies of –1.0°C or more. Only northernmost parts of European Russia were warmer than normal (+1.0°C). Southern areas of the region were affected in March when cold continental air from Siberia reached Kazakhstan and the Caucasus region (–3.0°C anomalies). Elsewhere, mild Atlantic air warmed northern parts of European Russia (close to 3.0°C above normal). In April, cold Arctic air reached Europe from the north, with western areas of the region most affected. Belarus, western Ukraine, and westernmost Romania reported anomalies around –2.0°C. In May, another cold spell originating from the north affected European Russia and West Kazakhstan, with temperatures 4.0°C below normal. Other parts of the region were also colder than normal, but less so, while western parts of Romania were 1.0°C warmer than normal.

Following these cold spells, summer was warm. Seasonal anomalies were mostly between +1.0°C and +2.0°C and as high as +3.0°C in northeastern European Russia. Warm airflow from southwestern Europe reached western parts of Eastern Europe in June, leading to monthly anomalies of around +2.0°C in western Romania, western Ukraine, and Belarus. In July, cooler air flowed in from Scandinavia over part of the region, but another strong warming took place in August as warm air arrived from both southwestern Europe and the Middle East. August temperatures were more than 4.0°C above normal in eastern European Russia.

Temperatures in autumn were mainly near normal. Only northernmost parts (northern coastal regions of European Russia) and southernmost parts (Romania, Moldova, southern European Russia, and West Kazakhstan) were around 1.0°C warmer than normal. In September, a cold spell affected western European Russia, Belarus, and northern Ukraine (–2.0°C anomaly), then warm air from the southwest spread over the entire region in October (+1°C to +2°C). In November, warm air flowed into both the northernmost and southernmost parts of the region, and cold continental air reached north-central European Russia. In December, cold air from Scandinavia affected Belarus and northern European Russia (–1.0°C anomaly), while southern parts experienced a warming from the southwest (+2.7°C anomaly in Romania).

(ii) Precipitation

The year was mostly drier than normal in Eastern Europe. Eastern Romania, parts of Moldova, southern and eastern Ukraine, and southern European Russia received less than 80% of their normal precipitation. Moldova reported a drought period during May–July, when only 30 mm to 90 mm (15% to 45% of normal) fell; this occurred for the first time in measurement history in Moldova. The year was wetter than normal across Belarus, northern Ukraine, central European Russia, and West Kazakhstan, with some areas receiving over 125% of normal. European Russia as a whole received 103% of its normal precipitation.

Precipitation in winter 2021/22 was mostly normal to above normal, mainly due to the positive North Atlantic Oscillation pattern (see overview of recent studies in McKenna and Maycock 2022). Locally, 150% to 200% of normal precipitation amounts fell, particularly in the mountains (Caucasus, Carpathians) and along the coasts of the Black Sea. In January, central parts of the region (Belarus, northern Ukraine, central European Russia, West Kazakhstan) received above-normal precipitation. In February, northwestern Russia was wetter than normal while southern areas (Romania, Moldova, Ukraine) were much drier than normal under the influence of high pressure.

Spring was wetter than normal (mostly above 125% of normal precipitation and 150% in certain places) in eastern Belarus, northern Ukraine, central European Russia, and West Kazakhstan. Other areas received less than 80% of their typical totals and less than 60% locally. March was dry in the west. Much of Belarus received less than 20% of its normal and large parts of Ukraine and western European Russia received below 40%; however, in April, some of these areas received 150% to 200% of their normal. May was again dry, with Romania, Moldova, and Ukraine receiving less than 60% of normal, while eastern parts of European Russia and West Kazakhstan were wetter than normal (125% to 200% of normal over large areas).

Summer was mainly drier than normal. July was the only summer month that was mostly wetter than normal, except for in Romania, Moldova, and Ukraine. In August, European Russia received only 44% of its monthly average total.

Autumn was wetter than normal in Belarus, Ukraine, central European Russia, West Kazakhstan, and western Romania. Conversely, it was drier than normal in northern European Russia and around the Black Sea, with the latter being an area where heavy precipitation frequently occurs. In autumn 2022, some northern Black Sea coastal areas received less than 80% of normal amounts. October was dry, with less than 20% of normal precipitation received in eastern parts of Romania and southern parts of Ukraine. In December, above-normal precipitation fell over Belarus, Ukraine, and central European Russia, while other areas were drier than normal.

(iii) Notable events and impacts

Heavy rain fell over European Russia in late June. On 24 June, 85 mm to 103 mm of rain led to a sharp rise in small river water levels in the Greater Sochi region close to the Black Sea. Two cars were swept into the sea due to flooding. On 26–27 June, heavy rains of 115 mm to 145 mm affected the Crimea Peninsula as water flooded streets, infrastructure, residential homes, and greenhouses.

8. MIDDLE EAST

This section includes Israel, Cyprus, Jordan, Lebanon, and Syria.

(i) Temperature

The Middle East saw near- to above-average annual temperatures in 2022. Anomalies were highest in northeastern Syria and eastern Jordan at +1.0°C. The year was in the top third of warmest years in Israel, but it was the coolest year since 2011.

Winter 2021/22 temperatures were normal to above normal, with anomalies increasing from the southwest (0°C in Israel) to the northeast (+1.0°C in northeastern Syria). A cold spell occurred in January, with the largest negative anomalies in the south (–1.0°C in southern Israel). Warming followed in February, expanding to the northern Middle East (up to +3.0°C anomaly in northern Syria).

Spring was slightly colder than normal in Cyprus, at the Mediterranean coast, and in northern Syria, while temperatures were above normal in southwestern Jordan (+1.0°C anomaly). In March, cold air from Russia flowed southward, resulting in below-normal temperatures throughout the region. Anomalies were largest in northwest Syria (–4.0°C) and decreased toward the southeast (–1.5°C in southeastern Jordan). During 10–26 March, temperatures were 7°C to 9°C below

normal in Israel. The duration of this cold wave was unusual and even unprecedented for March in many places. Israel and Cyprus each reported their coldest March on record. In April however, warming spread over the region, with temperatures 2°C to 3°C above normal across most of the region and as much as 4°C in southeastern Jordan. Israel recorded its third-warmest April, behind 2016 and 1989. In May, temperatures were below normal in northeastern Syria (–1.0°C anomaly), while the rest of the region had temperatures near or slightly above normal.

In summer, heat from the Arabic Peninsula affected eastern Syria and eastern Jordan (+1.0°C anomaly) and less so farther west. This mostly moderate warming persisted throughout the season.

Autumn was also warmer than normal across the region, with anomalies of +1.0°C or higher. In terms of anomalies, September, October, and November were similar. December was particularly mild, as a large-scale warming expanded over the Mediterranean region. Monthly anomalies ranged from +1.5°C in southeastern Jordan to +3.0°C in northern Syria. Cyprus observed its second-warmest December on record, behind 2010.

(ii) Precipitation

The year was mostly drier than normal across the Middle East. Syria, Lebanon, and northern parts of Israel and Jordan received less than 80% of their normal precipitation, while Syria received less than 40%. Southern Israel and southern Jordan were slightly wetter than normal. The 2021/22 rainy season (October–April) was wetter than the 1991–2020 average in Israel; the last four rainfall seasons have been wetter than average, which is unprecedented in the last 100 years.

Winter 2021/22 was dry in Syria and northeastern Jordan, with large areas receiving less than 30 mm total (less than 20% of normal in some areas). Lebanon also received below-normal precipitation, while the rest of the region was slightly wetter than normal. Notably, Israel experienced an unusually wet January (120% to 160% of normal). It was the third-rainiest January in the central-southern coastal plain in Israel since the 1940s (exact year depends on the stations), behind 2013 and 1974.

Spring was generally drier than normal throughout the region. Eastern parts of Syria and Jordan received less than 20% of their normal precipitation. In March, above-normal precipitation fell locally along the coasts, while eastern parts of the region remained mainly dry. In April, the entire region received little to no rain, which is unusual so early in the year, at least for the northern areas. This extreme dryness in the northern mountains of Israel last occurred in 2012. Cyprus had its driest April on record. May was also mostly dry, except for some rain in parts of Cyprus, western and northern Syria, and northern Lebanon.

Summer is the dry season in the Middle East. Monthly totals above 10 mm were only registered in Cyprus and western Syria in June, which were above normal. In northeastern Israel, a few millimeters of rain were measured. Locally, more than 5 mm were measured.

Autumn brought above-normal precipitation to Cyprus and parts of the continental region, at the coasts in localized places, and in the interior. Up to 250% of the seasonal normal fell in eastern Jordan, but in absolute terms this was only around 10 mm. September and October were mainly dry, except for Cyprus, which saw above-normal rainfall in October. November was wetter than normal, with heavy rain observed at Syria and Lebanon's coasts. December was unusually dry in much of the region. Large parts of Syria and northeastern Jordan saw no rain at all, whereas precipitation was above normal in southern Jordan. The first half of the rainy season 2022/23 in Israel was deficient at the end of 2022, despite significant rains at the end of December.

(iii) Notable events and impacts

Heavy precipitation (that included snow in the mountains) fell during 25–28 January in Israel. The first part of the system was named "Elpis" (as part of the windstorm naming in Europe) and brought snow to the mountains. In the northern and central Golan Heights, the snow depth

reached 20 cm to 40 cm. In Jerusalem, snow depth reached 15 cm to 25 cm, its largest snowfall since 2015. Precipitation totals during the event reached 100 mm to 150 mm in the northern and central mountains and the southern coastal plain.

Due to cold weather in March, significant and unusual snow fell in the northern mountains of Israel. For example, more than 30 cm fell on Mt. Hermon during a heavy precipitation event on 23–26 March.

During 24–26 April, severe haze prevailed for three consecutive days. The source of the haze was from the east (as opposed to the southwest, from which it typically originates). The haze caused sandstorms in the Jordanian and southern Syrian deserts due to strong winds and developed clouds in the area. The dust that rose into the air was transported to Israel by easterly to northeasterly winds in upper layers, so that elevated areas were most affected by it.

In Israel, temperatures reached 43°C to 45°C in the Jordan Valley and the Arava during a heatwave from 27 to 31 August.

9. TÜRKIYE AND SOUTH CAUCASUS

This section includes Türkiye, Armenia, Georgia, and Azerbaijan.

(i) Temperature

The year was warmer than normal for almost all of Türkiye and the South Caucasus region, with anomalies up to +1.0°C and slightly higher in eastern Türkiye. A few places in western Türkiye were slightly colder than normal. The average temperature in Türkiye was 0.6°C above normal.

Winter 2021/22 was mostly mild, especially in northeastern Türkiye and the South Caucasus with anomalies of +1°C to +2°C. Temperatures in the rest of Türkiye were generally near normal, with some places in western Türkiye slightly below normal. A cold spell in January affected mainly Türkiye (monthly anomaly of around –1.0°C), but February was warmer than normal everywhere in the region, most notably in the east.

Cold air from Russia resulted in a colder-than-normal spring in the region with seasonal anomalies around –1.0°C in places. In March, anomalies ranged from –1.0°C in eastern Azerbaijan to –5.0°C in parts of western Türkiye. A warmer-than-normal April followed, with anomalies between +1.0°C and +3.0°C. May again brought an influx of cold air, albeit less intense than that of March, with eastern parts of the region being most affected (anomalies ranged from –1.8°C in northern Georgia to +1.0°C in southwestern Türkiye).

Summer was mainly warmer than normal across the region, particularly in the South Caucasus and eastern Türkiye at 1.0°C above normal; only places in northwestern Türkiye were slightly colder than normal, which was mainly due to a cooler period in July. It was the fifth-warmest summer on record for Armenia.

Autumn was also warmer than normal, specifically 1.0°C or more above normal across much of the region. It was the second-warmest autumn on record in Armenia behind 2010. The greatest departures from average occurred in November in Türkiye and Georgia with anomalies of around +2.0°C in most parts, whereas September and October were particularly warm in Armenia. It was also warmer than average in December (up to +3.0°C in Türkiye).

(ii) Precipitation

The year was drier than normal in Türkiye, Georgia, and western Armenia. Some areas, particularly in Türkiye, received as little as 60% to 80% of their normal precipitation. Most of Azerbaijan and eastern Armenia by contrast received above-normal precipitation (mostly more than 125%). Armenia received 75% of its normal total on average, making 2022 its fourth-driest year since 1935.

Winter 2021/22 was wetter than normal in the western half of Türkiye, with some areas receiving more than 125% of normal. The eastern half of Türkiye and the South Caucasus were mainly drier than normal. Some of these areas received less than 80% of normal precipitation and some less than 60%. In Armenia, precipitation was only 36% of its normal in February.

In spring, the pattern was reversed compared to winter. Western Türkiye was considerably drier than normal with less than 80% in most areas and below 40% in westernmost Türkiye. Eastern Türkiye and the South Caucasus saw above-normal precipitation, with the highest anomalies in Azerbaijan (more than 250% of normal in certain places). Precipitation in March accounted for much of this excess. It was the second-wettest March in Armenia since 1935. April, however, was drier than normal in almost the entire region. Large parts of Türkiye, Armenia, and Azerbaijan received less than 60% of their typical rainfall, with less than 20% being received in southern Türkiye.

In summer, there was again a reversal of patterns. Western Türkiye was wetter than normal with locally heavy precipitation, including hail. Seasonal totals were more than 150% of normal in many places. In contrast, eastern Türkiye had a dry summer with widespread precipitation below 80% of normal. Summer precipitation was also below normal in most of the South Caucasus. Seasonal precipitation in Armenia was only 58% of normal, making this its second-driest summer on record.

Autumn was generally drier than normal across most of the region. Several areas received less than 80% of their normal precipitation, and western Türkiye and Armenia received less than 60%. December was also a dry month, with many places receiving less than 20% of normal, especially in Türkiye. Only Azerbaijan had above-normal precipitation that month, with some locations seeing more than 250% of normal.

(iii) Notable events and impacts

The year 2022 had the highest number of extreme weather- and climate-related events in Türkiye on record, with 1030 reported through the database of the Turkish Meteorological Service. Most of the reported events were heavy rain and floods (34%), severe storms (21%), and hail (19%). As an example, 336 landslides occurred in 11 districts of the Ordu Municipality (located at the eastern Black Sea coast of Türkiye) due to heavy rain on 18 July. There is an increasing trend in the number of extreme events, especially in the last two decades.

In Yerevan (Armenia), the daily maximum temperature reached 39.5°C on 17 August, setting a new record for that day of the year. The highest temperature overall during 2022 in Armenia was 41.2°C at Ararat station (southwest Armenia) during the same heatwave on 15–19 August. The highest temperature in Türkiye was 47.9°C in Silopi/Şırnak on 15 July.

g. Asia

—Z. Zhu, Ed.

Throughout this section, the base period for the climatological normal and anomalies is 1991–2020. All seasons refer to the Northern Hemisphere, with winter referring to December–February 2021/22, unless otherwise noted.

1. OVERVIEW

—P. Zhang, T.-C. Lee, A.-M. Setiawan, Y. Oikawa, K. Takemura, Y. Okunaka, K. Takahashi, M.-J, Kim, D. Dulamsuren, M.-V. Khiem, H.-P. Lam, H. Chen, and R. Lu

Annual mean surface air temperatures for 2022 were above normal across most of Asia and Siberia, except for Southeast and South Asia, with anomalies of more than +1.0°C in eastern China, from northwestern China to Central Asia, and in northern central and western Siberia (Fig. 7.45). Annual precipitation totals were more than 120% of normal across most of central Siberia, northeastern China, parts of Southeast Asia, from India to Pakistan, and western Central Asia. Annual precipitation totals were less than 80% of normal from western Mongolia to western China (Fig. 7.46).

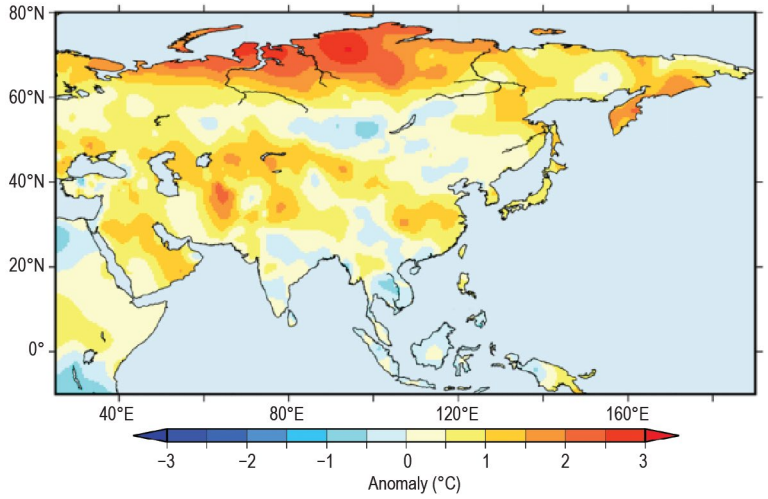

Fig. 7.45. Annual mean surface temperature anomalies (°C; 1991–2020 base period) over Asia in 2022. (Source: Japan Meteorological Agency, JMA.)

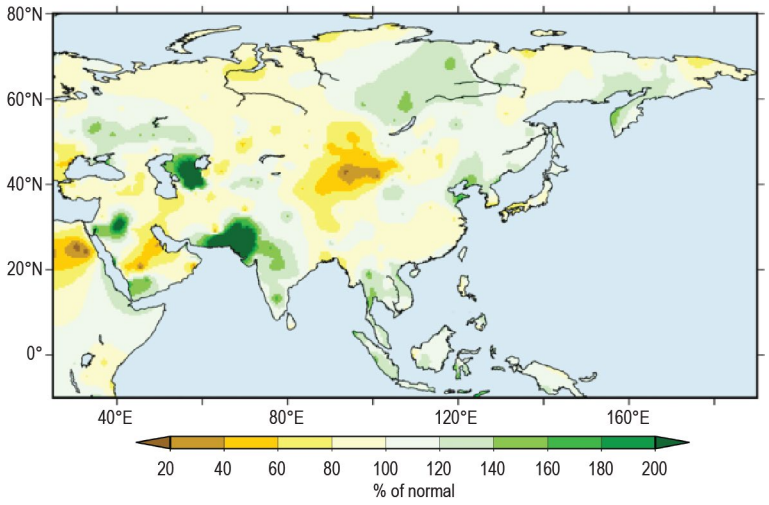

Fig. 7.46. Annual precipitation totals (% of normal; 1991–2020 base period) over Asia in 2022. (Source: JMA.)

In winter, above-normal temperatures dominated from northern central Siberia to northern India (Fig. 7.47a). Seasonal precipitation was much above normal from the Indochina Peninsula to India and below normal from western Japan to eastern China and from Mongolia to northwestern China (Fig. 7.47b). In spring, temperatures were above normal across most of Asia and Siberia, except for parts of eastern Siberia, Southeast Asia, and Central Asia (Fig. 7.47c). Seasonal precipitation was above normal from southern China to the Philippines and in western China, and below normal from Mongolia to northern China and from northwestern India to southwestern Asia (Fig. 7.47d). In summer, Pakistan experienced much-below-normal temperatures and much-above-normal precipitation (Figs. 7.47e,f). Positive temperature anomalies were observed in most of China, while temperatures were below normal from northern Mongolia to southern central Siberia (Fig. 7.47e). Seasonal precipitation was above normal in and around central Siberia, from northeastern China to northern Japan, and in Indonesia and southwestern Asia. Summer precipitation was below normal from western Mongolia to western China, and in southern Central Asia (Fig. 7.47f). In autumn, temperatures were above normal in northern central and western Siberia, southeastern China, and western Asia and below normal in far eastern

Siberia (Fig. 7.47g). Seasonal precipitation was much above normal from southwestern China to northern India as well as in Indonesia and western Central Asia and below normal in southwestern Asia and from southern Mongolia to northern China (Fig. 7.47h).

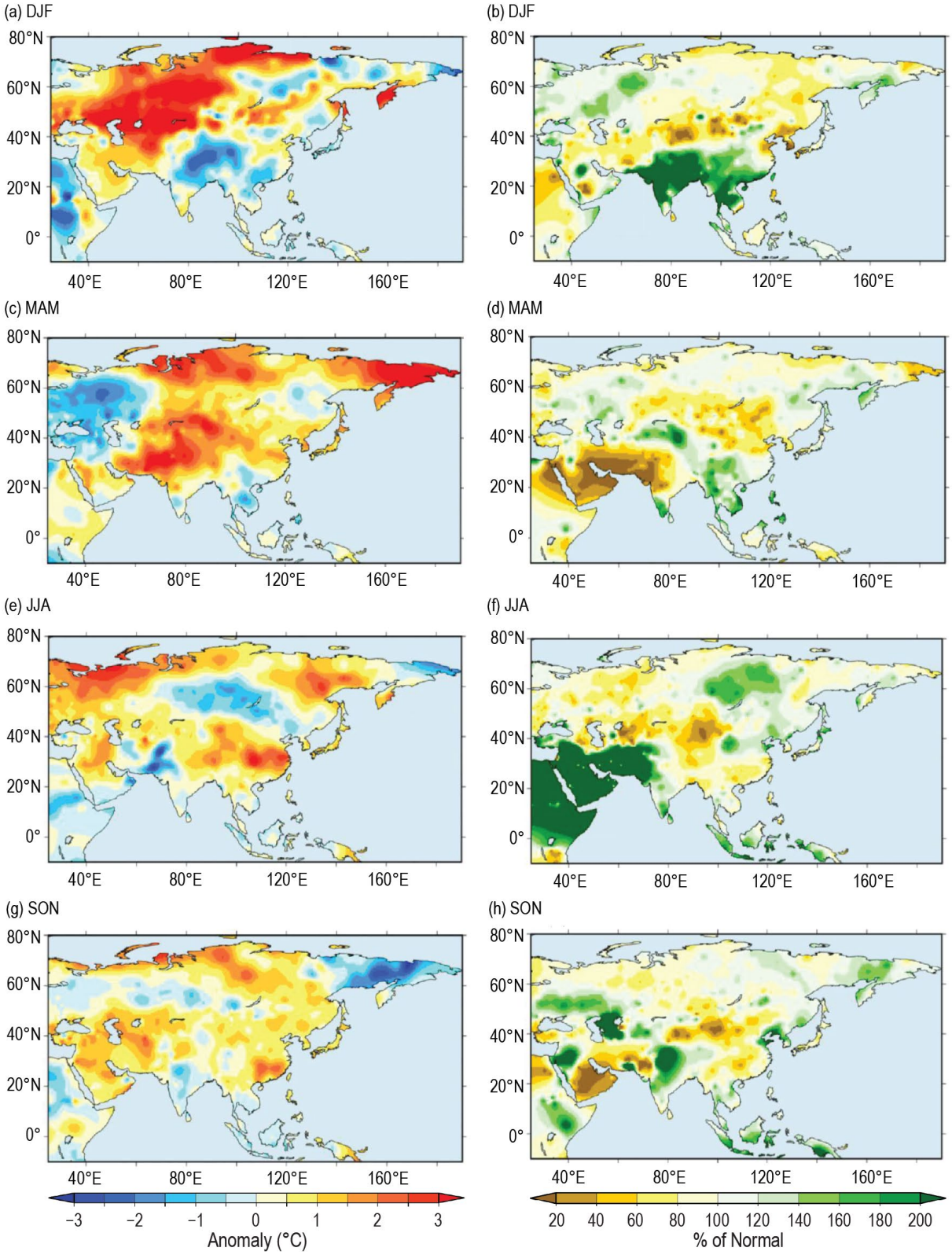

Fig. 7.47. Seasonal mean surface temperature anomalies (°C, left column) and precipitation ratios (% of normal, right column) over Asia in 2022 for (a),(b) winter, DJF; (c),(d) spring, MAM; (e),(f) summer, JJA; and (g),(h) autumn, SON. Anomalies and ratios are relative to 1991–2020. (Source: JMA.)

In winter, positive 500-hPa geopotential height anomalies were dominant from Central Asia to Siberia, while negative 500-hPa geopotential height anomalies accompanying negative 850-hPa temperature anomalies were observed from South Asia to East Asia (Fig. 7.48a). In spring, positive anomalies of geopotential height and temperature were seen over Central and East Asia (Fig. 7.48c). The enhanced convection from southwestern India to the seas east of the Philippines (Fig. 7.48d) was observed. In summer, above-normal geopotential heights and temperatures were observed over China (Fig. 7.48e). Convective activity was enhanced from the Arabian Sea to near Indonesia (Fig. 7.48f). In autumn, above-normal geopotential heights and temperatures were clearly seen in the midlatitudes from Eurasia to the North Pacific (Fig. 7.48g). Convective activity was enhanced near Indonesia, accompanied by 850-hPa cyclonic circulation anomalies straddling the equator over the eastern tropical Indian Ocean (Fig. 7.48h).

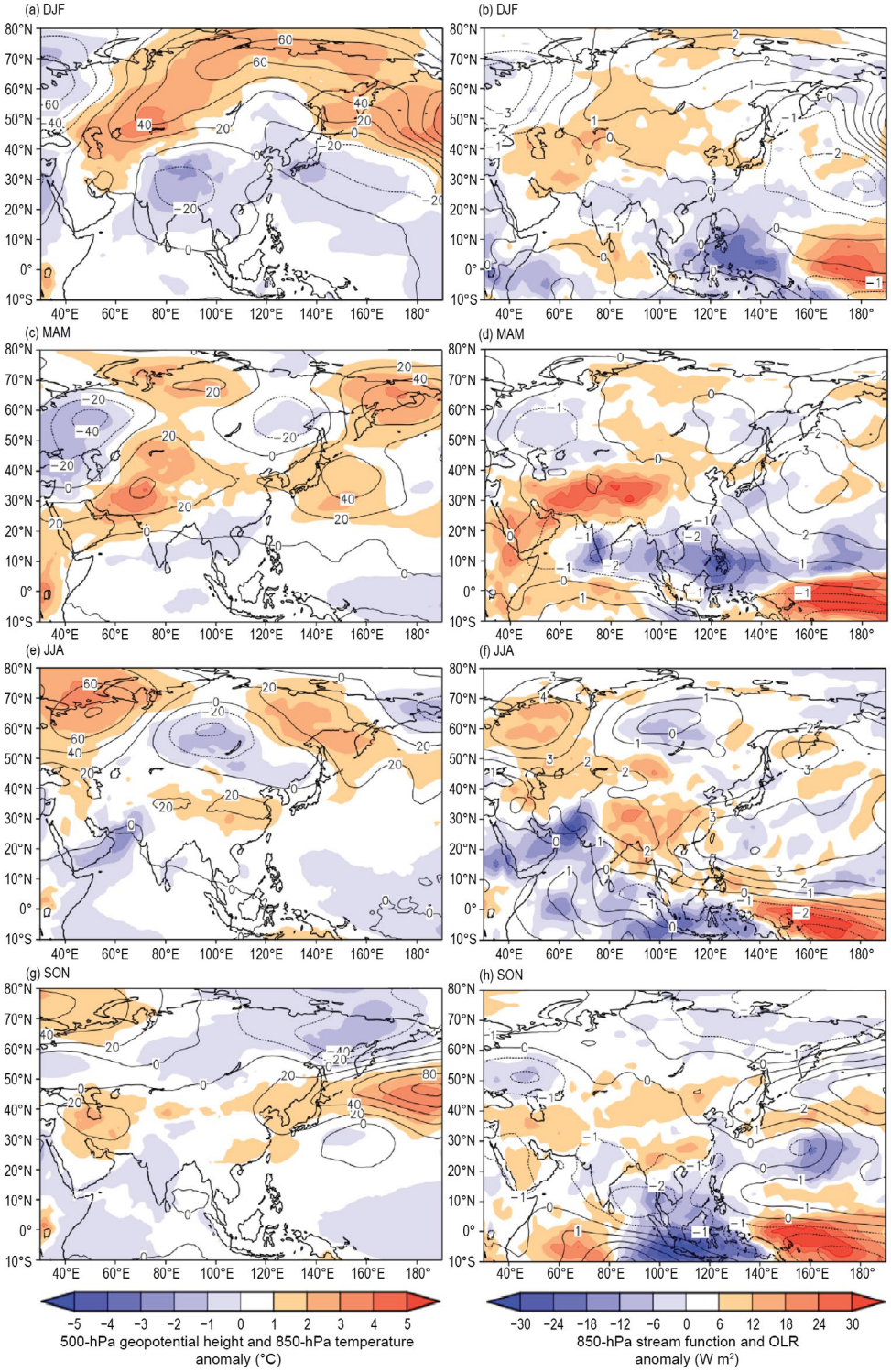

Fig. 7.48. Seasonal mean anomalies of atmospheric circulation variables in 2022 for (a),(b) winter, DJF; (c),(d) spring, MAM; (e),(f) summer, JJA; and (g),(h) autumn, SON. Left column: 500-hPa geopotential height (contour, gpm) and 850-hPa temperature (shading, °C). Right column: 850-hPa stream function (contour, 1 × 10^6 m^2 s^{-1}) using data from the JRA-55 reanalysis and outgoing longwave radiation (OLR; shading, W m^{-2}) using data originally provided by NOAA. Anomalies are relative to 1991–2020. (Source: JMA.)

2. RUSSIA

—M. Yu. Bardin and N. N. Korshunova

Estimates of climate features for Russia are obtained from hydrometeorological observations of the Roshydromet Observation Network. Anomalies are relative to the 1991–2020 base period, and national rankings and percentiles reflect the 1936–2022 period of record. Note that the temperature database was extended significantly, which in some cases changed previous rankings. The boundary between Asian Russia and European Russia is considered to be 60°E.

(i) Temperature

The year 2022 in Russia was the fifth warmest on record with an annual mean temperature 0.87°C above normal (Fig. 7.49), significantly higher than that of the previous year (0.15°C above normal) but below that of 2020 (2.02°C above normal), the record-warmest year.

The warmest areas, with respect to their climatology (anomalies above the 95th percentile), were the Arctic zone from the Kola peninsula to the Yenisei River, the southern Far East (Khabarovsk region, Kamchatka, Sakhalin), and the eastern North Caucasus.

Winter was the 10th warmest on record for Russia as a whole, with February in European Russia ranking among its five warmest on record (5.2°C above normal).

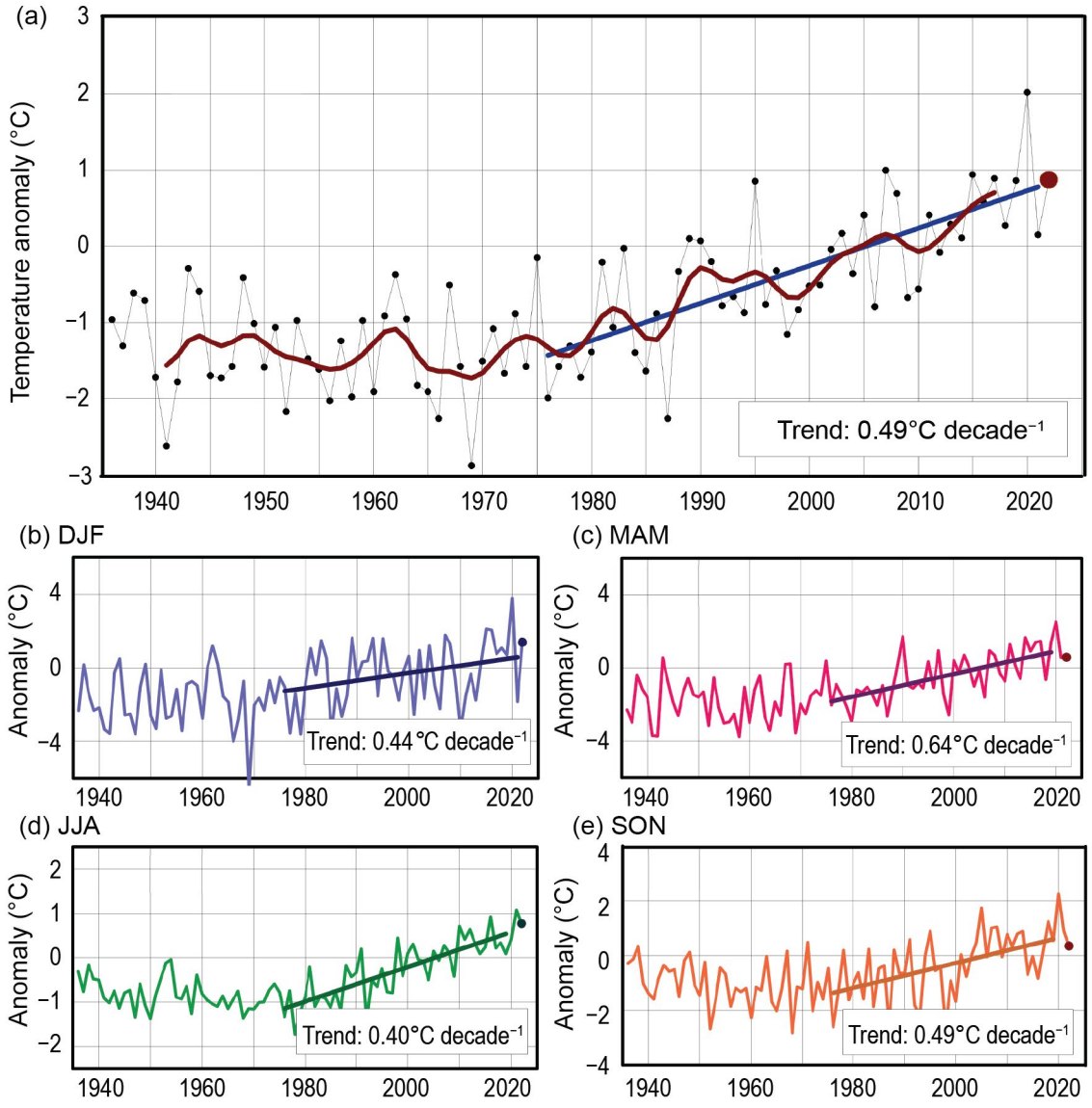

Fig. 7.49. Annual and seasonal mean temperature anomalies (°C; 1991–2020 base period) averaged over the territory of Russia for the period 1936–2022: (a) annual, (b) winter, (c) spring, (d) summer, and (e) autumn. The bold red line in (a) is an 11-point binomial filter. Linear trend (°C decade⁻¹) is calculated for the period 1976–2022.

Spring was colder than normal in European Russia (0.84°C below normal), but warmer than normal in its Asian counterpart (1.2°C above normal; 10th warmest). May in Asian Russia was the second warmest on record (1.6°C above normal), while in European Russia the May temperature was in the bottom quartile (2.1°C below normal). The largest positive anomalies in May were observed in the Yamalo-Nenets Autonomous Okrug. At the meteorological stations Nadym and Tarko-Sale, May 2022 was the second warmest after 2020 (Fig. 7.50). Conversely, abnormally cold

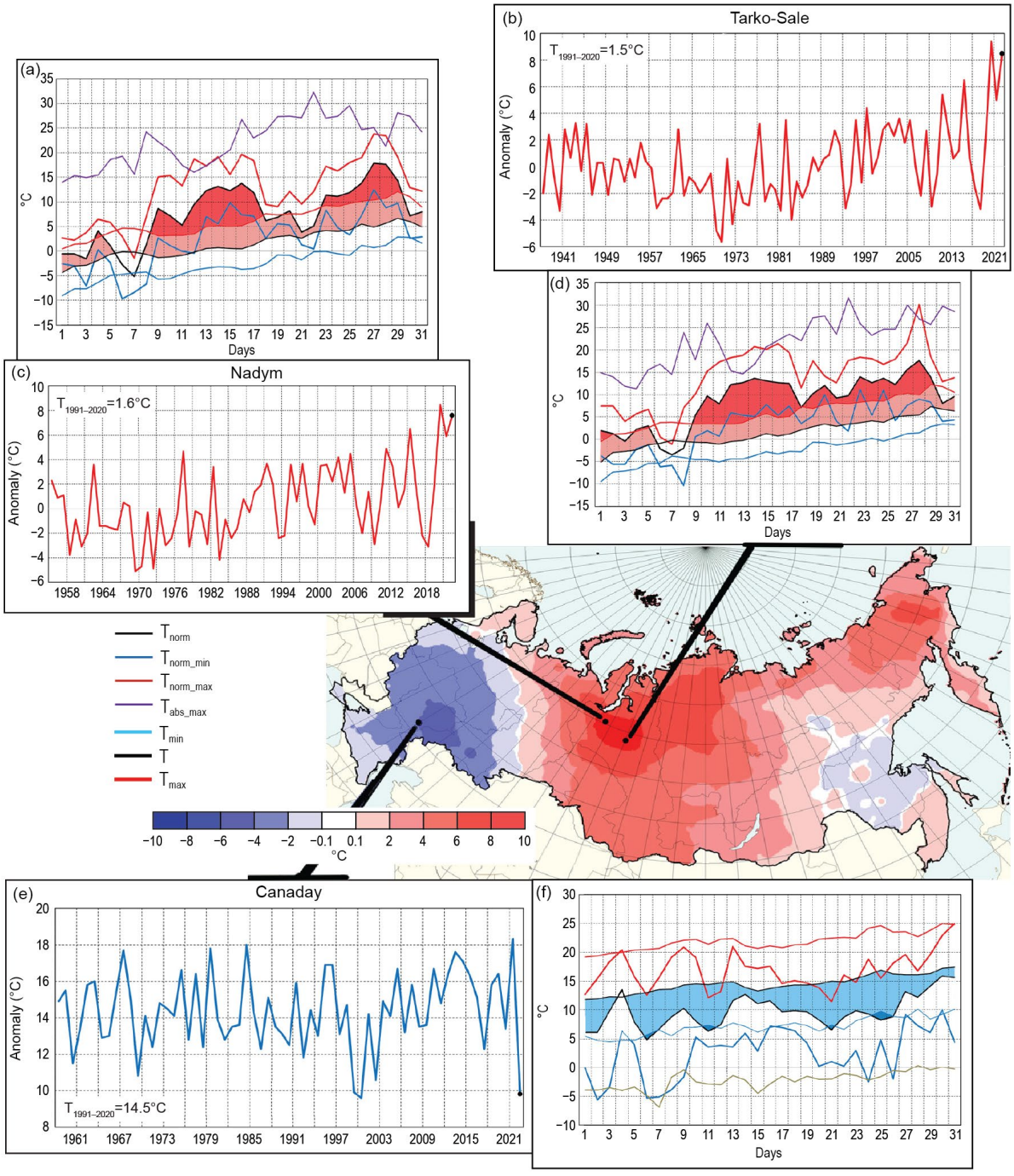

Fig. 7.50. Map: temperature anomalies across Russia (shading, contour interval is 2°C) for May 2022. Insets: Monthly mean temperature (°C) in (b) Tarko-Sale (1937–2022), (c) Nadym (1955–2022), and (e) Canaday (1958–2022), and mean, minimum, and maximum daily temperatures (°C) in May 2022 in (d) Tarko-Sale, (a) Nadym, and (f) Canaday. $T_{91\text{-}20}$ on plots of monthly mean temperatures is 1991–2020 mean. Plots of daily temperature show observed daily mean (T, black line), daily minimum (T_{min}, blue line), and daily maximum (T_{max}, red line) temperatures along with their climatological values (three lowermost curves: T_{norm}, black; T_{norm_min}, blue; T_{norm_max}, red) and absolute maximum temperature (T_{abs_max}, dark red). For (a) Nadym and (d) Tarko-Sale, the area between the normal daily mean curve T_{norm} and the observed daily mean curve is shaded pink where $T > T_{norm}$, and is shaded red if T was above normal daily maximum T_{norm_max}. For (f) Canaday, the area where $T < T_{norm}$ is shaded blue.

weather was observed in European Russia for almost the entire month. New daily temperature minima were recorded from the Vologda Oblast to the Lower Volga. At the Canaday meteorological station, the daily average temperature was below normal for 30 days in May. Daily minimum temperature records were broken six times at the same station. This contrasting temperature regime was associated with a pattern of tropospheric circulation, in which a deep trough located over European Russia provided an influx of arctic air while a large ridge over western Siberia provided an influx of warm air from the subtropics; this pattern persisted with some variations for almost the entire month.

Summer was the third warmest on record both for Russia as a whole (0.77°C above normal) and European Russia (1.69°C above normal). Summer for Asian Russia was the sixth warmest (0.43°C above normal). July was especially warm (0.73°C above normal; second warmest on record) there, and August was record warmest in European Russia (3.5°C above normal). Monthly temperatures above the 95th percentile were recorded in August at all European stations of Russia.

Autumn was moderately warm (0.35°C above normal), due primarily to a warm October (1.44°C above normal; sixth warmest on record). Temperatures in September and November were below normal, especially in the northern Far East Russia.

All seasons in Russia have warmed since the mid-1970s. Annual and seasonal trends are statistically significant at 1%, except winter. Due to long-term changes in atmospheric circulation in the Atlantic-European sector, winter temperatures showed no discernable trend from the mid-1990s to around 2010, then began to increase thereafter (Fig. 7.49), but the trend remained insignificant. After the abnormally warm winter of 2020, the trend became significant at least at the 5% level.

(ii) Precipitation

Across Russia as a whole, the total precipitation in 2022 was 105% of normal, the fourth wettest on record (equal with 1961, 1966, and 1990; Fig. 7.51). Asian Russia received 105% of its normal precipitation (fourth wettest), while European Russia had 104% (14th wettest). The seasons that ranked among their 10 wettest were: winter (120% of normal; third wettest) and autumn (118% of normal; seventh) in European Russia and summer in Asian Russia (112% of normal; sixth). In contrast, summer in European Russia was dry with only 83% of normal precipitation. In particular, August in European Russia was the second driest on record (50% of its normal precipitation).

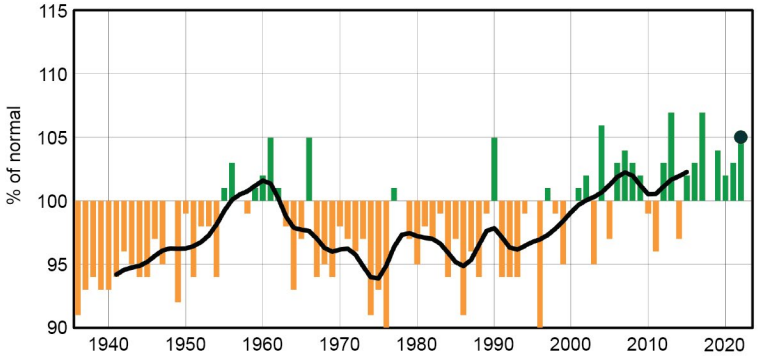

Fig. 7.51. Annual precipitation (% of normal; 1991–2020 base period) averaged over the Russian territory for 1936–2022. Bold black line denotes the smoothed time series (11-point binomial filter). The black dot indicates 2022 precipitation percentage.

Precipitation in Russia has increased during the period of warming since the mid-1970s by about 1.8% per decade. Increases are most notable in spring, with a rate of about +6% decade^{-1}. However, a vast area in southern European Russia is seeing decreasing precipitation; combined with the high rate of warming, this has led to an increasing risk of drought in this principal agricultural region.

(iii) Notable events and impacts

On 12 May, in the Bryansk region, heavy thunderstorms were accompanied by strong winds up to 27 m s^{-1}. Emergency power outages were recorded, 435 trees were felled, 272 houses were damaged, and three people were injured.

During 19–20 June, heavy rains (48 mm–74 mm) caused a sharp rise in water levels for the rivers of the Trans-Baikal Territory. Roads were washed out and bridges were destroyed. On one section of the Trans-Siberian Railway, the railway track was washed out, which led to a halt in the movement of trains.

On 24 June, heavy rain (85 mm–103 mm) caused a sharp water rise in small rivers in the Lazarevsky district of Greater Sochi. Twenty-eight adjacent territories were flooded and six people were swept out to sea. A landslide occurred at the railway station Chemitokvadzhe. Several trains were delayed, and the automobile bridge was washed away.

On 14–17 July, heavy rains (138 mm–311 mm) occurred in the Primorsky Territory and caused rivers to rise by 2.5 m–4 m. Roads and low-water bridges were destroyed, agricultural lands were flooded, and power lines were washed out. In the village of Timofeevka, mudslides descended on two houses, with one fatality recorded.

On 6 August, for two hours, inclement weather was observed in St. Petersburg; heavy rain (44 mm) was accompanied by winds up to 22 m s^{-1} and hail with a diameter of 5 mm. Several sections of roads as well as the lobby of a metro station were flooded, and the contact network of trolleybuses was broken. One person was injured.

On 19 September, in Moscow, wind speeds reached 19 m s^{-1} to 21 m s^{-1}, causing a power outage, 81 downed trees, damage to 65 cars, and one injury.

On 21–23 December, heavy snowfall (6 cm–13 cm) and blizzard conditions (27 m s^{-1} to 32 m s^{-1}) were recorded in the Primorsky Territory. The storm disrupted the power supply in 22 settlements, hindered traffic in 10 road sections, and canceled 128 bus trips.

3. EAST AND SOUTHEAST ASIA

—P. Zhang, T. C. Lee, A. M. Setiawan, A. Moise, Y. Oikawa, K. Takemura, K. Takahashi, M.-J. Kim, , D. Dulamsuren, M.-V. Khiem, and H.-P. Lam

Countries and places considered in this section include China, Hong Kong (China), Indonesia, Japan, Korea, Mongolia, Singapore, and Vietnam. Unless otherwise noted, anomalies refer to the 1991–2020 base period.

(i) Temperature

Annual mean temperature anomalies for 2022 across East and Southeast Asia are shown in Fig. 7.45. The annual mean temperature for China was 0.62°C above normal and the second highest since the start of the record in 1951. It was the sixth-warmest year in Hong Kong since its records began in 1884, at 0.4°C above normal.

In Japan, annual mean temperatures were above normal nationwide and significantly above normal in northern Japan. In western Japan, summer temperatures in 2022 were the highest on record since 1946, equal with 2013 and 2018. The annual mean temperature anomaly in South Korea was 0.4°C above normal, which was the ninth highest since its records began in 1973. Notably, it was significantly warmer than normal from spring to early summer. The annual mean temperature anomaly over Mongolia was 2.3°C above average (16th highest since 1940); the country recorded its fifth-warmest January and sixth-warmest May, 2.4°C and 1.7°C above normal, respectively.

Based on observation of 91 stations in Indonesia, the country recorded an annual average temperature that was 0.2°C above normal, making 2022 the 13th-warmest year since 1981. The maximum anomaly (+0.8°C) was recorded at Sentani–Jayapura meteorological station, while

the minimum anomaly (−0.7°C) was recorded at Karel Sadsuitubun–Maluku Tenggara meteorological station.

The annual mean temperature for Singapore in 2022 was 0.1°C above average. This was equal with 2021 as the 10th-warmest year since records began in 1929.

The monthly mean temperature was near-normal across Vietnam for most months in 2022. While the annual mean temperature was 0.4°C above normal, it was the coolest year since 2015.

(ii) Precipitation

Annual precipitation for 2022 as a percent of normal over East and Southeast Asia is shown in Fig. 7.46. The annual precipitation total for China was 95% of normal and the lowest total in the past 10 years. Total precipitation was significantly above normal in northeast China (124% of normal) and the Liaohe River Basin (135%; second wettest since 1961) and below normal in the Yangtze River Basin (86%). Total rainfall for Hong Kong in 2022 was about 91% of normal.

In Japan, annual precipitation totals were above normal in Okinawa/Amami and below normal on the Sea of Japan side of western Japan. The annual precipitation total for South Korea was 86.7% of its normal. Precipitation from winter 2021/22 to spring was below normal, mainly due to the influence of high-pressure systems. The annual precipitation in Mongolia was about 50% of normal.

Based on observed precipitation data from 115 BMKG official stations over the Indonesian region, 2022 was the second-wettest year since 1985 after 2010, with annual rainfall being 122% of normal. The highest rainfall anomaly (219% of normal) was recorded at Tampa Padang–Majene meteorological stations.

In Singapore, above-average annual total rainfall was recorded at most of the island stations in 2022. The annual total rainfall averaged across these stations (3012.0 mm) was 119% of the 1991–2020 average of 2534.3 mm, making 2022 the sixth-wettest year since 1980.

Total annual rainfall in 2022 in Vietnam varied from 80% to 120% of average across the country, except for the Red River Delta region to the Nghe An province, where annual rainfall was 140%–170% of average.

(iii) Notable events and impacts

In China, the Meiyu (also named Baiu in Japan and Changma in Korea) season, which started and ended earlier than usual, was eight days shorter than normal with 258.3 mm rainfall (81% of normal). The rainy season in North China, which was 23 days longer than normal (with a length of 53 days; third longest since 1961), had an average total rainfall of 214.7 mm (257% of normal).

In 2022, regional and periodic droughts occurred in China, especially in southern China which suffered from severe summer and autumn drought that had wide range, long duration, and heavy intensity. From July to the first half of November, the middle and lower reaches of the Yangtze River as well as Sichuan and Chongqing suffered from a series of summer and autumn droughts, impacting a maximum area of 1.63 million km^2. Seventy-seven days of drought accompanied high temperatures and little rainfall; the drought duration was the longest on record during this period since 1961. The persistent drought had a great impact on agriculture, water supply, energy, ecosystem balance, and human health in the Yangtze River basin.

From 13 June to 30 August, east-central China was affected by a widespread and enduring heatwave that lasted up to 79 days, the longest heatwave since 1961. Sichuan basin, Jianghuai, Jianghan, and Jiangnan all reported high temperatures above 35°C for 30 to 65 days, depending on the location. There were 361 stations (about 15% of the total number of stations in the country) in which the daily maximum temperature reached or exceeded its historical extreme. Beibei in Chongqing reached a daily maximum temperature of 45°C for two consecutive days.

In Hong Kong, total rainfall in April 2022 was only 3.5 mm, the lowest on record for the month. July 2022 was the hottest month on record with the monthly mean temperature reaching 30.3°C.

Contributing to this record were 25 hot nights (daily minimum temperature ≥28.0°C) and 21 very hot days (daily maximum temperature ≥33.0°C), both of which were the highest number in a month on record. Moreover, the consecutive 21 hot nights from 9 to 29 July were the hottest nights on record.

An extreme heavy rainfall event during 13–16 October in central Vietnam, from Quang Binh to Quang Ngai provinces, was the consequence of the combination of Tropical Storm Sonca (TS. No 5), the northeast monsoon, and easterly waves. Da Nang recorded record rainfall of 600 mm (Da Nang station) and 642 mm (Suoi Da station) in seven hours on 14 October, and level 3 floods (highest level in Vietnam's flood warning system) occurred in Kien Giang, Thach Han, Phu Oc, and Ai Nghia. These high floods, combined with high tide, caused prolonged inundation for central Vietnam that day.

South Korea observed its highest mean temperature from late June to early July (26.4°C; 3.5°C above normal) since 1973. From 8 to 11 August, South Korea experienced downpours (exceeding 140 mm h^{-1}) as a stationary front anchored over the central region. A few weeks later, on 6 September, Typhoon Hinnamnor made landfall in South Korea, bringing heavy rain and significant flooding.

In Semarang, Central Java of Indonesia, more than 200 mm of rainfall during 30–31 December caused massive flooding that inundated most of Semarang City and forced the government to stop operating the trans-Java train services.

Please refer to section 4g4 for details about the 2022 western Pacific tropical cyclone season.

Sidebar 7.2: The record-breaking hot summer of 2022 in the Yangtze River basin

—Z. ZHU, H. HUANG, H. CHEN, K. TAKEMURA, AND K. TAKAHASHI

The record-breaking hot summer of 2022 in Central and East Asia, especially in the Yangtze River basin (YRB), was long-lasting and extremely intense. Unusually high temperatures led to serious hydrological drought, agricultural failure, and ecological damage causing a direct economic loss of 32.8 billion yuan ($4.75 billion U.S. dollars) and affecting more than 38 million people.

The highest above-average temperatures were mainly located in the YRB in July and August (Figs. SB7.3a,b). Relative to the 90th percentile of temperature records in the period of 1991–2020, there were 30% more extreme high-temperature days (EHDs) during July and August across the YRB (slashed region in Fig. SB7.3a). The above-normal temperatures, averaged over the YRB, lasted about 80 days, with a maximum anomaly of +5.3°C on 22 August (Fig. SB7.3b). There were 35 EHDs from June to August, with 31 of those in July and August.

The detrended normalized July–August mean temperature averaged over the YRB (referred to as YT afterwards) in 2022 was more than two standard deviations, which was the largest since 1979 (Fig. SB7.3c).

The descending motion over the YRB was related to a local anomalous barotropic anticyclone (Figs. SB7.3d–f), which was one of the centers of anomalous anticyclones and cyclones. Based on regressions of the anomalous atmospheric fields onto the YT, the extreme high-temperature event was thought to be caused by: 1) the positive phase of North Atlantic Oscillation (NAO; Figs. SB7.3d–f), 2) the positive convection anomalies over the tropical Atlantic (Fig. SB7.3e), and 3) below-normal sea-surface temperatures (SSTs) due to La Niña in the tropical Pacific (Fig. SB7.3f).

The rare "triple-dip" La Niña event (see section 4b and Sidebar 3.1 for details), with negative SST anomalies in the central and eastern Pacific and positive SST anomalies in the western Pacific (Fig. SB7.3f), led to enhanced convection over the Maritime Continent (Fig. SB7.3e), which resulted in an anomalous local meridional cell favorable for the anomalous anticyclone (and descending motion) over the YRB. Furthermore, the anomalous convection over the tropical Atlantic, as well as the positive phase of NAO, could have also contributed to the anomalous anticyclone (and descending motion) over the YRB by stimulating the Rossby wave train propagating from the Atlantic to the North Pacific (Yang et al. 2023; Fu et al. 2023).

The three contributors noted above could be applied to reconstructing the YT index through a multiple linear

regression model (Fig. SB7.3c). Using the tropical Pacific SST (TPS) index (defined as the difference between the western and eastern tropical Pacific SSTs) as the only independent variable, the model was not able to reproduce the observed YT index or the extreme high-temperature event in 2022. When the NAO index was added as another independent variable, the simulated YT index was much closer to the observed one. It was found that the TPS index could be replaced by the precipitation over the tropical Atlantic (TAP) in the model. The observed YT index was reproduced to a large extent by the multiple regression model using the TAP and NAO indices, with a correlation coefficient of 0.67 ($p<0.01$) and root mean square error of 0.81. The record-breaking hot summer in 2022 over the YRB was also captured by this model, which suggests the irrelevance to the La Niña.

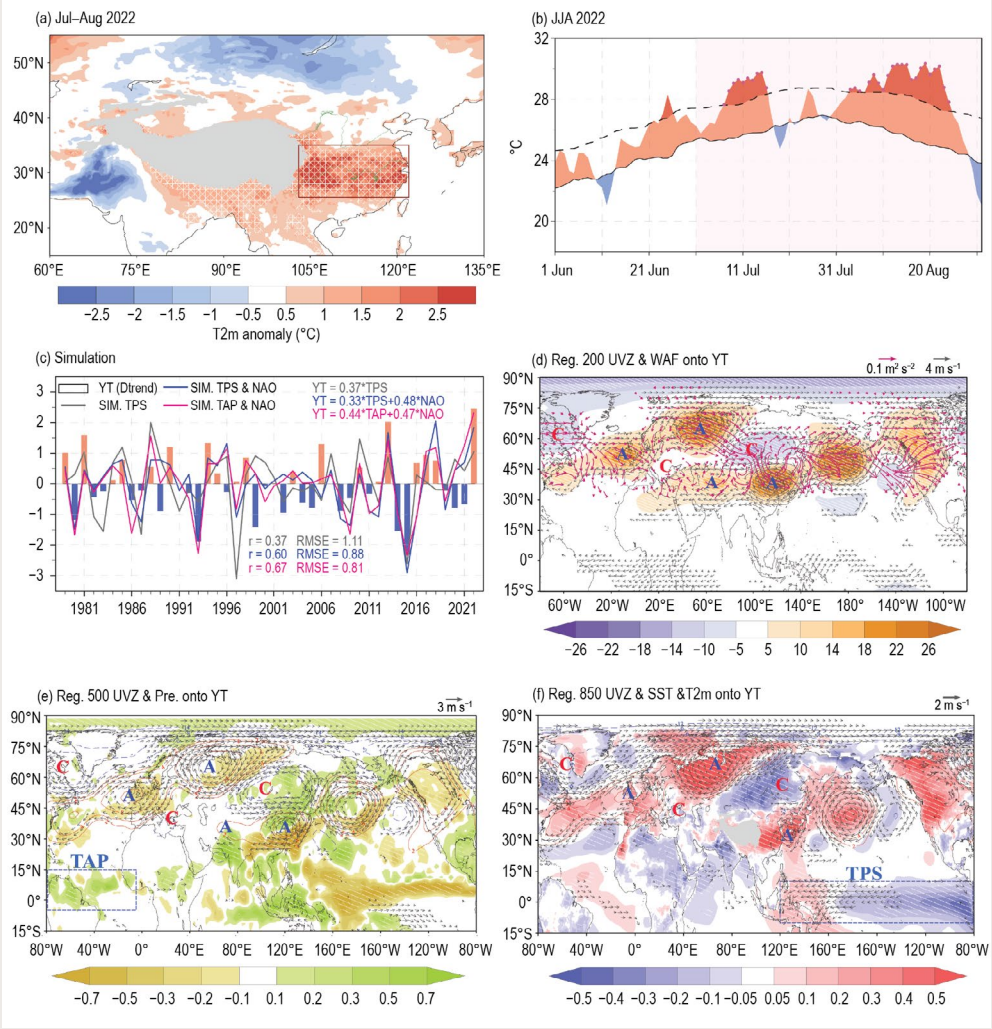

Fig. SB7.3. (a) 2-m air-temperature anomalies (T2m, shading, °C) for Jul–Aug 2022. Areas with extreme high-temperature days (EHDs) 30% more than normal (1991–2020) are slashed. (b) Daily evolution of temperatures averaged in the Yangtze River basin (YRB) from Jun to Aug 2022. The dashed (solid) curve represents the 90th percentile (climatological mean) of the temperature records, and the EHDs in Jul–Aug are marked (c) Time series of the detrended normalized Jul–Aug mean temperature averaged over the YRB (i.e., YT = 0.37*TPS, YT = 0.33*TPS+0.48*NAO, YT = 0.44*TAP+0.47*NAO) during 1979–2022 from observations (bar) and reconstruction by the multiple linear regression model (curves), with tropical Pacific sea-surface temperature (TPS) as the only independent variable (gray curve), with TPS and the North Atlantic Oscillation (NAO) indices as independent variables (blue curve), and with TAP and NAO as independent variables (red curve). (d) Regressions of the geopotential height (shading, gpm), wind (black vectors, m s^{-1}), and wave activity flux (red vectors, m^2 s^{-2}) at 200 hPa onto the YT index. (e) Regressions of the geopotential height (contours, gpm) and wind (vectors, m s^{-1}) at 500 hPa and precipitation (shading, mm day^{-1}) onto the YT index. (f) Regressions of the geopotential height (contours, gpm) and wind (vectors, m s^{-1}) at 850 hPa and SST/T2m (shading, °C) onto the YT index. In (d)–(f), the letters "A" and "C" represent the centers of anomalous anticyclones and cyclones, respectively, and regressions exceeding the 90% significance level are marked by white slashes. In (a) and (f), the Tibetan Plateau is denoted by gray shading. In (a), (e), and (f), the red and blue boxes are the domains for calculating the YT, TAP, and TPS indices.

4. SOUTH ASIA

—O. P. Sreejith, A. K. Srivastava, and M. Rajeevan

Countries in this section include Bangladesh, India, Pakistan, and Sri Lanka.

(i) Temperature

In 2022, South Asia generally experienced above-normal temperatures. The annual mean temperature in India was 0.51°C above the 1981–2010 average, making 2022 the fifth-warmest year on record since national records commenced in 1901 (Fig. 7.52). The seasonal mean temperatures in India were above normal for all seasons, except winter. The seasonal mean temperatures in India during the pre-monsoon season (March–May, anomaly of +1.06°C), monsoon season (June–September, +0.36°C), and post-monsoon season (October–December, +0.52°C) accounted for most of the warmth. The 10 warmest years on record have all occurred since 2009.

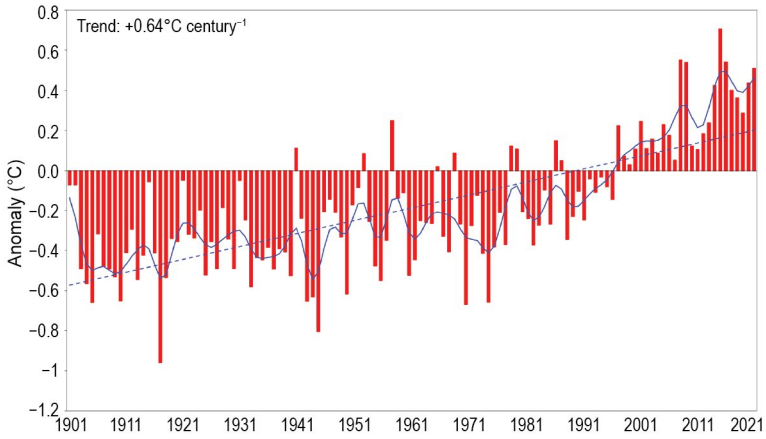

Fig. 7.52. Annual mean temperature anomalies (°C; with respect to 1981–2010 normal) averaged over India for the period 1901–2022. Continuous blue line indicates the smoothed time series (nine-point binomial filter). Dotted blue line indicates the trend over the period.

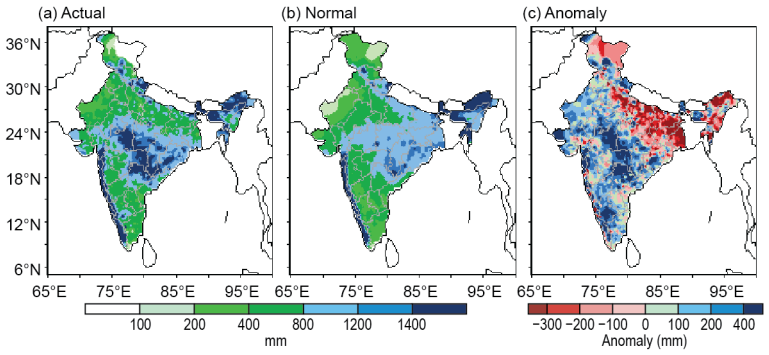

Fig. 7.53. Spatial distribution of actual, normal, and anomalous monsoon seasonal (Jun–Sep) rainfall (mm) over India in 2022.

(ii) Precipitation

The summer monsoon season (June–September) contributes about 75% of the annual precipitation over South Asia. The 2022 summer monsoon set in over Kerala (southwestern parts of peninsular India) on 29 May (normal is 1 June). The monsoon covered all of India by 2 July (normal is 8 July).

For India, the long-term average (LTA; 1971–2020) total of the summer monsoon rainfall is 869 mm with a standard deviation of about 10%; however, over smaller regions the standard deviation can be much larger. During 2022, the Indian summer monsoon rainfall (ISMR) averaged over the country as a whole was 106% of its LTA. Rainfall was fairly well distributed over the country except over the eastern and northeastern regions (Fig. 7.53). Seasonal rainfall over the homogeneous regions of Northwest India, Central India, South Peninsula, and East and Northeast India was 101%, 119%, 122%, and 82% of their respective LTA. On a monthly scale, rainfall for the country as a whole was above normal during July and September (117% and 108% of LTA, respectively), below normal during June (92%), and near normal during August (104%; Fig. 7.54).

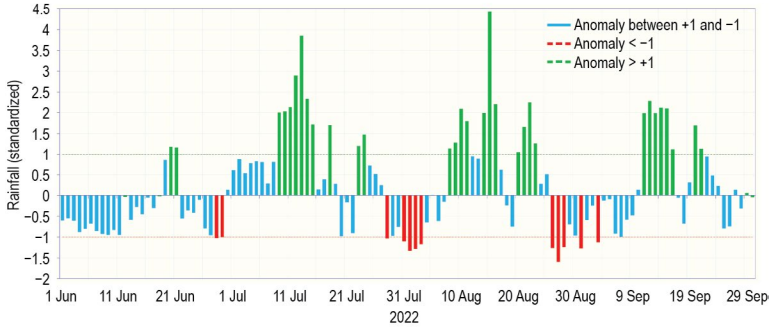

Fig. 7.54. Daily standardized rainfall time series averaged over the core monsoon zone of India (1 Jun–30 Sep 2022).

During the winter season (January–February), rainfall over India was above normal (147% of its LTA). It was near normal (99%) during the pre-monsoon season (March–May), and above normal (119%) during the post-monsoon season (October–December).

Pakistan, which is at the western edge of the pluvial region of the South Asian monsoon, typically receives 60%–70% of its annual rainfall during the summer monsoon season (July–September). The summer monsoon usually sets over eastern parts of Pakistan around 1 July with a standard deviation of five days. In 2022, the monsoon set over Pakistan on 30 June and withdrew during the third week of September. Summer monsoon rainfall was significantly above normal (175% of LTA). Pakistan experienced above-normal rains during July (183%) and August (241%), and below-normal rains during September (81%). Torrential rains during the season caused massive devastating floods in eastern and southern Balochistan, Sindh, Southwest Punjab, and Khyber Pakhtunkhwa. The seasonal rainfall (October–December) 2022 was 67% of the LTA value.

Bangladesh received normal (104% of LTA) rainfall during its summer 2022 monsoon season, while Sri Lanka received above-normal rainfall during its summer monsoon season (May–September).

Later in the year, the northeast monsoon (NEM) sets in over southern peninsular India during October and over Sri Lanka in late November. The NEM contributes 30%–50% of the annual rainfall over southern peninsular India and Sri Lanka as a whole. The NEM, which set in over southern peninsular India on 29 October, contributed to above-normal seasonal rainfall (110% of LTA).

(iii) Notable events and impacts

Fifteen cyclonic disturbances (three cyclonic storms and 12 depressions) formed over the North Indian Ocean in 2022, four more than the normal of 11 based on data from 1965–2021. The three tropical cyclones were: Severe Cyclonic Storms Asani and Mandous and Cyclonic Storm Sitrang. All three formed over the Bay of Bengal. The tracks of these cyclonic storms are shown in Fig. 7.55. Please refer to section 4g5 for details of the North Indian Ocean basin cyclone season.

In 2022, thunderstorms and lightning claimed around 1285 lives in India. On 25 July at least 26 people were killed in lightning strikes in Bihar and Uttar Pradesh.

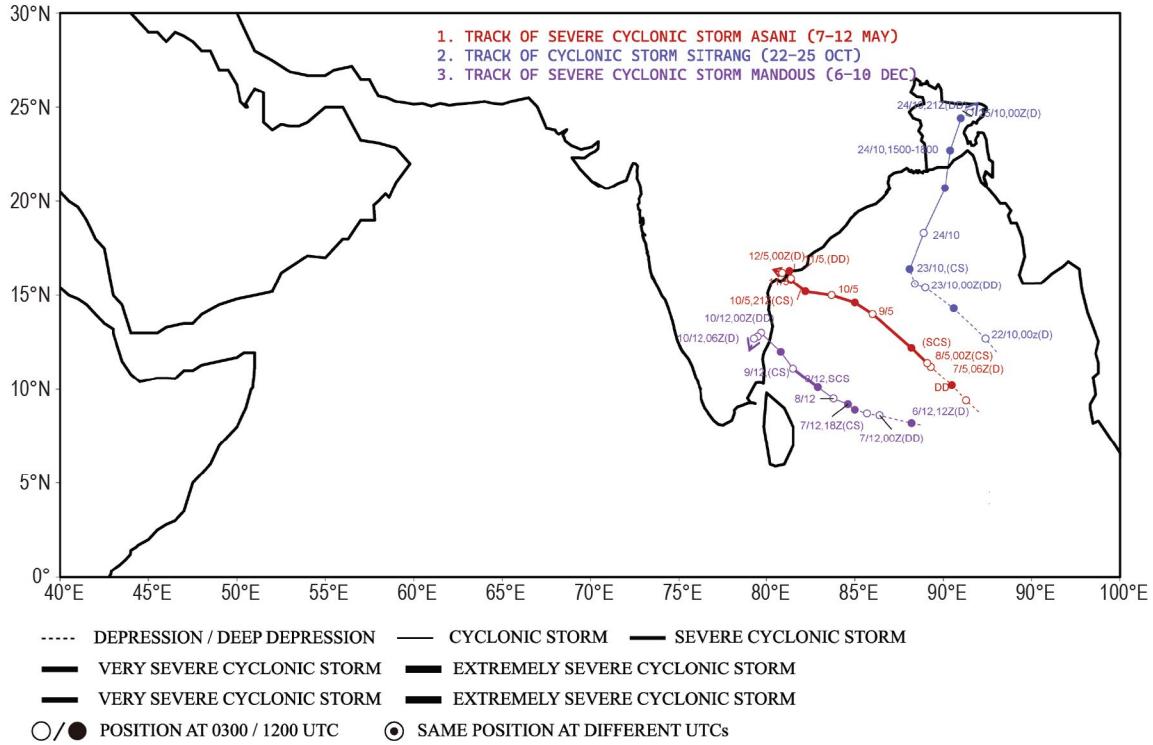

Fig. 7.55. Tracks of 2022 cyclonic storms over the North Indian Ocean.

During March and April, large parts of northwest India and Pakistan experienced prolonged heatwaves, prompting an early onset of the hot weather season. March 2022 was the hottest March in India since 1901. Mean temperatures in March and April were consistently 3°C to 8°C above normal, breaking many all-time records. In Pakistan, many stations recorded monthly all-time highs during the month. The city of Nawabshah recorded a high temperature of 49.5°C while the cities of Jacobabad and Sibi each recorded 47°C. This heatwave led to at least 90 deaths and reduced wheat crop yields across India and Pakistan. It also triggered forest fires in India.

Heavy rainfall and flood-related incidents claimed over 835 lives in different parts of India during 2022. Of these, 198 were from Assam, 116 from Maharashtra, 98 from Uttar Pradesh, 75 from Himachal Pradesh, and 56 from Manipur.

In Bangladesh, continuous heavy rains during the third week of June caused severe floods in several districts, claiming more than 60 lives. More than 4.3 million people were affected and there was a widespread loss of crops and houses. The Sylhet district was most affected, as almost two-thirds of the district was submerged.

Floods in Pakistan during June, July, and August caused over 1700 fatalities and led to major crop and property losses. Billions of dollars of damage and economic losses were reported. The flood in summer 2022 was also recorded as one of the world's costliest natural disasters of all time. The favorable monsoon circulation features enhanced monsoon lows and depressions that formed over the Bay of Bengal, moved up to Sindh-Balochistan, and caused heavy precipitation. In Bangladesh, 32 people died in June due to severe floods.

5. SOUTHWEST ASIA

—A. Vazife, A. F. Kazemi, and M. Mohammadi

This section covers Iran. Anomalies refer to the 1991–2020 base period.

(i) Temperature

The year 2022 was generally dry and warm in Iran, with anomalies of +0.5°C to +2.5°C; the eastern regions were exceptionally warm (Fig. 7.56a). Figure 7.56b shows that 2022 ranked in the top 20th percentile of all years since 1971.

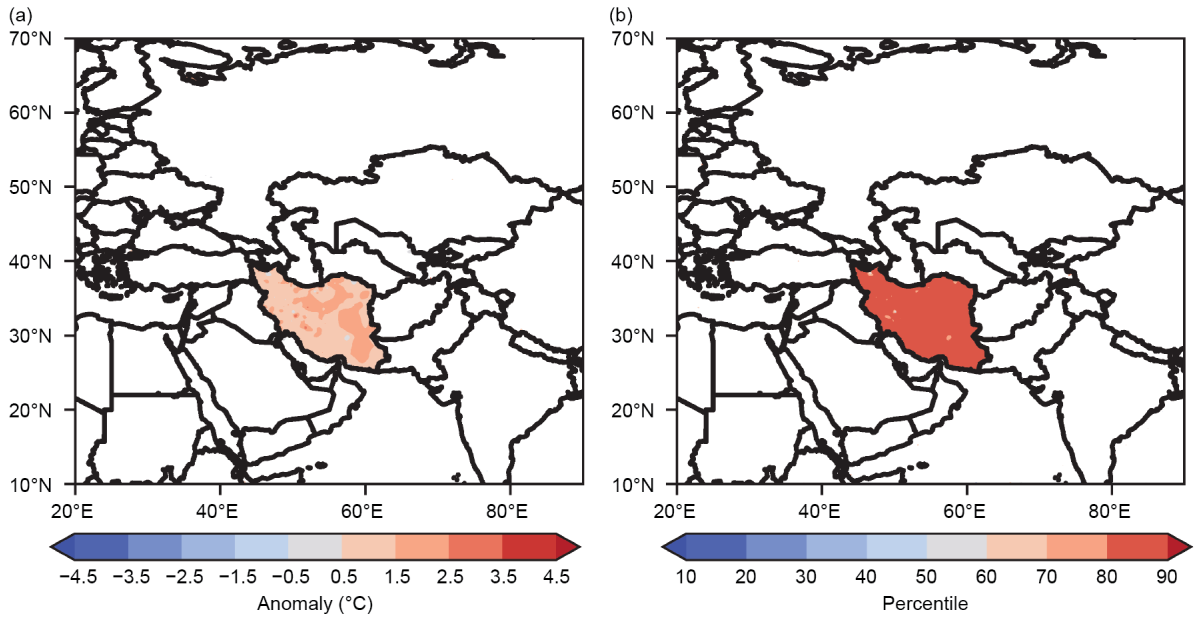

Fig. 7.56. (a) Mean annual temperature anomalies (°C; base period 1991–2020) and (b) percentile of the surface temperature for 2022 (period 1971–2020).

(ii) Precipitation

The annual precipitation total in 2022 averaged over Iran was 177.0 mm, which was more than that of 2021 (114.8 mm), but less than normal (236.9 mm). This marked the second-driest year (behind 2021) on record for the country.

Figure 7.57 shows precipitation anomalies in Iran for every season. Precipitation in the main rainy seasons of the year (winter, spring, and autumn) was below normal, and rain deficits were severe across parts of western, northwestern, and northeastern Iran.

Summer precipitation was above normal due to the northward track of the low-level Somali jet north of the Indian Ocean and the Oman Sea. Humid air currents in summer were pushed northward by the jet, and Iran received above-normal precipitation in the south and southeast via local thunderstorms. The normal range of summer precipitation typically provides less than 10% of annual precipitation in the country, but in summer 2022, Iran received more than 15% of its annual total. This was mainly attributed to the low-level humidity track of the Indian Ocean region surface and low-level winds.

Despite above-average summer precipitation, the annual 2022 precipitation was much less than normal since the main precipitation periods of the country (winter, spring, and autumn) were much drier than normal. Due to the dryness, Iran experienced severe and exceptional drought in many provinces of the country, especially in western mountainous provinces across the Zagross chain.

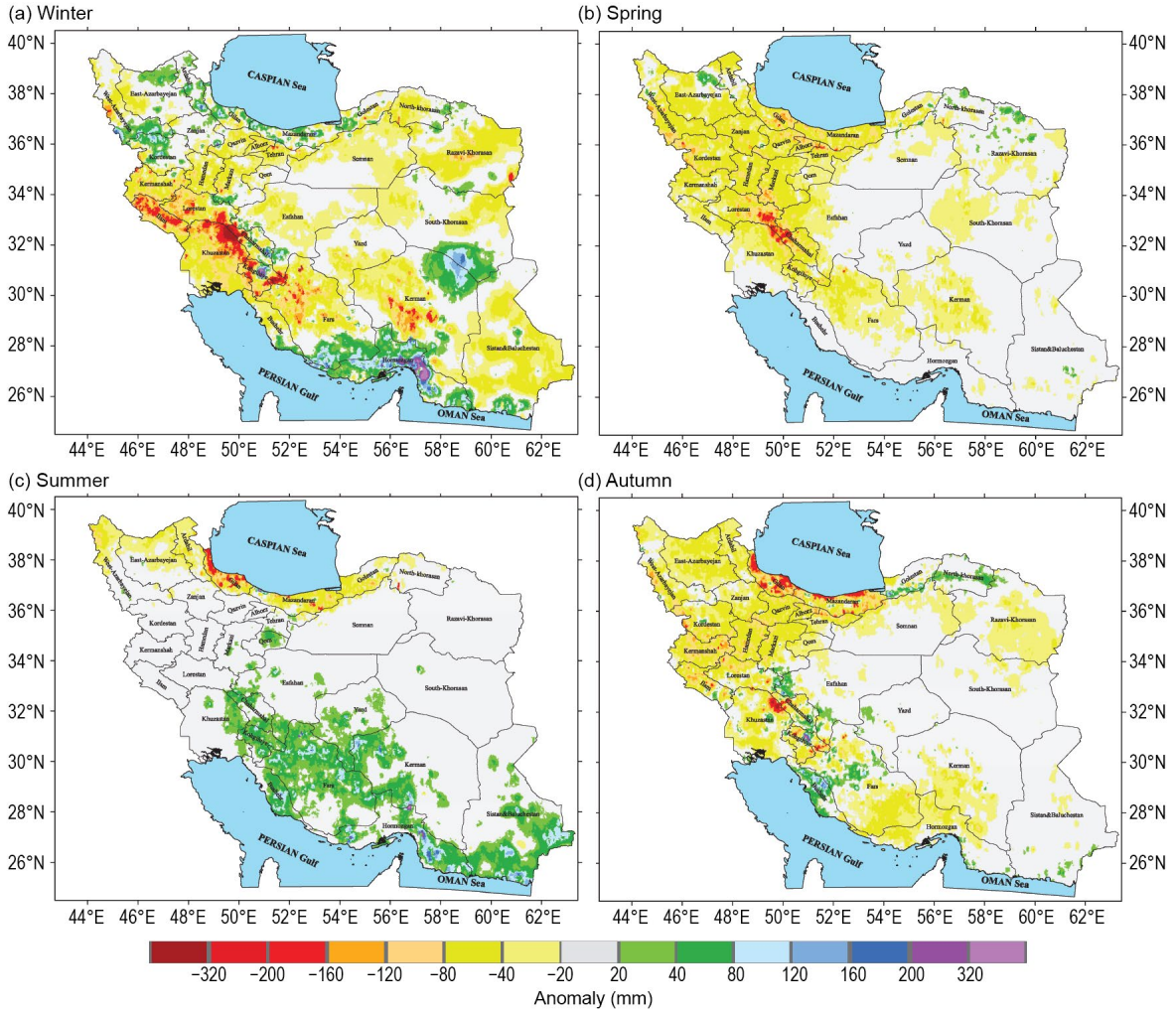

Fig. 7.57. Precipitation anomalies (mm) across Iran in 2022 for (a) winter (Jan–Mar, JFM), (b) spring (Apr–Jun, AMJ), (c) summer (Jul–Sep, JAS), and (d) autumn (Oct–Dec, OND).

(iii) Notable events and impacts

Droughts and summer flash floods in Iran caused enormous damage to crop yields and rural areas. The water shortages were more visible and severe in the central plateau of the country. Flash floods in Tehran and southern provinces in the north of the Persian Gulf during June and July caused dozens of deaths. Together, the drought and floods caused nearly $7 billion (U.S. dollars) in damage to the agriculture sector, with two-thirds of the damage due to drought and one-third due to floods.

6. CENTRAL ASIA

—R. Shukla, MD A. E. Bhuiyan, and W. M. Thiaw

Central Asia (CA) is a landlocked semi-arid region spanning a wide latitudinal area extending from the northern temperate zone with Russia at its northern border to the southern subtropics. It exhibits a complex topography ranging from vast plains to high mountains, and the Caspian Sea at its western edge. Its climate is diverse and influenced by terrain inhomogeneity. For the purpose of this analysis, we define CA as the region encompassing the countries of Afghanistan to the south, Turkmenistan, Uzbekistan, Tajikistan, Kyrgyzstan (from west to east) in the central part of the region, and Kazakhstan to the north. The climatological base period for both temperature and precipitation is 1991–2020.

(i) Temperature

During 2022, annual mean temperatures were lowest (–10°C–0°C) in central and eastern Tajikistan, southeast regions of Kyrgyzstan, and in northern high-elevation regions of Afghanistan (Fig. 7.58a). The northwest, central, northern, and eastern regions of Kazakhstan, western and northern Kyrgyzstan, western Tajikistan, and northern and northeast regions of Afghanistan registered 0°C–10°C. Annual mean temperatures were higher (10°C–20°C) across southwest and southern Kazakhstan, Uzbekistan, Turkmenistan, and western, southern, and southeast Afghanistan, with 20°C–25°C for the southern region of Afghanistan. The annual mean temperature anomalies were +0.5°C to +1.5°C in western and southern Karaganda, southeast Kazakhstan, western and central Uzbekistan, southwest Kyrgyzstan, and southern Afghanistan (Fig. 7.58b). 2022 ranked in the 90th–97th percentiles of warmest years on record in southwest Kazakhstan and southern Afghanistan. In contrast, the annual mean temperature anomalies were below normal (–1°C to –0.5°C) in the northern Kostanay regions of Kazakhstan and near the Kyrgyzstan/Tajikistan border, ranking 2022 in the 3rd–15th percentiles of coldest years on record for the latter area.

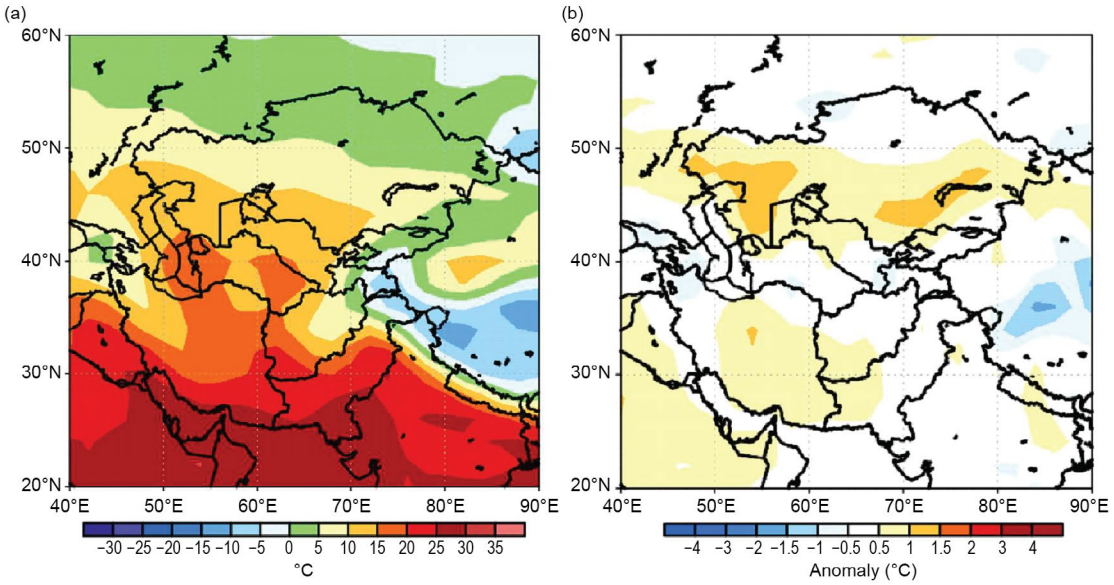

Fig. 7.58. Annual (a) mean temperature (°C) and (b) mean temperature anomalies (°C; 1991–2020 base period) for Central Asia. (Source: NOAA/NCEP.)

(ii) Precipitation

Annual precipitation totals for 2022 varied across Central Asia (Fig. 7.59a). About 100 mm–200 mm were received in southern Afghanistan, central and northern Turkmenistan, and central and southwest Uzbekistan during the year. Kazakhstan, Kyrgyzstan, Tajikistan, northwest and eastern Uzbekistan, western and eastern Turkmenistan, and the central, eastern, and northern regions of Afghanistan received 200 mm–500 mm. Larger precipitation totals (500 mm–600 mm) were observed in the high-elevation region of northern Afghanistan and in the northern and northeast regions of Kazakhstan.

Most regions in Central Asia received their maximum precipitation (rain and snowfall) during winter and spring seasons. Northern and eastern regions of Kazakhstan received precipitation during all months, while southern Kazakhstan, Uzbekistan, Turkmenistan, and western and southern Afghanistan received little to no rain during May–August. The annual precipitation totals were 10 mm–100 mm below average in the western, central, northern, and northeast regions of Afghanistan, western, southern, and eastern Turkmenistan, southeast Uzbekistan, and northern, northeast, and southwest Kazakhstan (Fig. 7.59b). In contrast, the annual precipitation totals were 10 mm–100 mm above normal in northwest, southern, and southeast Kazakhstan, western and northeast Uzbekistan, northern, central, and eastern Tajikistan and southeast Afghanistan, and were 100 mm–150 mm above average in northwest Kazakhstan and near the southeast border of Afghanistan and Pakistan.

Large precipitation deficits (–10 mm to –50 mm; lowest 10th percentile) were observed across Afghanistan during February–April. Most regions in Afghanistan received 25%–50% below-normal rainfall amounts during this period, according to data from the Global Precipitation Climatology Project (GPCP). The precipitation was 10 mm–30 mm below average across the northern, eastern, and southeast regions of Kazakhstan during April–September.

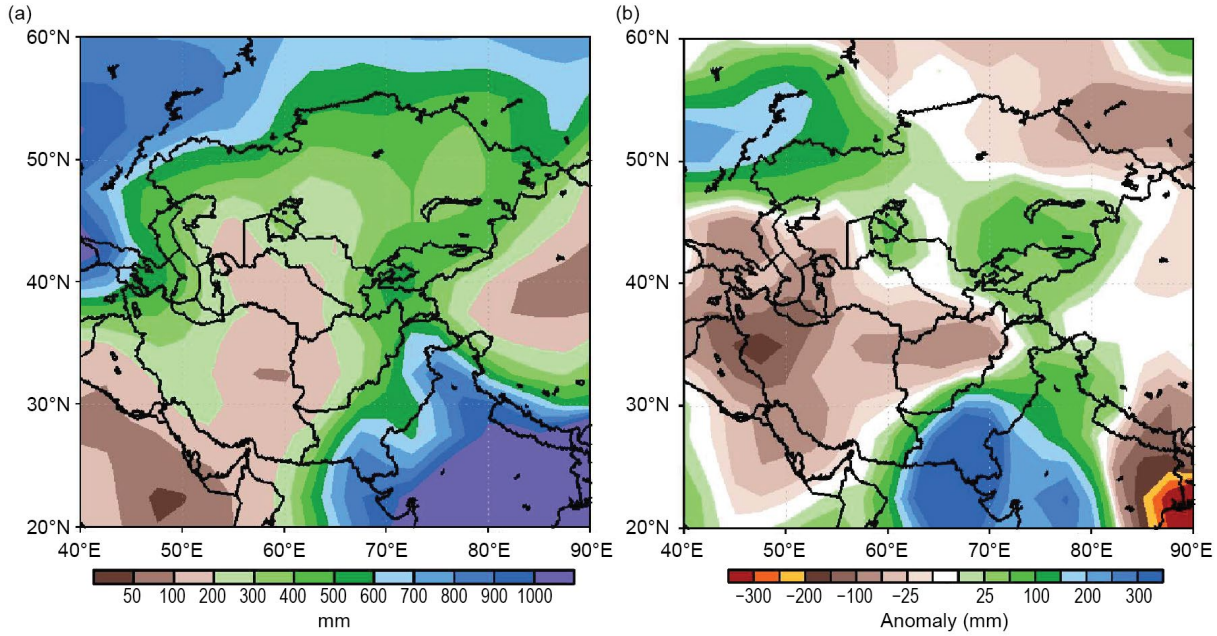

Fig. 7.59. Cumulative annual (a) precipitation (mm) and (b) precipitation anomalies (mm; 1991–2020 base period) for Central Asia. (Source: NOAA/NCEP GPCP data.)

(iii) Notable events and impacts

According to the Uzbekistan Hydrometeorological Service and analysis from NOAA's Climate Prediction Center (CPC) Unified Gauge, areas in the Samarkand and Jizzakh regions recorded 25 mm–50 mm of rainfall in two hours on 20 April, more than that normally received during the entire month. This rainfall damaged crops, homes, schools, and other buildings in the Bakhmal, Farish, Gallaaral, and Sharof Rashidov districts. Four fatalities were also reported.

According to the United Nations Office for the Coordination of Humanitarian Affairs (UN-OCHA), heavy and unseasonal rainfall (25 mm–75mm), based on analysis from the CPC Morphing Technique (CMORPH), fell in the Badakhshan, Herat, Badghis, Helmand, Takhar, Parwan, Kandahar, Wardag, Kunduz, Baghlan, Logar, and Juzjan regions of Afghanistan on 2–3 May, which caused flash flooding and affected nearly 3400 people. The flooding caused 22 fatalities and infrastructure damage.

According to UN-OCHA, eastern Afghanistan experienced flash flooding due to heavy rainfall (25 mm–75 mm) on 22 June that affected 1288 people. There were 19 fatalities and 131 injuries, and 356 houses were damaged or destroyed. Throughout July, heavy rains also caused floods and flash floods across several provinces in eastern, central, southern, and western Afghanistan, according to Afghan Red Crescent Society (ARCS) branches and the Ministry for Disaster Management. Also during the month, 25 mm–200 mm rainfall was observed across eastern regions of Afghanistan, based on analysis from CPC Unified Gauge rainfall. According to UN-OCHA, 39 people lost their lives and more than 1200 houses were damaged or destroyed, affecting at least 3000 families. Critical infrastructure, such as wheat mills and bridges, was also destroyed. Throughout August, heavy rains and flash floods were reported in several provinces across eastern, central, southeastern, southern, and northern Afghanistan, according to the United Nations International Children's Emergency Fund (UNICEF) and the International Federation of Red Cross and Red Crescent Societies (IFRC). Total rainfall across these regions ranged from 25 mm to 300 mm, according to analysis from the CPC Unified Gauge rainfall. From rainfall events in August, 141 fatalities were reported and 124 people were injured, with 44 others reported missing. Based on the Afghanistan National Disaster Management Authority (ANDMA) report, more than 16,000 houses were destroyed and 19,700 were damaged, and 249,900 people were affected. Thousands of hectares of crops were destroyed. From 11 to 15 August, most of eastern and southeastern Afghanistan received heavy rainfall (10 mm–50 mm) that caused flash flooding, resulting in 41 fatalities and significant infrastructure damage, according to UN-OCHA. In the following six days (16–21 August), the same regions received more heavy rainfall (25 mm–100 mm based on analysis from the CPC Unified Gauge). These rains also caused flash flooding, resulting in 63 fatalities and significant infrastructure damage.

h. Oceania

—C. Ganter, Ed.

1. OVERVIEW

—C. Ganter

The region of Oceania was dominated by La Niña conditions in 2022. This follows on from the past two years, which were also under its influence. As is typical for a La Niña year, most parts of Oceania were affected. Drier conditions were seen in some Southwest Pacific islands near the equator, while rainfall was higher than usual to the southwest of the South Pacific Convergence Zone. Broad areas of Australia had wetter conditions and persistent flooding. Micronesia had a quiet year for typhoon activity along with dryness near the equator, which is also typical of La Niña. In New Zealand, air and sea-surface temperatures were generally higher than average, as is typical of La Nina conditions.

In addition to La Niña, a negative Indian Ocean dipole (IOD) during the austral winter and spring, as well as persistently positive Southern Annular Mode (SAM) conditions for much of the year, influenced Australia during 2022. Both the negative IOD and the positive SAM contributed alongside the La Niña to Australia's second-wettest spring in 123 years. The positive SAM was associated with higher-than-normal pressure over New Zealand and, in combination with La Niña, it contributed to the country's warmest year, marking the second consecutive year to break the record.

2. NORTHWEST PACIFIC AND MICRONESIA

—B. Bukunt and C. P. Guard

This assessment covers the area from the date line west to 130°E, between the equator and 20°N. It includes the U.S.-Affiliated Islands of Micronesia, but excludes the western islands of Kiribati and nearby northeastern islands of Indonesia (see Fig. 7.61). Temperature and rainfall station data anomalies are reported with respect to the 1991–2020 base period.

For much of Micronesia, the weather and climate of 2022 was similar to that of 2021—quiet, with few extremes of rainfall, wind, or ocean waves. Of note were the wet conditions in eastern (Kwajalein, Majuro, Kosrae) and western (Yap, Palau) non-equatorial regions of Micronesia during the first six months of 2022. Only the central Micronesian island of Chuuk and the Marianas (Saipan, Guam) exhibited rainfall totals near or slightly below average. There was a low number of typhoons in the western North Pacific basin (see section 4g4 for details). With the third consecutive year of La Niña, three climate characteristics typical of La Niña were of note and similar to 2021: extreme dryness confined to locations along the equator, higher-than-normal sea levels across all of Micronesia, and a dearth of tropical cyclone activity in Micronesia.

(i) Temperature

While temperatures across most of Micronesia during 2022 were a mix of above and below average, most locations were near average. Wet locations had below-normal daytime temperatures due to persistent cloudy conditions, especially during the first half of the year. Nighttime temperatures were less attributable, but Yap and Pohnpei had large nighttime (minimum) temperature anomalies for the entire year, likely due to nighttime cloudiness.

The average six-month maximum and minimum temperature anomalies and the six-month and annual rainfall values for selected locations across Micronesia are summarized in Table 7.1.

Table 7.1. Average six-month temperature anomalies (first half and second half), and six-month and annual rainfall totals as well as percent of average values for selected Micronesia locations during 2022. The average values are for the 1991–2020 base period. Latitudes and longitudes are approximate. "Kapinga" stands for Kapingamarangi Atoll in Pohnpei State, Federated States of Micronesia. The color coding indicates: red highlights for above-average temperature (up arrow) and blue highlights for below-average temperature (down arrow); green fill for above-average rainfall (up arrow) and yellow fill for below-average rainfall (down arrow). The excessive coolness at Palau is likely an effect of the relocation of the weather station from the municipality of Koror to the international airport in Airai. Official stations inspections have been spotty since COVID started in early 2020. This lack of maintenance may have introduced some unknown issues to the station data.

Location	Jan-Jun Max, Min Temp (°C)	Jul-Dec Max, Min Temp (°C)	Jan-Jun AVG Rainfall (mm)	Jan-Jun 2022 Rainfall (mm)	Jan-Jun % Rainfall (mm)	Jul-Dec AVG Rainfall (mm)	Jul-Dec 2022 Rainfall (mm)	Jul-Dec % Rainfall (mm)	Jan-Dec 2022 Rainfall (mm)	Jan-Dec % Rainfall (mm)
Saipan 15°N, 146°E	+0.56 ↑, +0.22 ↑	+0.77 ↑, +0.73 ↑	462.8	527.3 ↑	113.9 ↑	1306.1	1412.5 ↑	108.1 ↑	1939.8 ↑	109.7 ↑
Guam 13°N, 145°E	–0.37 ↓, +0.03 ↑	–0.55 ↓, –0.22 ↓	678.7	542.8 ↓	80.0 ↓	1813.6	1745.0 ↓	96.2 ↓	2287.8 ↓	91.8 ↓
Yap 9°N, 138°E	–1.26 ↓, +1.37 ↑	–0.64 ↓, +1.37 ↑	1191.5	1511.8 ↑	126.9 ↑	1943.4	1968.8 ↑	101.3 ↑	3480.6 ↑	110.0 ↑
Palau 7°N, 134°E	–1.19 ↓, –1.02 ↓	–0.48 ↓, –1.45 ↓	1798.1	2391.7 ↑	133.0 ↑	2279.4	2154.4 ↓	94.5 ↓	4546.1 ↑	111.5 ↑
Chuuk 7°N, 152°E	–0.44 ↓, +0.58 ↑	–0.11 ↓, +1.03 ↑	1678.2	1666.5 ↓	99.3 ↓	1917.7	1856.5 ↓	96.8 ↓	3523.0 ↓	98.0 ↓
Pohnpei 7°N, 158°E	–0.29 ↓, +1.30 ↑	–0.29 ↓, +1.45 ↑	2361.2	3160.3 ↑	133.8 ↑	2308.4	2827.0 ↑	122.5 ↑	5987.3 ↑	128.2 ↑
Kapinga 1°N, 155°E	n/a	n/a	1880.6	1040.1 ↓	55.3 ↓	1485.1	768.4 ↓	51.7 ↓	1808.5 ↓	53.7 ↓
Kosrae 5°N, 163°E	–0.35 ↓, –0.19 ↓	–0.90 ↓, +0.14 ↑	2635.8	3451.6 ↑	131.0 ↑	2354.8	3111.8 ↑	132.1 ↑	6563.4 ↑	131.5 ↑
Majuro 7°N, 171°E	–0.51 ↓, +0.33 ↑	–0.31 ↓, +0.25 ↑	1459.0	1819.9 ↑	124.7 ↑	1875.0	1989.8 ↑	106.1 ↑	3809.8 ↑	114.3 ↑

(ii) Precipitation

Two particular characteristics of Micronesian regional precipitation during 2022 stood out: 1) extreme dryness at Kapingamarangi, which was considerably more extreme than in 2021 and 2) very wet conditions in eastern (Kwajalein, Majuro, Kosrae) and western (Yap, Palau) non-equatorial regions of Micronesia during the first six months of the year.

A sharp north-to-south gradient was observed across Pohnpei State. While Kapingamarangi (1°N latitude) had its second-driest January–June on record, the main island of Pohnpei reported its second-wettest January–June. Kapingamarangi ended the year as second driest on record

while Pohnpei ended the year as the third-wettest year. This unusual meridional gradient in rainfall is likely due to the strengthening La Niña during the April–July timeframe, which led to a compressed Intertropical Convergence Zone (ITCZ) constantly meandering over Pohnpei at 7°N latitude while the cold tongue sea-surface temperature signal along the equator limited convection around Kapingamarangi.

Typical rainfall distribution during a La Niña event includes moderate-to-extreme dryness at western Pacific locations near and along the equator, especially from May to November, while wet conditions are typical across the latitudes of the ITCZ (4°N–8°N; He et al. 1998). During a prolonged La Niña event, dryness is often experienced in eastern Micronesia, including Majuro and Kwajalein; however, this was not the case in 2022. An early and active tropical upper tropospheric trough (Sadler 1976) contributed to the wetness of the Marshall Islands in eastern Micronesia.

Table 7.2 illustrates the rainfall variability, comparing the percent of average between the 2021 and 2022 rainfall totals for selected islands. Negative values indicate greater rainfall in 2021 than in 2022. Despite both 2021 and 2022 being in an extended La Niña status, there was

Table 7.2. Difference (Δ%) of 2021 and 2022 percent of average six-month rainfall (first half and second half) and annual rainfall values for selected Micronesia locations. Negative values indicate greater rainfall in 2021 than in 2022. The average values are for the 1991–2020 base period. Latitudes and longitudes are approximate. The fill color of the boxes indicates green for values of ±0%–10% difference between 2021 and 2022 (right arrow), blue for values of ±11%–25% difference (northeast arrow), and purple for greater than ±25% difference (up arrow).

Location	2021 % Jan-Jun Rainfall (mm)	2022 % Jan-Jun Rainfall (mm)	Δ% Jan-Jun Rainfall (mm)	2021 % Jul-Dec Rainfall (mm)	2022 % Jul-Dec Rainfall (mm)	Δ% Jul-Dec Rainfall (mm)	2021 % Jan-Dec Rainfall (mm)	2022 % Jan-Dec Rainfall (mm)	Δ% Jan-Dec Rainfall (mm)
Saipan 15°N, 146°E	92.7	113.9	21.2 ↗	105.6	108.1	2.5 →	102.2	109.7	7.5 →
Guam 13°N, 145°E	86.3	80.0	–6.3 →	107.6	96.2	–11.4 ↗	101.8	91.8	10.0 →
Yap 9°N, 138°E	139.5	126.9	–12.6 ↗	86.9	101.3	14.4 ↗	106.9	110.0	3.1 →
Palau 7°N, 134°E	120.7	133.1	12.40 ↗	110.8	94.5	–16.3 ↗	115.2	111.5	–3.7 →
Chuuk 7°N, 152°E	125.3	99.3	–26.0 ↑	110.7	96.8	–13.9 ↗	117.5	98.0	–19.5 ↗
Pohnpei 7°N, 158°E	128.6	133.8	5.2 →	102.0	122.5	20.5 ↗	115.5	128.2	12.7 ↗
Kapinga 1°N, 155°E	90.0	55.3	–34.7 ↑	71.7	51.7	–20.0 ↗	81.9	53.7	–28.2 ↑
Kosrae 5°N, 163°E	149.5	131.0	–18.5 ↗	114.1	132.1	18.0 ↗	132.8	131.5	–1.3 →
Majuro 7°N, 171°E	141.5	124.7	–16.8 ↗	99.9	106.1	6.2 →	118.1	114.3	–3.8 →
Kwajalein 9°N, 168°E	92.6	141.2	48.6 ↑	84.9	102.0	17.1 ↗	87.7	116.3	28.6 ↑

substantial variability in rainfall amounts. Some differences were large, especially at Kwajalein where it was much wetter and at Kapingamarangi and Chuuk where it was much drier in the first half of 2022. Differences at all locations were within 25% in the second half of the year. Six of the 10 locations had differences of 10% or less by the end of the year.

(iii) Notable events and impacts

In keeping with a typical response to La Niña, conditions were very dry at Kapingamarangi (1.1°N, 154.8°E). Prolonged dry conditions there led to severe drought that impacted potable water supplies, local vegetation, and food crops. Abundant rainfall needed at Kapingamarangi to help the island recover from the effects of the long-term 2022 drought did not appear by year's end. Overall, impacts to the residents were minimized by the early import of water and food resources by the Federated States of Micronesia government and the U.S. Agency of International Development through the International Office for Migration.

Within Micronesia, Ulithi (10.0°N, 139.7°E) and Fais (9.8°N, 140.5°E) in Yap State were affected when Tropical Storm Malakas passed nearby in early April. Several tropical disturbances made significant contributions to seasonal rainfall at islands across western Micronesia.

Much-higher-than-average sea level across the tropics of the western Pacific is typical during La Niña. Sea-level heights by boreal summer 2022 were near their historical peaks throughout Micronesia. Time series of the sea level from two widely separated stations (Guam and Kwajalein) illustrate the strength of the coherence of the regional sea level and the historical perspective of the high stands during 2022 (Fig. 7.60). There were no reports of significant coastal inundation from any of the selected islands.

Since 1998, the tropics of the western North Pacific has experienced the largest magnitude of sea-level rise across the globe. The character of this rise was not gradual, but instead is best described as a step-function jump during 1998. The sea level increased by 30 cm from its low stand at the end of 1997 to a historically high stand at the end of 1998 (Merrifield et al. 2012). Elevated sea levels then persisted to the present, with three major short-term dips during the 2002, 2015, and 2018 El Niño events. Absolute historical high stands during 2010–12 and 2020–22 occur with periods of prolonged La Niña. At Guam, the high stands reached during 2021 and 2022 were the second and fourth highest in the historical record, respectively. The high sea level in the tropics of the western North Pacific is not primarily a signal of climate change, but rather an artifact of a substantial increase in the strength of the Pacific trade-wind system (Merrifield et al. 2012). An abrupt increase in the strength of the trade winds in 1998 separates the recent historical climate of the western Pacific into two regimes: 1) weak trades, low sea level (1975–98); and 2) strong trades, high sea level (1998–present).

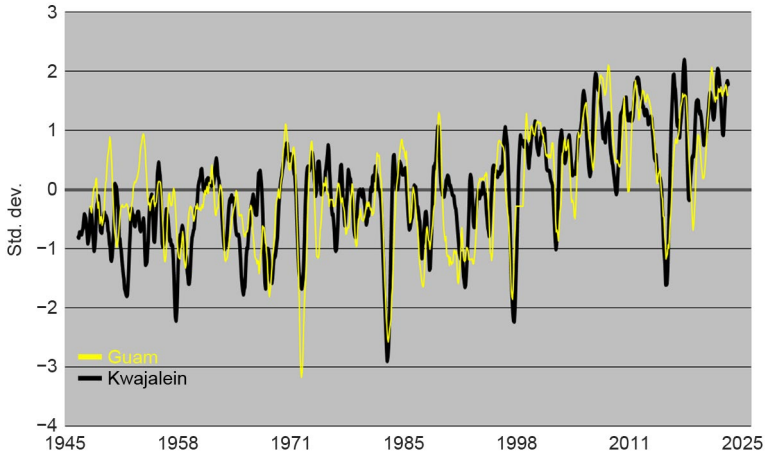

Fig. 7.60. A six-month moving average of the sea level at Guam (yellow) and at Kwajalein (black) from 1948 to 2022. Plotted values are normalized: (average)/(std. dev). Strong El Niño events stand out as sharp dips. (Data source: NOAA's Center for Operational Oceanographic Products and Services (CO-OPS).)

3. SOUTHWEST PACIFIC

—E. Chandler

Countries considered in this section include American Samoa, the Cook Islands, Fiji, French Polynesia, Kiribati, New Caledonia, Niue, Papua New Guinea (PNG), Samoa, the Solomon Islands, Tonga, Tuvalu, Vanuatu, and Wallis and Futuna (Fig. 7.61). The temperature analysis is based on the Climate Anomaly Monitoring System (CAMS) Monthly Surface Air Temperature Anomalies (https://iridl.ldeo.columbia.edu/maproom/Global/Atm_Temp/Anomaly.html). Anomalies are calculated with respect to the 1991–2020 base period. The precipitation analysis is based on the Multi-Source Weighted-Ensemble Precipitation (MSWEP) monthly analyses as presented for the South Pacific (http://www.bom.gov.au/climate/pacific/outlooks/) and the COSPPac Online Climate Outlook Forum (https://www.pacificmet.net/products-and-services/online-climate-outlook-forum). The base period for precipitation is 1980–2021.

The year began with a mature La Niña event that persisted into the second quarter of the year, before atmospheric and oceanic indicators in the Pacific briefly eased. La Niña strengthened again towards the end of 2022. Below-normal sea-surface temperatures (SSTs) were present across the central and western equatorial Pacific during the first half of 2022 before the cool regions contracted, although rainfall patterns remained persistently La Niña-like. Signs that La Niña would strengthen later in the year were present in the cloud and pressure patterns as early as June, with trade winds re-strengthening during August. The ocean lagged the atmospheric indicators but began to cool during the third quarter of the year.

Air temperatures and rainfall patterns were both typical of a La Niña event throughout 2022. Air temperatures at the start of the year were below normal along the central to eastern equatorial region. In the second quarter, the below-normal air temperatures expanded westward across the date line, in line with expanding negative sea-surface temperature anomalies. These cooler air temperatures persisted along the central and western equator during the third quarter while

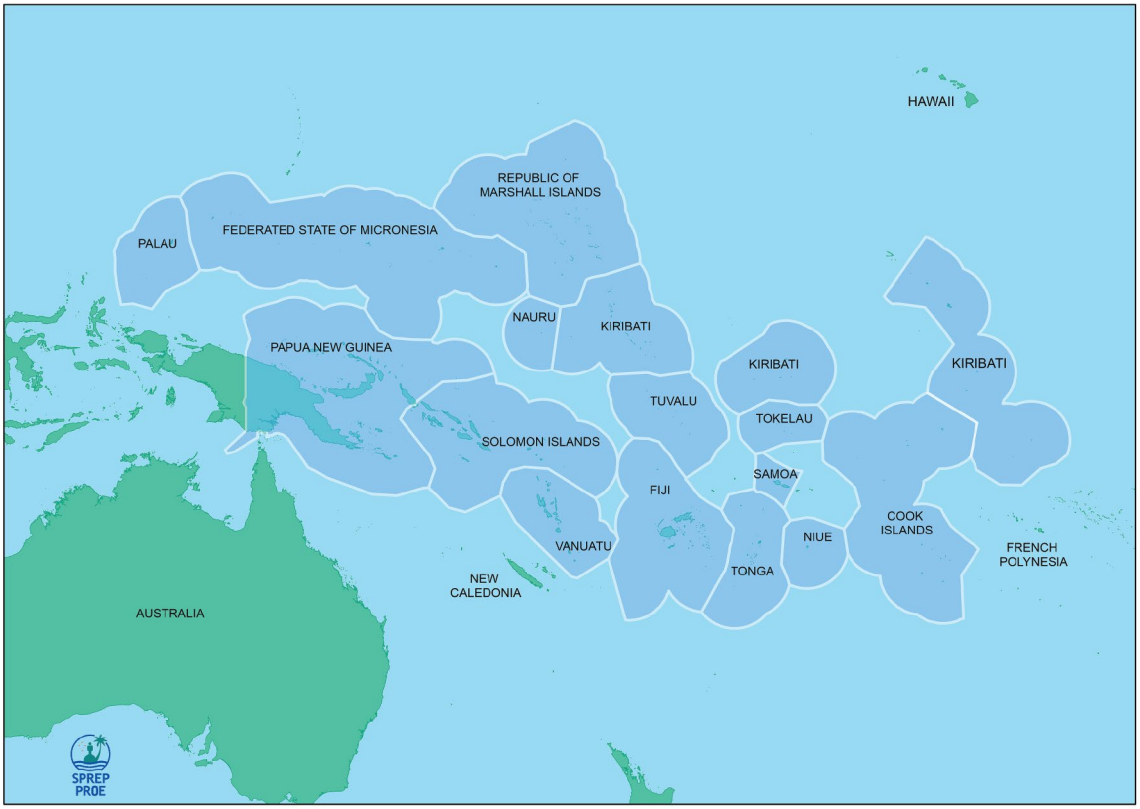

Fig. 7.61. Islands (highlighted in blue) in the Oceania region. (Source: SPREP.)

easing slightly in the far eastern Pacific during the middle months of the year. During the second and third quarter, above-normal air temperatures emerged in a band between Papua New Guinea and the south of Fiji, extending southeast across the Solomon Islands and New Caledonia and persisting through to the end of the year.

Rainfall was suppressed along the equator throughout the year, as is typical with La Niña. The negative rainfall anomalies eased slightly in the third quarter of the year in the central and eastern equatorial Pacific before re-strengthening again towards the end of the year. In the off-equatorial South Pacific, positive rainfall anomalies were strongest in a band from southern PNG to New Caledonia and Vanuatu during the second half of the year. Generally, rainfall was higher than usual throughout the year in the region to the southwest of the South Pacific Convergence Zone (SPCZ), as is usual during La Niña.

(i) Temperature

Along the equator, air temperatures were 1°C to 2°C below normal to the east of the date line during January and February, extending as far west as Kiribati during March. These temperatures were associated with the underlying region of below-normal SSTs. A large region with air temperatures 1°C to 2°C above normal was present in the far South Pacific (south of 20°S) during January. However, this region had cooled and returned to near-normal levels by the end of the first quarter (Fig. 7.62a).

The broad area of below-normal air temperatures along the equator contracted in spatial extent through April to June (AMJ; Fig. 7.62b), associated with increasing SSTs, although cool air-temperature anomalies persisted across Nauru and Kiribati during these months. A region with air temperatures 1°C to 2°C above normal developed over southern French Polynesia during April, spreading west to cover the southern Cook Islands during May before becoming patchy in June. A small region of above-average air temperatures was also present over south-east PNG

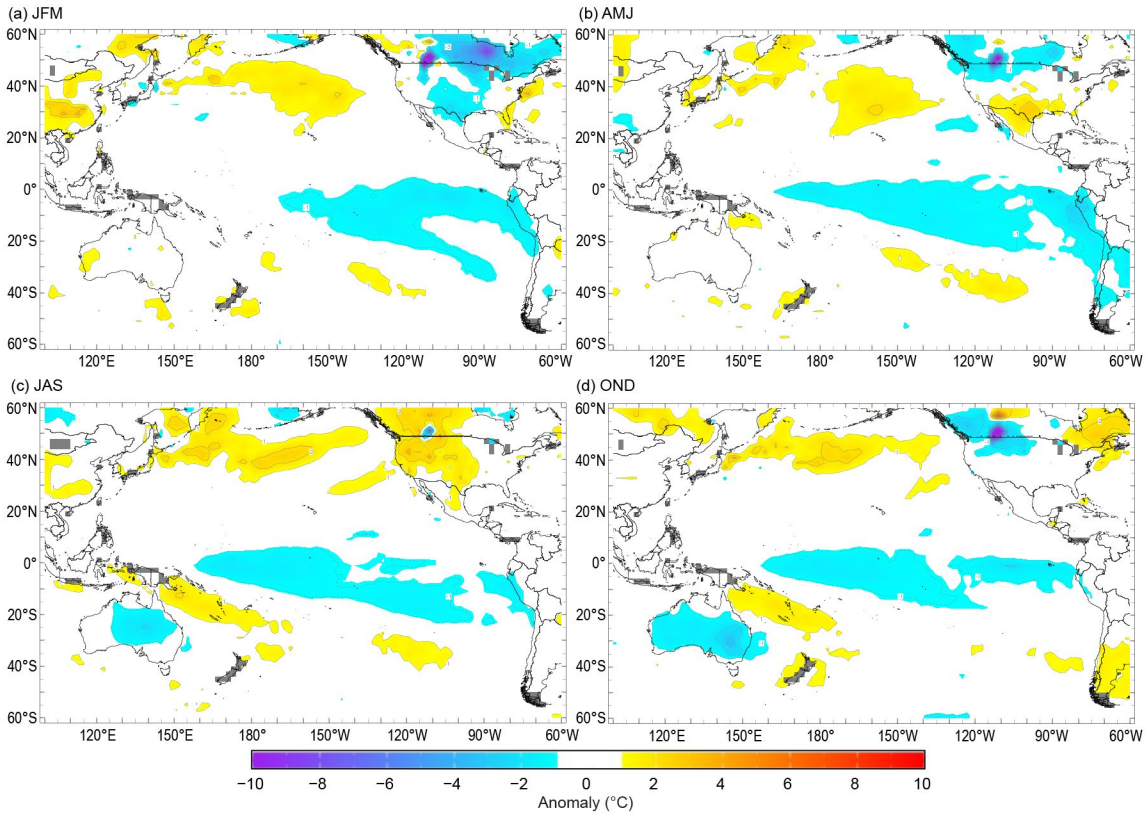

Fig. 7.62. Seasonal air-temperature surface anomalies (°C) across the Pacific for (a) Jan–Mar, (b) Apr–Jun, (c) Jul–Sep, and (d) Oct–Dec. (Source: CAMS.)

during May. This region grew in extent and continued to warm in parts with anomalies of up to +2°C as it expanded southeast to cover the southern Solomon Islands, Vanuatu, and New Caledonia during June.

During July–September (JAS), the area of –1°C to –2°C anomalies expanded westward along the equator in the South Pacific (Fig. 7.62c), matching the expanding region of below-average SSTs as La Niña re-emerged. The band of warmer air temperatures between PNG and New Caledonia continued to increase in strength with anomalies of greater than +2°C covering southeastern PNG by September. This region of air temperatures 1°C to 2°C above normal also expanded to the southeast covering Fiji and southern Tonga.

During October–December (OND), the region of negative air-temperature anomalies along the central equatorial region persisted, although the anomalies became patchy in the far east as the waters in the coastal area of South America warmed. The region of positive anomalies in the off-equatorial western South Pacific persisted through October and November before reducing in spatial extent during December (Fig. 7.62d). The peak positive anomaly area of +2°C located west of Vanuatu in November shifted eastward during December to the south of Fiji, matching the peak positive anomaly locations of SSTs at the time.

(ii) Precipitation

Rainfall patterns at the start of the year reflected typical La Niña patterns across the tropical Pacific. Rainfall deficits were observed along the equator east of 160°E during January–March (JFM), with the strongest negative rainfall anomalies occurring over Kiribati. Patchy positive rainfall anomalies occurred over most off-equatorial South Pacific Islands between the Solomon Islands and Niue (Fig. 7.63a), with some islands in Vanuatu receiving twice their usual JFM rainfall totals. The SPCZ was located to the south of its climatologically normal position during JFM, bringing it closer to Vanuatu and Fiji. As a result, rainfall totals above the 90th percentile were recorded at stations in Fiji, Vanuatu, Niue, and Tonga. In Vanuatu, Bauerfield and Port Vila recorded their wettest JFM on record with 1670 mm (50-year climatology) and 1667 mm (70-year

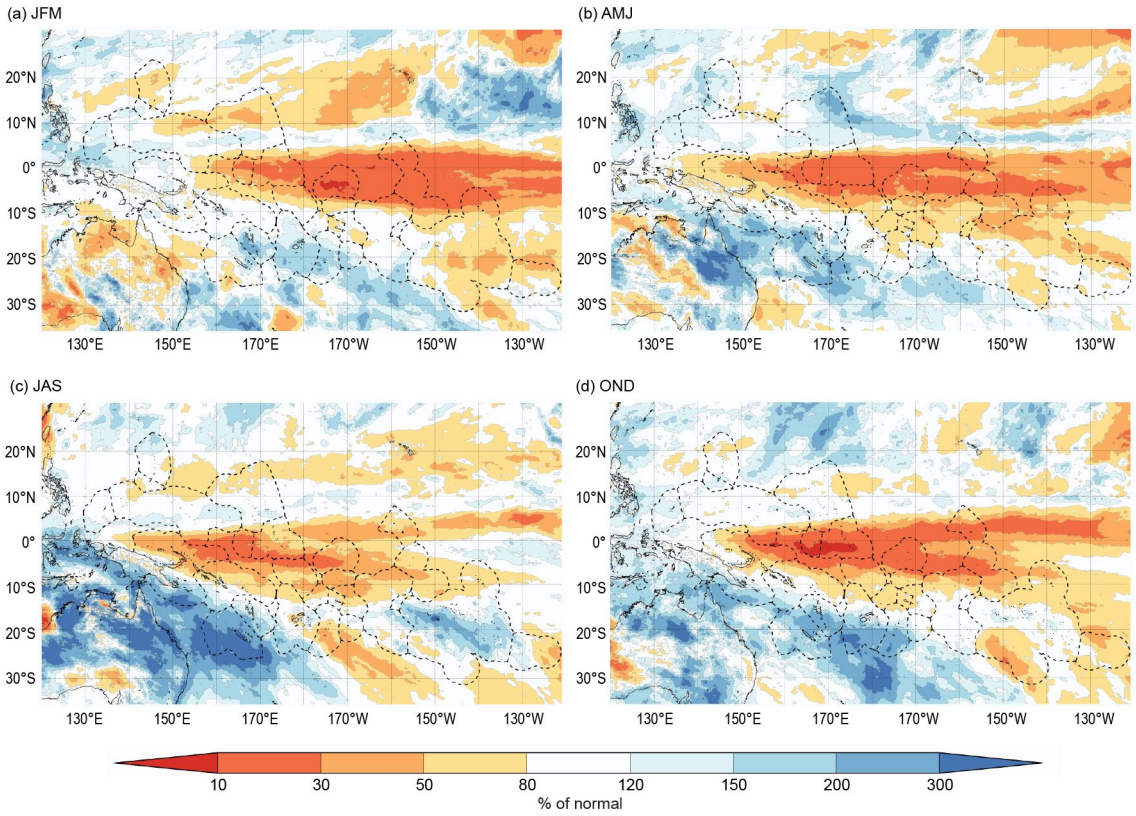

Fig. 7.63. Seasonal percentage of normal rainfall (%) across the Southwest Pacific for (a) Jan–Mar, (b) Apr–Jun, (c) Jul–Sep, and (d) Oct–Dec. (Source: MSWEP.)

climatology), respectively. In stark contrast, parts of Kiribati, Tuvalu, and Samoa recorded rainfall in the lowest 10th percentile on record.

The rainfall deficiencies along the equator persisted into the second quarter of the year (Fig. 7.63b), expanding south to cover Tuvalu, Wallis and Futuna, Tokelau, Samoa, American Samoa, northern Tonga, the northern Cook Islands, and large parts of French Polynesia. Conversely, the positive off-equatorial rainfall anomalies remained in a band from southeastern PNG, extending southeast to Vanuatu, New Caledonia, and southern Fiji. Rainfall was largely close to normal in the Solomon Islands, central and northern Fiji, central Tonga, Niue, and the southern Cook Islands, coinciding with the start of the dry season and the SPCZ becoming less active (as is usual for the time of year). Kiribati, northeastern PNG, the Solomon Islands, northern Fiji, and Tuvalu all recorded rainfall in their bottom 10th percentiles for AMJ. Arorae (Gilbert Islands, Kiribati) recorded its lowest AMJ total in its 55-year record with 66 mm. Conversely, in Vanuatu, Whitegrass recorded its third-wettest AMJ in 48 years (600 mm) and Aneityum recorded its second-wettest AMJ on record (1045 mm) in its 68-year record.

During JAS, the largest positive rainfall anomalies shifted to the southwest over New Caledonia and Australia, with parts of southern PNG, patches of Vanuatu and Fiji as well as New Caledonia receiving above-average rainfall (Fig. 7.63c). The region of reduced rainfall along the equator persisted eastward past the Line Islands of Kiribati from northern PNG. The spatial extent of the dry anomalies over Wallis and Futuna, Samoa, and American Samoa shrank, and rainfall became closer to normal in this region. Fiji, Tonga, the Solomon Islands, Tuvalu, and Kiribati recorded rainfall below the 10th percentile for JAS, with Arorae in Kiribati recording 52 mm, the lowest in its 54-year record, and Kavieng in northeast PNG recording 189 mm, its driest JAS in 90 years.

Rainfall patterns during the last quarter of 2022 reflected the re-emergence of La Niña, although the SPCZ remained less active than usual during this time. Rainfall during October–December continued to be suppressed along the equator. The off-equatorial region of reduced rainfall observed south of 20°S in the area during JAS contracted eastward during OND, which impacted the southern Cook Islands and French Polynesia (Fig 7.63d). Enhanced rainfall anomalies covered a broad region from southern PNG southeast over Vanuatu, New Caledonia, Fiji, Tonga, and Niue, coinciding with a region of above-normal SSTs. Rainfall totals below the 10th percentile for OND were recorded at several locations across the Gilbert Islands (Kiribati), Rotuma (northern Fiji), and over northern Papua New Guinea. Arorae in Kiribati recorded its second-driest OND in its 56-year history (10 mm). Conversely, Fiji and Tonga recorded rainfall above the 90th percentile. Ono-i-Lau (Fiji) recorded 807 mm, its second-wettest OND in 75 years, and Ha'apai in Tonga recorded 863 mm, its third-wettest OND on record (76 years).

(iii) Notable events and impacts

The most powerful tropical cyclone to impact the South Pacific for 2022 was Tropical Cyclone Dovi, which formed early in February 2022 as the third named storm of the western North Pacific season. Dovi formed to the west of New Caledonia before tracking eastward toward southern Vanuatu and then turned in a southerly direction past southern New Caledonia towards New Zealand. At its peak, Dovi had one-minute sustained winds of 175 km h^{-1} (94 kt) and a lowest central pressure of 940 hPa.

Tropical Cyclone Dovi caused heavy rainfall and flash flooding across Vanuatu. Several rivers overflowed, causing damage to housing and crops in nearby areas, and mudslides destroyed several bridges in Port Vila, Vanuatu's capital. In southern New Caledonia, Dovi caused all flights from the country to be cancelled for two days and businesses and schools to be closed. The heavy rainfall led to landslides and mudslides and resulted in some evacuations in the capital Nouméa. As Dovi weakened and tracked west of Norfolk Island and across northern New Zealand, the storm brought strong winds and heavy rainfall to both regions. In total, there was approximately $80 million (U.S. dollars) of damage across the four regions according to AON's Global Catastrophe Recap, with one fatality recorded in New Caledonia.

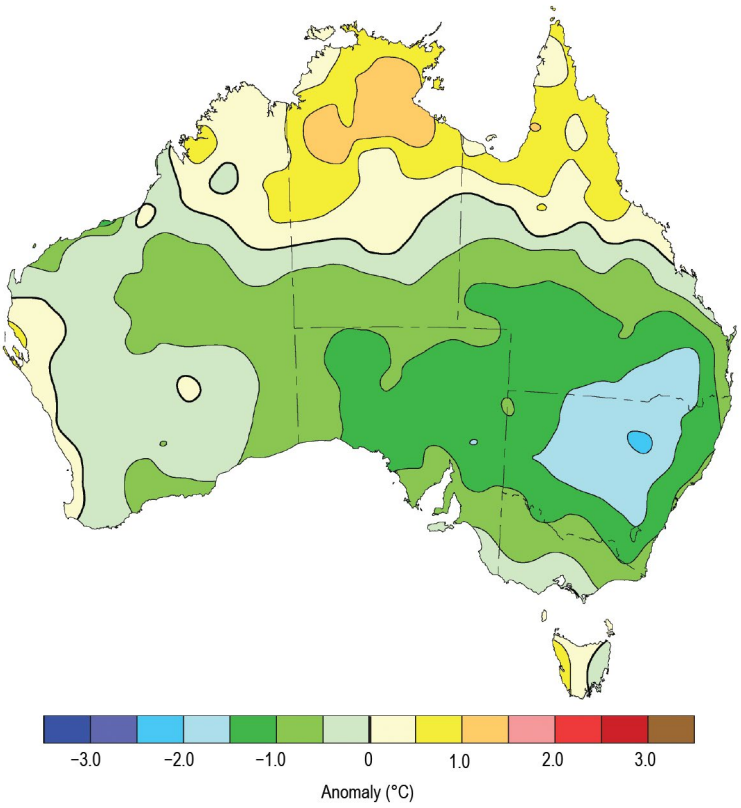

Fig. 7.64. Maximum temperature anomalies (°C) for Australia, averaged over 2022, relative to a 1991–2020 base period. Australian States/Territories are as follows, starting clockwise from the west: Western Australia, the Northern Territory, Queensland, New South Wales, Victoria, and South Australia, with the island of Tasmania in the southeast. (Source: Australian Bureau of Meteorology.)

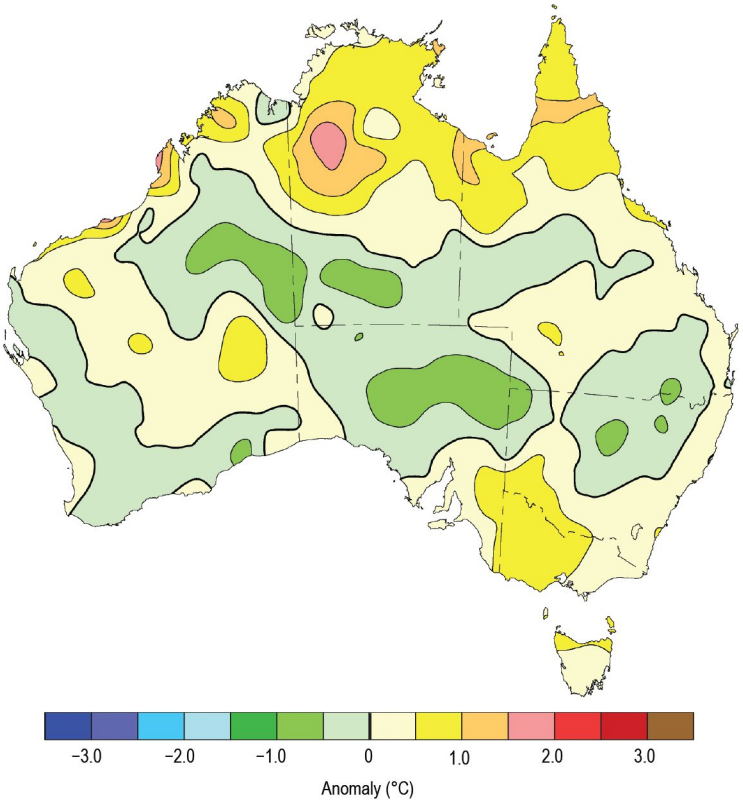

4. AUSTRALIA

—S. Tobin

In this section, monthly area-averaged temperatures are based on the Australian Climate Observations Reference Network–Surface Air Temperature (ACORN-SAT) dataset (Trewin 2018), while mapped temperature analyses are based on the Australian Water Availability Project (AWAP) dataset (Jones et al. 2009), both of which begin in 1910. Area-averaged rainfall values and mapped analyses use the Australian Gridded Climate Data (AGCD) dataset (Evans et al. 2020), which begins in 1900. Anomalies are based on the 1991–2020 average.

(i) Temperature

The area-averaged annual mean temperature for 2022 was slightly below the 1991–2020 average (0.13°C below average), but overall was the 22nd warmest in Australia's 113-year record. The decade 2013–22 was the warmest 10-year period on record for Australia, 0.38°C above the 1991–2020 average, despite recurrent La Niña and high rainfall bringing relatively cool years during 2021 and 2022. Only six years prior to 2000 were warmer than 2022.

The annual nationwide mean maximum temperature (Fig. 7.64) was 0.40°C below average, and the mean minimum temperature (Fig. 7.65) was 0.13°C above average.

In terms of annual anomalies, both mean annual maximum and minimum temperatures were above average for most of tropical northern Australia. Compared to the distribution across all 113 years of observations (1910–2022), maximum temperatures were in the highest 10% of observations for most of the Top End in the Northern Territory and Queensland's Cape York Peninsula, and also in western Tasmania. New South Wales, much of southern Queensland, and large parts of South Australia were in the bottom 30% of observations. The mean annual minimum

Fig. 7.65. Minimum temperature anomalies (°C) for Australia, averaged over 2022, relative to a 1991–2020 base period. (Source: Australian Bureau of Meteorology.)

temperature was in the top 30% of observations compared to all years 1910–2022 across the majority of Australia.

In the first half of the year, most months were warmer than average for large parts of Australia. In the second half of the year, temperatures generally remained warmer than average for the tropics, but were cooler than average across large areas, particularly the central and southern mainland during spring.

Warm sea-surface temperature anomalies to the west and northwest of Western Australia as well as a ridge of high pressure south of the Great Australian Bight played an important role early in the year, with extreme heatwave conditions affecting the north and west throughout the first quarter of 2022.

July was unusually cool for large parts of the tropics due to unusual dry-season rainfall, although farther south much of southwest Australia and parts of the southeast continued to experience warmer-than-average days and nights.

During August, September, October, and December, far-northern Australia experienced above-average temperatures, with heatwave conditions in some parts of the tropics.

Spring (September–November; SON) brought a shift to cooler-than-average days for most of the mainland south of the tropics. In November, both mean maximum and mean minimum temperatures were below average for most areas except the very far north. Nationally, November was Australia's coolest since 1999 and the eighth-coolest November on record.

December was also cooler than average for much of eastern Australia, with cold outbreaks during the month leading to a large number of stations across the region observing a record-low daily minimum temperature during the first half of the month.

(ii) Precipitation

Averaged across Australia, rainfall for 2022 was 587.8 mm, the ninth-wettest year on record for Australia and 20.9% above the 1991–2020 average of 486.0 mm. Compared to the distribution across all 123 years of observations (1900–2022), annual rainfall was above average for most of mainland Australia and in the top 10 percent for most of the southeastern quarter of the mainland (Fig. 7.66). Rainfall was below average for western Tasmania, much of the north of the Northern Territory, and for parts of the south-west of Western Australia.

La Niña was a dominant influence on Australia's climate during 2022, persisting through summer 2021/22, weakening during autumn, and returning to neutral before a third successive La Niña re-emerged in early September. A negative Indian Ocean dipole (IOD) during winter and spring as well as a persistently positive phase of the Southern Annular Mode (SAM) from mid-autumn also influenced Australia's climate and weather patterns during 2022 (Ashok et al. 2003; Hendon et al. 2007; Risbey et al. 2009).

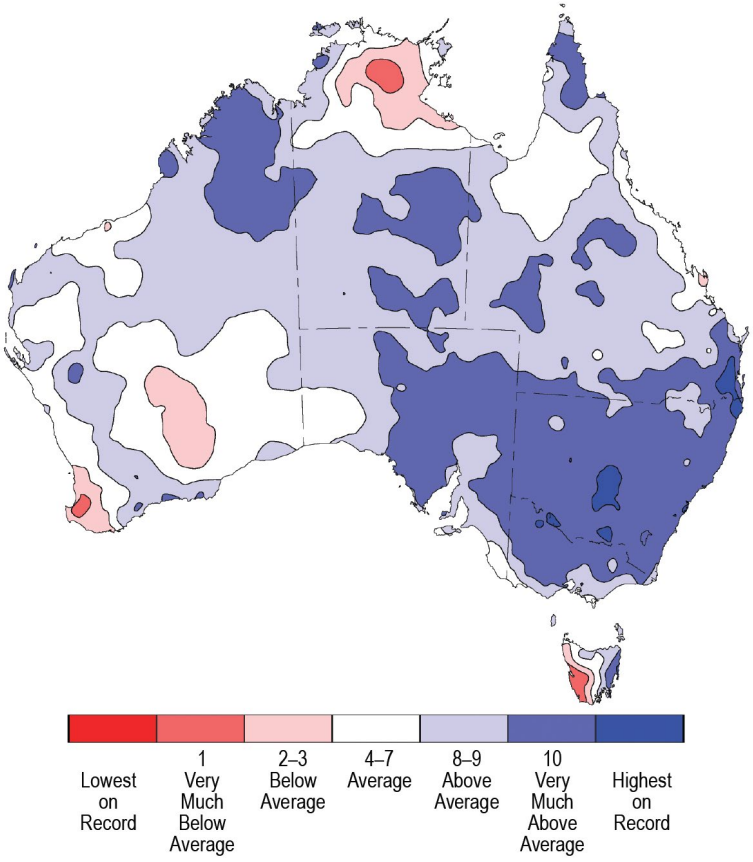

Fig. 7.66. Rainfall deciles for Australia for 2022, based on the 1900–2022 distribution. (Source: Australian Bureau of Meteorology.)

La Niña typically brings wetter conditions to much of northern and eastern Australia, and when La Niña and negative IOD conditions combine, the likelihood of above-average rainfall over Australia is further increased. Together, they also increase the chances of warmer nights for northern Australia and cooler days for much of the eastern mainland. SAM is often positive during La Niña, and during 2022 the persistently positive SAM was also boosted by a strong polar vortex over Antarctica. The positive SAM likely contributed both to above-average rainfall across parts of eastern Australia and below-average rainfall in parts of southern Australia, particularly in areas with west-facing coastlines (Fig. 7.66).

In northern Australia, the latter part of the 2021/22 northern wet season (October–April) was particularly dry, with rainfall for February–April 2022 being in the lowest 10% of observations for much of the northern half of the Northern Territory. A lack of days with the Madden-Julian Oscillation (MJO) in phases 5–7, typically associated with wetter conditions for northern Australia (see Wheeler et al. 2009) in the second half of the northern wet season meant that there was a reduction in the number of rainy monsoon bursts. This MJO behavior, with a persistent pattern of MJO events stalling in the Indian Ocean and/or weakening rapidly as they approached Australia, may have been influenced by above-average sea-surface temperatures in the Indian Ocean (Marshall et al. 2023).

In eastern Australia, persistent rain caused significant flooding that affected large areas multiple times during the year, with some areas in the east seeing a third wet year in a row. Flooding affected southeastern Queensland and eastern New South Wales from late February into March, inland central and northern Queensland and inland northern New South Wales during May, around Sydney and the New South Wales coast in early July, and across large parts of the eastern states from August. Flooding affected many parts of the Murray–Darling Basin over prolonged periods or on multiple occasions throughout spring.

Austral spring was the second wettest on record for Australia as a whole, and the wettest on record for the Murray–Darling Basin, New South Wales, and Victoria. Numerous locations near the coast of New South Wales and in southern Queensland broke their annual rainfall record by the end of October, and for Victoria, October was the state's wettest month on record for any time of the year. In the north of Western Australia, the Kimberley region was affected by flooding near both the start and the end of the year.

High rainfall, wet soils, and high streamflows meant that water storage levels were high across much of Australia during 2022. In parts of northern Australia and southeast Queensland, water storages started the year well below capacity and experienced significant increases during February. Surface water storage levels remained at near-full capacity for many parts of the country across the year, including most of those in the Murray–Darling Basin. However, storage levels remained low in parts of central coastal Queensland, western Tasmania, southeast New South Wales, and western Victoria.

Predominantly easterly winds over much of Australia influenced by La Niña, a generally positive SAM, and persistent blocking highs were associated with below-average rainfall in parts of southern Australia, particularly in areas with west-facing coastlines. Summer 2021/22 was the fifth driest on record for Tasmania as a whole, and the driest since 1980/81.

Serious rainfall deficiencies (defined as totals in the lowest 10% of historical observations since 1900) emerged across western Tasmania and parts of coastal southern Australia from early in the year. Despite heavy rain and periods of flooding in eastern Australia, these rainfall deficiencies persisted into spring 2022 for much of the west-facing coasts of southeastern Australia, with deficiencies still in place in western Tasmania at the end of the year.

(iii) Notable events and impacts

Ex-tropical Cyclone Tiffany brought heavy rain and damaged transport infrastructure across northwest Australia through to southern South Australia during the second half of January. Tiffany also contributed to extreme high temperatures over the Pilbara during mid-January. Onslow Airport reached 50.7°C on 13 January, equaling Australia's highest temperature on record. Heatwave conditions continued along the west coast on and off into February, contributing to high fire danger in early February, with multiple fires breaking out across Western Australia's South West Land Division.

The remnants of Tropical Cyclone Seth caused significant flooding in Queensland in early January in the Wide Bay and Burnett districts in the southeast of the state. The Mary River catchment received rainfall totals in excess of 600 mm.

Extreme multi-day rainfall in late February to early March produced record-breaking floods in southeast Queensland and eastern New South Wales. Record flooding resulted in multiple catchments extending from Maryborough in Queensland to Grafton in New South Wales. Parts of southeast Queensland observed their highest flood peaks since 1893, including the Mary River at Gympie. In parts of northeast New South Wales, peak flood levels surpassed previous observations by considerable margins, and in the Hawkesbury–Nepean they were comparable to levels that occurred in 1978.

From late winter and into spring, persistent rain falling onto already wet catchments led to renewed river-level rises and flooding along many rivers in southern Queensland, inland New South Wales, and northern and central inland Victoria. In many parts of the Murray–Darling Basin, flooding occurred over prolonged periods or on multiple occasions, and continued to affect a number of communities throughout October and into November. Flooding continued during December as flood waters progressed through inland rivers in southern Queensland and the southeastern mainland. Multiple flood peaks were observed at some locations in the generally flat downstream catchments of the Murray–Darling Basin.

December was the seventh wettest on record for the Northern Territory, partly due to the passage of ex-Tropical Cyclone Ellie over northern and central parts of the region during the last week of the year. Significant flooding occurred on the Fitzroy River in Western Australia's Kimberley region, with heavy rain continuing into the start of 2023.

5. NEW ZEALAND

—T. Meyers

In the following discussion, the base period is 1981–2010. The nationwide average temperature is based upon New Zealand's National Institute of Water and Atmospheric Research (NIWA) seven-station temperature series that began in 1909. All statistics are based on data available as of 11 January 2023.

(i) Temperature

According to NIWA's seven-station temperature series, 2022 was New Zealand's warmest year since records began in 1909, surpassing the record set just the previous year. The nationwide average temperature for 2022 was 13.76°C, which was 1.15°C above the annual average. Annual temperatures were above average (+0.51°C to +1.20°C) or well above average (>1.20°C) for almost all of New Zealand, although near-normal (±0.50°C of average) temperatures occurred in pockets around the eastern South Island and also parts of Marlborough and Nelson (Fig. 7.67a).

Various climate drivers contributed to the exceptional warmth, with La Niña being the primary driver. In New Zealand, La Niña is typically linked with higher-than-normal air pressure near and to the east of the country with lower pressures to the north. These circulation anomalies were observed in 2022, which led to more northeasterly winds than usual and were likely a major cause of the above-average air temperatures. Throughout 2022, coastal sea-surface temperatures (SSTs) were either above or well above average every month, with January, November, and December having the most anomalously warm SSTs. This resulted in a protracted marine heatwave (MHW), where SSTs are above the 90th percentile as derived from a 30-year climatology, with ocean temperatures staying unseasonably warm over thousands of kilometers for much of the year. The MHWs of 2022 also likely contributed to the observed above-average air temperatures over New Zealand. Additionally, the Southern Annular Mode was positive for the vast majority of 2022, which is associated with higher-than-normal pressures over the New Zealand region. Climate change also continues to affect New Zealand's long-term temperature trend, which is increasing at a rate of around 1.17°C (±0.2°C) per century, according to NIWA's seven-station series.

It was the warmest year on record for 47 locations while an additional 33 locations experienced annual average temperatures among their four warmest on record. No locations experienced a record or near-record cold year, and no locations experienced below-average annual mean daily temperatures. The last year New Zealand observed any locations where annual temperatures were record or near-record cold was 2015.

Unlike 2021, which featured high temperatures in the high 30s during summer, no station recorded a temperature over 35°C in 2022. The last time New Zealand failed to reach a temperature higher than 35°C during a calendar year was 2007.

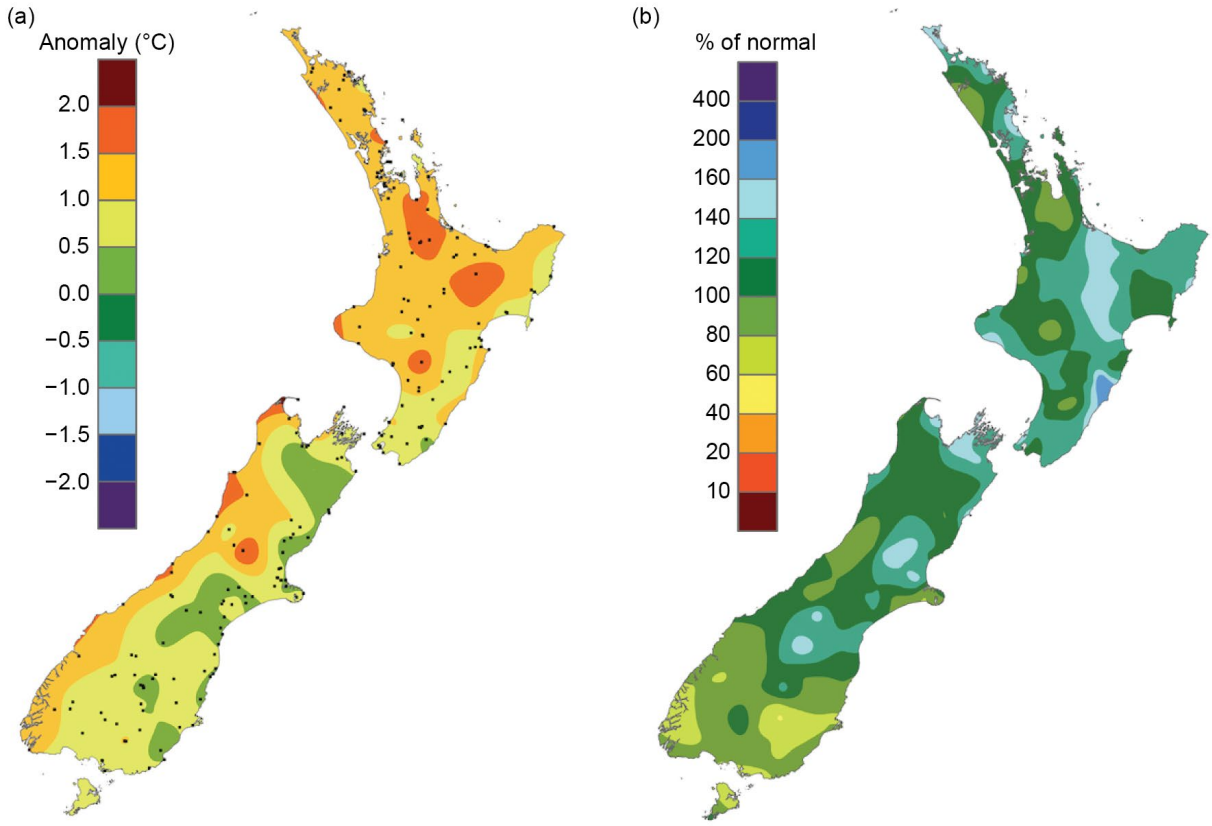

Fig. 7.67. 2022 annual (a) average temperature anomaly (°C) and (b) total rainfall (% of normal), relative to the 1981–2010 base period. The black dots on (a) represent the locations of climate stations used to create both the temperature and rainfall maps. Note: some data used to create these plots have been identified as not homogenized. As NIWA switches to the 1991–2020 normal period, these data will be homogenized (Source: NIWA.)

(ii) Precipitation

The majority of the country experienced near-normal annual rainfall (80%–119%) in 2022, although rainfall totals were above normal (120%–149% of normal) or well above normal (>150%) for parts of Northland, Tauranga, Gisborne, the Central Plateau, southern Taranaki, parts of Manawatū-Whanganui, much of Wellington, Nelson, northern Marlborough, parts of Tasman, the West Coast near Westport, and pockets of Canterbury and below normal (50%–79%) for pockets of Southland and Dunedin (Fig. 7.67b). Overall, 2022 was New Zealand's eighth-wettest year on record, based on an analysis of NIWA's Virtual Climate Station Network (https://niwa.co.nz/climate/our-services/virtual-climate-stations) dating to 1960. Of all the regularly reporting gauges, the wettest location in 2022 was Cropp River (West Coast), 975 meters a.s.l. with 11,034 mm for the year. The driest of the regularly reporting rainfall sites in 2022 were Roxburgh and Middlemarch in the Otago region of the South Island, both reporting just 368 mm.

(iii) Notable Events

Widespread meteorological drought and dryness (based on the NZ Drought Index; https://niwa.co.nz/climate/information-and-resources/drought-monitor) developed by the end of January. The city of Auckland experienced a 37-day dry spell (defined as less than 1 mm of rain observed in the 24 hours to 9am local time) from 17 December 2021 to 22 January 2022, which was its second-longest dry spell since records began in 1943. Many areas around New Zealand introduced water restrictions during January due to the dry conditions. While these conditions eased for the North Island during February, parts of the South Island continued to experience dryness or meteorological drought well into autumn.

On 13 February, the landfall of ex-Tropical Cyclone Dovi brought heavy rainfall and strong wind gusts to the North Island and upper South Island. This was the first cyclone to make landfall in New Zealand since Fehi and Gita in February 2018. Widespread power outages occurred, numerous roads were temporarily closed due to surface flooding or landslides, and homes in Wellington were evacuated due to landslides.

From 16 to 20 August, an atmospheric river (AR) that extended from the tropics led to a long-duration heavy rain and flooding event. ARs are long, narrow, and transient corridors of strong horizontal water vapor transport that are typically associated with a low-level jet stream ahead of a cold front or an extratropical cyclone. Although ARs are responsible for the majority of annual normal precipitation for sections of the country, they also disproportionately account for the amount of extreme precipitation in some parts of New Zealand; over 90% of extreme (6-hourly) precipitation occurs due to AR activity for parts of the West Coast on the South Island and over 70% for Nelson (Prince 2019). An analysis from the European Centre for Medium-Range Weather Forecasts Reanalysis version 5 (ERA5) dataset revealed that the August AR was the strongest landfalling August AR for New Zealand since at least 1950, with the total amount of water vapor flowing through an atmospheric column (known as integrated water vapor transport) reaching a maximum value of 1749 kg m^{-1} s^{-1}. The AR resulted in a 1-in-120-year rain event in Nelson, severe flooding, and numerous landslides, as two to four times the normal August rainfall was recorded in just a few days across parts of the upper South Island and North Island.

Acknowledgments

Europe

Much of the information in this section is based on national climate reports kindly provided by the National Meteorological and Hydrological Services (NMHSs) of the WMO RA VI Region. The information has been compiled at the WMO RA VI Regional Climate Centre (RCC) Node on Climate Monitoring, located at Deutscher Wetterdienst (DWD) in Germany. The national contributions have been provided as part of the cooperation between NMHSs and the RCC.

Specifically, we acknowledge the Instytut Meteorologii i Gospodarki Wodnej PIB in Poland for its kind cooperation with RCC in this subject.

Oceania

The editors acknowledge and thank the numerous national meteorological and hydrological services for collecting and providing data for this report. Data centers like NCEP/NCAR, ECMWF-ERA, and CHIRPS are also acknowledged for making their data freely available.

Appendix 1: Chapter 7 – Acronyms

ACORN-SAT	Australian Climate Observations Reference Network–Surface Air Temperature
AGCD	Australian Gridded Climate Data
AMJ	April–June
ANDMA	Afghanistan National Disaster Management Authority
AR	atmospheric river
ARCS	Afghan Red Crescent Society
ASO	August–October
AWAP	Australian Water Availability Project
CA	Central America
CA	Central Asia
CAMS	Climate Anomaly Monitoring System
CA-NWS	CA-NWS
CAR	Central African Republic
CMORPH	Climate Prediction Center Morphing Techinique
CNE	National Emergency Commission
CONRED	National Coordination for Disaster Reduction
CONUS	contiguous United States
COPECO	Permanent Contingency Commission of Honduras
CPC	Climate Prediction Center
DJF	December–February
DRC	Democratic Republic of the Congo
DWD	Deutscher Wetterdienst
ECCC	Environment and Climate Change Canada
EF	Enhanced Fujita
EHD	extreme high-temperature days
EM-DAT	Emergency Events Database
ERA 5	European Centre for Medium-Range Weather Forecasts Reanalysis version 5
FEWS NET	Famine Early Warning Systems Network
GHA	Greater Horn of Africa
GHCN	Global Historical Climate Network
GPCC	Global Precipitation Climatology Centre
GPCP	Global Precipitation Climatology Project
HAC	Humanitarian Aid Commission
IDI	Integrated Drought Index
IFRC	International Federation of Red Cross and Red Crescent Societies
IOD	Indian Ocean dipole
ISMR	Indian summer monsoon rainfall
ITCZ	Intertropical Convergence Zone
JAS	July–September
JFM	January–March
JJA	June–August
JJAS	June–September
JMA	Japan Meteorological Agency
LTA	long-term average
MAM	March–May
MHW	marine heatwave
MJO	Madden-Julian Oscillation
MSWEP	Multi-Source Weighted-Ensemble Precipitation
NAO	North Atlantic Oscillation

NCAR	National Center for Atmospheric Research
NCEP/NCAR	National Centers for Environmental Prediction/National Center for Atmospheric Research
NEM	northeast monsoon
NIWA	National Institute of Water and Atmospheric Research
NMHS	National Meteorological and Hydrological Services
OLR	outgoing longwave radiation
OND	October–December
P	accumulated pentad precipitation
PNG	Papua New Guinea
RA VI	(WMO) Regional Association VI
RCC-CM	Regional Climate Centre on Climate Monitoring
RFE2	RainFall Estimate version 2
SAM	Southern Annular Mode
SINAPROC	National Civil Protection System
SON	September–November
SPCZ	South Pacific Convergence Zone
SPI	standardized precipitation index
SSA	southern South America
SST	sea-surface temperature
TAP	tropical Atlantic precipitation
Tm	mean temperature
Tmax	maximum temperature
Tmin	minimum temperature
TPS	tropical Pacific SST
UNICEF	United Nations Children's Fund
UN-OCHA	United Nations Office for the Coordination of Humanitarian Affairs
WMO	World Meteorological Association
YRB	Yangtze River Basin
YT	mean temperature averaged over the YRB

Appendix 2: Chapter 7 – Supplemental Materials

Table A7.1. Temporal coverage of nationally averaged temperature and precipitation in situ observations for Europe / WMO RA VI Region. For some countries, only one station (preferably with long time series) has been used (name of the location in brackets). All records extend to the present. Anomalies refer to the 1991–2020 reference unless otherwise specified. Data are checked for consistency with the text. Inconsistencies with maps shown in the figures might occur because not all national data have been available for generation of maps.

Nation	Temperature start of record	Precipitation start of record	Source	Temperature anomaly (°C)	Rank (ordered from warmest to coldest)	Precipitation anomaly (annual total in % of normal)	Rank (ordered from wettest to driest)
European average	1950	1881	GHCN[1] data (temperature), GPCC (precipitation)	+1.0	2	95%	91
Albania (Korce)	1963	1963	CLIMAT[2]	-	-	-	-
Andorra	1931	1927	NMHS[3]	+2.6	1	78%	76
Armenia	1935	1935	NMHS	+1.7	5	75%	85
Austria	1767	1858	NMHS	+1.1	3	85%	155
Azerbaijan (Astara)	1991	1991	CLIMAT	-	-	-	-
Belarus	1881	1945	NMHS	-	-	-	-
Belgium	1833	1833	NMHS	+1.2	1	84%	29
Bosnia & Herzegovina (Banja Luka)	1950	1950	NMHS	+1.1	1	82%	66
Bulgaria	1930	1930	NMHS	+0.8	4	80%	-
Croatia	1961	1961	NMHS	+1.2	1	84%	56
Cyprus (Nicosia)	1899	1899	NMHS	+0.6	14	-	-
Czechia	1961	1961	NMHS	+0.9	5	93%	-
Denmark	1873	1874	NMHS	+0.8	3	91%	66
Estonia	1961	1961	NMHS	+0.7	8	80%	56

[1] GHCN = Global Historical Climatology Network (Menne et al. 2018), GPCC = Global Precipitation Climatology Centre (Schneider et al. 2018), averaged over RA VI land areas without Greenland

[2] CLIMAT station data as reported worldwide via the WMO Global Telecommunication System

[3] NMHS = National Meteorological and Hydrological Service; for individual names of NMHSs see https://public.wmo.int/en/about-us/members

[4] reference period 1971–2000

[5] reference period 1981–2010

Nation	Temperature start of record	Precipitation start of record	Source	Temperature anomaly (°C)	Rank (ordered from warmest to coldest)	Precipitation anomaly (annual total in % of normal)	Rank (ordered from wettest to driest)
Finland (Helsinki)	1900	1961	NMHS	+0.9	-	-	-
France	1900	1959	NMHS	+1.6	1	76%	63
Georgia	1956	1881 (Tbilisi)	NMHS	-	-	-	-
Germany	1881	1881	NMHS	+2.3	1	85%	119
Greece	1960	1960	NMHS	+0.7[5]	5	80%[5]	59
Hungary	1901	1901	NMHS	+1.1	3	81%	106
Iceland (Stykkishólmur for temperature, Reykjavik for precipitation)	1900	1921	NMHS	+0.0	-	-	8
Ireland	1900	1941	NMHS	+0.7	1	97%	37
Israel	1951	1935 (Deganya)	NMHS	+0.1	19	102%	30
Italy	1961	1961	NMHS	+1.1	1	77%	62
Jordan (Amman)	1981	1981	NMHS	-	-	-	-
Kazakhstan	1941	1941	NMHS	-	-	-	-
Latvia	1924	1924	NMHS	+0.5	12	100%	39
Lebanon (Beirut)	1949	1949	CLIMAT	-	-	-	-
Lithuania	1961	1887 (Vilnius)	NMHS	+0.5	11	97%	31
Luxembourg (Findel)	1838	1854	NMHS	+1.1	1	85%	110
Malta (Luqa)	1923	1949	NMHS/CLIMAT	-	-	-	-
Moldova (Chisinau)	1886	1891	NMHS	+0.9	4	80%	30

[1] GHCN = Global Historical Climatology Network (Menne et al. 2018), GPCC = Global Precipitation Climatology Centre (Schneider et al. 2018), averaged over RA VI land areas without Greenland

[2] CLIMAT station data as reported worldwide via the WMO Global Telecommunication System

[3] NMHS = National Meteorological and Hydrological Service; for individual names of NMHSs see https://public.wmo.int/en/about-us/members

[4] reference period 1971–2000

[5] reference period 1981–2010

Nation	Temperature start of record	Precipitation start of record	Source	Temperature anomaly (°C)	Rank (ordered from warmest to coldest)	Precipitation anomaly (annual total in % of normal)	Rank (ordered from wettest to driest)
Monaco	1969	1969	NMHS	+1.4	1	60%	51
Montenegro (Podgorica)	1949	1949	NMHS	+1.2	1	-	-
Netherlands	1901	1901	NMHS	+1.1	3	66%	53
North Macedonia	1981	1981	NMHS	+0.7[5]	12	91%	31
Norway	1900	1900	NMHS	+0.7	9	104%	17
Poland	1951	1951	NMHS	+0.8	7	87%	59
Portugal	1931	1931	NMHS	+1.4[4]	1	90%[4]	-
Romania	1961	1961	NMHS	+1.0	3	82%	53
Russia, European part	1936	1936	NMHS	+0.8	-	103%	-
Serbia	1951	1951	NMHS	+1.0	2	93%	46
Slovakia	1951	1961	NMHS	+1.0	4	81%	57
Slovenia	1961	1961	NMHS	+1.2	1	84%	56
Spain	1961	1961	NMHS	+1.7[5]	1	84%[5]	57
Sweden	1860	1880	NMHS	+0.8	4	88%	79
Switzerland	1864	1864	NMHS	+1.6	1	82%	137
Syrian Arab Republic (Aleppo)	1960	1960	-	-	-	.	-
Türkiye	1971	1991	NMHS	+0.6	7	88%	
Ukraine	1891	1891	NMHS	+0.7	19	99%	43
United Kingdom	1884	1836	NMHS	+0.9	1	94%	76

[1] GHCN = Global Historical Climatology Network (Menne et al. 2018), GPCC = Global Precipitation Climatology Centre (Schneider et al. 2018), averaged over RA VI land areas without Greenland

[2] CLIMAT station data as reported worldwide via the WMO Global Telecommunication System

[3] NMHS = National Meteorological and Hydrological Service; for individual names of NMHSs see https://public.wmo.int/en/about-us/members

[4] reference period 1971–2000

[5] reference period 1981–2010

References

Alcântara, E., and Coauthors, 2023: Deadly disasters in the southeastern South America: Flash floods and landslides of February 2022 in Petrópolis, Rio de Janeiro. *Nat. Hazards Earth Syst. Sci.*, **23**, 1157–1175, https://doi.org/10.5194/nhess-23-1157-2023.

Amador, J. A., 1998: A climatic feature of the tropical Americas: The trade wind easterly jet. *Top. Meteor. Oceanogr.*, **5**, 91–102.

——, 2008: The Intra-Americas Seas Low-Level Jet (IALLJ): Overview and future research. *Ann. N. Y. Acad. Sci.*, **1146**, 153–188, https://doi.org/10.1196/annals.1446.012.

——, E. J. Alfaro, H. Hidalgo, and B. Calderon, 2011: Central America and the Caribbean [in "State of the Climate in 2010"]. *Bull. Amer. Meteor. Soc.*, **92** (6), S182–S183, https://doi.org/10.1175/1520-0477-92.6.S1.

——, E. R. Rivera, A. M. Durán-Quesada, G. Mora, F. Sáenz, B. Calderón, and N. Mora, 2016a: The easternmost tropical Pacific. Part I: A climate review. *Rev. Biol. Trop.*, **64** (S1), S1–S22, https://doi.org/10.15517/rbt.v64i1.23407.

——, A. M. Durán-Quesada, E. R. Rivera, G. Mora, F. Sáenz, B. Calderón, and N. Mora, 2016b: The easternmost tropical Pacific. Part II: Seasonal and intraseasonal modes of atmospheric variability. *Rev. Biol. Trop.*, **64** (S1), S23–S57, https://doi.org/10.15517/rbt.v64i1.23409.

——, H. G. Hidalgo, E. J. Alfaro, B. Calderón, and N. Mora, 2018: Central America and the Caribbean [in "State of the Climate 2017"]. *Bull. Amer. Meteor. Soc.*, **99** (8), S199–S200, https://doi.org/10.1175/2018BAMSStateoftheClimate.1.

Ashok, K., Z. Guan, and T. Yamagata, 2003: Influence of the Indian Ocean dipole on the Australian winter rainfall. *Geophys. Res. Lett.*, **30**, 1821, https://doi.org/10.1029/2003GL017926.

Biasutti, M., 2019: Rainfall trends in the African Sahel: Characteristics, processes, and causes. *Wiley Interdiscip. Rev.: Climate Change*, **10**, e591, https://doi.org/10.1002/wcc.591.

Espinoza, J. C., J. A. Marengo, J. Schongart, and J. C. Jimenez, 2022: The new historical flood of 2021 in the Amazon River compared to major floods of the 21st century: Atmospheric features in the context of the intensification of floods. *Wea. Climate Extremes*, **35**, 100406, https://doi.org/10.1016/j.wace.2021.100406.

Evans, A., D. Jones, R. Smalley, and S. Lellyett, 2020: An enhanced gridded rainfall analysis scheme for Australia. Bureau of Meteorology Research Rep. 41, 45 pp., http://www.bom.gov.au/research/publications/researchreports/BRR-041.pdf.

Fu, S., Z. Zhu, and R. Lu, 2023: Changes in the factors controlling Northeast Asian spring surface air temperature in the past 60 years. *Climate Dyn.*, **61**, 169–183, https://doi.org/10.1007/s00382-022-06569-7.

Giannini, A., 2015: Climate change comes to the Sahel. *Nat. Climate Change*, **5**, 720–721, https://doi.org/10.1038/nclimate2739.

He, Y., A. G. Barnston, and A. C. Hilton, 1998: A precipitation climatology for stations in the tropical Pacific Basin: Effects of ENSO. NCEP/Climate Prediction Center Atlas 5, NOAA, 280 pp.

Hendon, H. H., D. W. Thompson, and M. C. Wheeler, 2007: Australian rainfall and surface temperature variations associated with the Southern Hemisphere annular mode. *J. Climate*, **20**, 2452–2467, https://doi.org/10.1175/JCLI4134.1.

Hidalgo, H., E. Alfaro, J. Amador, and A. Bastidas, 2019: Precursors of quasi-decadal dry-spells in the Central America Dry Corridor. *Climate Dyn.*, **53**, 1307–1322, https://doi.org/10.1007/s00382-019-04638-y.

Jones, D. A., W. Wang, and R. Fawcett, 2009: High-quality spatial climate data-sets for Australia. *Aust. Meteor. Oceanogr. J.*, **58**, 233–248, https://doi.org/10.22499/2.5804.003.

Magaña, V., J. A. Amador, and S. Medina, 1999: The mid-summer drought over México and Central America. *J. Climate*, **12**, 1577–1588, https://doi.org/10.1175/1520-0442(1999)0122.0.CO;2.

Lindsey, R., and L. Dahlman, 2009: Climate variability: North Atlantic Oscillation. Climate.gov, 30 August, www.climate.gov/news-features/understanding-climate/climate-variability-north-atlantic-oscillation.

Marengo, J. A., and Coauthors, 2023: Flash floods and landslides in the city of Recife, Northeast Brazil after heavy rain on May 25–28, 2022: Causes, impacts, and disaster preparedness. *Wea. Climate Extremes*, **39**, 100545, https://doi.org/10.1016/j.wace.2022.100545.

McKenna, C. M., and A. C. Maycock, 2022: The role of the North Atlantic Oscillation for projections of winter mean precipitation in Europe. *Geophys. Res. Lett.*, **49**, e2022GL099083, https://doi.org/10.1029/2022GL099083.

Menne, M. J., C. N. Williams, and B. E. Gleason, 2018: The Global Historical Climatology Network monthly temperature dataset, version 4. *J. Climate*, **31**, 9835–9854, https://doi.org/10.1175/JCLI-D-18-0094.1.

Merrifield, M. A., P. R. Thompson, and M. A. Lander, 2012: Multidecadal sea level anomalies and trends in the western tropical Pacific. *Geophys. Res. Lett.*, **39**, L13602, https://doi.org/10.1029/2012GL052032.

Naumann, G., and Coauthors, 2022: Extreme and long-term drought in the La Plata Basin: Event evolution and impact assessment until September 2022. JRC Tech Rep. 132245, 53 pp., https://doi.org/10.2760/62557.

Nicholson, S. E., A. H. Fink, and C. Funk, 2018: Assessing recovery and change in West Africa's rainfall regime from a 161-year record. *Int. J. Climatol.*, **38**, 3770–3786, https://doi.org/10.1002/joc.5530.

Prince, H. D., N. J. Cullen, P. B. Gibson, J. Conway, and D. G. Kingston, 2021: A climatology of atmospheric rivers in New Zealand. *J. Climate*, **34**, 4383–4402, https://doi.org/10.1175/JCLI-D-20-0664.1.

Risbey, J. S., M. J. Pook, P. C. McIntosh, M. C. Wheeler, and H. H. Hendon, 2009: On the remote drivers of rainfall variability in Australia. *Mon. Wea. Rev.*, **137**, 3233–3253, https://doi.org/10.1175/2009MWR2861.1.

Sadler, J. C., 1976: A role of the tropical upper tropospheric trough in early season typhoon development. *Mon. Wea. Rev.*, **104**, 1266–1278, https://doi.org/10.1175/1520-0493(1976)1042.0.CO;2.

Schneider, U., P. Finger, A. Meyer-Christoffer, M. Ziese, and A. Becker, 2018: Global precipitation analysis products of the GPCC. Deutscher Wetterdienst (DWD), 15 pp., https://opendata.dwd.de/climate_environment/GPCC/PDF/GPCC_intro_products_v2018.pdf.

Trewin, B., 2018: The Australian Climate Observations Reference Network–Surface Air Temperature (ACORN-SAT) version 2. Bureau of Meteorology Research Rep. 032, 67 pp., http://www.bom.gov.au/research/publications/researchreports/BRR-032.pdf.

Wheeler, M. C., H. H. Hendon, S. Cleland, H. Meinke, and A. Donald, 2009: Impacts of the Madden–Julian Oscillation on Australian Rainfall and Circulation. *J. Climate*, **22**, 1482–1498, https://doi.org/10.1175/2008JCLI2595.1.

WMO, 2023: *State of the Climate in Europe 2022*. WMO-No. 1320, 40 pp., https://library.wmo.int/index.php?lvl=notice_display&id=22285

Yang, Y., Z. Zhu, X. Shen, L. Jiang, and T. Li, 2023: The influences of Atlantic sea surface temperature anomalies on the ENSO-independent interannual variability of East Asian summer monsoon rainfall. *J. Climate*, **36**, 677–692, https://doi.org/10.1175/JCLI-D-22-0061.1.